

Suppressing SIV after removing
antiretrovirals pp. 157, 177, & 197

Politics trumps science
in Antarctic ocean p. 185

Polymers for perovskite
solar cells pp. 203 & 206

Science

\$15
14 OCTOBER 2016
sciencemag.org

AAAS

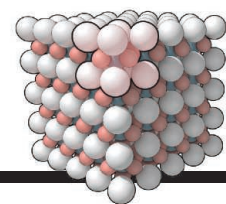
TAKING AIM

The new science of mosquito control p. 162



CONTENTS

14 OCTOBER 2016 • VOLUME 354 • ISSUE 6309



180
Materials
in silico



FEATURES

162 BITING BACK

By M. Enserink and L. Roberts

164 WINGED WARRIORS

Brazil plans to release billions of designer mosquitoes to stop the spread of infectious diseases. Will it work? By K. Servick

► PODCAST

168 THE ELIMINATOR

In humankind's war against insect-borne disease, Dutch entomologist Bart Knols is one of the most creative warriors By K. Kupferschmidt

171 PICK YOUR POISON

As mosquitoes develop resistance to pyrethroid insecticides, researchers are forced to look for alternatives By K. Kupferschmidt

ON THE COVER



An *Aedes aegypti* mosquito engorged with blood, perched on a human arm. This species can transmit viral diseases such as dengue,

Zika, chikungunya, and yellow fever. This week, a special news package examines new strategies in humanity's battle against mosquito-borne disease. See page 162.

Photo: © Alex Wild

NEWS

IN BRIEF

152 News at a glance

IN DEPTH

155 SPY AGENCIES TEAM UP WITH NATIONAL ACADEMIES

Expanded ties include new board, first-ever survey of social sciences and security By J. Mervis

156 AS HAWAII DELIBERATES, GIANT TELESCOPE CONSIDERS NEW HOME

State could prove inhospitable even if TMT wins permit By D. Clery

157 SURPRISING TREATMENT 'CURES' MONKEY HIV INFECTION

Antibody keeps SIV suppressed, but it's unclear how By J. Cohen

► PERSPECTIVE P. 177; REPORT P. 197

158 CHEMISTRY NOBEL HERALDS AGE OF MOLECULAR MACHINES

Primitive parts have evolved into more useful devices that pump, drill, move, and assemble other molecules

By R. F. Service

159 JOINT RESEARCH PUSH TARGETS FAST-MELTING ANTARCTIC ICE

U.K.-U.S. "Thwaites invasion" aims to refine sea-level rise estimates

By P. Voosen

160 CHINESE SCIENTIST JAILED OVER THEFT OF HYBRID CORN

Investigators used secret terrorism warrant to gather evidence and unravel plot By M. Hvistendahl

INSIGHTS

PERSPECTIVES

174 SICK BIRDS DON'T FLY...OR DO THEY?

Migratory birds were key to the spread of H5N8 viruses By C. A. Russell

► REPORT P. 213

176 YOUNG PHOSPHORYLATION IS FUNCTIONALLY SILENT

Phosphorylation sites younger than 18 million years prevail in numbers, but not in function By O. Matalon et al.

► REPORT P. 229

177 SHOCK AND KILL WITH CAUTION

Strategies to silence latent HIV infection should be explored By R. C. Gallo

► NEWS STORY P. 157; REPORT P. 197

179 MULTISITE PHOSPHORYLATION BY MAPK

Progressive phosphorylation controls the activity of a transcription factor By A. J. Whitmarsh and R. J. Davis

► REPORT P. 233

180 MAKING THE MOST OF MATERIALS COMPUTATIONS

Databases of theoretical structures and properties of materials can speed real-world discovery By K. S. Thygesen and K. W. Jacobsen

182 THE TROUBLE WITH NEGATIVE EMISSIONS

Reliance on negative-emission concepts locks in humankind's carbon addiction By K. Anderson and G. Peters



160

CONTENTS



225

An extraterrestrial impact

14 OCTOBER 2016 • VOLUME 354 • ISSUE 6309

184 A MICROBIAL ROUTE FROM COAL TO GAS

Microbes isolated from an oil reservoir directly convert coal to methane *By C. U. Welte*

► REPORT P. 222

POLICY FORUM

185 SCIENCE-BASED MANAGEMENT IN DECLINE IN THE SOUTHERN OCEAN

The burden of proof is being turned upside down *By C. M. Brooks et al.*

BOOKS ET AL.

188 ASYLUMS AND AFTER

A new exhibition probes the ever-evolving treatment of mental illness *By A. Robinson*

189 THE MYTHOLOGY OF CRISPR

An optimistic outlook on gene editing seeks to reconcile scientific progress with wisdom from the humanities *By G. J. Annas*

LETTERS

190 RETRACTION

By J. M. Berg

190 COLOMBIA: DEALING IN CONSERVATION

By N. Clerici et al.

191 COLOMBIA'S TAX ON WILDLIFE STUDIES

By V. P. Páez

191 ERRATA

RESEARCH

IN BRIEF

192 From *Science* and other journals

REVIEW

195 QUANTUM MATERIALS

Polaritons in van der Waals materials
D. N. Basov et al.

REVIEW SUMMARY; FOR FULL TEXT:

[dx.doi.org/10.1126/science.aag1992](https://doi.org/10.1126/science.aag1992)



RESEARCH ARTICLES

196 FOREST ECOLOGY

Positive biodiversity-productivity relationship predominant in global forests *J. Liang et al.*

RESEARCH ARTICLE SUMMARY; FOR FULL TEXT:

[dx.doi.org/10.1126/science.aaf8957](https://doi.org/10.1126/science.aaf8957)

197 HIV-1 THERAPY

Sustained virologic control in SIV⁺ macaques after antiretroviral and $\alpha_4\beta_7$ antibody therapy *S. N. Byrareddy et al.*

► NEWS STORY P. 157; PERSPECTIVE P. 177

REPORTS

SOLAR CELLS

203 Improving efficiency and stability of perovskite solar cells with photocurable fluoropolymers
F. Bella et al.

206 Incorporation of rubidium cations into perovskite solar cells improves photovoltaic performance
M. Saliba et al.

209 BIOPHYSICS

Bifurcating electron-transfer pathways in DNA photolyases determine the repair quantum yield *M. Zhang et al.*

213 INFLUENZA

Role for migratory wild birds in the global spread of avian influenza H5N8
The Global Consortium for H5N8 and Related Influenza Viruses

► PERSPECTIVE P. 174

217 POLITICAL SCIENCE

How economic, humanitarian, and religious concerns shape European attitudes toward asylum seekers
K. Bansak et al.

222 MICROBIAL PHYSIOLOGY

Methane production from coal by a single methanogen *D. Mayumi et al.*

► PERSPECTIVE P. 184

225 GLOBAL CLIMATE CHANGE

Impact ejecta at the Paleocene-Eocene boundary *M. F. Schaller et al.*

229 PROTEIN EVOLUTION

Evolution of protein phosphorylation across 18 fungal species *R. A. Studer et al.*

► PERSPECTIVE P. 176

233 SIGNAL TRANSDUCTION

Opposing effects of Elk-1 multisite phosphorylation shape its response to ERK activation *A. Mylona et al.*

► PERSPECTIVE P. 179

237 VACCINES

Rapid development of a DNA vaccine for Zika virus *K. A. Dowd et al.*

DEPARTMENTS

151 EDITORIAL

Business backs the basics
By Subra Suresh and Robert A. Bradway

254 WORKING LIFE

Making my own home
By Fatma Kaplan

Science Staff	150
New Products	241
Science Careers	242

SCIENCE (ISSN 0036-8075) is published weekly on Friday, except the last week in December, by the American Association for the Advancement of Science, 1200 New York Avenue, NW, Washington, DC 20005. Periodicals mail postage (publication No. 484460) paid at Washington, DC, and additional mailing offices. Copyright © 2016 by the American Association for the Advancement of Science. The title SCIENCE is a registered trademark of the AAAS. Domestic individual membership and subscription (51 issues): \$165 (\$74 allocated to subscription). Domestic institutional subscription (51 issues): \$1522. Foreign postage extra: Mexico, Caribbean (surface mail) \$55; other countries (air assist delivery) \$89. First class, airmail, student, and emeritus rates on request. Canadian rates with GST available upon request. GST #R1254 88122. Publications Mail Agreement Number 1069624. Printed in the U.S.A. Change of address: Allow 4 weeks, giving old and new addresses and 8-digit account number. Postmaster: Send change of address to AAAS, P.O. Box 96178, Washington, DC 20090-6178. Single-copy sales: \$15.00 current issue, \$20.00 back issue prepaid includes surface postage; bulk rates on request. Authorization to photocopy material for internal or personal use under circumstances not falling within the fair use provisions of the Copyright Act is granted by AAAS to libraries and other users registered with the Copyright Clearance Center (CCC) Transactional Reporting Service, provided that \$35.00 per article is paid directly to CCC, 222 Rosewood Drive, Danvers, MA 01923. The identification code for Science is 0036-8075. Science is indexed in the Reader's Guide to Periodical Literature and in several specialized indexes.

Editor-in-Chief Jeremy Berg

Executive Editor Monica M. Bradford **News Editor** Tim Appenzeller

Deputy Editors Lisa D. Chong, Andrew M. Sugden(UK), Valda J. Vinson, Jake S. Yeston

Research and Insights

DEPUTY EDITOR, EMERITUS Barbara R. Jasny **SR. EDITORS** Caroline Ash(UK), Gilbert J. Chin, Julia Fahrenkamp-Uppenbrink(UK), Pamela J. Hines, Stella M. Hurlley(UK), Paula A. Kiberstis, Marc S. Lavine(Canada), Kristen L. Mueller, Ian S. Osborne(UK), Beverly A. Purnell, L. Bryan Ray, Guy Riddihough, H. Jesse Smith, Jelena Stajic, Peter Stern(UK), Phillip D. Szuroni, Sacha Vignieri, Brad Wible, Nicholas S. Wigginton, Laura M. Zahn **ASSOCIATE EDITORS** Brent Grocholski, Keith T. Smith **ASSOCIATE BOOK REVIEW EDITOR** Valerie B. Thompson **LETTERS EDITOR** Jennifer Sills **LEAD CONTENT PRODUCTION EDITORS** Harry Jach, Lauren Krnec **CONTENT PRODUCTION EDITORS** Jeffrey E. Cook, Chris Filatreau, Cynthia Howe, Barbara P. Ordway, Catherine Wolner **SR. EDITORIAL COORDINATORS** Carolyn Kyle, Beverly Shields **EDITORIAL COORDINATORS** Aneera Dobbins, Joi S. Granger, Jeffrey Hearn, Lisa Johnson, Maryrose Madrid, Anita Wynn **PUBLICATIONS ASSISTANTS** Nida Masiulis, Dona Mathieu, Le-Toya Mayne Flood, Shannon McMahon, Scott Miller, Jerry Richardson, Alice Whaley(UK), Gwen Grant(UK), Brian White **EXECUTIVE ASSISTANT** Anna Bashkirova **ADMINISTRATIVE SUPPORT** Janet Clements(UK), Lizanne Newton(UK), Sarah Harrison (UK)

News

NEWS MANAGING EDITOR John Travis **INTERNATIONAL EDITOR** Richard Stone **DEPUTY NEWS EDITORS** Elizabeth Culotta, David Grimm, Eric Hand David Malakoff, Leslie Roberts **CONTRIBUTING EDITOR** Martin Enserink(Europe) **SR. CORRESPONDENTS** Daniel Clery(UK), Jeffrey Mervis, Elizabeth Pennisi **NEWS WRITERS** Adrian Cho, Jon Cohen, Jennifer Couzin-Frankel, Carolyn Gramling, Jocelyn Kaiser, Catherine Maticic, Kelly Servick, Robert F. Service, Erik Stokstad(Cambridge, UK), Paul Voosen, Meredith Wadman **INTERNS** Jessica Boddy, Ben Panko **CONTRIBUTING CORRESPONDENTS** John Bohannon, Warren Cornwall, Ann Gibbons, Mara Hvistendahl, Sam Kean, Eli Kintisch, Kai Kupferschmidt(Berlin), Andrew Lawler, Mitch Leslie, Charles C. Mann, Eliot Marshall, Virginia Morell, Dennis Normile(Shanghai), Heather Pringle, Tania Rabesandratana(London), Emily Underwood, Gretchen Vogel(Berlin), Lizzie Wade(Mexico City) **CAREERS** Donisha Adams, Rachel Bernstein(Editor), Maggie Kuo **COPY EDITORS** Julia Cole, Dorie Chevien, Jennifer Levin (Chief) **ADMINISTRATIVE SUPPORT** Jessica Adams

Executive Publisher Rush D. Holt

Publisher Bill Moran **Chief Digital Media Officer** Rob Covey

BUSINESS OPERATIONS AND PORTFOLIO MANAGEMENT DIRECTOR Sarah Whalen **PRODUCT DEVELOPMENT DIRECTOR** Will Schweitzer **PRODUCT DEVELOPMENT ASSOCIATE** Hannah Heckner **BUSINESS SYSTEMS AND FINANCIAL ANALYSIS DIRECTOR** Randy Y. SENIOR SYSTEMS ANALYST Nicole Mehmedovich **DIRECTOR, BUSINESS OPERATIONS & ANALYSIS** Eric Knott **MANAGER, BUSINESS OPERATIONS** Jessica Tierney **SENIOR BUSINESS ANALYST** Cory Lipman **BUSINESS ANALYSTS** David Garrison, Michael Hardesty Meron Kebede, Sandy Kim **FINANCIAL ANALYST** Drew Sher **DIRECTOR, COPYRIGHTS LICENSING SPECIAL PROJECTS** Emilie David **PERMISSIONS ASSOCIATE** Elizabeth Sandler **RIGHTS, CONTRACTS, AND LICENSING ASSOCIATE** Lili Kiser **RIGHTS & PERMISSIONS ASSISTANT** Alexander Lee

MARKETING DIRECTOR Elise Swinehart **ASSOCIATE MARKETING DIRECTOR** Stacey Burke Bowers **MARKETING ASSOCIATE** Steven Goodman **CREATIVE DIRECTOR** Scott Rodgersen **SENIOR ART ASSOCIATES** Paula Fry **ART ASSOCIATE** Kim Huynh

FULFILLMENT SYSTEMS AND OPERATIONS membership@aaas.org **MANAGER, MEMBER SERVICES** Pat Butler **SPECIALISTS** Terrance Morrison, Latashia Russell **MANAGER, DATA ENTRY** Mickie Napoleoni **DATA ENTRY SPECIALISTS** Brenden Aquilino, Fiona Giblin **MARKETING ASSOCIATE** Isa Sesay-Bah

PUBLISHER RELATIONS, EASTERN REGION Keith Layson **PUBLISHER RELATIONS, WESTERN REGION** Ryan Rexroth **SALES RESEARCH COORDINATOR** Aiesha Marshall **ASSOCIATE DIRECTOR, INSTITUTIONAL LICENSING OPERATIONS** Iquo Edim **SENIOR OPERATIONS ANALYST** Lana Guz **MANAGER, AGENT RELATIONS & CUSTOMER SUCCESS** Judy Lillibridge

WEB TECHNOLOGIES **PORTFOLIO MANAGER** Trista Smith **TECHNICAL MANAGER** Chris Coleman **PROJECT MANAGER** Nick Fletcher **DEVELOPERS** Ryan Jensen, Jimmy Marks, Brandon Morrison **BUSINESS ANALYST** Christina Wofford

DIGITAL MEDIA DIRECTOR OF ANALYTICS Enrique Gonzales **DIGITAL REPORTING ANALYST** Eric Hossinger **SR. MULTIMEDIA PRODUCER** Sarah Crespi **MANAGING DIGITAL PRODUCER** Alison Crawford **PRODUCER** Liana Birke **VIDEO PRODUCER** Chris Burns, Nguyễn Khởi Nguyễn **DIGITAL SOCIAL MEDIA PRODUCER** Brice Russ

DIRECTOR OF OPERATIONS PRINT AND ONLINE Lizabeth Harman **DIGITAL/PRINT STRATEGY MANAGER** Jason Hillman **QUALITY TECHNICAL MANAGER** Marcus Spiegler **PROJECT ACCOUNT MANAGER** Tara Kelly **DIGITAL PRODUCTION MANAGER** Lisa Stanford **ASSISTANT MANAGER DIGITAL/PRINT** Rebecca Doshi **SENIOR CONTENT SPECIALISTS** Steve Forrester, Antoinette Hodal, Lori Murphy, Anthony Rosen **CONTENT SPECIALISTS** Jacob Hedrick, Kimberley Oster **ADVERTISING OPERATIONS SPECIALIST** Ashley Jeter

DESIGN DIRECTOR Beth Rakouskas **DESIGN EDITOR** Marcy Atarod **SENIOR DESIGNER** Chrystal Smith **GRAPHICS MANAGING EDITOR** Alberto Cuadra **GRAPHICS EDITOR** Garvin Grullón **SENIOR SCIENTIFIC ILLUSTRATORS** Chris Bickel, Katharine Sutliff **SCIENTIFIC ILLUSTRATOR** Valerie Altounian **INTERACTIVE GRAPHICS EDITOR** Jia You **SENIOR GRAPHICS SPECIALISTS** Holly Bishop, Nathalie Cary **PHOTOGRAPHY MANAGING EDITOR** William Douthitt **SENIOR PHOTO EDITOR** Christy Steele **PHOTO EDITOR** Emily Petersen

DIRECTOR, GLOBAL COLLABORATION, CUSTOM PUBLICATIONS, ADVERTISING Bill Moran **EDITOR, CUSTOM PUBLISHING** Sean Sanders: 202-326-6430 **ASSISTANT EDITOR, CUSTOM PUBLISHING** Jackie Oberst: 202-326-6463 **ADVERTISING MARKETING MANAGER** Justin Sawyers: 202-326-7061 science_advertising@aaas.org **ADVERTISING SUPPORT MANAGER** Karen Foote: 202-326-6740 **ADVERTISING PRODUCTION OPERATIONS MANAGER** Deborah Tompkins **SR. PRODUCTION SPECIALIST/GRAPHIC DESIGNER** Amy Hardcastle **SR. TRAFFIC ASSOCIATE** Christine Hall **SALES COORDINATOR** Shirley Young **ASSOCIATE DIRECTOR, COLLABORATION, CUSTOM PUBLICATIONS/CHINA/TAIWAN/KOREA/SINGAPORE** Ruolei Wu: +86-186 0082 9345, rwu@aaas.org **COLLABORATION/CUSTOM PUBLICATIONS/JAPAN** Adarsh Sandhu + 81532-81-5142 asandhu@aaas.org **EAST COAST/FE**: +86-186 0082 9345, FAX 617-507-8189 **WEST COAST/W. CANADA** Lynne Stickrod: 415-931-9782, FAX 415-520-6940 **MIDWEST** Jeffrey Dembski: 847-498-4520 x3005, Steven Loerch: 847-498-4520 x3006 **UK EUROPE/ASIA** Roger Goncalves: TEL/FAX +41 43 243 1358 **JAPAN** Katsuyoshi Fukamizu(Tokyo): +81-3-3219-5777 kfukamizu@aaas.org **CHINA/TAIWAN** Ruolei Wu: +86-186 0082 9345, rwu@aaas.org

WORLDWIDE ASSOCIATE DIRECTOR OF SCIENCE CAREERS Tracy Holmes: +44 (0) 1223 326525, FAX +44 (0) 1223 326532 tholmes@science-int.co.uk

CLASSIFIED advertise@sciencecareers.org **U.S. SALES** Tina Burks: 202-326-6577, Nancy Toerna: 202-326-6578 **EUROPE/ROW SALES** Sarah Lelarge **SALES ASSISTANT** Kelly Grace **JAPAN** Hiroyuki Mashiki(Kyoto): +81-75-823-1109 hmmashiki@aaas.org **CHINA/TAIWAN** Ruolei Wu: +86-186 0082 9345 rwu@aaas.org **MARKETING MANAGER** Allison Pritchard **MARKETING ASSOCIATE** Aimee Aponte

AAAS BOARD OF DIRECTORS, CHAIR Geraldine L. Richmond **PRESIDENT** Barbara A. Schaaf **PRESIDENT-ELECT** Susan Hockfield **TREASURER** David Evans **SHAW CHIEF EXECUTIVE OFFICER** Rush D. Holt **BOARD** Cynthia M. Beall, May R. Berenbaum, Carlos J. Bustamante, Stephen P.A. Fodor, Claire M. Fraser, Michael S. Gazzaniga, Laura H. Greene, Elizabeth Loftus, Mercedes Pascual

SUBSCRIPTION SERVICES For change of address, missing issues, new orders and renewals, and payment questions: 866-434-AAAS (2227) or 202-326-6417, FAX 202-842-1065. Mailing addresses: AAAS, P.O. Box 96178, Washington, DC 20090-6178 or AAAS Member Services, 1200 New York Avenue, NW, Washington, DC 20005

INSTITUTIONAL SITE LICENSES 202-326-6730 **REPRINTS:** Author Inquiries 800-635-7181 **COMMERCIAL INQUIRIES** 803-359-4578 **PERMISSIONS** 202-326-6765, permissions@aaas.org **AAAS Member Services** 202-326-6417 or <http://membercentral.aaas.org/discourts>

Science serves as a forum for discussion of important issues related to the advancement of science by publishing material on which a consensus has been reached as well as including the presentation of minority of conflicting points of view. Accordingly, all articles published in Science—including editorials, news and comment, and book reviews—are signed and reflect the individual views of the authors and not official points of view adopted by AAAS or the institutions with which the authors are affiliated.

INFORMATION FOR AUTHORS See pages 624 and 625 of the 5 February 2016 issue or access www.sciencemag.org/authors/science-information-authors

SENIOR EDITORIAL BOARD

Gary King, *Harvard University*, Susan M. Rosenberg, *Baylor College of Medicine*, Ali Shalatifard, *Northwestern University Feinberg School of Medicine*

BOARD OF REVIEWING EDITORS

(Statistics board members indicated with \$)

Adriano Aguzzi, *U. of Hospital Zurich*
Takuzo Aida, *U. of Tokyo*
Leslie Aiello, *Wenner-Gren Foundation*
Judith Allen, *U. of Edinburgh*
Sonia Altizer, *U. of Georgia*
Sebastian Amigorena, *Institut Curie*
Meinrat O. Andreae, *Max-Planck Inst. Mainz*
Paola Arlotta, *Harvard U.*
Johan Auwerx, *EPFL*
David Awschalom, *U. of Chicago*
Clare Baker, *University of Cambridge*
Nenad Ban, *ETH Zurich*
Franz Bauer, *Pontificia Universidad Católica de Chile*
Ray H. Baughman, *U. of Texas, Dallas*
David Baum, *U. of Wisconsin*
Carlo Beenakker, *Leiden U.*
Kamran Behnia, *ESPCI-ParisTech*
Yasmine Belkaid, *NIAID, NIH*
Philip Benfey, *Duke U.*
May Berenbaum, *U. of Illinois*
Gabriele Bergers, *U. of California, San Francisco*
Bradley Bernstein, *Massachusetts General Hospital*
Peer Bork, *EMBL*
Bernard Bourdon, *Ecole Normale Supérieure de Lyon*
Chris Bowler, *Ecole Normale Supérieure*
Ian Boyd, *U. of St. Andrews*
Emily Brodsky, *U. of California, Santa Cruz*
Ron Brookmeyer, *U. of California Los Angeles* (\$) **\$**
Christian Büchel, *U. Hamburg-Eppendorf*
Joseph A. Burns, *Cornell U.*
Carter Tribble Butts, *U. of California, Irvine*
Gyorgy Buzsaki, *New York U. School of Medicine*
Blanche Capel, *Duke U.*
Mats Carlsson, *U. of Oslo*
Ib Chorkendorff, *U. of Denmark*
David Clapham, *Children's Hospital Boston*
Joel Cohen, *Rockefeller U., Columbia U.*
James J. Collins, *MIT*
Robert Cook-Deegan, *Duke U.*
Lisa Coussens, *Oregon Health & Science U.*
Alan Cowman, *Walter & Eliza Hall Inst.*
Robert H. Crabtree, *Yale U.*
Roberto Croce, *Vrije Universiteit*
Janet Currie, *Princeton U.*
Jeff L. Dangl, *U. of North Carolina*
Tom Daniel, *U. of Washington*
Frans de Waal, *Emory U.*
Stanislas Dehaene, *Collège de France*
Robert Desimone, *MIT*
Claude Desplan, *New York U.*
Sandra Diaz, *Universidad Nacional de Cordoba*
Dennis Discher, *U. of Pennsylvania*
Gerald W. Dorn II, *Washington U. School of Medicine*
Jennifer A. Doudna, *U. of California, Berkeley*
Bruce Dunn, *U. of California, Los Angeles*
William Dunphy, *Caltch*
Christopher Dye, *WHO*
Todd Ehlers, *U. of Tuebingen*
David Ehrhardt, *Carnegie Inst. of Washington*
Tim Elston, *U. of North Carolina at Chapel Hill*
Jennifer Elisseeff, *Johns Hopkins U.*
Gerhard Ertl, *Fritz-Haber-Institut, Berlin*
Barry Everitt, *U. of Cambridge*
Ernst Fehr, *Johns Hopkins U.*
Anne C. Ferguson-Smith, *U. of Cambridge*
Michael Feuer, *The George Washington U.*
Toren Finkel, *NHLBI, NIH*
Kate Fitzgerald, *U. of Massachusetts*
Peter Fratzl, *Max-Planck Inst.*
Elaine Fuchs, *Rockefeller U.*
Daniel Geschwind, *UCLA*
Karl-Heinz Glassmeier, *TU Braunschweig*
Ramón González, *Rice U.*
Elizabeth Grove, *U. of Chicago*
Nicolas Gruber, *ETH Zurich*
Kip Guy, *St. Jude's Children's Research Hospital*
Teekjip Ha, *U. of Illinois at Urbana-Champaign*
Wolf-Dietrich Hardt, *ETH Zurich*
Christian Haass, *Ludwig Maximilians U.*
Sharon Hammes-Schiffer, *U. of Illinois at Urbana-Champaign*
Michael Hasselmo, *Boston U.*
Martin Heimann, *Max-Planck Inst. Jena*
Yka Helariutta, *U. of Cambridge*
James A. Hendler, *Rensselaer Polytechnic Inst.*
Janet G. Hering, *Swiss Fed. Inst. of Aquatic Science & Technology*
Kai-Uwe Hinrichs, *U. of Bremen*
David Hodell, *U. of Cambridge*
Lora Hooper, *UT Southwestern Medical Ctr. at Dallas*
Tamas Horvath, *Yale University*
Raymond Huey, *U. of Washington*
Fred Hughson, *Princeton U.*
Auke Ijspeert, *EPFL Lausanne*
Stephen Jackson, *USGS and U. of Arizona*
Steven Jacobsen, *U. of California, Los Angeles*
Seema Jayachandran, *Northwestern U.*
Kai Jonsson, *EPFL Lausanne*
Peter Jonas, *Inst. of Science & Technology (IST) Austria*
Matt Kaeberlein, *U. of Washington*
William Kaelin Jr., *Dana-Farber Cancer Inst.*
Daniel Kahne, *Harvard U.*
Daniel Kammen, *U. of California, Berkeley*
Abby Kanner, *U. of California, Los Angeles*
Hitoshi Kawakatsu, *U. of Tokyo*
Masashi Kawasaki, *U. of Tokyo*
V. Naray Kim, *Seoul National U.*
Robert Kingston, *Harvard Medical School*

Etienne Koechlin, *Ecole Normale Supérieure*
Alexander Kolodkin, *Johns Hopkins U.*
Thomas Langer, *U. of Cologne*
Mitchell A. Lazar, *U. of Pennsylvania*
David Lazer, *Harvard U.*
Thomas Lecuit, *IDM*
Virginia Lee, *U. of Pennsylvania*
Stanley Lemon, *U. of North Carolina at Chapel Hill*
Ottoline Leyser, *Cambridge U.*
Wendell Lim, *U.C. San Francisco*
Marcia C. Linn, *U. of California, Berkeley*
Jianguo Liu, *Michigan State U.*
Luis Liz-Marzan, *CIC biomaGUNE*
Jonathan Losos, *Harvard U.*
Ke Lu, *Chinese Acad. of Sciences*
Christian Lüscher, *U. of Geneva*
Laura Machesky, *CRUK Beatson Inst. for Cancer Research*
Aime Magurran, *U. of St. Andrews*
Oscar Marin, *CSIC & U. Miguel Hernández*
Charles Marshall, *U. of California, Berkeley*
C. Robertson McClung, *Dartmouth College*
Rodrigo Medellín, *U. of Mexico*
Graham Medley, *U. of Warwick*
Jane Memmott, *U. of Bristol*
Tom Misteli, *NCI*
Yasushi Miyashita, *U. of Tokyo*
Mary Ann Moran, *U. of Georgia*
Richard Morris, *U. of Edinburgh*
Alison Moutter-Reif, *NC State U.* (\$) **\$**
Thomas Murray, *The Hastings Center*
Daniel Neuman, *U. of California, Berkeley*
Kitty Nijmeijer, *U. of Twente*
Helga Nowotny, *European Research Advisory Board*
Rachel O'Reilly, *Warwick U.*
Joe Orenstein, *U. of California*
Berkeley & Lawrence Berkeley National Lab
Harry Orr, *U. of Minnesota*
Pilar Ossorio, *U. of Wisconsin*
Andrew Oswald, *U. of Warwick*
Isabella Pagano, *Istituto Nazionale di Astrofisica*
Margaret Palmer, *U. of Maryland*
Steve Palumbi, *Stanford U.*
Jane Parker, *Max-Planck Inst. of Plant Breeding Research*
Giovanni Parmigiani, *Dana-Farber Cancer Inst.* (\$) **\$**
John H. J. Petrini, *Memorial Sloan-Kettering Cancer Center*
Samuel Pfaff, *Salk Institute for Biological Studies*
Kathrin Plath, *U. of California, Los Angeles*
Joshua Plotkin, *U. of Pennsylvania*
Albert Polman, *FOM Institute AMOLF*
Philippe Poulin, *CNRS*
Jonathan Pritchard, *Stanford U.*
Wim van der Putten, *Netherlands Institute of Ecology*
David Randall, *Colorado State U.*
Sarah Reisman, *Caltch*
Felix Rey, *Institut Pasteur*
Trevor Robbins, *U. of Cambridge*
Jim Roberts, *Fred Hutchinson Cancer Research Ctr.*
Amy Rosenzweig, *Northwestern University*
Mike Ryan, *U. of Texas, Austin*
Shinji Saitoku, *Kyoto U.*
Shimon Sakaguchi, *Kyoto U.*
Miguel Salmeron, *Lawrence Berkeley National Lab*
Jürgen Sandkühler, *Medical U. of Vienna*
Alexander Schier, *Harvard U.*
Vladimir Shalaev, *Purdue U.*
Robert Siliciano, *Johns Hopkins School of Medicine*
Denis Simon, *Arizona State U.*
Uri Simonsohn, *U. of Pennsylvania*
Alison Smith, *Johns Hopkins U.*
Richard Smith, *U. of North Carolina* (\$) **\$**
John Speakman, *U. of Aberdeen*
Allan C. Spradling, *Carnegie Institution of Washington*
Jonathan Sprent, *Garvan Inst. of Medical Research*
Eric Steig, *U. of Washington*
Paula Stephan, *Georgia State U. and National Bureau of Economic Research*
Molly Stevens, *Imperial College London*
V. S. Subramanian, *U. of Maryland*
Ira Tabas, *Columbia U.*
Sarah Teichmann, *Cambridge U.*
John Thomas, *North Carolina State U.*
Shubha Tole, *Jata Institute of Fundamental Research*
Christopher Tyler-Smith, *The Wellcome Trust*
Sanger Inst.
Herbert Virgin, *Washington U.*
Bert Vogelstein, *Johns Hopkins U.*
David Wallace, *Weizmann Inst. of Science*
Ian Walsmley, *U. of Oxford*
Jane-Ling Wang, *U. of California, Davis* (\$) **\$**
David Waxman, *Fudan U.*
Jonathan Weissman, *U. of California, San Francisco*
Chris Wikle, *U. of Missouri* (\$) **\$**
Ian A. Wilson, *The Scripps Res. Inst.* (\$) **\$**
Timothy D. Wilson, *U. of Virginia*
Rosemary Wyse, *Johns Hopkins U.*
Jan Zaenen, *Leiden U.*
Kenneth Zaret, *U. of Pennsylvania School of Medicine*
Jonathan Zehr, *U. of California, Santa Cruz*
Len Zon, *Children's Hospital Boston*
Maria Zuber, *MIT*

BOOK REVIEW BOARD

David Bloom, *Harvard U.*, Samuel Bowring, *MIT*, Angela Creager, *Princeton U.*, Richard Swedder, *U. of Chicago*, Ed Wasserman, *DuPont*

Business backs the basics

Earlier this year, a number of leaders from major U.S. corporations gathered at Sunnylands in California to discuss the critical importance of basic scientific research. For decades, the private sector has withdrawn from some areas of basic research, as accelerating market pressures, the speed of innovation, and the need to protect intellectual property in a global marketplace made a Bell Labs-style, in-house model of discovery and development hard to sustain. However, the leaders who gathered for the “CEOs and Leaders for Science” retreat* (which we convened) agreed that basic research will make or break corporations in the long term. Why?

Long-term basic research, substantially funded by the U.S. government, underlies some of industry’s most profitable innovations. Global positioning system technology, now a staple in every mobile phone, emerged from Cold War Defense Department research and decades of National Science Foundation explorations. As well, long-term public-private partnerships in basic research have driven U.S. leadership, from information technology to drug development and medical advancement. For example, the Human Genome Project combined \$14.5 billion in federal investment with a private-sector initiative, generating nearly \$1 trillion in jobs, personal wealth for entrepreneurs, and taxes by 2013. Such endeavors created a science ecosystem that in turn generated the talent pipeline upon which it depended.

Although for-profit corporations still invest in proprietary product development and expensive clinical trials, industry finds itself unable to invest in basic research the way it once did. The need for increased corporate secrecy, market force-driven short-term decision-making, and narrowing windows to monetize new technologies have whittled away industry’s willingness and ability to conduct basic research. This change threatens U.S. preeminence in research. For instance, the nation may lose its ability to attract and retain the finest talent from around the world. A good fraction of the students who earn ad-

vanced degrees in science and technology in the United States come from abroad because of the nation’s scientific excellence. For decades, American companies could attract and retain the finest talent from around the world. But if the U.S. loses its edge in research, it may also lose this vital resource of expertise and innovation.

Consequently, business leaders assembled at Sunnylands resolved to use their individual and collective cred-

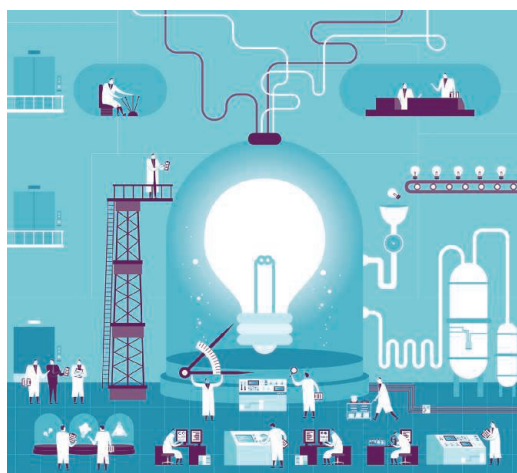
ibility, and their stature as heads of enterprises that fuel the economy, to advocate for greater government support for basic scientific research to revitalize the science ecosystem. However, they will need to lift sagging public opinion because many Americans now see basic research as a luxury rather than a necessity. A 2015 Pew poll found that Americans who view publically funded basic research as “not worth it” rose from 18 to 24% between 2009 and 2014. At the same time, those who believe private investment is enough to ensure scientific progress also increased from 29 to 34%.

With that in mind, the CEOs will partner with academic leaders to educate the public about the importance of basic research. Together, they will advocate for this in meetings with federal officials, through various media channels, and by asking presidents in the Association of American Universities to identify corporate leaders in their respective communities to join the effort. The hope is that this concerted action positions basic research atop the next U.S. president’s agenda.

History has shown that investments in basic research are the primary engine by which humanity has advanced, and major economic gains—often unanticipated when the research was initially funded—have been realized. In the United States, that will require a long-term commitment from the government, complementing the ongoing investment of risk capital and key industry sectors.

America’s leadership role in scientific innovation is an inherited responsibility and an economic imperative. It must not be neglected.

—Subra Suresh and Robert A. Bradway



**“...basic research will
make or break corporations
in the long term.”**



Subra Suresh is the president of Carnegie Mellon University, Pittsburgh, PA, and is the former director of the U.S. National Science Foundation. Email: president@cmu.edu



Robert A. Bradway is the chairman and chief executive officer of Amgen, Thousand Oaks, CA. Email: rbradway@amgen.com

*www.annenbergpublicpolicycenter.org/business-leaders-agree-u-s-funding-of-basic-research-advances-prosperity-security-well-being/

“Science is global. ... If I look back to my old country, it's in a real mess because it thinks it can raise borders to people coming in. This is not good for science.”

U.K. native Fraser Stoddart of Northwestern University in Evanston, Illinois, who last week was one of three winners of the 2016 Nobel Prize in Chemistry. <http://scim.ag/2016chemnobel>

IN BRIEF

Pangolins to get more protection

Numbers of several highly endangered species, including pangolins (pictured), African grey parrots, and Barbary macaques, have plummeted due to uncontrolled international trade—but delegates to the 17th Convention on International Trade in Endangered Species of Wild Fauna and Flora (CITES) in Johannesburg, South Africa, have now voted to ban that trade. Delegates from 182 countries approved 51 of 61 proposals to tighten protections for hundreds of species, including devil rays, chambered nautilus, and several species of shark. An effort to reauthorize selling rhinoceros horn was defeated; the rhinoceros will remain on CITES's Appendix I, receiving its highest protection. A proposal to list all African elephants on Appendix I, effectively banning ivory trade, did not pass—although populations shrank from 1.2 million in 1980 to 400,000. The United States opposed the listing after Namibia warned it would ignore restrictions, and the European Union said each country should manage its own elephant population. Meanwhile, a proposal to prohibit trade in African lions was weakened from a ban on exports of products from all lions to a ban on the sale of bones, claws, and teeth of wild lions.



AROUND THE WORLD

India drives rise in TB cases

GENEVA, SWITZERLAND | Tuberculosis (TB) in 2015 sickened an estimated 10.4 million people, a jump of 500,000 from 2014, and killed 1.8 million—more than HIV. But the apparently alarming rise mainly reflects improved surveillance in India, which accounts for 24% of the cases, says the annual *Global Tuberculosis Report* released this week by the World Health Organization (WHO) in Geneva, Switzerland. “India’s always been a major problem,” says Mario Ravigliione, head of the TB program at WHO. “They have 400 million people living in poverty.” The poor often share rooms, have little access to health care, and depend on alternatives like Ayurvedic medicine that keep them away from proven cures. The report also emphasizes that the world has made scant progress against multidrug-resistant TB, and needs to increase its investment by \$1.7 billion a year in low- and middle-income countries to properly combat it.

Contract theory nabs econ Nobel

STOCKHOLM | The 2016 Nobel Prize in Economic Sciences has been awarded to key figures in the development of contract theory—conceptual work that explains the logic of CEO bonuses, privatization of government services, and other kinds of contracts. Bengt Holmström of the Massachusetts Institute of Technology and Oliver Hart of Harvard University, both in Cambridge, Massachusetts, will share the prize. Holmström’s theories inform how compensation packages should be structured: In 1979, he published the informativeness principle, which says that pay should be based on information about effort. He later noted that fixed pay might be better than bonuses for jobs with many kinds of output, some more quantifiable than others, as an incentive structure would encourage employees to prioritize easily measured aspects over others—such as student test scores over critical thinking. In the mid-1980s, Hart and colleagues studied the idea of incomplete contracts, which lay out how disagreements will be resolved, such as who will take control



Gender bias in telescope time

Astronomers wanting time on the European Southern Observatory's (ESO's) telescopes are less likely to get it if they're women, an internal ESO study reported last week on the preprint server arXiv. The study examined 13,420 proposals submitted by 3017 principal investigators from 2008 to 2016. Male-led proposals were selected 22.2% of the time, compared with 16% for female-led proposals. One reason may be that men are overrepresented at more senior career levels: Professional astronomers tended to win out over postdoctoral

fellows and students—and there were four times as many professional male applicants. But after accounting for the career level of the proposer, a gender gap persisted: The success rate for men was 22.1%, whereas women's success rate inched up to 19.3%. Both male and female reviewers tended to rank proposals from female applicants at all career levels more poorly. A 2014 study of proposal reviews for the Hubble Space Telescope also found that men were more successful than women in getting time. <http://scim.ag/ESOgender>

of assets. His group also examined when governments should privatize services, noting the potential for a tradeoff between cost and quality, but also the possibility for competition to avert quality declines. <http://scim.ag/2016EconNobel>

Nuclear R&D pact suspended

MOSCOW | Even during the Cold War, things were never this bad. Last week, the Russian government suspended an agreement with the United States on nuclear R&D cooperation and terminated another agreement to retrofit Russian research reactors to

no longer run on weapons-grade uranium fuel. The suspensions are largely symbolic, but nonetheless plunged relations between Russian and U.S. nuclear science communities to a new low. The Russian government framed the suspension of the September 2013 R&D agreement as a “countermeasure” to U.S. sanctions imposed on Russia after its annexation of Crimea in March 2014 and U.S. support for rebels in eastern Ukraine. That suspension “is particularly unfortunate,” says a U.S. official, because the agreement was “the first framework following the collapse of the Soviet Union in which the two sides came together as equals.” After

the Soviet Union collapsed in 1991, U.S. assistance to Russia's nuclear establishment for many years was geared toward securing nuclear materials and redirecting weapons scientists to civilian projects. The Russian government stated that cooperation could resume when “justified by the general context of relations with the United States.”

Europe signs onto climate deal

STRASBOURG, FRANCE | The European Union and seven member states, including Germany and France, last week officially signed onto the global treaty to curb climate change reached in Paris last November. The deal sets a global target of slowing the flow of greenhouse gases into the atmosphere and holding temperature increases during this century to below 2°C. The European backing means the Paris agreement will have been adopted by more than 55 nations totaling more than 55% of greenhouse gas emissions—the level required for the agreement to take effect. The climate deal takes effect 30 days after hitting the two “55” targets. Although 195 nations endorsed the agreement in Paris, each country then needs to go through its national process of approving the deal. In early September, the United States and China jointly pledged to officially sign the agreement; India, another



Despite the suspension of nuclear R&D cooperation, joint U.S.-Russia efforts to remove highly enriched uranium from Poland continue.

major player in climate politics, approved it on 2 October. New Zealand and Canada also signed last week. Under the agreement, once a country has adopted it and it has taken effect, the country must wait at least 4 years to withdraw. <http://scim.ag/climate55>

NEWSMAKERS

Three Qs

Biologist **Cory Williams** of Northern Arizona University in Flagstaff is using activity trackers akin to Fitbits to track the energy consumption of arctic ground squirrels in Alaska. In a recent study in *Royal Society Open Science*, he found that male squirrels spend more time outside of their burrows but are less active than females, which have limited time to spare when caring for their young but use it to forage for food. He chatted with *Science*



A tracker detects the arctic ground squirrel's activity.

about creating a squirrel Fitbit and how technology is improving ecological research. <http://scim.ag/squirrelfitbit>

Q: Why arctic ground squirrels?

A: [They're] one of the only Arctic animals that keep a rigid schedule even when there's no light/dark cycle for 6 weeks—meaning, they emerge from and return to their burrows the same time every day and they eat the same time each day.

Q: What technology did you use for the trackers?

A: The trackers were epoxied onto a collar that the animals wore. We used light loggers that ... detect the presence or absence of light to see if the squirrels are in their burrows. The accelerometers take measurements once every second in three axes of direction, which lets us measure the index of movement.

Q: What could be done with the technology in the future?

A: I'd like to implant a single device in an animal that can give us measures of physiology and behavior besides energy expenditure. ... Data on heart rate, metabolism, and what hormones it's producing. And now that wireless charging is more common, we could recharge the implanted device and send the animal on its way. I'm interested to see how we can implement technology more into ecological studies.



Bumble bees mastered a test used to assess the intelligence of birds and apes.

Bumble bees prove their smarts



Apes, crows, and parrots often get acclaim for their intelligence. But small-brained bumble bees can solve tasks that may impress even a bird cognition researcher, a new study suggests. String pulling is often used to assess the intelligence of animals such as birds and apes. So a team of cognitive scientists from Queen Mary University of London designed one for bees: a clear plastic table containing

three flat artificial blue flowers that each held a well of sugar water. To get the sugar water, the bee had to pull the flower out by tugging on an attached string (inset). The team put 110 bees, one at a time, next to the table—and watched. Some tugged at the strings and gave up, but two kept at it until they retrieved the reward, the team reported last week in *PLOS Biology*. The team also placed untrained bees behind a clear plastic wall, where they could watch the other bees retrieve the water. More than 60% of the watchers knew to pull the string when it was their turn; furthermore, when trained bees were returned to their colony, a majority of the workers picked up string pulling by watching them—hinting at a rudimentary form of culture, the team says.

BY THE NUMBERS

401

Lowest concentration of carbon dioxide, in parts per million (ppm), measured for 2016 at Mauna Loa in Hawaii in late September, before values climb again. The site may now have passed the 400-ppm mark permanently.

50%

Proportion of sperm count in boys conceived by injecting sperm directly into the egg, compared with boys conceived naturally. The sons probably inherited their fathers' poor fertility, scientists say (*Human Reproduction*).

3

Number of the seven new Nobel laureates in the natural sciences who were born in Scotland.

U.S. INTELLIGENCE

Expanded ties include new board, first-ever survey of social sciences and security

In an unprecedented move, U.S. intelligence agencies are teaming up with the nation's most prestigious scientific body in a bid to make better use of findings from the country's leading social and behavioral scientists.

David Honey, ODNI director of science and technology under Director of National Intelligence James Clapper, says he hopes that the new partnership will help the intelligence community improve how it collects and analyzes information. He and others are eager for help picking out useful and relevant research, as well as grasping where there is a lack of good science. Understanding “the

One area in dire need of better research is figuring out when people are lying, Fein says.

Charles Gaukel, National Intelligence Council

Even research that generated solid results had serious flaws, he adds. "For example,

“Scholars like to say, ‘In general, X is the case.’ But as practitioners, we are asked to respond to a specific situation,” explained Charles Gaukel of the National Intelligence Council in Washington, D.C., which consists of senior officials from each of the 16 intelligence agencies across the government. Gaukel also debunked the popular notion that intelligence analysts try to forecast global events. “Our role is not to make predictions,” he said. “Rather, we try to give policymakers a sense of what’s out there, and how the enemy is likely to respond.”

SCIENCE sciencemag.org

blueprint for so-called decadal surveys, which look ahead 10 years. Traditionally, decadal studies help a particular discipline, such as astrophysics or geoscience, set priorities among competing facilities and projects. They may also recommend how federal agencies can fill gaps and maximize their research portfolios.

In contrast, the new study won't seek to balance competing demands for scientific facilities or examine existing research portfolios at the intelligence agencies. Instead, Honey hopes it will identify current and future research areas that might be useful for national security. Speaking at the summit, Fein suggested that those on the decadal survey might want to convene a panel of intelligence practitioners who would propose areas "that might benefit from the relevant perspectives, data, and knowledge" of social and behavioral scientists.

"I can't forecast what we will learn" from the study, Honey says. "But the history of decadal studies shows their value in pointing to where the research community is headed."

The survey is expected to take 2 years, and more than 300 people have been nominated for the panel's 18 slots. Despite that strong show of interest, some scientists who support the effort worry that getting involved could harm their research because of public unease about the spy agencies' activities.

"I'm a citizen scientist, and I think this collaboration is great," says Paul Glimcher, a neuroeconomist at New York University in New York City who spoke at the summit about the Kavli HUMAN project, a deep dive into the behavior and characteristics of 10,000 New York City residents that he leads. But he says his team has "promised our subjects that the data will never be shared with the government. And I'm concerned they might react negatively to my being involved in a study funded by U.S. intelligence agencies."

Some observers see the new intelligence board as a successor to an ODNI science advisory panel that Clapper abolished after becoming the nation's top spy in 2010. "It seems like at least an admission that the abandonment of [that advisory board] was a mistake and that there is an important role for independent advice from academics to the intelligence community," says Steven Aftergood, who leads the government secrecy project at the Federation of American Scientists in Washington, D.C.

Gaukel may have inadvertently given the pending decadal survey its marching orders during his summit talk on what intelligence analysts do. "We're looking for truth," he said. "But we're particularly looking for truth that works." ■

Artist's impression of the Thirty Meter Telescope.



ASTRONOMY

As Hawaii deliberates, giant telescope considers new home

State could prove inhospitable even if TMT wins permit

By Daniel Clery

If you are going to spend more than a billion dollars building one of the world's biggest telescopes, you'll want to put it in a place with the best possible view of the stars. But in the case of the Thirty Meter Telescope (TMT), an instrument that promises unprecedented images of everything from the most distant galaxies to nearby exoplanets, builders may have to settle for second best.

Next week, the fierce legal and cultural battle that has engulfed efforts to build the TMT on Mauna Kea, a 4,207-meter-high peak in Hawaii, will reignite as state of-

ficials open a pivotal hearing on whether to allow construction. The peak is rated as the best observing site in the Northern Hemisphere, but for Native Hawaiians it is sacred land, and many residents oppose the project. "The risk [to the project] is by no means small," says project manager Gary Sanders of the TMT International Observatory in Pasadena, California, and "the cost of delay is significant." So the project is also hedging its bets by considering alternative sites.

The TMT is one of three giant telescopes expected to dominate ground-based optical astronomy beginning in the next decade. The European Extremely Large Telescope (with a 39-meter mirror) and the Giant Magellan Telescope (24.5 meters) are already under construction, both in Chile. The TMT was also supposed to be underway by now, having won a construction permit from Hawaiian officials in 2011 after a long approval process. But the project ground to a halt after Native Hawaiian protesters disrupted a 2014 groundbreaking ceremony and later blocked workers from reaching the site. Then in December 2015, native activists won a ruling from Hawaii's supreme court that invalidated the TMT's building permit because of procedural violations. The court ordered the state's Board

The sky's the limit

Troubles at Mauna Kea have forced the Thirty Meter Telescope to consider alternative sites. Lower elevations generally offer inferior observing conditions.

LOCATION	ELEVATION (METERS)
Mauna Kea, Hawaii	4050
San Pedro Mártir, Mexico	2830
Roque de los Muchachos, Spain	2400
Antofagasta region, Chile	2300–4500

of Land and Natural Resources to reopen hearings designed to give the public a voice in the decision.

The new hearings begin on Hawaii's Big Island on 18 October and will last into late November. Sanders says the TMT's application is essentially unchanged. Witnesses have already supplied written statements, and more than a dozen parties, mostly opposing the project, will have a chance to ask questions. In the end, "it seems likely we'll get the permit," says astronomer Robert Kirshner, head of science programs at the Gordon and Betty Moore Foundation in Palo Alto, California, which has so far ploughed \$180 million into the TMT. But any decision, which is unlikely before the end of the year, will probably end up again in Hawaii's supreme court.

Even if the TMT ultimately gets a go-ahead, supporters worry that continuing opposition may make it difficult to build, staff, and operate the telescope. Protests on the mountain have become heated at times, according to press reports, and there have been arrests. "We can't take risks with people's safety," Sanders says.

If Hawaii proves inhospitable, the TMT will try to relocate. Since this past February, experts have been reviewing alternative sites, including several that were studied when the TMT began serious planning in the mid-2000s. Cerro Armazones, a peak in northern Chile, was a favorite for the TMT, but it is now ruled out because Europe's giant scope is taking up residence. Other sites nearby are in contention. But moving the TMT to Chile would put all three giant telescopes in the Southern Hemisphere, where they would be unable to see much of the northern sky.

Potential Northern Hemisphere sites include San Pedro Mártir in Baja California in Mexico and Roque de los Muchachos on La Palma, a Spanish island off the Atlantic coast of Morocco. "Our friends in La Palma are pushing hard" to get the TMT, says Matt Mountain, president of the Association of Universities for Research in Astronomy in Washington, D.C. But neither alternative matches the seeing conditions on Mauna Kea, and they would bring extra cost and complication. The project has already ruled out sites in the Himalayas, put forward by India and China—both TMT partners along with the United States, Japan, and Canada—because they are too far from ports and have short construction seasons.

The TMT governors are expected to choose their top alternative site later this month. Regardless of what happens in Hawaii, the governors have vowed to start construction—on Mauna Kea or elsewhere—no later than April 2018. ■

AIDS

Surprising treatment 'cures' monkey HIV infection

Antibody keeps SIV suppressed, but it's unclear how

By Jon Cohen

Fascinating." "A complete first." "Striking." "Too amazing to be real." Those are some of the reactions researchers are having to a provocative, baffling monkey study suggesting that a monoclonal antibody used to treat inflammatory bowel disease in humans might lead to a "functional" cure of an infection with the AIDS virus.

HIV therapies have improved to the point that combinations of antiretroviral (ARV) drugs routinely knock down the virus so effectively that standard tests cannot detect it in the blood. Researchers have long sought strategies that would allow people to stop taking their ARVs without the virus rebounding—a functional rather than complete cure, because patients would still harbor the virus, which integrates its genes into the DNA of a host's cells. Yet save for a few notable exceptions, almost everyone who has stopped taking ARVs has seen the virus jump back to high levels a few weeks later. To keep the virus at bay, HIV-infected people must take ARVs for life.

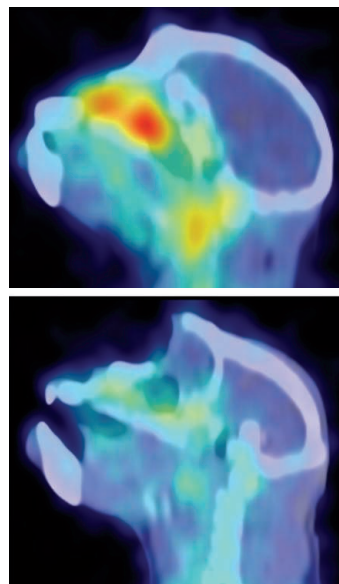
On p. 197, a team led by immunologist Aftab Ansari of Emory University School of Medicine in Atlanta describes infecting eight monkeys with SIV, the simian version of HIV, treating them with ARVs, and then infusing them with an antibody similar to an approved drug for Crohn's disease and ulcerative colitis that targets a receptor on immune cell surfaces known as $\alpha 4\beta 7$. More than 9 months after the ARVs and antibody treatments were stopped, all eight animals had low or undetectable levels of SIV in their blood. In seven SIV-infected control animals that received what amounts to a placebo antibody, the virus rebounded to high levels

within 2 weeks of stopping ARVs. "The results knocked us out, they were so stunning," says co-author Anthony Fauci, an immunologist who heads the U.S. National Institute of Allergy and Infectious Diseases (NIAID) in Bethesda, Maryland.

Ansari stresses that animals treated with anti- $\alpha 4\beta 7$ remain infected. "They're not cured—far from it," Ansari says. Moreover, he and Fauci don't know how the treatment works. "It has made us think 10 times over, 'What the hell is going on in the system?'" Ansari says. "It's really a puzzle."

He, Fauci, and other AIDS researchers became interested in $\alpha 4\beta 7$ because it is found on the surface of CD4 cells, the immune cells that are the main target of HIV. The protein helps CD4 cells home in on the gut, where they gather in large numbers. Unfortunately, $\alpha 4\beta 7$ can also bind to HIV's surface protein, which makes CD4 cells far more susceptible to infection and explains why the virus destroys those cells in the gut early in an infection. Ansari and Fauci were also tantalized by results from an earlier monkey study they conducted, which showed that the $\alpha 4\beta 7$ antibody could thwart infection with SIV. They proposed a straightforward mechanism for the protection: The antibody reduced the CD4 cells' tendency to home in on the gut, providing fewer targets for any AIDS virus there.

Weirdly, the monkeys in the new experiment had higher levels of $\alpha 4\beta 7$ -studded CD4 cells in their guts. And a novel positron emission tomography/computerized tomography scan that can show tagged viruses revealed that the animals treated with the anti- $\alpha 4\beta 7$ had higher levels of SIV than the control animals in some parts of the body, such as the small intestine. The treated monkeys did show signs



This SIV-infected monkey shows far less virus (red-yellow) after treatment with an antibody to $\alpha 4\beta 7$ (bottom).

of immune responses that might have helped them control SIV, but none was particularly strong.

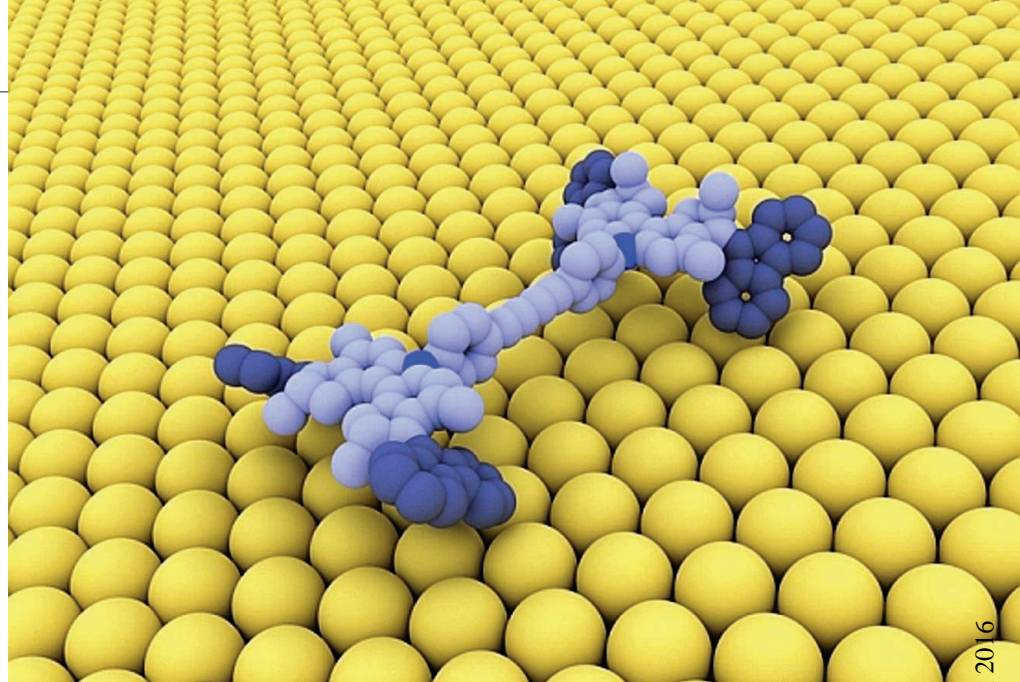
"Everything they expected to happen didn't happen, but what did happen was interesting," says Steven Deeks, a clinician who conducts HIV cure studies at the University of California, San Francisco. "The immune system is unknowable, dynamic, complicated, and it always surprises you."

Despite the lack of a clear-cut mechanism, immunologist Rafick-Pierre Sékaly at Case Western Reserve University in Cleveland, Ohio, predicts the apparent success will trigger a bevy of new studies. "That paper is going to orient the research in a completely new direction," he says. Sharon Lewin, a leading HIV cure researcher at the Peter Doherty Institute for Infection and Immunity in Melbourne, Australia, says the work "has very convincing data" and that it's "a really impressive finding." But Lewin adds a word of caution echoed by many, including the study authors: "Whether it's a quirk of the monkey model, we don't know," she says.

It's also possible that anti- $\alpha 4\beta 7$ worked because the experimental design tipped the scales toward success in a way that doesn't reflect a typical HIV infection. For one thing, Ansari and Fauci's team started the monkeys on ARVs 5 weeks after infection, which is far earlier than most people start treatment. Louis Picker, an immunologist who develops AIDS vaccines at Oregon Health & Science University, Beaverton, also wonders whether the SIV used might have been weakened, as his own experiments with the same strain have produced far higher peak levels of virus in the blood of untreated animals.

Picker suspects some undefined immune response explains the viral control. "What this experiment appears to be doing is nudging the viral/immune balance to the host rather than the virus," he says. "I suspect if you took an antibody to CD4 and did the same experiment you'd see the same thing."

But Picker allows that no other group has yet published similar results. And perhaps most important, unlike the CD4 monoclonal antibody, the one against $\alpha 4\beta 7$ has a human version, vedolizumab, already approved for clinical use. Indeed, NIAID began studies of it in HIV-infected people 3 weeks ago. The trial, which hopes to enroll 20 people, is mainly a safety assessment, but participants will go off ARVs, and then the researchers will closely monitor them to see whether their HIV levels rise or remain suppressed. "We're going to find out very soon whether this is all a bunch of nonsense or actually works," Fauci says. ■



NANOTECHNOLOGY

Chemistry Nobel heralds age of molecular machines

Primitive parts have evolved into more useful devices that pump, drill, move, and assemble other molecules

By Robert F. Service

The automated textile loom, patented in 1785, helped launch the Industrial Revolution. But early specimens were finicky and fussy handmade contraptions. Gears, rollers, and yarn shuttles regularly broke down, and inventor

Edmund Cartwright never made any money. Yet 40 years later, fully automated, steam-powered looms were the norm, and the world never looked back.

That developmental arc could now be happening for molecular machines. Last week, the 2016 Nobel Prize in Chemistry went to a trio of researchers who in the 1980s and '90s painstakingly created the first simple devices out of molecular rings and rods: Jean-Pierre Sauvage of the University of Strasbourg in France, Fraser Stoddart of Northwestern University in Evanston, Illinois, and Bernard Feringa of the University of Groningen in the Netherlands. Today, more than 3 decades later, the components they devised are giving birth to mechanisms with potentially useful abilities: pumping, drilling, transporting, and assembling other molecules. "I think we will see this nascent field take off with applications over the next

several years," says R. Dean Astumian, a physicist at the University of Maine, Orono.

In 1983, Sauvage started things off by using a copper ion to knit together two interlocking rings of organic compounds. He later figured out how to inject ions to chemically trigger the rotation of one ring as it passed through the other. Though that simple motion

didn't do anything useful, the efficiency of the reactions enticed other researchers. Stoddart followed that up nearly a decade later by looping an electron-deficient molecular ring around a dumbbell-shaped molecule with electron-rich patches at either end, to which the ring would stick. He then added heat to flip

the ring back and forth between the ends: a rudimentary shuttlecock. Feringa upped the complexity another notch in 1999 when he created a rotary motor capable of using light to spin a pair of molecular paddles.

Like Cartwright's loom, these primitive molecular machines were quirky, difficult to control, and wholly impractical. But today's molecular machines work better and accomplish much more. Since developing the original paddle wheel motor, Feringa's team has developed dozens more that, for example, move water droplets and control

CHEMISTRY NOBEL

"... for the design and synthesis of molecular machines."

Jean-Pierre Sauvage
Fraser Stoddart
Bernard Feringa

Artist's impression of an electrically powered nanocar on a copper surface.

chemical reactions. In 2011, he and his colleagues attached four motors to the corners of a chassis, creating a molecular car able to drive across a surface. Next spring, six teams are scheduled to race their electrically powered molecular cars across a gold surface in the first-ever NanoCar Race in Toulouse, France.

Other researchers are dreaming up new uses for molecular motors. Last month, for example, Jim Tour, a chemist at Rice University in Houston, Texas, reported preliminary work at a meeting that he and his colleagues had modified a motor to act as a molecular drill bit able to target cancer cells. Attached to the drill are small protein fragments, called peptides, which home in on cell surface receptors specific to cancer cells, bringing the drill into position. When let loose in cell culture media, the machine drilled holes in the cell membranes. Down the road, Tour hopes to use the approach not only to tear apart cancer cells, but also to create openings in other diseased cells for inserting gene therapy drugs or other medicines.

Stoddart's original shuttlecock has spawned a set of switchlike devices that respond to light or heat. In 2007, he teamed up with Jim Heath, a chemist at the California Institute of Technology in Pasadena, and others to assemble millions of switches into a molecular memory device. The devices were fragile, lasting only a hundred switching cycles or so, Heath says. Since then, Stoddart and his Northwestern colleagues have packed their switches inside porous crystals to make these memories more durable. Eventually, Stoddart says, assemblies of nanoswitches could form the basis for molecular scale sensors, and possibly even computers.

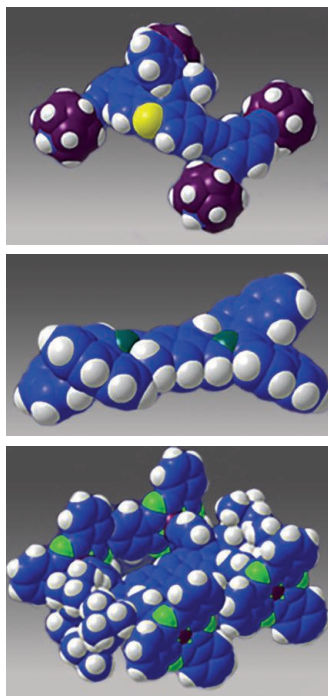
Not all ideas are so Silicon Valley. At the University of Manchester in the United Kingdom, researchers led by chemist David Leigh are taking an approach that would have been at home in his city's 19th century mills. In 2010, Leigh reported that he

and his colleagues made a small molecule that walks down a molecular track—a miniature railroad—much as biological motor proteins called kinesins haul cargo across cells by walking along scaffolds known as microtubules. Last year, his team made another device evoking heavy industry: a sort of robotic arm capable of lifting a small hydrocarbon, swinging it around, and dropping it a couple of nanometers away. Combining the two machines could make a molecular assembly line.

Biology is providing other inspiration. During photosynthesis, plants use proteins driven by the sun's energy to pump ions against a chemical gradient, storing energy that other proteins harness to synthesize sugars needed for the plant to grow. Researchers can't accomplish anything so sophisticated yet. But last year, Stoddart and his colleagues reported creating a simple molecular pump that uses chemical energy to squeeze molecular rings onto a rod, in effect storing energy. And in 2013, Leigh's group imitated a ribosome, the cellular organelle that builds proteins, by triggering a molecule to march down a molecular rod, pick up three amino acids and link them together. That's not anything macro-scale machines can't do already. But it may spur other molecular-scale chemical synthesizers.

For now, these chemists struggle with powering, controlling, and even imaging their devices. When it comes to nanomachines, molecular biologists have it easier: They can edit genomes to code for novel protein-based pumps and motors, then rely on cells to actually build them. But the new molecular machines that the chemists are devising have the potential to operate efficiently in harsh environments, without the need to keep organisms alive.

Molecular machines haven't exploded into a new industrial revolution just yet. Tour says the revolution will come in time, and could be even more far-reaching than that of the 19th century. "In 100 to 200 years, I think we will fabricate everything from the bottom up" using molecular machines, he says. ■



Six teams are set to drive molecular cars across a gold surface next year at the NanoCar Race.

POLAR SCIENCE

Joint research push targets fast-melting Antarctic ice

U.K.-U.S. "Thwaites invasion" aims to refine sea-level rise estimates

By Paul Voosen, in Sterling, Virginia

If there's one question that scientists working on the West Antarctic Ice Sheet hear from their friends and families, it's this: "How fast is the sea going to rise?"

The ice sheet is one of the biggest wild cards in sea-level projections for the next century, threatening up to several meters of rise. It was once expected to be stable for centuries, but satellite and airplane observations have shown that parts of the sheet are thinning and could become unstable. When that might happen is uncertain, with estimates ranging from as soon as the next few decades to the next few centuries.

In a bid to refine these estimates, this month the National Science Foundation (NSF) and the United Kingdom's Natural Environment Research Council will announce a project to support coordinated fieldwork on the Thwaites Glacier, a remote, Oklahoma-sized expanse of ice that is emerging as the epicenter of melt on the West Antarctic Ice Sheet. Although NSF declined to disclose exact figures, the initiative will likely provide tens of millions of dollars for Antarctic research and infrastructure over 5 years.

The "Thwaites invasion" will be "the biggest thing to happen in our area of science for quite a long time," said David Vaughan, director of science at the British Antarctic Survey in Cambridge at an annual interdisciplinary workshop for West Antarctic scientists held last week in Virginia. The initiative aims to feed data directly into the sea-level forecasts produced by the Intergovernmental Panel on Climate Change. "We want real outcomes that improve projections," he said.

Several recent studies have found evidence of ice retreat and thinning at Thwaites and other West Antarctic glaciers draining into the Amundsen Sea. Thwaites is a textbook example of why the health of such glaciers concerns scientists. It has a

wide front on the ocean's edge and sits on ground below sea level, where warming waters can slowly melt its base. For now, this deep water is held back by a submerged ridge, but on the landward side the bedrock slopes down into a basin of uncertain topography and slipperiness. Once water surmounts this grounding line, it could trigger a slow but irreversible collapse of the ice sheet. If the entire West Antarctic Ice Sheet melts over many centuries, it would raise sea levels by 3.3 meters, inundating cities. The rise would be 30% worse for the coastal United States thanks to a decline in Antarctica's gravitational pull.

Thwaites seems to be thinning faster than neighboring glaciers, adding to concerns. But from the evidence coming from satellites, airplanes, and models, it remains difficult to say for sure whether the melting at Thwaites represents a true tipping point for the planet or how fast it might happen.

Those alarming studies “set the tone for the [past] 2 years,” said Ted Scambos, a scientist at the U.S. National Snow and Ice Data Center in Boulder, Colorado, who helped devise the initiative. At a series of meetings, U.K. and U.S. scientists realized they were both focusing on Thwaites. Given tight budgets, a joint, targeted campaign made sense. “We already know what the right things to do are,” Scambos said. They just have to do them.

Many measures are needed to improve projections, including a clear picture of the land hidden beneath Thwaites: Is it smooth and slippery, or rough enough to hold the sheet in place? Another vital question is the stability of ocean-facing ice cliffs as they grow in height during glacial retreat: At what height do they fail? To answer such questions, the initiative will support a mix

of fieldwork on the ice sheet and in the surrounding sea. Projects could include new automatic weather stations, sub-ice shelf moorings, robotic submersibles, shallow ice cores, and radar and seismic surveys of the bedrock. The project will also finance modeling, paleoclimate reconstruction, and research on glaciers deemed directly relevant to Thwaites. It will support 5-year missions, beginning next October, with the primary field seasons expected between fall 2019 and spring 2021.

Thwaites is far from any U.S. station, and about as remote from existing infrastructure as one can get in Antarctica. Working there is “at the limit of people's comfort level,” says Chris Shuman, an Arctic scientist at NASA Goddard Space Flight Center in Greenbelt, Maryland. It has a rugged surface and harsh weather. To make these campaigns happen, Vaughan said at the meeting, “we are committing a huge amount of our logistics resources.”

Although NSF will continue to support investigator-driven research in Antarctica, this campaign will unavoidably ding the financing for other projects, Eric Saltzman, head of NSF's Antarctic science program in Arlington, Virginia, told the meeting. “Will it have an impact? Yes.” U.K. polar research will likely feel a similar strain.

Despite the sacrifices, the approach seems “sensible,” says Martin Siegert, a polar scientist at Imperial College London who has worked on the East Antarctic Ice Sheet. Thwaites surely holds universal lessons, he notes. At the meeting, Robin Bell, an Antarctic scientist at Columbia University, added that she and her colleagues have a responsibility to the public to provide answers about the fate of West Antarctica. “This is a moral and social imperative.” ■

INDUSTRIAL ESPIONAGE

Chinese scientist jailed over theft of hybrid corn

Investigators used secret terrorism warrant to gather evidence and unravel plot

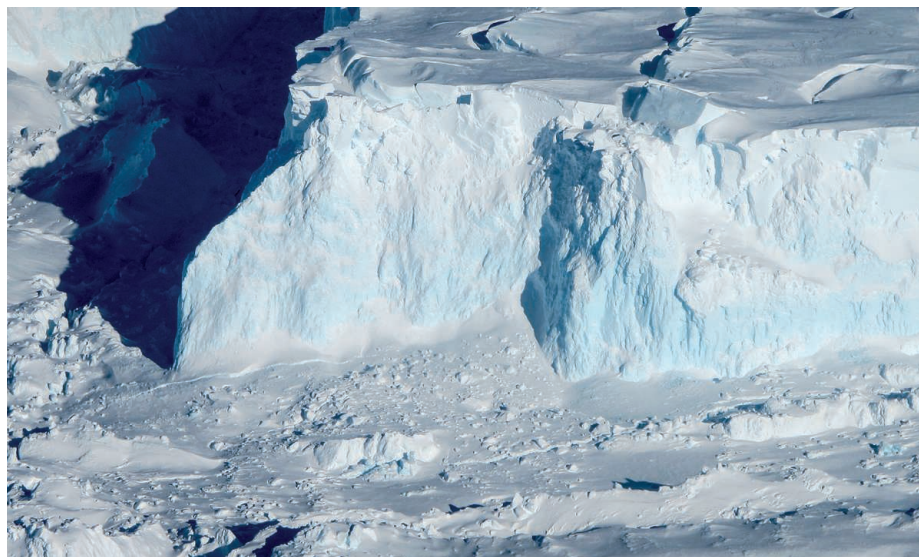
By Mara Hvistendahl, in Des Moines

“I have destroyed everything that I wanted,” said Mo Hailong, sobbing with remorse here in U.S. District Court on 5 October. “My reputation, my job security, my family's respect. My heart is broken because I know that I am to blame.” An engineer by training, Mo had earlier pleaded guilty to having participated in an elaborate plot to steal proprietary hybrid corn seed and transport it to China, where scientists could presumably analyze and reconstruct its traits. After his searing statement and plea for mercy last week, Mo was sentenced to 36 months in prison.

The U.S. Department of Justice of late has aggressively pursued charges of industrial espionage against Chinese scientists. Several high-profile cases have unraveled, including one involving the chair of Temple University's physics department (*Science*, 13 November 2015, p. 732). This time, the charges stuck. “The theft of agricultural trade secrets, and other intellectual property, poses a grave threat to our national economic security,” U.S. Attorney Kevin E. VanderSchel for the Southern District of Iowa here said on 5 October.

The case, which began in 2011 when Mo was discovered on his knees in a remote test field in Tama County in Iowa, led to the indictment of Mo and five co-defendants in December 2013, for what the U.S. government alleged was a highly orchestrated conspiracy to steal the germplasm, or genetic makeup, of DuPont Pioneer and Monsanto corn seed. The companies and the U.S. Attorney's office declined in court filings to release details about the seed varieties in question, citing the need to protect trade secrets. New hybrid seeds are so closely guarded that even the farmers who manage test fields aren't given many details about the varieties they are growing.

The government claimed that Mo, as director of international business for Beijing



Antarctica's Thwaites Glacier is shattering and thinning at its margin. But its future is uncertain.



Corn dries on the ground in China's Shandong province. A Chinese scientist was sentenced to prison last week for his role in a plot to spirit stolen corn seed to China.

Dabeinong Technology Group, or DBN, a leading Chinese agricultural firm, was enlisted in a scheme to swipe whole ears of corn as well as spring seedlings and transport them to China.

DBN was apparently looking for a shortcut to producing new, high-yielding varieties. Government restrictions on selling foreign seed mean China lags behind the United States in seed technology, says Carl Pray, an agriculture expert at Rutgers University, New Brunswick, in New Jersey. Companies have to develop their own varieties, an effort that, if done right, has “about a 10-year pipeline,” says David Miller, director of research for the Iowa Farm Bureau Federation here. By “stealing [seed] in year 9 of the research,” he says, a company could sidestep significant groundwork.

China has a pressing need for high-yielding corn. Most corn in China is fed to pigs, chickens, and cows, and as the Chinese improve their standard of living and eat more meat, corn has supplanted rice as China's leading crop. But the U.S. Department of Agriculture forecasts Chinese corn yield for 2016–17 at 6 metric tons per hectare, compared with nearly 11 metric tons per hectare for the United States. That's because of a combination of poor agronomy practices and inferior seed lines, Miller says.

The alleged kingpin of DBN's scheme to rapidly close that yield gap was Li Shaoming, the head of DBN subsidiary Beijing Kings Nower Seed. According to court proceedings, Mo, a 47-year-old U.S. permanent resident with a Ph.D. in mechanical engineering from Kansas State University in Manhattan who has taught at several universities in Florida, took directions from Li and DBN's founder,

Shao Genhuo, who is Mo's brother-in-law. “There is no evidence that [Mo] was either the decision-maker or the organizer of what occurred in the United States,” stated U.S. District Judge Stephanie Rose here in Des Moines. Charges are still pending against Li and four other defendants, who are overseas and have not been apprehended. The case against Mo's sister, Mo Yun—the wife of DBN Founder Shao and the company's head of research—was dropped in 2015 after a judge ruled out critical evidence.

When a DuPont Pioneer manager caught Mo in the test field, according to an affidavit submitted by Federal Bureau of Investigation (FBI) agent Kevin Kohler, Mo claimed that he worked for the University of Iowa and was on his way to a

“The theft of agricultural trade secrets, and other intellectual property, poses a grave threat to our national economic security.”

Kevin E. VanderSchel, U.S. attorney

conference. Suspicious, the manager took down Mo's license plate number. The seed grown in the test field was a “highly anticipated” variety—no other details about it were made public—that DuPont Pioneer planned to bring to market within 2 to 3 years, Kohler wrote.

FBI agents spent months collecting evidence implicating Mo and his co-defendants by installing GPS tracking devices on their

rental cars, bugging the vehicles' interiors, and even flying drones overhead. They did so using a warrant intended for monitoring terrorists and foreign government agents, which investigators obtained under the Foreign Intelligence Surveillance Act. In a court filing, Mo's attorneys called the warrant a “breathtaking and unprecedented expansion” of the government's use of the act. Judge Rose disagreed, however, allowing evidence collected under the warrant.

In January, Mo pleaded guilty to one count of conspiracy to steal trade secrets. The crime carries a maximum of 10 years in prison and a \$250,000 fine, but as a condition of his plea agreement, Judge Rose agreed to limit prison time to 5 years. She reduced his sentence to 36 months in the hearing last week because Mo is in remission from synovial sarcoma, a rare cancer. “Mo appreciates the certainty that the sentencing hearing brings and the ability to begin putting this matter behind him and his family,” defense attorney Mark Weinhardt of Weinhardt & Logan here wrote in a statement emailed to *Science*.

Meanwhile, Chinese firms are making more legitimate inroads into agricultural R&D beyond its borders. Last February, for instance, China National Chemical Corporation announced a planned \$43 billion takeover of Swiss seed company Syngenta. Two months later, Bill Niebur, a former general manager for DuPont Pioneer who oversaw the company's Asia operations, was appointed CEO of the Chinese seed company Origin Agritech. As Mo sat in court awaiting his sentence, Origin Agritech quietly opened its first branch outside China—here in Des Moines. ■

BITING BACK





By Martin Enserink and Leslie Roberts

Most people would not shed a tear if mosquitoes disappeared from the planet. At best, the bloodsucking critters are a nuisance; at worst, as events such as this year's massive Zika epidemic in Latin America have shown, they spread devastating diseases far and wide. But for now, the best we can do is beat back the threat. That's because the weapons we have developed—including insecticides, window screens and bed nets, repellents, and plain old swatting—are far from perfect.

The mosquito that infects untold millions with malaria every year—*Anopheles gambiae*, pictured on these pages—is developing resistance to pyrethroids, a class of insecticides developed decades ago. No alternatives have come online for years, in part because the compounds don't promise big profits for companies. Scientists are busy working on long-overdue replacements; meanwhile, they are devising ways to use pyrethroids more efficiently while they last. Others hope to turn African homes into clever mosquito traps using humans as bait.

Insecticides have never worked very well against *Aedes aegypti*, the species on the cover of this issue, which transmits not just Zika, but also dengue, chikungunya, and yellow fever. Some scientists hope to fight it by releasing billions of designer mosquitoes. They would carry either a lethal gene that can cause populations to crash, or a helpful bacterium that protects mosquitoes from viral invaders. Brazil, which has suffered more from Zika than any other country, is a testing ground for both strategies. The battle continues.

<http://science.sciencemag.org/>




PHOTO: © ALEX WILD

WINGED WARRIORS

Brazil plans to release billions of designer mosquitoes to stop the spread of infectious diseases. Will it work?

By Kelly Servick, in Brazil

Every Saturday morning, Maria do Carmo Tunussi goes door to door asking her neighbors to scour their houses and yards for flowerpots, buckets, clogged gutters—anything that could collect water and offer mosquitoes a place to breed. For 17 years, Tunussi has been a community health agent at the local clinic in CECAP/Eldorado, a district of about 5000 people in the small city of Piracicaba, 2 hours northwest of São Paulo, Brazil. She has seen many surges of the mosquito-borne dengue virus, which causes fever, nausea, and agonizing joint pain. The task sometimes feels futile. “You remove the breeding site one day, and the next day, it’s back,” she says. “It never ends.”

Last April, CECAP became the first neighborhood in Piracicaba to try something new—a mosquito control tool that Tunussi believes not only stamped out dengue, but kept the Zika virus from taking hold. That tool is OX513A—a strain of transgenic *Aedes aegypti* mosquitoes designed to reduce the population by passing a lethal gene to their offspring.

In Florida, a planned release by Oxitec, the company behind the insects, is mired in public resistance. But here in Piracicaba, few residents seem to bat an eye at the little clouds of mosquitoes spilling out the window of the Oxitec van on its slow morning route.

That may be because dengue is so common here. The virus sickened about a million and a half people in Brazil last year, and more than 1600 in Piracicaba between July 2015 and July 2016. Panic over the spread of the Zika virus has only amplified interest in solutions beyond pesticides, which aren’t all

that effective against *A. aegypti*, and breeding site removal, which, despite Tunussi’s efforts, is hard to keep up year after year. So it’s not surprising that, 7 years after releasing the world’s first genetically modified (GM) mosquito, Oxitec has chosen Brazil as the site of a major scale-up. It is moving from small-scale pilot projects like the one in CECAP to planned releases covering tens of thousands of people.

Indeed, Brazil is becoming a proving ground for tailored mosquitoes. About 600 kilometers to the east, in the coastal cities of Niterói and Rio de Janeiro, another lab strain of mosquitoes is on the wing. Bred by a nonprofit organization called Eliminate Dengue, this one is infected with a bacterium called *Wolbachia pipientis* that protects it from infection with dengue, Zika, and a third virus named chikungunya.

Most scientists are confident that both mosquito strains are safe for humans and the environment. But the two projects are radically different in both their scientific approaches and their funding models. Whether either one can actually reduce rates of mosquito-borne disease is still an open question. And if either proves effective, Brazil and many other developing countries will face one more question: Does buying and releasing billions of mosquitoes make economic sense?

OXITEC’S BRAZILIAN headquarters, in the industrial city of Campinas, stinks of the soggy fish food used to feed mosquito larvae. Here, the company can usher about 4 million mosquitoes a week through their life cycles: from an ashy powder of eggs to writhing gray strands of larvae, then dense black pupae the size of rice grains, and, finally, flying adults



Oxitec's transgenic mosquitoes swarm out of a container in Piracicaba, Brazil.

bouncing around in plastic tubs the size of take-out containers.

They are roughly the 200th generation of descendants from a single mosquito created 14 years ago in a University of Oxford lab in the United Kingdom, where geneticist Luke Alphey and his team inserted a new gene into insect embryos. It codes for a protein known as a transcriptional activator, which drives the expression of other genes by binding to DNA and certain proteins involved in transcription. But the gene Oxitec uses, known as *tTAV* (tetracycline-repressible transcriptional activator variant) is designed to drive the expression of even more *tTAV* in what becomes a fatal feedback loop.

How the process kills mosquitoes isn’t entirely clear; the excess *tTAV* protein may tie up the cell’s protein production machinery. “It basically causes genetic havoc, and the organism dies,” says Al Handler, an insect geneticist at the U.S. Department of Agriculture in Gainesville, Florida.



Oxitec mosquitoes bearing the lethal gene grow up feeding on tetracycline, an antibiotic that blocks *tTAV* activity and keeps them alive. Males, which don't bite humans, are released in towns and cities, where they mate with wild females. Their offspring quickly accumulate the lethal protein, and the vast majority die before maturing.

Alphey focused on *A. aegypti* in part because it's the principal transmitter of dengue, a major global health problem. Malaria, although a greater burden, is carried by multiple *Anopheles* species, making genetic control more difficult. *Aedes* is also easier to rear, exists at low population densities that seemed easier to cut down, and, compared with other mosquitoes, is harder to control with measures such as bed nets, Alphey says.

Picking *Aedes* also made business sense. It is prevalent in middle-income countries like Brazil that could potentially afford to evaluate and regulate the new product—and, eventually, to buy it. Alphey spun out a

company in 2002, backed by private venture capital firms and Oxford. Last year, the U.S. synthetic biology behemoth Intrexon Corporation purchased Oxitec for \$160 million.

Oxitec has built up scientific evidence—and a business case—through field trials in countries where regulators were friendly to experimental releases. The first, in the Cayman Islands in 2009, was largely unknown to the world until Oxitec shared results, and it stirred criticism that the company had rushed a GM organism into the field without properly consulting the public (*Science*, 19 November 2010, p. 1030). But the results were encouraging: Oxitec reported roughly a 96% reduction in the mosquito population in the tiny 0.16-square-kilometer release area.

Oxitec also did field tests in Panama and Malaysia, and it put down roots in Brazil through an academic collaboration with the University of São Paulo and the nonprofit research facility Moscamed. Between 2011 and 2013, the team released Oxitec mosquitoes

in three neighborhoods in the northeastern state of Bahia. It reported at least 90% population reductions in all three.

But the collaboration was rocky. Oxitec provided the mosquitoes and its expertise, but funding for releases and data collection came primarily from Bahia, and collaborators clashed over how involved the company should be in the research. An independent evaluation of the product would have been more valuable, says Margareth Capurro, a University of São Paulo, São Paulo, biochemist who co-led the project. “We [fought] for a year because they wanted to be first and last authors.” Andrew McKemey, Oxitec's head of field operations in Abingdon, U.K., says company scientists were rightfully included in the papers they helped produce.

The Bahia results helped Oxitec win approval from Brazil's National Technical Commission for Biosecurity to release mosquitoes commercially. They also impressed Pedro Mello, Piracicaba's health secretary. Mello's

quitoes actually reduce disease? “The goal here is not to kill mosquitoes. It’s to prevent people from getting infected and sick and dying,” says Thomas Scott, an epidemiologist and insect ecologist at the University of California, Davis. So far there’s no proof that either approach does that. It may seem intuitive that fewer infectious mosquitoes mean fewer infections, but just a few *A. aegypti* may be enough to transmit disease through a susceptible population, Scott says.

In July, Oxitec published numbers showing that dengue cases in CECAP dropped 91% over the previous year—from 133 to 12. The rest of the municipality saw only a 52% reduction. But Scott notes that dengue outbreaks are episodic: “You can have an epidemic in one town and no transmission in the one next door, and the next year, it can be flipped.”

The last word on efficacy would come from trials that monitor disease in residents of neighborhoods randomized to receive mosquitoes or act as controls. These two groups are inherently leaky, because people are mobile; that means such studies have to be large—and costly—to be meaningful. In March, a World Health Organization working group chaired by Scott deemed both Oxitec’s and Eliminate Dengue’s strategies worthy of “carefully planned pilot development” but called for large epidemiological studies.

Eliminate Dengue already has an efficacy study underway in Yogyakarta, Indonesia, which will track disease rates in 24 areas of about 14,500 people each, half of which will receive *Wolbachia* mosquitoes. A network of clinics across the city is testing continuously for dengue over 2 years. An even larger study is being planned in Vietnam. Oxitec, meanwhile, is enlisting independent experts to design a trial tentatively slated for 2018.

Over the long term, both kinds of modified mosquito could lose their edge, because evolutionary pressure could select for resistance to either Oxitec’s lethal gene or *Wolbachia*’s virus-fighting powers.

EVEN IF EITHER TYPE of mosquito—or both—proves a success, there’s still the issue of the cost. Not every community in Brazil will likely be able to afford mosquitoes, which raises new questions, says Fred Gould, an insect geneticist at North Carolina State University in Raleigh. “There’s a whole issue of justice: Who gets these mosquitoes and who doesn’t? Who gets Zika and who doesn’t?”

The Fiocruz facility makes about 40,000 *Wolbachia*-infected mosquitoes a week to supply roughly 300 release containers, but a new facility will have a capacity of about 12 million a week. Eliminate Dengue was not able to provide an estimate of current costs in Brazil, but aims to bring them down to

\$1 per person or less.

Oxitec’s mosquitoes are currently more expensive. The Piracicaba expansion will cost the city roughly \$1.1 million over 2 years—some \$10 per person in the treated area—about half of which will come out of the existing mosquito control budget. Oxitec itself is paying even more than that, says Slade, but it’s too early to tell how much the mosquitoes will cost if they are reared on a much larger scale. “It’s only when you roll up your sleeves and build a factory that you know what your costs are.”

Oxitec’s plan to sell the mosquitoes before the epidemiological evidence is in troubles some scientists. “They’re good salesmen—that’s the bottom line,” says population geneticist Jeffrey Powell of Yale University. “They go out and they talk to the people

She, like a handful of other researchers, is betting on so-called gene drives, which bias the inheritance of a particular gene to quickly and irreversibly spread it through the population (*Science*, 27 November 2015, p. 1014). Capurro is working on a gene allowing mosquito cells to recognize an enzyme produced by the dengue virus and release a self-destruct signal.

Such strategies may be more difficult to get approved because they would make an entire wild population transgenic. Oxitec’s transgenic males and their offspring die within days, which has gone a long way to appease GM-wary regulators, says entomologist Zach Adelman of Texas A&M University, College Station.

In the long run, Adelman and Capurro envision a time when public health



Technicians separate male from female mosquito larvae in Oxitec’s Brazil production facility.

in various countries saying, ‘We’ve got this magic bullet.’” And the need for continuous mosquito releases is a serious economic downside, adds molecular entomologist Marcelo Jacobs-Lorena of Johns Hopkins University in Baltimore, Maryland. “It is a forever proposal,” he says. “That may be good for the company, but maybe not so good for the overall control efforts.”

For Slade, the dramatic population reductions already show that Oxitec’s approach works far better than pesticides, which are also a “forever proposal.” “I personally don’t accept that without [an epidemiology study], we don’t have the evidence that this is the best tool,” he says.

EVENTUALLY, other alternatives will hatch. In Margareth Capurro’s São Paulo lab, larvae from new transgenic strains line the shelves.

departments can shop for a strain of disease-fighting mosquito that makes the most sense for them. Some may want an inexpensive option that doesn’t require indefinite releases, for instance, whereas residents in some areas may be uncomfortable with biting females. Some may want to combine approaches—knocking the population down before introducing a new gene. “You’ll have a market rather than one game in town,” Adelman says.

Piracicaba does not want to wait for that market—or even for more definitive evidence that Oxitec’s mosquitoes work. Being the first city in Brazil to pay for an experimental disease-fighting mosquito was a calculated risk, Mello says. “Everything you do in the public sector has risks,” he says. “But I still think the biggest risk is to let people die without giving them any kind of alternatives.” ■



"Everything in my life
involves mosquitoes,"
Bart Knols says.
"They're my passion."

THE ELIMINATOR

In humankind's war against insect-borne disease, Dutch entomologist Bart Knols is one of the most creative warriors

By Kai Kupferschmidt

There is only a faint glimmer of blue light on the stage, barely illuminating the man who just sat up in bed. A mosquito can be heard buzzing about, then a slap. “Gotcha,” the man says. As the lights go up, he points to a blood fleck in the palm of his right hand. The location is Maastricht, the Netherlands, and the man is Dutch entomologist Bart Knols. Still in bed, he stares at the audience through his round glasses. “Mosquitoes. I hate them,” he says. “Don’t you?” Then Knols gets up, and, dressed in boxer shorts and a polo shirt, delivers a 10-minute talk entitled “Three new ways of killing mosquitoes.”

Knols has studied mosquitoes for a quarter-century. He seems to have come up with a new way of killing them every other year. In the 2012 TEDx Talk, he presented three ideas: simulating human odor to lure mosquitoes into traps; teaching dogs to recognize the smell of mosquito larvae, so they can sniff out breeding sites; and flooding human blood with a drug that kills mosquitoes when they bite.

Knols has since championed other schemes; using drones to spray insecticides, for instance, or letting a fungus kill mosquitoes. His latest plan, modifying African houses to become big mosquito traps, is now being tested in a huge, \$10 million trial. In humanity's war with mosquitoes, Knols is one of its most creative warriors.

And creativity is needed. Despite decades of research, mosquitoes are still the deadliest animals in the world, spreading diseases that sicken hundreds of millions of people annually and kill more than 600,000. Decades-old insecticides are still the most important weapon (see Feature, p. 171). “Where is the innovation?” Knols asks.

His obsession has led to an unusual career. Knols has won both the Ig Nobel Prize, a spoof award for unusual or trivial research results, and the prestigious Dutch Eijkman Medal for tropical medicine. He has an im-

pressive list of high-profile publications, but feels academic science doesn't nearly have enough impact. That's why in 2012 he left Wageningen University & Research (WUR) in the Netherlands to co-found a startup named In2Care, which sells human odor-baited mosquito traps. Knols is also the Dutch media's go-to guy for mosquito stories. He combines sometimes-dire predictions about the threat of mosquito-borne disease with what some call a knack for public engagement. Others call it a knack for self-promotion.

Many say Knols can be difficult to get along with, and he has a history of getting into tussles with collaborators. Just last month—after *Science* had interviewed him—Knols announced that his relationship with In2Care would soon end. “I think one of Bart's key strengths is his energy and commitment to make change and ultimately save lives,” says entomologist Matthew Thomas of Pennsylvania State University (Penn State), University Park, who leads the mosquito trap trial in Africa. “The downside is that his doggedness can ruffle feathers.”

KNOLS STARTED MAKING headlines early on. As a Ph.D. student at WUR, he and his colleague Ruurd de Jong tried to find out which human odors attract mosquitoes. “Man, we turned the lab into a smelly place,” Knols says. They lured mosquitoes with everything from pads worn under their armpits or in their groin area to used tampons. One day Knols put his worn socks on top of a cage. “These things went crazy for it,” he says. Feet often have a cheesy odor, so the next question seemed natural: Does cheese work as bait? As it happened, mosquitoes found cheese from Limburg, the southern province where Knols was born, particularly irresistible.

It was vintage Knols: quirky research with a serious core. “The bacteria that create the aroma of some of these smelly cheeses may actually originate from human skin, and therefore you may attract malaria mosqui-

toes with the aroma,” he says. When *Parasitology Today* published the study in 1996, Knols also penned a letter in *The Lancet*, bragging that medical entomologists were now taking cheese with them around the globe. “Whether or not they will manage to attract another mosquito species with Limburger cheese remains to be seen,” he wrote; “(if not, they can always eat it.)”

Journalists around the world loved it—as did the Ig Nobel jury—but the study's impact on the field was modest, some scientists say. “It's a nice story, but you wouldn't use cheese to catch mosquitoes,” says Janet Hemingway, an entomologist at the Liverpool School of Tropical Medicine (LSTM) in the United Kingdom. Today, scientists are still working on a good attractant for malaria mosquitoes, she notes. Knols says they are still testing blends based on his work with cheese.

After getting his Ph.D., Knols worked at the International Centre of Insect Physiology and Ecology (ICIPE) in Nairobi for 5 years, three of them leading the malaria program at a field station in Mbita Point, Kenya, on the shores of Lake Victoria. In 2003, he joined the International Atomic Energy Agency in Vienna, which has a long-running research program that uses radiation to create sterile insects, which can help reduce natural populations. He went back to WUR in 2006.

“Everything in my life involves mosquitoes. They're my passion,” Knols writes on his website. “I love to research them. But I prefer to eliminate them.” His torrent of proposals for doing so elicits mixed reactions. “He is adopting a bit of a shotgun approach,” says LSTM entomologist Philip McCall. “Maybe if he had fewer, refined weapons, he might press people more” to try them. But Andreas Rose, an entomologist at Biogents, a company in Regensburg, Germany, sees his prolific creativity as a strength, though he notes that Knols at times unwittingly adopts other people's ideas as well. “He's like a composer who maybe has heard a melody on the radio that

he then incorporates in his work,” Rose says.

Knols’s media presence has raised eyebrows among colleagues, and some find him too alarmist. He often warns about the threat of epidemics and exotic mosquitoes; when the Asian bush mosquito (*Aedes japonicus*) showed up in the Netherlands, for instance, Knols said it might be able to transmit Zika, and, if so, a major door-to-door eradication effort would be called for. “Sometimes we are watching with surprise how strongly he asserts things,” a spokesperson for the Dutch National Institute for Public Health and the Environment told the newspaper *NRC Handelsblad*.

KNOLS IS AN ADMIRER of Fred Soper, a legendary U.S. scientist at The Rockefeller Foundation who in the late 1930s helped Brazil get rid of a massive infestation of *Anopheles gambiae*, Africa’s main malaria vector. An authoritarian figure, Soper hired thousands of workers in a military-style campaign to fumigate buildings and treat breeding sites with a poison called Paris green. “Soper had the willpower, the passion, the energy and the leadership qualities necessary to carry out a campaign in such a large area,” Knols wrote in a 2009 book.

He is a force to be reckoned with himself. “He is uncompromising and he pushes a singular Knolsian view of the world,” McCall says. “His approach to getting traction is to really push ideas hard,” Thomas says—and sometimes the rhetoric gets ahead of the science. “His contribution is as an agent of change and someone who is trying to shake the system up.”

His stint at ICIPE ended in a dramatic fashion after he accused a fellow scientist of misconduct, a claim then-ICIPE Director-General Hans Herren dismissed. Herren says he fired Knols for insubordination and called in the police after Knols blocked the main entrance at Mbita Point, essentially trying to take control of the station. “It was a pity really, because Knols had great ideas. But you can only tackle malaria by working together,” Knols says Herren must be confused about the 14-year-old incident: “I never ever was involved in any protests or demonstrations,” he says. Both say they have since buried the hatchet.

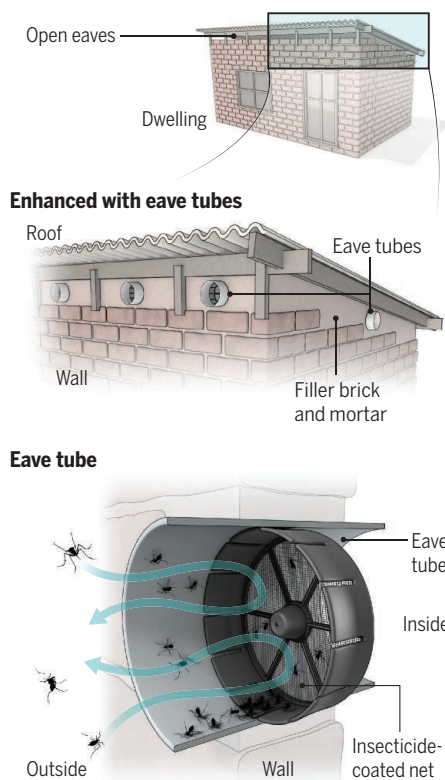
Irish entomologist Gerry Killeen resigned from ICIPE at the same time to protest Knols’s dismissal. “Am I always thrilled about the way Bart approaches myself or other people? No. But it doesn’t mean that he’s wrong,” he says. Killeen, now at the Ifakara Health Institute in Dar es Salaam, Tanzania, says Knols fostered a great atmosphere at Mbita Point. “People felt they were really doing something; that they could make a contribution, develop as

scientists, and compete globally.”

Knols’s most ambitious project so far brought both his talents and problems into sharp focus. In 2012, In2Care partnered with Biogents, Penn State, and others on an EU-funded project to develop a new way to kill mosquitoes. The partners met in Tanzania in February 2013 to discuss the project. “After looking at some houses, we just sat down in the shade of a mango tree and started brainstorming,” Rose recalls. One result was what’s now called the “eave tube.” African

Turning a house into a trap

A big study in Ivory Coast seeks to kill mosquitoes by bricking up the open space under the roofs of houses and installing eave tubes that have an insecticide-coated net on the inside.



houses often have open eaves, which mosquitoes use as an entryway. The idea was to brick off these openings and install a few polyvinyl chloride, or PVC, tubes, open to the outside to allow mosquitoes in; inside the house, the tubes are closed off by an electrostatic netting coated with an insecticide.

The concept unites several ideas. Instead of a chemical attractant, it uses the humans in the house as bait. The netting—originally developed to filter pollen out of the air—gives insecticide particles an electric charge, making them stick better to the insects. The idea is “brilliant,” Killeen says. “I wish I had thought of that.” In 2014, the first eave tubes were tested in houses in Tanzania. After

the EU project ended, the partners secured \$10 million from the Bill & Melinda Gates Foundation for a randomized controlled trial in Ivory Coast. In 20 villages, houses are being equipped with eave tubes, while villagers receive insecticide-treated bed nets; 20 other villages get only bed nets. The team will test blood samples from 50 to 60 kids per village for malaria every 2 weeks. Results should be in by 2019.

It would seem like the chance of a lifetime for Knols—an opportunity to see at least one plan all the way through a large trial. But his apparent conflict with In2Care has made further involvement unlikely. The company says Knols is no longer working for it, but its co-founders—including two younger entomologists trained at WUR—declined to answer questions. Knols himself says he will leave in the near future but provided no details. “I’m a man who is constantly on the search for new things, and I explore things,” he says. “And that is not always what other people like—let’s put it that way.”

IN HIS 2009 BOOK, Knols drew a sobering conclusion about his academic work until then. “I doubt whether the knowledge I added has saved the life of even one African child,” he said. Seven years later, he’s more optimistic: With the traps and the eave tube project, “I strongly feel that we have made contributions to public health improvement.”

But much more is possible, he says. The problem with today’s mosquito control is that it suffers from too much talking and increasingly relies on “community participation,” which is difficult to sustain, Knols wrote in his book; he scorned Aruba, where during a dengue outbreak schoolchildren were given a note asking their parents to remove mosquito breeding sites around the home. “Soper ... would have cleaned up this entire island of fewer than 200 square kilometers within a few months,” he lamented.

That’s why in 2010, he co-founded another company, Soper Strategies, which seeks to combine his hero’s approaches with modern technology to rid islands or entire countries of their mosquito populations in “meticulously planned elimination campaigns, executed with military precision and discipline,” as the website puts it. Candidate countries include Cape Verde, South Africa, and Saudi Arabia. Knols hoped to use Aruba to show that elimination Soper-style can work, but failed to secure the funding. Other clients have yet to come forward.

Knols believes it’s just a matter of time. In his book, he even wondered whether “one day soon, a new Soper will stand up.” It seemed clear who he had in mind. ■

With reporting by Martin Enserink.



To test insecticide efficacy, mosquitoes are exposed to strips of treated bed nets.

PICK YOUR POISON

As mosquitoes develop resistance to pyrethroid insecticides, researchers are forced to look for alternatives

By Kai Kupferschmidt

When Janet Hemingway started her career in mosquito research in 1977, a child was dying of malaria every 10 seconds. Yet the disease, and the mosquitoes that carry it, were low on the global health priority list.

Today, the landscape has

been transformed. Scientists at the prestigious Liverpool School of Tropical Medicine (LSTM) in the United Kingdom, which Hemingway now heads, and elsewhere have sequenced the genomes of at least 23 mosquito species, looking for clues that might help them conquer the disease. And malaria has surged to the top of the global agenda. Thanks to a bolus of new funds,

deaths have been halved. And halved again.

But one thing hasn't changed. The world still relies on the same class of insecticides, known as pyrethroids, as it did in 1977. Now, in part because of that neglect, these compounds may be nearing the end of their useful lives as mosquitoes develop resistance to them at alarming rates, and there is little in the pipeline to replace



A fogging machine is tested at Jones Beach in New York in 1945. Mass spraying of DDT led mosquitoes to develop resistance.

them. “If we don’t do something about this very quickly, we have a public health catastrophe on our hands,” Hemingway says.

Pyrethroids have played an outsize role in the global fight against malaria in the last decades. They are the main compounds used to spray the inside walls of homes—so-called indoor residual spraying, or IRS—to kill the *Anopheles* mosquitoes that transmit the disease. And they are the only insecticides that can be used on bed nets. Much of the global success in fighting malaria has come from these two interventions. In a *Nature* paper last year, a group led by Simon Hay at the University of Oxford in the United Kingdom estimated that between 2000 and 2015, some 633 million malaria deaths were averted, with 68% of that decline due to insecticide-treated bed nets and 10% to IRS. (Treating people with antimalarial drugs accounted for the remaining 22%.) Pyrethroids have also played a role in the fight against *Aedes aegypti*, the main mosquito transmitting the yellow fever, dengue, and Zika viruses, even though bed nets are less effective against *A. aegypti* because it predominantly bites people outdoors and during the day.

Pyrethroids have several distinct advantages: They kill mosquitoes efficiently, act rapidly, and, although toxic, are safer for humans than the alternatives. But when the massive rollout of insecticide-treated

bed nets began in Africa in the early 2000s—more than a billion have been distributed—little thought was given to resistance, says Maureen Coetzee, director of the Wits Research Institute for Malaria at the University of the Witwatersrand in Johannesburg, South Africa. “Nobody dreamt that insecticide resistance would spread the way it has spread throughout Africa.”

Scientists shouldn’t have been surprised, however. An earlier insecticide, DDT, played a major role in driving down malaria cases starting in the 1940s. But in many places, resistance reversed those gains. In Sri Lanka, for instance, malaria was all but wiped out with the help of DDT, but by the end of the 1960s, when resistance was widespread, cases surged to more than half a million a year. By that time, Rachel Carson had highlighted the toxic effects of DDT in *Silent Spring*, and many nations banned its use.

Nor has there been much incentive for companies to develop new mosquito-killing insecticides, which could be used in tandem with existing ones to slow the development of resistance. Most R&D has focused on agricultural chemicals, a far more lucrative market. “No publicly traded company is going to spend the money required to discover and develop and take to the market an insecticide for public health,” says Nick Hamon, who heads the Innovative Vector Control Consortium

(IVCC) in Liverpool. “These companies are looking for \$100 million in sales every year to have any chance of recouping the money for a new compound.”

First detected in Ivory Coast in 1993, resistance to pyrethroids was relatively rare until about 10 years ago, when it began racing across the continent (see map, p. 173). “Some countries are seeing an increase in malaria transmission, and resistance is one of the probable causes,” Coetzee says. It’s hard to be sure, she says, because drug shortages or cutbacks of control programs may also be taking a toll. But Hilary Ranson of LSTM thinks the problem is real and will only get worse. “I think insecticide resistance is a time bomb.”

Many scientists have their hopes pinned on new approaches to vector control that would be less likely to run into resistance or prove toxic, such as mosquitoes genetically modified to die young, traps that lure the insects to their death, or insecticidal bacteria or fungi (see Features, pp. 164 and 168). “We need to diversify in terms of the kind of tools that we use to control mosquitoes and not focus it entirely on chemical control,” says Willem Takken, a medical entomologist at Wageningen University & Research in the Netherlands. But Hemingway and other scientists caution that even if these new tools prove their mettle, they are years away at best. The first priority, Hemingway says, is to preserve and im-

prove the tools we know work. And to her, that means insecticides.

That's why, in 2005, Hemingway started IVCC, a public-private partnership that aims to develop entirely new classes of insecticides and get them on the market in 5 to 8 years. Since IVCC's inception, the Bill & Melinda Gates Foundation has kicked in more than \$200 million, and the U.S. Agency for International Development, the Wellcome Trust, and others have each contributed millions. In the meantime, IVCC is scrambling to help scientists find smarter ways to use existing insecticides or combine them with other interventions in a way that keeps resistance at bay.

With IRS, one option is to switch to an insecticide from one of the other available classes: organochlorides, carbamates, and organophosphates. South Africa went back to using DDT, an organochloride, after an epidemic of malaria transmitted by pyrethroid-resistant mosquitoes in 1999 and 2000. But many other countries avoid the insecticide—and not just for environmental reasons. DDT and pyrethroids also work through a very similar mechanism, so some mosquitoes resistant to pyrethroids are also resistant to DDT.

Some countries have switched from pyrethroids to an organophosphate insecticide called actellic. But actellic is four times as expensive, Hemingway says. "Fewer houses are getting sprayed, because the money available hasn't increased fourfold." And with many countries switching to the same compound, there is a danger that resistance will emerge to it as well.

Two new mosquito killers could be on the market as soon as 2017: SumiShield, developed by Japanese company Sumitomo Chemical, and chlorfenapyr, an insecticide mostly used to control cat fleas, developed by BASF. But both are seen as stop-gap measures. Although they are new to public health, these compounds have been used in agriculture for years, so some mosquitoes may be resistant already. And SumiShield is a neonicotinoid, a class of compounds that faces public opposition because it has been implicated in the mass die-off of pollinators.

Finding replacement insecticides for bed nets is far trickier. Any insecticide used in a bed net "has to be safe enough that a child can put it in their mouth," says Ranson, and only pyrethroids fit the bill. Pyrethroids also have a trait scientists call excito-repellency: They stimulate mosquitoes to leave the net. Neither SumiShield nor chlorfenapyr does that.

Not only are bed nets the best weapon in the fight against malaria-carrying mosquitoes, in many countries they are the only one. "Some countries still don't have IRS as part of their program. They view it as too expensive and difficult to implement," Ranson says.

From 2011 to 2016, Ranson headed an EU-funded project called AvecNet to evaluate new weapons to fight mosquitoes and take one through a clinical trial. The researchers eventually chose a net that combines pyrethroids with a compound called pyriproxyfen, which prevents mosquitoes from producing fertile eggs. "The idea is that if the mosquitoes are fully susceptible they will be killed by the insecticide, and if they are resistant they will pick up a dose of the sterilizing agent and the population

will crash as well," Ranson says. The group began testing the nets in 40 clusters of villages in Burkina Faso in 2014; results of the trial should be known in a few weeks. "There is a lot riding on this," Ranson says. "If it doesn't show any improvement, then I doubt there will be any further clinical trials of it."

Another combination net is already on the market, but it's not widely used because its efficacy is still in doubt. The net combines pyrethroids with a chemical called piperonyl butoxide (PBO). PBO blocks enzymes that help resistant mosquitoes break down pyrethroids, so, in theory, the mosquitoes should become susceptible again. Small-scale studies have suggested that the nets do work, but there haven't been any large-scale clinical trials.

To find new compounds for spraying and nets, IVCC has partnered with several large chemical companies including BASF, Syngenta, and Sumitomo to screen more than 4 million compounds in their libraries. Over the next few months they will choose three to go into large-scale toxicology testing, Hamon says. Any candidates for bed nets will have to pass other demanding tests: In addition to being safe, they will have to survive at least 20 washes and perform well for 3 years. "We were just very lucky with the pyrethroid insecticides in the '70s and '80s," Hamon says.

Luck may not run out quite as fast as many fear. Although resistance to pyrethroids is widespread, its impact on public health is still unclear. Even though a mosquito may survive a dose of an insecticide, the chemical may weaken it in some way. And the genes needed for resistance may take their own toll, perhaps by shortening a mosquito's life span. If the insect survives for fewer than 14 days, the malaria parasites won't have enough time to mature to the stage where they can infect humans, says Matthew Thomas, an entomologist at Pennsylvania State University, University Park. "There is some evidence to show that things like that can happen," Thomas says.

Insecticide resistance is going to matter at a certain point, he says—"What we don't know is whether we are just approaching that point, whether it is 1 year away, or five or 10." Defeating diseases like malaria may depend not only on finding chemicals to kill mosquitoes, but also on understanding how the insects manage to survive them. ■

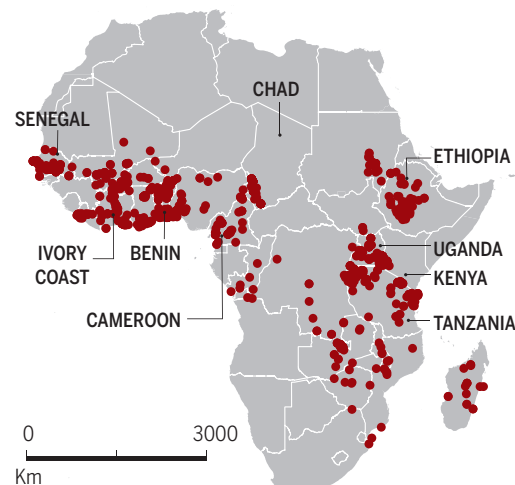
Resistance movement

Malaria mosquitoes that are resistant to pyrethroids have spread across Africa in recent years, stoking fears that malaria cases will rise again.

Confirmed resistance to pyrethroids, 1993–2003



Confirmed resistance to pyrethroids, 1993–now



INSIGHTS

PERSPECTIVES

EPIDEMIOLOGY

Sick birds don't fly...or do they?

Migratory birds were key to the spread of H5N8 viruses

By **Colin A. Russell**

In 2014, a new, highly pathogenic avian influenza virus (HPAIV) called H5N8 caused outbreaks in poultry in East and Southeast Asia and spread across the Northern Hemisphere to Europe and North America. In the United States alone, H5N8 outbreaks resulted in the destruction of more than 48 million poultry birds (1). International live-poultry trade and wild-bird migration have both been implicated in the intercontinental movement of H5N8 and other HPAIVs. H5N8 viruses have been found in wild birds (2–4), but strong

links between poultry outbreaks and live-poultry trade or wild-bird migration have been elusive. On page 213 of this issue, the Global Consortium for H5N8 and Related Influenza Viruses (5) delineates the contributions of live-poultry trade and wild-bird migration to the global spread of H5N8 viruses.

Live-poultry trade and wild-bird migration are both plausible mechanisms for the global movement of HPAIVs. The world's poultry population exceeds 50 billion animals, and the global network of live-poultry trade is extensive. Furthermore, HPAIVs are most commonly found in, and are thought to originate from, poultry (6). Al-

though HPAIVs are less often found in wild birds, they have been collected from various wild-bird species, and wild birds are the natural reservoir of all avian influenza virus subtypes. Wild-bird migration has the potential to move viruses long distances and introduce them to new populations, particularly where migratory flyways overlap (see the figure) (6, 7).

To investigate the spread of H5N8 viruses, the Global Consortium combined analyses of epidemiological, genetic, and ornithological data from Asia, Europe, and North America. These data consistently point to a prominent role of wild birds in spreading the viruses from Asia into Europe and North America via circumpolar migratory flyways (see the figure). In contrast, international trade data from the Food and Agriculture Organization

Department of Veterinary Medicine, University of Cambridge, Madingley Road, Cambridge CB3 0ES, UK.
Email: car44@cam.ac.uk

PROTEIN EVOLUTION

Young phosphorylation is functionally silent

Phosphorylation sites younger than 18 million years prevail in numbers, but not in function

By Or Matalon,* Benjamin Dubreuil,*
Emmanuel D. Levy

In cell biology, important discoveries often relate to mechanisms that are conserved throughout evolution. Yet what makes any species unique are specific molecular changes accumulated during the course of evolution. Thus, it is just as important to identify differences between species as it is to characterize their underlying similarities (1). On page 229 of this issue, Studer *et al.* present such an evolutionary comparative analysis, revealing similarities and, remarkably, substantial differences in the phosphorylation landscapes of fungal species (2).

Phosphorylation is a reversible posttranslational modification of proteins that can alter their structures and functions. This regulatory mechanism is ubiquitous throughout eukaryotes, where it controls and amplifies responses to intra- and extracellular signals. Although the chemical process of phosphorylation is evolutionarily conserved, the positions targeted for phosphorylation in protein sequences are not necessarily so.

To characterize the evolution of this regulatory mechanism, Studer *et al.* identified phosphorylation events in the proteomes of 18 fungal species, expanding our view of this covalent mark beyond the canonical model organisms (3–5). The work focuses on fungi, but covers a broad evolutionary time period. The group of closely related “*Saccharomyces*” fungi spans a divergence time of ~18 million years, which is comparable with the time separating humans from their last common ancestor (LCA) with the apes (see the figure).

The authors analyzed 18 fungal proteomes with mass spectrometry, allowing identification of 73,340 phosphorylated sites or “phosphosites” across the lineage, with 3000 to 5000 sites per species. The subsequent comparison of these sites enabled the

reconstruction of their probable evolutionary history. Sites specific to a species or a group of related species were inferred as having emerged recently, whereas those conserved throughout the lineage were inferred as being old and likely present in their LCA.

Studer *et al.* found that a mere ~2% of today’s phosphosites have been conserved since the LCA, ~700 million years ago (Ma). To put this in context, >73% of protein domains have been retained in all these fungi since their split from the LCA (6, 7), highlighting that phosphorylation sites can be lost during evolution much more rapidly than protein domains are. Accordingly, the authors also found phosphosites to be gained rapidly, with 69% being younger than 18 million years in the baker’s yeast *S. cerevisiae*. In several control experiments, the authors ruled out data coverage and condition-specific regulation as being responsible for this large fraction of young phosphosites. Moreover, using an even more conservative approach that takes adjacent sequence positions into account, 39% of phosphosites were still found to be young and therefore not conserved. Such a

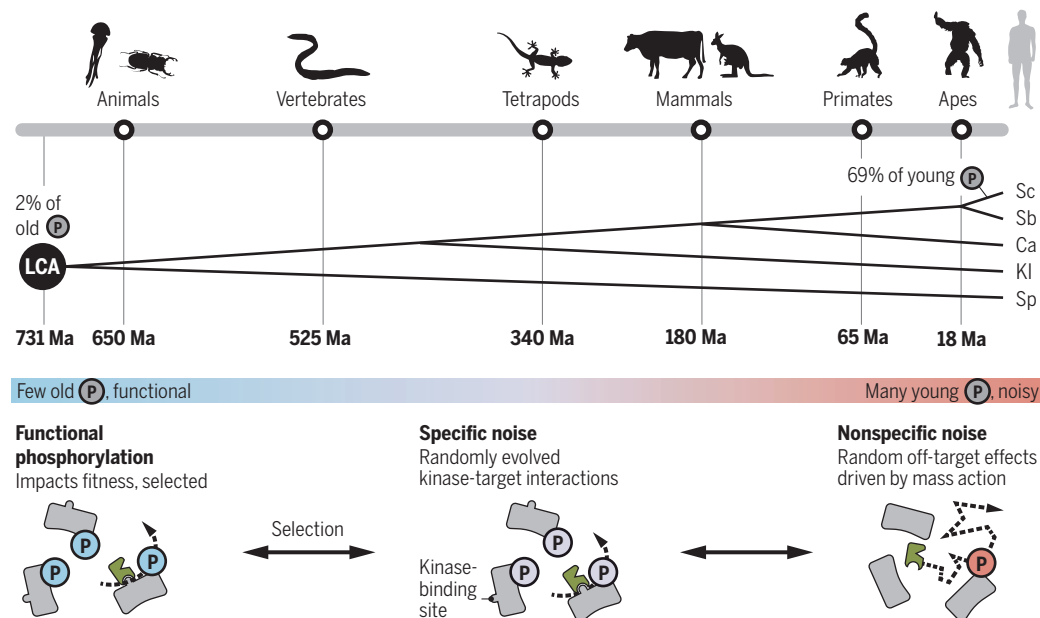
lack of conservation appears to contradict the textbook view that phosphorylation is strictly controlled and regulates important functions. Whereas certain phosphorylation events do surely regulate function, many may not. Edwin Krebs himself, who received the 1992 Nobel Prize with Edmond Fischer for the characterization of “reversible protein phosphorylation,” noted that there likely exists a degree of phosphorylation noise (8).

Noise—phosphorylation events not selected to carry out a specific function—can provide a simple explanation for the weak evolutionary conservation of phosphosites (9). Mechanistically, the low degree of sequence specificity required for phosphorylation implies that new kinase recognition motifs can frequently emerge by chance, without having been selected for, and hence need not be conserved. Kinase promiscuity means that even noncanonical substrates may be phosphorylated occasionally, so that abundant proteins can yield subpopulations detectable with mass spectrometry (10).

Evolutionary noise—mutations that are not selected to carry out a specific func-

Evolutionary phosphorylation insight

(Top) Evolutionary tree of five representative fungal species for which Studer *et al.* characterized the phosphorylation (P) landscape (Sc, *S. cerevisiae*; Sb, *S. bayanus*; Ca, *C. albicans*; Kl, *K. lactis*; Sp, *S. pombe*). For reference, divergence times are shown between humans and their LCA for different branches of the tree of life (14). (Bottom) Phosphorylation is not invariably associated with function; many phosphosites are likely noisy, as reflected in their young age and lack of conservation.



Weizmann Institute of Science, Department of Structural Biology, Rehovot, 7610001, Israel.
*These authors contributed equally to this work. Email: emmanuel.levy@weizmann.ac.il

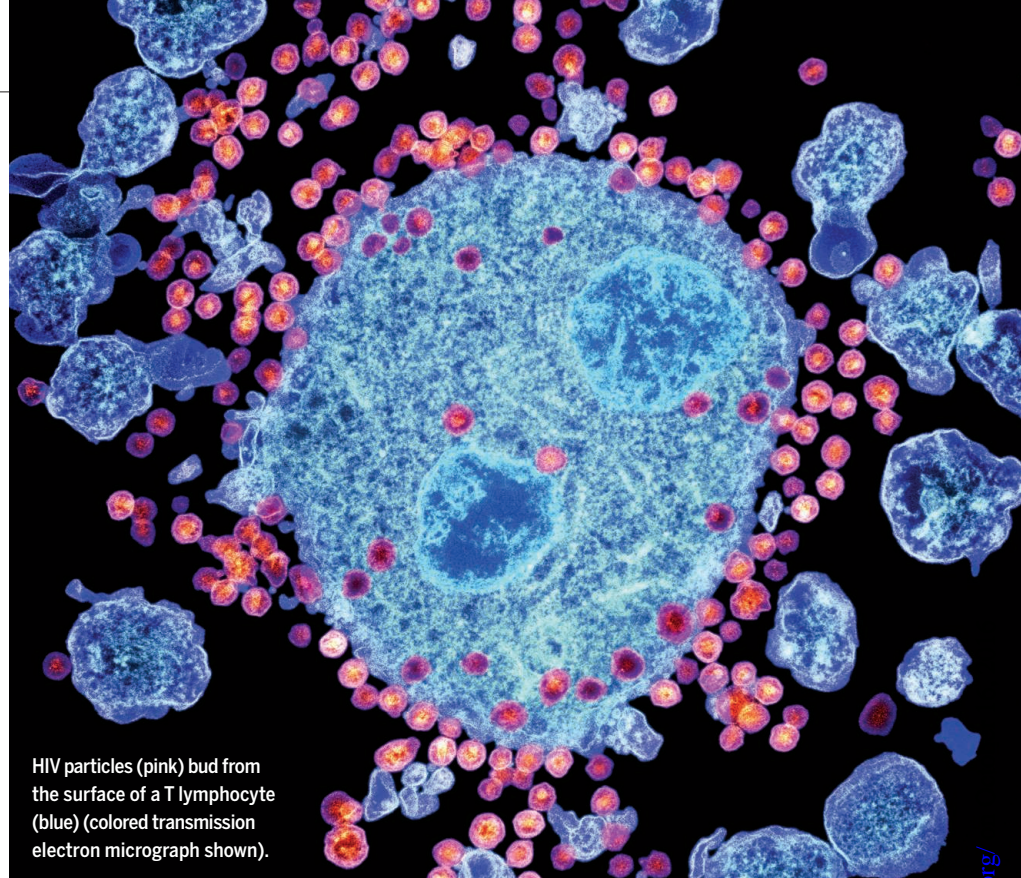
tion—is in fact seen during evolutionary adaptation. Whether in yeast adapting to a new environment (11) or in cancer cells escaping growth-control mechanisms (12), rare “driver” mutations arise in a background of “passenger” mutations that have a negligible impact on fitness. A common strategy to identify driver mutations is to find recurrent patterns across independent laboratory evolution experiments or cancer cell lines, such as mutations falling in the same genes. But to identify functional phosphosites, alternative approaches must be envisioned because evolution cannot be replayed multiple times. The work of Studer *et al.* opens new avenues in this respect. They reveal that lineage-specific preferences in phosphosite context have arisen across the fungal evolutionary tree. For example, proteins in the baker's yeast lineage show a depletion in proline-based phosphosite context and an increase in negatively charged context. They also found that specific classes of proteins acquired phosphosites in a coordinated fashion during specific time periods. These analyses suggest that global properties of phosphoproteomes are selected and therefore could be used to predict functional phosphorylation events. Equally important to predicting function will be our ability to filter out noise, which will require a more systematic consideration of protein abundance (10) and phosphorylation stoichiometry (13). More generally, the large data set of ancient sites identified in this work will make it possible to contrast structural and cellular properties of ancient and young sites (such as structural environment, presence of specific motifs, substrate interactions, expression, and localization) to discover new mechanisms and circuits involved in functional versus noisy phosphorylation.

Evolutionary cell biology is still in its early days (1). Thus, comparative proteomics efforts will be increasingly important to complement the postgenomic revolution, elucidate molecular differences between cell machineries across species, and fuel our understanding of life and its history. ■

REFERENCES AND NOTES

1. M. Lynch *et al.*, *Proc. Natl. Acad. Sci. U.S.A.* **111**, 16990 (2014).
2. R. A. Studer *et al.*, *Science* **354**, 229 (2016).
3. C. S. Tan *et al.*, *Sci. Signal.* **2**, ra39 (2009).
4. J. Boekhorst *et al.*, *Genome Biol.* **9**, R144 (2008).
5. B. Bodenmiller *et al.*, *Nat. Biotechnol.* **26**, 1339 (2008).
6. M. E. Oates *et al.*, *Nucleic Acids Res.* **43**, D227 (2015).
7. 73% is a conservative estimate, corresponding to the domain superfamilies common to the 18 species, divided by the total number of superfamilies in those species.
8. P. Cohen, *Nat. Cell Biol.* **4**, E127 (2002).
9. C. R. Landry *et al.*, *Trends Genet.* **25**, 193 (2009).
10. E. D. Levy, S. W. Michnick, C. R. Landry, *Philos. Trans. R. Soc. London B Biol. Sci.* **367**, 2594 (2012).
11. G. I. Lang *et al.*, *Nature* **500**, 571 (2013).
12. C. Greenman *et al.*, *Nature* **446**, 153 (2007).
13. H. Steen *et al.*, *Proc. Natl. Acad. Sci. U.S.A.* **102**, 3948 (2005).
14. J. Rosindell, L. J. Harmon, *PLOS Biol.* **10**, e1001406 (2012).

10.1126/science.aai8833



HIV particles (pink) bud from the surface of a T lymphocyte (blue) (colored transmission electron micrograph shown).

HIV

Shock and kill with caution

Strategies to silence latent HIV infection should be explored

By Robert C. Gallo

Antiretroviral therapy has made life-long suppression of human immunodeficiency virus (HIV) replication a possibility for some patients. But with the 2015 estimate of 36.7 million people infected worldwide, there is a great need to explore other ways to address this epidemic—from preventing new infections by treating uninfected high-risk individuals, to developing a vaccine, to targeting latent HIV that hides in immune cells and persists in patients. The idea of clearing latent infection has prompted strategies aimed at an HIV-1 cure. Although this approach should continue to be tested, other approaches, including those that seek to permanently suppress the latent virus, should also be explored. Different strategies may target different viral reservoirs, and may turn out to be complementary.

The existence of T cells harboring latent HIV-1 provirus was first described in 1986 (1),

as was the demonstration that activation of those T cells “reawakened” HIV-1 expression (2). The importance of these latently infected cells, however, came to the forefront following the work of several clinical investigators (3) who showed that these cells persist long after anti-HIV therapy and virus suppression, and periodically release HIV-1, presumably in response to a milieu favorable to T cell activation. The idea then arose that HIV-1 infection would be curable if latent virus could be deliberately reactivated. This would lead to T cell death, either directly from HIV-1 cytopathic effects or by cytotoxic T lymphocytes (CTLs). Concurrent anti-HIV therapy would block new rounds of infection. This idea has been called “shock and kill” or “kick and kill,” and has spawned numerous studies (4), clinical trials, and discussions at meetings. Part of this impetus was provided by an enduring focus on one patient, the so-called “Berlin patient” (5), who—through a series of fortunate events—is the only known example of complete HIV-1 cure. This individual was HIV-1-positive, but also had leukemia, which allowed physicians to treat him with total body irradiation. Fortunately, he survived this aggressive treatment, and his leukemia.

Institute of Human Virology, University of Maryland School of Medicine, 725 West Lombard Street, Baltimore, MD 21201, USA. Email: rgallo@ihv.umaryland.edu

Another fortunate circumstance was the availability of bone marrow cells from an HIV-1-negative donor who carried a rare homozygous mutation in the HIV-1 co-receptor CCR5 (CCR5 Δ 32), which renders cells resistant to HIV-1 infection (6). With the ablation of his own bone marrow cells and the acceptance by his weakened immune system of T cells lacking functional CCR5, he became free of HIV-1 and presumably unable to be infected. Although no new principles came from this study, it did provide a proof of concept for a “cure.” The results are indeed germane to developing approaches, such as gene therapy, that destroy or remove CCR5 from infected persons (7). However, the study’s relevance to almost all other HIV-1-infected patients, as well as its connection to currently envisioned “shock and kill” approaches, is not apparent.

Clinical testing of the “shock and kill” approach has begun only recently, and therefore merits further evaluation (8). However, this strategy presents a few issues of concern that should not be overlooked. It is assumed that all latently infected cells will die following viral reactivation and/or by CTL attack, but there is no evidence for this; rather, these cells do not die. This may be because only weak latency-reversing agents (LRAs) have been tested clinically. Therefore, it is possible that more effective agents (alone or in combination) might do a better job at reawakening the virus and killing the infected cell, which should be tested. Also, there is no assurance that combination antiretroviral therapy (cART) will completely block the released virus from infecting new cells, especially in the brain or lymphoid tissues where the antiretroviral drugs may not reach fully suppressive concentrations. The effectiveness of these drugs in anatomical sites is still being debated. Treatment intensification does not seem to reduce the size of the viral reservoir, and there appears to be no genetic evolution of the virus in patients under suppressive cART therapy, both of which suggest that current regimens completely block virus spread. However, some have suggested that poor drug penetrance in certain anatomical sites plays against drug-resistant strains. Because this issue is still unresolved, we should use caution and consider that current regimens may not achieve suppressive concentrations (in at least some anatomical sites), and thus may be unable to block virus spread in the context of “shock and kill” strategies.

Another issue of concern is that some LRAs may activate uninfected T cells, rendering them new targets for infection. This could possibly be the case with Toll-like receptor agonists that are being evaluated as LRAs. More recently, the idea has emerged to combine certain LRAs with therapeutic vac-

cines, as a new version of the “shock and kill” approach. This is of course attractive, but it remains to be established whether a therapeutic vaccine can be devised to raise effective CTL responses in immunocompromised individuals. Indeed, in one case, a vaccine could raise protective CTL responses prior to infection (9), but its efficacy in infected patients is questionable.

Latent viruses other than HIV-1 may also be reactivated and spread by LRAs, thereby giving rise to serious side effects later on. Such viruses include Epstein-Barr virus, cytomegalovirus, human T cell lymphotropic virus, hepatitis C virus, human herpes virus, human herpes virus 8 (Kaposi sarcoma herpes virus), and human endogenous retroviruses. Moreover, the use of agents that target host factors (all LRAs tested so far fall into this category) will also modulate host gene expression (including inheritable epigenetic

“‘Shock and kill’ and ‘soothe and snooze’ may turn out to be two non-mutually exclusive approaches to a functional cure for HIV-1 infection.”

marks), which may cause unwanted side effects. Indeed, any approach involving T cell activation could be toxic beyond just the potential of activating other disease-causing viruses and making cells more sensitive to HIV-1 infection. We should not forget that although cART does not represent a cure, it allows HIV-1-infected individuals a full life, especially with simpler drug regimens.

There are HIV-1-infected cell types other than CD4⁺ T cells that are not given consideration in the “shock and kill” approach. For example, macrophages are infected by HIV-1 (10) and generally do not die from infection. Brain cells are also an HIV-1 sanctuary (11), mainly in microglial cells. A recent study has shown that viral replication persists in lymphoid tissues of infected individuals despite suppressed viremia (12). Although not directly addressed, myeloid cells could be the source of this persistent viral replication. Indeed, macrophages are a source of continual low-level production of HIV-1 (13). Whether or not myeloid cells represent a long-lived viral reservoir remains to be conclusively addressed, but until then, their role should not be ignored or discounted. In short, there is more to HIV-1 persistence in the context of suppressive cART than CD4⁺ T cell reservoirs.

Agents such as histone deacetylase inhibitors show limited efficacy in reactivating HIV-1 because they target only one molecular mechanism that maintains viral latency. Many other blocks are still in place, including the lack of key transcription factors, the presence of other epigenetic blocks, and a cellular environment that is quiescent and unable to support viral replication.

Another approach to address latent HIV infection is to force the latent virus to remain quiescent by stronger and more durable virus-suppressing agents. So far, the only example of this “soothe and snooze” strategy is the use of the HIV-1 Tat inhibitor, didehydrocortistatin A (14). This drug appears to be highly specific for Tat, without off-target effects. However, other latency-promoting agents, particularly those acting in an HIV-1-specific manner, should be explored. Other goals in developing this strategy include drugs targeting cellular factors that play a role in viral replication, and those that reach anatomical sanctuaries more efficiently. Durable HIV suppression could be concurrently supported by gene therapy strategies that target the HIV-1 provirus and/or CCR5 with gene-editing tools. In line with longer-term virus suppression, Byraredy *et al.* (15) report that combining ART with antibodies that block T cells sustained low viremia in simian immunodeficiency virus (SIV)-infected monkeys.

Despite the success of cART, there are still very high-priority areas that must be supported, including HIV-1 testing, promoting preexposure prophylaxis, and developing a vaccine (16). Therapeutic strategies aimed at an HIV-1 cure through viral reactivation should continue to be tested, but other strategies such as viral suppression should also be explored. Indeed, funding agencies are starting to support research aimed at permanently silencing the latent provirus. “Shock and kill” and “soothe and snooze” may turn out to be two non-mutually exclusive approaches to a functional cure for HIV-1 infection. ■

REFERENCES AND NOTES

1. M. E. Harper *et al.*, *Proc. Natl. Acad. Sci. U.S.A.* **83**, 772 (1986).
2. D. Zagury *et al.*, *Science* **231**, 850 (1986).
3. D. Finzi *et al.*, *Science* **278**, 1295 (1997).
4. D. D. Richman *et al.*, *Science* **323**, 1304 (2009).
5. G. Hutter *et al.*, *N. Engl. J. Med.* **360**, 692 (2009).
6. R. Liu *et al.*, *Cell* **86**, 367 (1996).
7. N. Holt *et al.*, *Nat. Biotechnol.* **28**, 839 (2010).
8. D. M. Margolis *et al.*, *Science* **353**, aaf6517 (2016).
9. S. G. Hansen *et al.*, *Nature* **473**, 523 (2011).
10. S. Gartner *et al.*, *Science* **233**, 215 (1986).
11. G. M. Shaw *et al.*, *Science* **227**, 177 (1985).
12. R. Lorenzo-Redondo *et al.*, *Nature* **530**, 51 (2016).
13. J. B. Honeycutt *et al.*, *J. Clin. Invest.* **126**, 1353 (2016).
14. G. Mousseau *et al.*, *MBio* **6**, e00465-15 (2015).
15. S. N. Byraredy *et al.*, *Science* **354**, 197 (2016).
16. A. S. Fauci, H. D. Marston, *N. Engl. J. Med.* **370**, 495 (2014).

ACKNOWLEDGMENTS

I thank F. Romero, M. S. Reitz, and A. Garzino-Demo for helpful discussions and critical reading of the manuscript.

10.1126/science.aaf8094

of sensitivity than might be achieved by the opposing actions of ERK together with protein phosphatases that dephosphorylate Elk-1. Nevertheless, both of these mechanisms likely contribute to the broader resetting of chromatin to allow cells to respond to subsequent signals. However, it is possible that fully phosphorylated Elk-1 could be reactivated by dephosphorylation of those sites that had the slowest rate of phosphorylation, as the graded dephosphorylation by protein phosphatases is an additional mechanism for controlling protein function (14).

The Elk-1 transcriptional activation domain is also a target of the c-Jun N-terminal kinase (JNK) and p38 groups of MAPK in response to stress (15). Mylona *et al.* provide some tantalizing initial data suggesting that the rates of Elk-1 phosphorylation at individual sites by these kinases are distinct from the pattern observed with ERK. This suggests that a group of phosphorylation sites on a transcription factor may be bar-coded by different kinases, with different phosphorylation patterns eliciting distinct transcriptional responses.

“...multisite phosphorylation substantially increases the scope for modulating protein function...”

It will be important to determine if this mechanism of multisite phosphorylation is unique to Elk-1 and its relatives or is more widely used to regulate transcriptional responses or the functions of other proteins. It is also possible that additional posttranslational modifications can utilize a similar mechanism. The study by Mylona *et al.* emphasizes the importance of performing detailed quantitative analysis of the molecular roles of protein modifications if we wish to fully understand the complex mechanisms regulating protein function. ■

REFERENCES

1. A. Mylona *et al.*, *Science* **354**, 233 (2016).
2. P. Cohen, *Trends Biochem. Sci.* **25**, 596 (2000).
3. P. Nash *et al.*, *Nature* **414**, 514 (2001).
4. M. Koivomägi *et al.*, *Nature* **480**, 128 (2011).
5. M. A. Pfaller *et al.*, *Science* **309**, 142 (2005).
6. S. C. Strickfaden *et al.*, *Cell* **128**, 519 (2007).
7. J. Schlessinger, *Cell* **103**, 211 (2000).
8. M. Springer *et al.*, *PLOS Biol.* **1**, e28 (2003).
9. N. Hao *et al.*, *Science* **339**, 460 (2013).
10. C. Salazar *et al.*, *Trends Cell Biol.* **20**, 634 (2010).
11. R. Marais *et al.*, *Cell* **73**, 381 (1993).
12. J. L. Stevens *et al.*, *Science* **296**, 755 (2002).
13. S.-H. Yang *et al.*, *Mol. Cell. Biol.* **21**, 2802 (2001).
14. K.-S. Park *et al.*, *Science* **313**, 976 (2006).
15. A. J. Whitmarsh *et al.*, *Mol. Cell. Biol.* **17**, 2360 (1997).

10.1126/science.aai9381

MATERIALS SCIENCE

Making the most of materials computations

Databases of theoretical structures and properties of materials can speed real-world discovery

By Kristian S. Thygesen and
Karsten W. Jacobsen

For more than a century, materials scientists have accumulated experimental data on the structures of chemical compounds and the thermal, electronic, and mechanical properties that they exhibit. These data have been a cornerstone in the development, selection, and design of materials (1). In the past decade, experimental data have been augmented by an explosion of computational data from quantum-mechanical calculations, which can be obtained more quickly and in some cases with comparable accuracy. Most of the data have been obtained via density functional theory (DFT), which calculates the electronic structure of a material and thereby provides atomic-scale information about its properties. Although databases can store all of these data, managing and fully utilizing this vast resource presents many challenges.

The computational databases supplement the experimental ones [as, for example, the Inorganic Crystal Structure Database (2)] mainly by providing additional systematic information about materials, but they also provide information about the properties of materials that do not occur naturally or that have never been synthesized in a laboratory. The databases therefore provide a playground for exploration of new materials. Some of the larger repositories, together containing more than 1 million material entries, are the Materials Project (3), the Automatic Flow for Materials Discovery (AFLOWLIB) (4), the Open Quantum Materials Database (OQMD) (5), the Novel Materials Discovery (NoMaD) Repository (6), the CatApp Database (7), and the Computational Materials Repository (CMR) (8) (see the top panel of the figure). All of these have web interfaces that provide free access to the data.

A popular application of DFT databases is thermodynamic stability analysis, where, for a given combination of chemical elements,

stable compositions and structures at low temperatures are identified. This feature is available in most of the major databases and is, for example, used as a first check of the stability of a given hypothetical material composition. Combining the computed data with experimental data for the free energy of dissolution makes it possible to extend this analysis to Pourbaix diagrams, which map out the stability of the material as a function of pH and applied potential, and indicate the ionic species that forms if it dissolves (9, 10).

The databases are steadily growing in size both because of systematic inclusion of new crystal structures and compositions, and because computational screening studies aimed at identifying useful materials within, for example, batteries or solar energy contribute with new materials. Many materials screening projects can be expected to take their starting point directly in the computational materials databases. Below, we discuss a few of the important opportunities and challenges for the further development of computational materials databases to improve their quality and their applicability for materials science and design.

DATA REPRESENTATION

Compared to experimental data, computed materials data have the advantage of being very well defined and easy to reproduce. A DFT calculation is specified by the atomic numbers and positions of all the atoms, plus a few additional parameters to describe the approximations being made. In practice, it may be a challenge to label the computed materials in a way that is both useful and sufficiently unique for the user. For example, should two calculations be considered to describe the same phase of a material if the atomic positions are not exactly the same?

DATA QUALITY

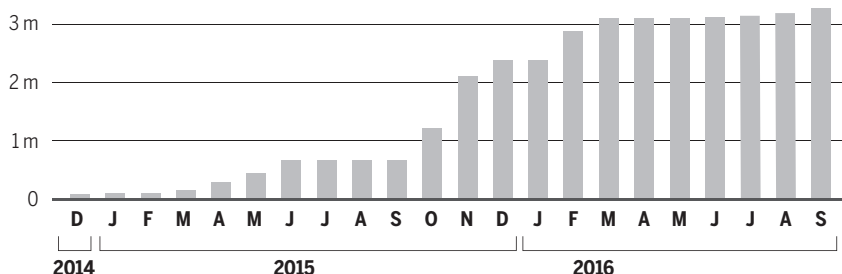
Computational materials scientists apply a range of different codes that all solve the same fundamental equations of DFT but apply diverse numerical approaches. In a large community effort, it was recently shown that in simple situations, like the calculation of the equation of state of elemental crystals, agreement between different codes can be

Department of Physics, CAMD, Technical University of Denmark, DK-2800 Kongens Lyngby, Denmark.
Email: thygesen@fysik.dtu.dk; kwj@fysik.dtu.dk

Materials data and discovery

DFT calculations in the NoMaD repository (in millions)

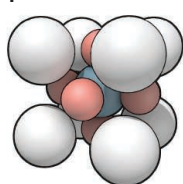
The number of DFT calculations in the NoMaD repository from December 2014 to September 2016. The large jumps in October/November 2015 and February 2016 arose from inclusion of data from the AFLOWLIB and OQMD repositories, respectively.



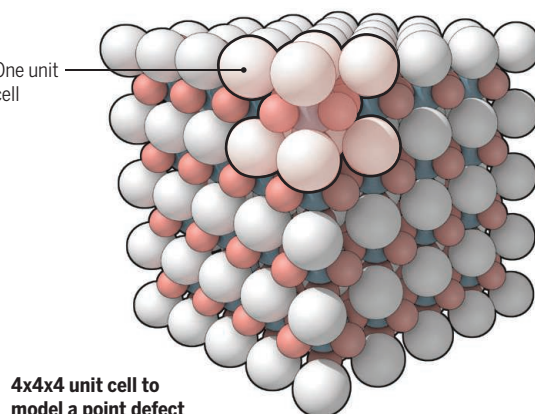
Materials data and discovery

An example of a small unit cell that repeats periodically to represent a simple periodical solid, versus a much larger unit cell required to model defects.

A simple SrTiO_3 perovskite unit cell



One unit cell



4x4x4 unit cell to model a point defect

established (11). More complex materials properties still represent a challenge, and accuracies need to be estimated. Unfortunately, different codes produce output in different formats. This issue is currently addressed by the NOMAD project (12), where parsers for the 40 most popular codes are developed to obtain a common file format. At a more fundamental level, DFT calculations require physical approximations for the so-called exchange-correlation energy of the electrons. Further refinements of these approximations will be necessary to increase the accuracy of the calculations, depending on the application.

COMPLEX SYSTEMS

Computational databases mainly contain entries for bulk solids in simple crystal structures, primarily because calculation times grow quickly with the number of atoms N in the unit cell (typically as N to a power between 2 and 3). However, many materials properties are determined by defects, such as vacancies, atoms in interstitial sites, or impurities, or by grain boundaries or surfaces. For many applications, the simple materials described in the databases are not directly relevant, and more complex structures and

materials must be included. However, as structural complexity increases, the number of possible materials also grows tremendously (see the bottom panel of the figure). An example of a first step to systematically address the more complicated situation of molecules reacting at surfaces is a DFT database of adsorption energies (7) of relevance to heterogeneous catalysis.

BEYOND DFT

Many materials properties or phenomena lie beyond the present capabilities of DFT for a quantitative description, including descriptions of electronic excitations and strongly correlated systems. For example, different corrections to the standard DFT approaches can be applied to study light absorption of materials for photovoltaics or photocatalysis, but today the best calculations of properties such as electronic band structures or optical spectra are based on many-body perturbation theory applying the so-called GW or Bethe-Salpeter approximations. However, these calculations are computationally much more expensive and numerically involved than DFT calculations, which makes the issue of data quality and consistency even more important. The first steps toward estab-

lishing GW databases for code benchmarking (13) and for the electronic structure of two-dimensional materials (14) have recently been taken, but much more work is needed to establish consistent and accurate “beyond-DFT” data.

MACHINE LEARNING

It might be debatable whether computational materials databases have the characteristics (volume, variety, and velocity) to qualify as “big data” (15). However, as computational databases grow, new possibilities for investigating the materials space will certainly arise. It will be necessary to develop or adapt tools from machine learning for searching and analyzing many millions of computed materials, and it will be possible to apply these tools to learn new correlations or structure-property relations of materials. Simple relations of this type are an integral part of materials science and chemistry. Examples include valence rules and geometrical tolerance factors for predicting chemical and structural stability. These rules have emerged from empirical observations performed over decades of research, but when considering large numbers of computed materials, these rules can be systematically deduced as correlations in the data. The use of modern machine learning may potentially allow researchers to identify deeper and more complex patterns in the materials space, and to use correlations to accelerate the prediction of new materials or to design materials with specific tailored properties. ■

REFERENCES AND NOTES

1. M. F. Ashby, *Materials Selection in Mechanical Design* (Butterworth-Heinemann, Oxford, ed. 4, 2010).
2. ICSD; www.fiz-karlsruhe.de/de/leistungen/kristallographie/icds.html.
3. A. Jain *et al.*, *APL Mater.* **1**, 011002 (2013).
4. S. Curtarolo *et al.*, *Comput. Mater. Sci.* **58**, 218 (2012).
5. J. E. Saal, S. Kirklin, M. Aykol, B. Meredig, C. Wolverton, *JOM* **65**, 1501 (2013).
6. <http://nomad-repository.eu>; <https://nomad-coe.eu>
7. J. S. Hummelshøj, F. Abild-Pedersen, F. Studt, T. Bligaard, J. K. Nørskov, *Angew. Chem. Int. Ed.* **51**, 272 (2011).
8. D. D. Landis *et al.*, *Computing. Sci. Eng.* **14**, 51 (2012).
9. K. A. Persson, B. Walldwick, P. Lázic, G. Ceder, *Phys. Rev. B* **85**, 235438 (2012).
10. I. E. Castelli, K. S. Thygesen, K. W. Jacobsen, *Top. Catal.* **57**, 265 (2014).
11. K. Lejaeghere *et al.*, *Science* **351**, aad3000 (2016).
12. L. M. Ghiringhelli *et al.*, *Psi-k Highlight July 2016*; http://psi-k.net/download/highlights/Highlight_131.pdf.
13. M. J. van Setten *et al.*, *J. Chem. Theory Comput.* **11**, 5665 (2015).
14. F. Rasmussen, K. S. Thygesen, *J. Phys. Chem. C* **119**, 13169 (2015).
15. J. Hill *et al.*, *MRS Bull.* **41**, 399 (2016).

ACKNOWLEDGMENTS

We thank C. Draxl and T. Zastrow for data on the NoMaD Repository. The research in the groups of the authors is supported by the Danish National Research Foundation's Center for Nanostructured Graphene; a research grant (9455) from Villum Fonden; and the European Union Center of Excellence, Novel Materials Discovery Laboratory (NOMAD).

10.1126/science.aah4776

CLIMATE CHANGE

The trouble with negative emissions

Reliance on negative-emission concepts locks in humankind's carbon addiction

By **Kevin Anderson**^{1,2} and **Glen Peters**³

In December 2015, member states of the United Nations Framework Convention on Climate Change (UNFCCC) adopted the Paris Agreement, which aims to hold the increase in the global average temperature to below 2°C and to pursue efforts to limit the temperature increase to 1.5°C. The Paris Agreement requires that anthropogenic greenhouse gas emission sources and sinks are balanced by the second half of this century. Because some nonzero sources are unavoidable, this leads to the abstract concept of “negative emissions,” the removal of carbon dioxide (CO₂) from the atmosphere through technical means. The Integrated Assessment Models (IAMs) informing policy-makers assume the large-scale use of negative-emission technologies. If we rely on these and they are not deployed or are unsuccessful at removing CO₂ from the atmosphere at the levels assumed, society will be locked into a high-temperature pathway.

CARBON BUDGETS

To understand the implications of the Paris Agreement for mitigation policy, we must translate its qualitative temperature limits into quantitative carbon budgets, specifying how much CO₂ can be emitted across the remainder of the century to keep warming below a given temperature level (1). Uncertainties in the climate system mean that such budgets are specified with quantitative likelihoods. Borrowing from the taxonomy of likelihoods used by the Intergovernmental Panel on Climate Change (IPCC), the most generous interpretation of the Paris Agreement's requirement to keep the temperature rise well below 2°C is, at least, a likely (66 to 100%) chance of not exceeding 2°C.

The IPCC has assessed 900 mitigation scenarios from about 30 IAMs (2). Of these, 76 scenarios from five IAMs had sufficient data to estimate the carbon budget for a likely chance of not exceeding 2°C. These scenarios give a carbon budget of between 600 and 1200 billion metric tons (Gt) CO₂ (10 to 90% range) for the period from 2016

until the peak in temperature [updated from (7)]. Increasing the likelihood of keeping temperatures below 2°C (or shifting the ceiling to 1.5°C) will reduce still further the available carbon budget (3). The budget is also subject to a reduction each year, currently around 40 Gt CO₂, due to continued fossil fuel, industry, and land-use change emissions.

It is important to keep in mind that despite their intuitive appeal, the complexity of carbon budgets make it impossible to assign a specific budget to a given temperature rise.

FROM BUDGETS TO EMISSION PATHWAYS

Because the carbon budgets represent cumulative emissions, different emission pathways can be consistent with a given budget. Using the 76 scenarios consistent with a likely chance of not exceeding 2°C (see the figure), two key features are immediately striking. First, the scenarios assume that the large-scale rollout of negative-emission technologies is technically, economically, and socially viable (2, 4). In many scenarios, the level of negative emissions is comparable in size with the remaining carbon budget (see the figure) and is sufficient to bring global emissions to at least net zero in the second half of the century. Second, there is a large and growing deviation between actual emis-

sion trends and emission scenarios. The sum of the national emission pledges submitted to the Paris negotiations (COP21) lead to an increase in emissions, at least until 2030. They thus broaden the division between pathways consistent with the temperature goals of the Paris Agreement (5) and require either much more severe near-term mitigation (6) or additional future negative emissions.

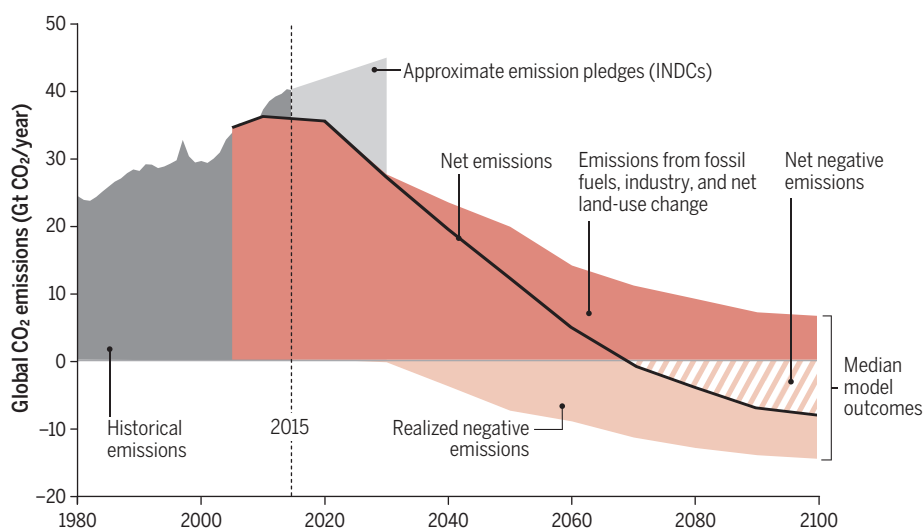
It is not well understood by policy-makers, or indeed many academics, that IAMs assume such a massive deployment of negative-emission technologies. Yet when it comes to the more stringent Paris obligations, studies suggest that it is impossible to reach 1.5°C with a 50% chance without significant negative emissions (3). Even for 2°C, very few scenarios have explored mitigation without negative emissions (2). Negative emissions are also prevalent in scenarios for higher stabilization targets (7). Given such a pervasive and pivotal role of negative emissions in mitigation scenarios, their almost complete absence from climate policy discussions is disturbing and needs to be addressed urgently.

NEGATIVE-EMISSION TECHNOLOGIES

Negative-emission technologies exist at various levels of development (8–11). Afforestation and reforestation, although not

No quick fixes

Modelers generally report net carbon emissions, unintentionally hiding the scale of negative emissions. Separating out the positive CO₂ emissions from fossil fuel combustion, industry, and land-use change reveals the scale of negative CO₂ emissions in the model scenarios (16). INDCs, Intended Nationally Determined Contributions.



¹Tyndall Centre, University of Manchester, Manchester M13 9PL, UK. ²Centre for Sustainable Development, Uppsala University, 75236 Uppsala, Sweden. ³Center for International Climate and Environmental Research—Oslo (CICERO), Pb. 1129 Blindern, 0318 Oslo, Norway. Email: kevin.anderson@manchester.ac.uk; glen.peters@cicero.oslo.no

strictly technologies, are already claimed by countries as mitigation measures. Bioenergy, combined with carbon capture and storage (BECCS), is the most prolific negative-emission technology included in IAMs and is used widely in emission scenarios. It has the distinct feature of providing energy while also, in principle (12), removing CO₂ from the atmosphere. Assuming that carbon is valued, BECCS can thus provide an economic benefit that may offset, at least in part, the additional costs of using the technology (13). Generally, carbon is assumed to be fully absorbed during biomass growth, captured before or after combustion, and then stored underground indefinitely. Despite the prevalence of BECCS in emission scenarios at a level much higher than afforestation, only one large-scale demonstration plant exists today.

Other negative-emission technologies have not moved beyond theoretical studies or small-scale demonstrations. Alternative and adjusted agricultural practices, including biochar, may increase carbon uptake in soils (9). It may also be possible to use direct air capture to remove CO₂ from the atmosphere via chemical reactions, with underground storage similar to CCS. Enhancing the natural weathering of minerals (rocks) may increase the amount of carbon stored in soils, land, or oceans. Introduction of biological or chemical catalysts may increase carbon uptake by the ocean. New technologies, designs, and refinements may emerge over time.

BECCS: A POLITICAL PANACEA

The allure of BECCS and other negative-emission technologies stems from their promise of much-reduced political and economic challenges today, compensated by anticipated technological advances tomorrow. Yet there are huge opportunities for near-term, rapid, and deep reductions today at little to modest costs, such as improving energy efficiency, encouraging low-carbon behaviors, and continued deployment of renewable energy technologies. Why, then, is BECCS used so prolifically in emission scenarios?

The answer is simple. Integrated assessment models often assume perfect knowledge of future technologies and give less weight to future costs. In effect, they assume that the discounted cost of BECCS in future decades is less than the cost of deep mitigation today. In postponing the need for rapid and immediate mitigation, BECCS licenses the ongoing combustion of fossil fuels while ostensibly fulfilling the Paris commitments.

“Negative-emission technologies are not an insurance policy, but rather an unjust and high-stakes gamble.”

The idea behind BECCS is to combine bioenergy production with CCS, but both face major and perhaps insurmountable obstacles. Two decades of research and pilot plants have struggled to demonstrate the technical and economic viability of power generation with CCS, even when combusting relatively

homogeneous fossil fuels (14). Substituting for heterogeneous biomass feedstock adds to the already considerable challenges.

Moreover, the scale of biomass assumed in IAMs—typically, one to two times the area of India—raises profound questions (10) about carbon neutrality, land availability, competition with food production, and competing demands for bioenergy from the transport, heating, and industrial sectors. The logistics of collating and transporting vast quantities of bioenergy—equivalent to up to half of the total global primary energy consumption—is seldom addressed. Some studies suggest that BECCS pathways are feasible, at least locally (15), but globally there are substantial limitations (10). BECCS thus remains a highly speculative technology.

Although BECCS, like all negative-emission technologies, is subject to scientific and political uncertainties, it dominates the scenario landscape. Yet, as recognition of the ubiquitous role of BECCS in mitigation scenarios has grown, so have concerns about its deployment (10, 11). Its land-use impacts could include terrestrial species losses equivalent to, at least, a 2.8°C temperature rise (11), leading to difficult trade-offs between biodiversity loss and temperature rise. There is also little robust analysis of the trade-offs between large-scale deployment of BECCS (and all negative-emission technologies) and the Sustainable Development Goals (SDGs). But such a level of caution is far removed from the technical utopia informing IAMs. Despite BECCS continuing to stumble through its infancy, many scenarios assessed by the IPCC propose its mature and large-scale rollout as soon as 2030 (see the figure).

MORAL HAZARD AND INEQUITY

The appropriateness or otherwise of relying, in significant part, on negative-emission technologies to realize the Paris commitments is an issue of risk (7). However, the distribution of this risk is highly inequitable. If negative-emission technologies fail to deliver at the scale enshrined in many IAMs, their failure will be felt most by low-emitting communities that are geographically and financially vulnerable to a rapidly changing climate.

The promise of future and cost-optimal negative-emission technologies is more politically appealing than the prospect of developing policies to deliver rapid and deep mitigation now. If negative-emission technologies do indeed follow the idealized, rapid, and successful deployment assumed in the models, then any reduction in near-term mitigation caused by the appeal of negative emissions will likely lead to only a small and temporary overshoot of the Paris temperature goals (3). In stark contrast, if the many reservations increasingly voiced about negative-emission technologies (particularly BECCS) turn out to be valid, the weakening of near-term mitigation and the failure of future negative-emission technologies will be a prelude to rapid temperature rises reminiscent of the 4°C “business as usual” pathway feared before the Paris Agreement (5).

Negative-emission technologies are not an insurance policy, but rather an unjust and high-stakes gamble. There is a real risk they will be unable to deliver on the scale of their promise. If the emphasis on equity and risk aversion embodied in the Paris Agreement are to have traction, negative-emission technologies should not form the basis of the mitigation agenda. This is not to say that they should be abandoned (14, 15). They could very reasonably be the subject of research, development, and potentially deployment, but the mitigation agenda should proceed on the premise that they will not work at scale. The implications of failing to do otherwise are a moral hazard par excellence. ■

REFERENCES AND NOTES

1. J. Rogelj et al., *Nat. Clim. Change* **6**, 245 (2016).
2. L. Clarke et al., in *Climate Change 2014: Mitigation of Climate Change. Contribution of Working Group III to the Fifth Assessment Report of the Intergovernmental Panel on Climate Change*, O. Edenhofer et al., Eds. (Cambridge Univ. Press, Cambridge/New York, 2014), pp. 413–510.
3. J. Rogelj et al., *Nat. Clim. Change* **5**, 519 (2015).
4. H. J. Buck, *Clim. Change* **10**, 1007/s10484-016-1770-6 (2016).
5. J. Rogelj et al., *Nature* **534**, 631 (2016).
6. K. Anderson, *Nat. Geosci.* **8**, 898 (2015).
7. S. Fuss et al., *Nat. Clim. Change* **4**, 850 (2014).
8. M. Tavoni, R. Socolow, *Clim. Change* **118**, 1 (2013).
9. P. Smith, *Glob. Change Biol.* **22**, 1315 (2016).
10. P. Smith et al., *Nat. Clim. Change* **6**, 42 (2015).
11. P. Williamson, *Nature* **530**, 153 (2016).
12. A. Gilbert, B. K. Sovacool, *Nat. Clim. Change* **5**, 495 (2015).
13. D. L. Sanchez et al., *Nat. Clim. Change* **5**, 230 (2015).
14. D. M. Reiner, *Nat. Energy* **1**, 15011 (2016).
15. D. L. Sanchez, D. M. Kammen, *Nat. Energy* **1**, 15002 (2016).
16. The figure shows the median of the 76 IPCC scenarios that limit the global temperature rise to 2°C with 66% likelihood (2). Realized negative emissions are estimated by converting the BECCS energy consumption [exajoules (EJ) per year], assuming an average biomass emission factor of 100 metric tons of CO₂ per terajoule (TJ) and assuming that 90% of the CO₂ is captured. The emission pledges (INDCs) in 2030 are estimated based on cumulative emissions from 2011 to 2030 (5).

ACKNOWLEDGMENTS

G.P. is funded by the Research Council of Norway (Strategic Challenges in International Climate and Energy Policy, project number 209701).

10.1126/science.aah4567

MICROBIOLOGY

A microbial route from coal to gas

Microbes isolated from an oil reservoir directly convert coal to methane

By Cornelia U. Welte^{1,2}

Many coal wells produce methane through the microbial decomposition of coal (1). About 7% of methane that reaches the atmosphere is derived from coal beds and contributes considerably to the greenhouse effect (2). But how is coal converted into methane? Which compounds in the coal are degraded, and which microbes are responsible? On page 222 of this issue, Mayumi *et al.* (3) report the discovery of methanogenic archaea that convert complex organic compounds released from coal directly into methane by a previously unknown type of metabolism.

Coal is a complex mixture of unreactive organic compounds that most microorganisms find difficult to consume. The key step in coal gasification is the production of methane by methanogenic archaea. However, known methanogens only use small carbon

compounds like carbon dioxide, methylated amines, or acetate for gas production (4). Analysis of microbial communities in coal wells has suggested that breakdown products of coal are first converted to simpler, more palatable carbon compounds through the activity of microbial food chains (5–7), thus supplying the methanogens with substrates. In fact, different classes of methanogens seem to govern methane formation in unrelated coal wells (2, 8, 9). It is unclear which organic molecules of the coal are actually converted to methane, although immature coal (lignite) seems to be more biologically accessible than mature (bituminous) coal (1, 10).

Mayumi *et al.* now show that methanogens from the genus *Methermicoccus* can convert coal-derived methoxylated compounds (R-O-CH₃) directly into methane. These methanogens, thus, bypass the entire microbial food chain. The authors report that 35 different methoxylated organic molecules are substrates for direct methane production by a culture of *Methermicoccus* isolated from a high-temperature oil reservoir. *Methermicoccus*, thus, has even more different substrates than the metabolically versatile metha-

nogen *Methanosarcina*; however, *Methermicoccus* cannot grow on acetate or H₂/CO₂.

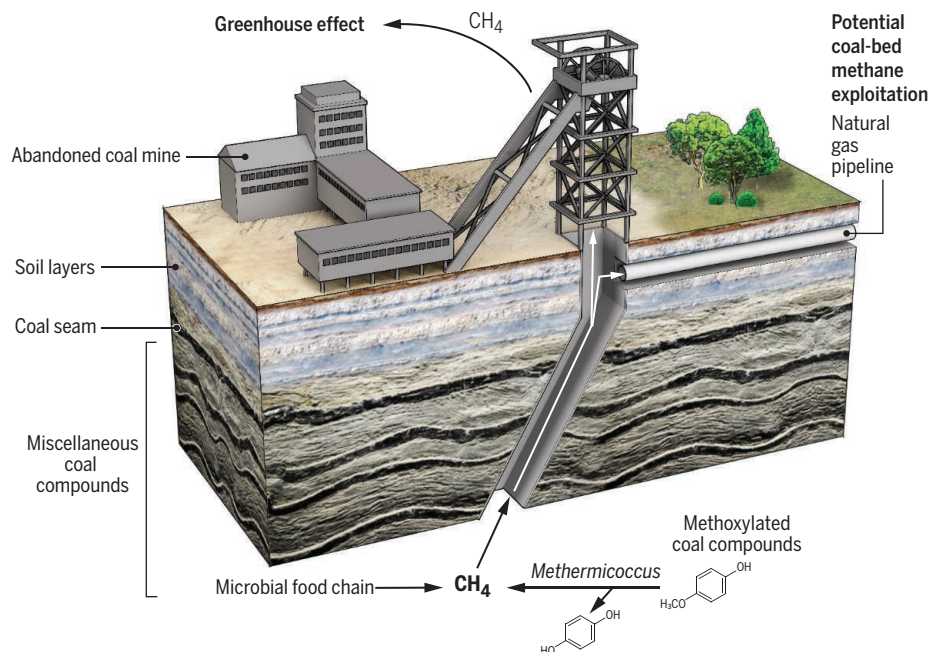
Methermicoccus seem to have an entirely different metabolism than other methanogens. In this metabolism, methyl groups of the methoxy moieties are removed by O-demethylation and used to build acetyl coenzyme A, which disproportionates to methane and carbon dioxide. This “methoxydotrophic methanogenesis” involves as yet unidentified methyl transferase enzymes not previously detected in methanogens. These exciting findings show that, even in the metagenomics era, cultivation of fastidious microorganisms is necessary to discover novel types of metabolism.

The discovery that methanogens can use complex organic compounds for methanogenesis opens up exciting opportunities for research and applications. Earth's subsurface harbors large reservoirs of sedimentary organic matter derived from lignin of higher plants, including methoxylated organic compounds. Methane is produced in the deep subsurface (11), but it is unknown whether methoxydotrophic or other yet unidentified methanogenic pathways play a role. If methane can be directly produced from methoxylated organic compounds in coal, which other complex organic compounds might be substrates for as yet unidentified methanogens?

Finally, coal-bed methane may become an economical alternative to shale gas, which is exploited through hydraulic fracturing (“fracking”). At the moment, methane production rates from coal beds are too low to allow cost-efficient exploitation (12), but understanding the biological mechanism of methane generation from coal—of which methoxydotrophic methanogenesis is an exciting part—may provide important clues. ■

Methane from coal

Coal seams produce natural gas (methane) through the activity of microbial food chains or the methanogen *Methermicoccus* discovered by Mayumi *et al.*



REFERENCES

1. D. Strapoč *et al.*, *Annu. Rev. Earth Planet. Sci.* **39**, 617 (2011).
2. M. Krüger *et al.*, *Geomicrobiol. J.* **25**, 315 (2008).
3. D. Mayumi *et al.*, *Science* **354**, 222 (2016).
4. R. K. Thauer, A. K. Kaster, H. Seedorf, W. Buckel, R. Hedderich, *Nat. Rev. Microbiol.* **6**, 579 (2008).
5. R. M. Fakoussa, M. Hofrichter, *Appl. Microbiol. Biotechnol.* **52**, 25 (1999).
6. F. Gründler *et al.*, *Front. Microbiol.* **6**, 200 (2015).
7. C. E. Lawson *et al.*, *Appl. Environ. Microbiol.* **81**, 7924 (2015).
8. D. Strapoč *et al.*, *Appl. Environ. Microbiol.* **74**, 2424 (2008).
9. S. Beckmann *et al.*, *Appl. Environ. Microbiol.* **77**, 3749 (2011).
10. S. J. Robbins, P. N. Evans, J. S. Esterle, S. D. Golding, G. W. Tyson, *Int. J. Coal Geol.* **154**, 205 (2016).
11. F. Inagaki *et al.*, *Science* **349**, 420 (2015).
12. D. Ritter *et al.*, *Int. J. Coal Geol.* **146**, 28 (2015).

10.1126/science.aai8101

MARINE CONSERVATION POLICY

Science-based management in decline in the Southern Ocean

The burden of proof is being turned upside down

By **Cassandra M. Brooks,¹ Larry B. Crowder,^{1,2} Lisa M. Curran,¹ Robert B. Dunbar,¹ David G. Ainley,³ Klaus J. Dodds,⁴ Kristina M. Gjerde,⁵ U. Rashid Sumaila⁶**

With an internationally lauded approach to conserving Southern Ocean ecosystems (1), the healthiest marine ecosystems on Earth, the Commission on the Conservation of Antarctic Marine Living Resources (CCAMLR), has committed to adopting marine protected areas (MPAs) in the waters around Antarctica (2). But conflict over MPAs has led CCAMLR member states to disregard the best available science, distort the foundational rules of their convention, break trust, and threaten the integrity of one of the world's most well-regarded science-based multinational governance efforts. With negotiations resuming at the CCAMLR meeting beginning 17 October, we offer recommendations aimed at implementing effective Southern Ocean MPAs, upholding CCAMLR's mandate, and maintaining its global leadership in ecosystem-based management. Given the historic conservation and diplomatic success of CCAMLR and Antarctic governance writ large, if we cannot adopt meaningful MPAs in the Southern Ocean, it does not bode well for doing so in the rest of the high seas.

EXEMPLARY SCIENCE-BASED MANAGEMENT

Antarctica is exceptional. The coldest, windiest, most pristine, and most remote continent is set aside by the Antarctic Treaty System (ATS) as a global commons dedicated to peace and science (3). The Convention on the Conservation of Antarctic Marine Living Resources (CAMLRL Convention) is the arm of the ATS that governs the use of marine life

in the ocean surrounding the continent (see the figure). Its primary objective is conservation, defined to include "rational use," which permits fishing by CCAMLR's 24 member states (plus the European Union) but only under conservation principles of precautionary, ecosystem-based management (1, 4). All management decisions require consensus, and that management takes full account of the best scientific information available, as determined by CCAMLR's Scientific Committee, an advisory body composed of international scientists (4). Commercial fishing is only permitted in regions where CCAMLR has developed scientifically grounded rules (e.g., total allowable catch) via consensus. Almost half of the CCAMLR area is closed to fishing on a year-to-year basis due to lack of data to support fishing, conservation rules to protect benthos, lack of known fish stocks, extensive ice, or other reasons.

"The Commission has a critical window of opportunity to uphold its status as a leader in resource management."

CCAMLR's exemplary management exceeds best practices for regional fisheries management organizations (1). CCAMLR operates by ecological rather than political boundaries in that it manages a discrete ecosystem, the Southern Ocean defined as south of the Antarctic Convergence, as demanded by the scientists who crafted the CAMLR Convention (see the figure). Successes include implementing management for Antarctic krill (*Euphasia superba*) that includes precautionary catch limits and monitoring for effects on krill predators and dramatically reducing illegal, unregulated, and unreported fishing in the Southern Ocean (1, 5).

In 2002, in line with this leadership, CCAMLR committed to designating a network of MPAs in the Southern Ocean (2). MPAs are broadly recognized as invaluable tools to assess, manage, and mitigate negative human effects and maintain biodiversity

(6). CCAMLR scientists identified priority areas for protection (2), and commission states mandated that MPAs be based on the best available science, protect key ecosystem processes, habitats, and biodiversity, and include scientific reference areas to monitor long-term effects of fishing and climate change (7).

The Antarctic is changing rapidly with potential global repercussions for sea-level rise, ocean circulation, and climate regulation. Locally, climate change is driving fluctuations in ice cover, shifts in population distributions, and alterations in primary productivity (8). Declines of ice-dependent Antarctic krill are potentially causing cascades throughout the ecosystem (8). Still, many CCAMLR fishing States advocate for increased catches of krill and toothfish (9). With decreases in ice and krill, fishing vessels are increasingly encroaching upon penguin and whale foraging grounds, compounding climate change stressors (10). To meet rising demands for toothfish (*Dissostichus eleginoides* and *D. mawsoni*) sold as lucrative "Chilean sea bass," fishers have pushed for higher catches and expanding fishing grounds (2, 9). Ecological repercussions of removing toothfish, the region's top fish predator, are unknown (11).

COMPROMISING PROTECTIONS

Moving toward an MPA network, CCAMLR adopted the world's first high seas MPA near the South Orkney Islands in 2009 (see the figure). Although the stated goal of the MPA is biodiversity conservation, conflicts between

preservation and fishing access produced a compromised result. The modified MPA excluded areas of highest ecological value to avoid conflict with commercial krill fisheries operated by several CCAMLR States (2) (see the figure). Japan, with the endorsement of South Korea and

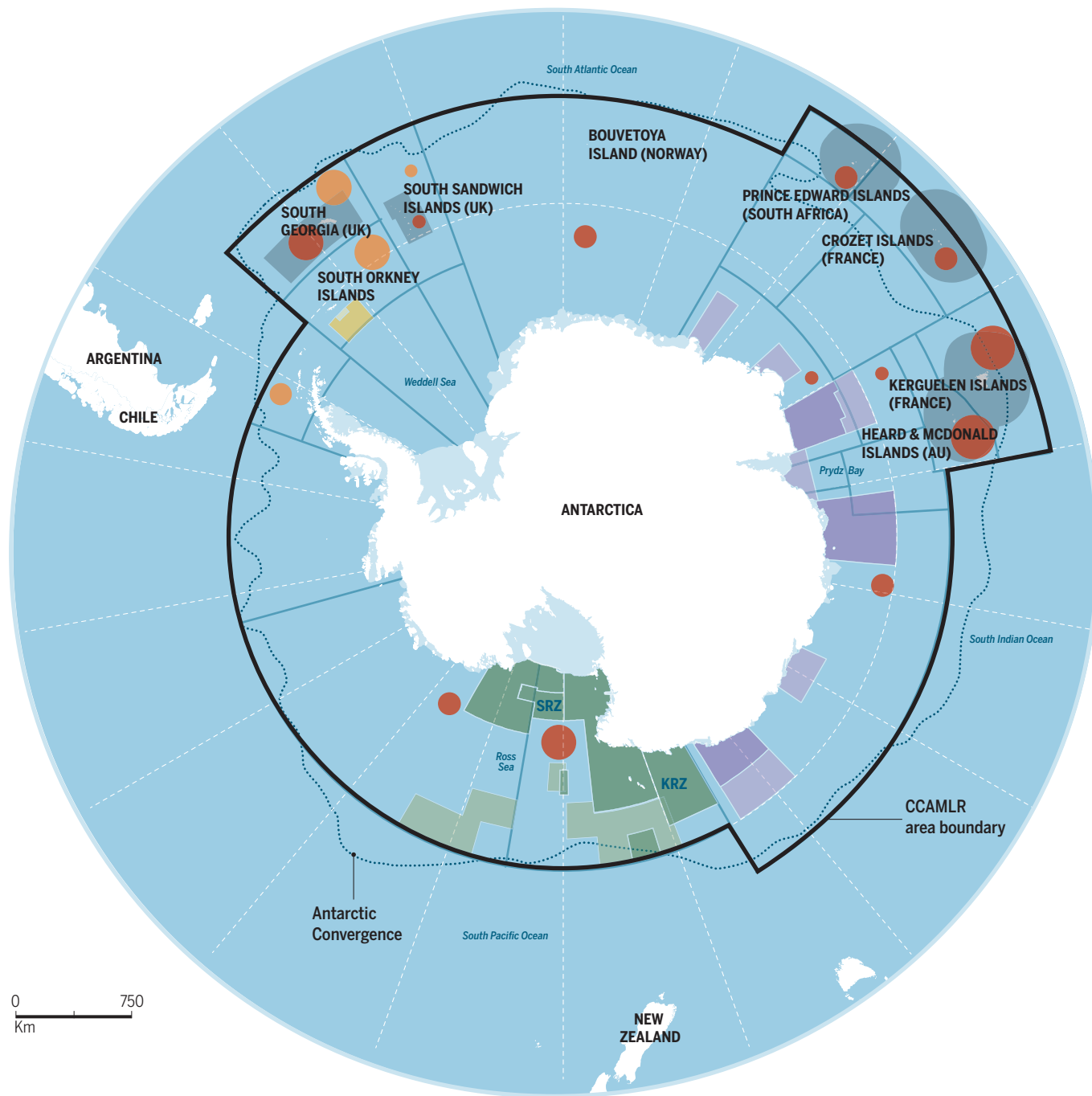
Russia, stated that "the amended MPA constitutes a good precedent" (12) because fisheries were not restricted. Other states objected to "the notion...that MPAs and fishing activities should be mutually exclusive" (12).

In 2012, CCAMLR considered MPA proposals in the Ross Sea and the East Antarctic. Both proposals were designed to protect ecological structure and function, with reference areas for evaluating climate change and fishery impacts, and both were deemed to be based on the best available science (2). Yet by 2015, the areas proposed for protection in the Ross Sea and the East Antarctic were reduced by 30 and 50%, respectively, with ecologically important areas omitted to enable fishing access (see the figure and fig. S1). Research fishing zones, which permit commercial fishing for toothfish and/or krill with additional requirements (e.g., increased fish tagging), were added to the Ross Sea MPA. These

¹Stanford University, Palo Alto, CA 94305, USA. ²The Center for Ocean Solutions, Monterey, CA 93940, USA. ³H. T. Harvey and Associates, Los Gatos, CA 95032, USA. ⁴Royal Holloway, University of London, London, UK. ⁵IUCN Global Marine and Polar Programme and World Commission on Protected Areas, Cambridge, MA 02138, USA. ⁶University of British Columbia, Vancouver, BC, Canada. Email: cbrooks1@stanford.edu

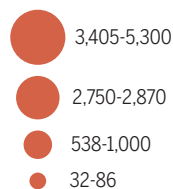
Fisheries and proposed marine protected areas in the Southern Ocean

CCAMLR's MPA concessions from 2012 to 2015. Total Allowable Catch (TAC) circle location is specified per subarea and does not represent the actual location of catch. CCAMLR boundaries, adopted MPA, and fisheries data from (18); Ross Sea MPA boundaries based on (19); East Antarctic MPA boundaries based on (20).

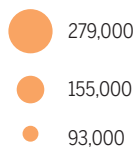


Captures in metric tons

Toothfish TAC 2015–16



Krill TAC 2015–16



- Nationally managed areas
- CCAMLR statistical subareas and divisions
- SRZ Special Research Zone
- KRZ Krill Research Zone

- 2012 Proposed East Antarctic MPA
- 2015 Proposed East Antarctic MPA
- 2012 Proposed Ross Sea MPA (- KRZ)
- 2015 Proposed Ross Sea MPA
- 2009 Proposed South Orkney MPA
- Adopted South Orkney MPA

fishing zones encompassed foraging grounds for seabirds and whales and jeopardized a scientific reference area that had been proposed to measure fishery ecosystem effects (2) (fig. S1). Even though the East Antarctic MPA proposal employs a multi-use approach, it omitted no-take zones, and the area of highest conservation value, Prydz Bay, was removed during negotiations (see the figure).

Temporal concessions, or “sunset clauses,” have marred negotiations. MPAs are usually established in perpetuity, and their duration has been linked to ecosystem benefits (6). The largely terrestrial protected areas adopted via the Antarctic Treaty are permanent, as are nationally designated subantarctic MPAs. Although duration was not discussed during the 2009 South Orkney MPA negotiations, it has become a major barrier to consensus, with many CCAMLR fishing states asserting that MPAs must include an expiration date. China proposed a limit of 20 years (9), shorter than the life spans of most Antarctic top predators and inconsistent with the stated goals of the MPAs, as well as CCAMLR’s provisions for rational use. As of 2015, the proposed Ross Sea and East Antarctic MPAs have 50- and 30-year expiration dates, respectively.

Current MPA proposals only prohibit fishing in 3.2% of CCAMLR’s waters (see the figure) for a fixed period of time, yet consensus still lags. Past conservation successes in CCAMLR depended on having an open political window of opportunity, trust within the Commission, and alignment of incentives among member states (5). Yet, currently, states have become entrenched in their positions for or against MPAs, breaking trust. States blocking adoption of MPAs continue to do so even after concessions were made to meet those states’ requests (9), not negotiating in good faith. Negotiations have been tainted by geopolitical disputes elsewhere in the world (e.g., United States–Russia tensions over Crimea) (13). States proposing MPAs in their former territories have been accused of using political rather than ecological boundaries as a tool for asserting sovereignty (14).

This stalemate may reflect the scramble for Southern Ocean resources as other fisheries become less productive (13). As a commons, the Southern Ocean continues to be a contested space. Although CCAMLR was historically composed mainly of states without active fisheries in the Southern Ocean, membership has grown, member stances on fishing have changed, and it is now dominated by fishing states (2) whose national positions reflect intent on economic gain and asserting power while securing future access by occupying the Southern Ocean via fishing (13).

The idea of “rational use”—defined in the Convention as a mandate to employ precaution in resource exploitation, a critical part

of conservation—is being reinterpreted by several states to defend an unequivocal right to fish and to argue against MPAs that in any way restrict fishing access (15). Although CCAMLR’s historic precautionary management paradigm was not to allow fishing unless sufficient data was available to manage the fishery, MPA opponents are reversing the burden of proof, demanding that sufficient data be available to show that fishing is damaging the ecosystem to warrant an MPA that restricts fishing (9). If the current amended proposals are adopted, their concessions will compromise MPA effectiveness, thus undermining the conservation mandate of CCAMLR and the implementation of science-based marine management broadly.

STABILIZING A KEYSTONE AGREEMENT

The Commission has a critical window of opportunity to uphold its status as a leader in resource management. We offer five recommendations for the upcoming meeting.

Endorse only MPAs that are designed with the best available science and combine no-take areas with effective enforcement. Ineffective MPAs that only “protect” ocean areas that may not have otherwise been heavily fished anyway undermine CCAMLR’s mandated best practices (7) and credibility while impairing the value of MPAs as a management tool.

Establish MPAs in perpetuity. CCAMLR’s MPA rules specify, “the period of designation...shall be consistent with the specific objectives of the MPA” (7). Proposed arbitrary sunset clauses of 20 to 30 years are insufficient for achieving MPA conservation objectives. Further, they will not meet internationally established criteria for protected areas (16) and thus may not qualify toward global MPA targets.

Uphold CCAMLR’s mandate. The Convention was designed as a conservation convention with fisheries management grounded in precautionary and ecosystem-based approaches (4). The use of closed areas “for purposes of scientific study or conservation” (4) is an essential component of ecosystem-based management. Redefinition of “conservation” as an unequivocal right to fish compromises the purpose of MPAs and the integrity of the Southern Ocean ecosystem and the high seas beyond.

Rebuild trust through science. The historic diplomatic and environmental success of CCAMLR and the broader ATS is fundamentally rooted in science (3). Science-based decision-making provides transparency and credibility and can reduce geopolitics within the forum. In adhering to its mandate for making conservation decisions based on the best available science, CCAMLR can rebuild trust and progress for MPA negotiations.

Demonstrate leadership. In adopting effective MPAs in the Ross Sea and the East Antarctic, CCAMLR could protect more than 2 million km², 6% of the Southern Ocean. With proposals for additional MPAs under way, CCAMLR could become the first international marine management organization to meet global protection targets agreed to by the Convention on Biological Diversity (10% of waters protected by 2020) (17), of which almost all CCAMLR states are members. This precedent would inform the current United Nations’ development of a legally binding agreement for conserving marine biodiversity beyond national jurisdiction (17) and influence governance of emerging resource frontiers (e.g., the Arctic). In upholding CCAMLR’s charter, member states could safeguard Southern Ocean ecosystems and avoid destabilizing a keystone of science-based international environmental agreements. ■

REFERENCES AND NOTES

1. D. G. Miller, N. M. Slicer, in *Governance of Marine Fisheries and Biodiversity Conservation* (Wiley Blackwell, Hoboken, NJ, 2014), chap. 18.
2. C. M. Brooks, *Polar J.* **3**, 277 (2013).
3. P. Berkman, M. Lang, W. Walton, O. Young, *Science Diplomacy: Antarctica, Science and the Governance of International Spaces* (Smithsonian Institution Scholarly Press, Washington, DC, 2011).
4. The Convention on the Conservation of Marine Living Resources, Canberra, Australia, 7 to 20 May 1980.
5. H. R. Osterblom, U. R. Sumaila, *Glob. Environ. Change* **21**, 972 (2011).
6. G. J. Edgar *et al.*, *Nature* **506**, 216 (2014).
7. CCAMLR, “Conservation Measure 91-04,” in General Framework for the establishment of CCAMLR Marine Protected Areas (CCAMLR, 2011).
8. O. Schofield *et al.*, *Science* **328**, 1520 (2010).
9. CCAMLR, “Report of the XXXIV Meeting of the Commission,” Hobart Australia, 19 to 30 October 2015 (CCAMLR, 2015).
10. W. Z. Trivelpiece *et al.*, *Proc. Natl. Acad. Sci. U.S.A.* **108**, 7625 (2011).
11. P. A. Abrams *et al.*, *Fish Fish.* **2016**, 10.1111/faf.12162 (2016).
12. CCAMLR, “Report of the XXVIII Meeting of the Commission,” Hobart Australia, 26 October to 6 November 2009 (2009).
13. K. Dodds, M. Nuttall, *The Scramble for the Poles* (Polity Press, Boston, MA, 2016).
14. V. V. Lukin, *Polar J.* **4**, 199 (2014).
15. J. Jacquet *et al.*, *Mar. Policy* **63**, 28 (2016).
16. J. C. Day *et al.*, “Guidelines for Applying the IUCN Protected Area Management Categories to MPAs” (IUCN, Gland, Switzerland, 2012).
17. K. M. Gjerde *et al.*, *Aquat. Conserv.* **26**, 45 (2016).
18. CCAMLR (2016); www.ccamlr.org.
19. New Zealand Foreign Affairs and Trade (2016); <https://mfat.govt.nz/en/environment/antarctica/ross-sea-region-marine-protected-area-proposal/>.
20. Australian Antarctic Division, Department of the Environment and Energy (Australian government, 2016); www.antarctica.gov.au/law-and-treaty/ccamlr/marine-protected-areas.

ACKNOWLEDGMENTS

We acknowledge support from the Price Fellowship and the Switzer Foundation (C.M.B.), the Center for Ocean Solutions (L.B.C.), the National Science Foundation (D.G.A. and R.B.D.), and OceanCanada (U.R.S.). We thank D. G. Miller, M. R. Caldwell, John B. Weller, and two anonymous reviewers for helpful comments on the manuscript. We thank the CCAMLR Secretariat, Commission States, and the Antarctic and Southern Ocean Coalition for allowing C.M.B. participant observation. CCAMLR meeting reports, papers, and fisheries data are available online at www.ccamlr.org.

SUPPLEMENTARY MATERIALS

www.sciencemag.org/content/354/6309/185/suppl/DC1

10.1126/science.aah4119



EXHIBITION

Asylums and after

A new exhibition probes the ever-evolving treatment of mental illness

By **Andrew Robinson**

Vincent van Gogh's only etching forms a small but profoundly significant part of *Bedlam: The Asylum and Beyond*, the Wellcome Collection's mind-stretching new exhibition on madness and the history of its treatment. It is a melancholy portrait of Paul Gachet, a professional physician and amateur painter who treated van Gogh after his release from a famously productive year spent in a French mental asylum in 1889–1890.

According to the exhibition's caption, van Gogh referred to Gachet as “a ready-made friend and something like a new brother ... he's very nervous and very bizarre himself.” But in a letter from van Gogh to his actual brother Theo, he wrote, “I think that we must not count on Dr. Gachet at all. First of all, he is sicker than I am, I think, or shall we say just as much.... Now when one blind man leads another blind man, don't they both fall into the ditch?” (1).

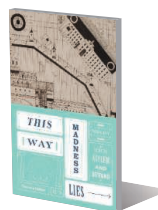
Such insights from a great but mentally ill artist remind us how difficult it has been—and still is—to fix a boundary between sanity and insanity. Would today's physicians, with their arsenal of brain-scanning techniques and mood-changing drugs, have had more success than Gachet in curing van Gogh? Prob-

Bedlam

The Asylum and Beyond
Wellcome Collection, London.
Through 15 January 2017.
<http://wellcomecollection.org/bedlam>

This Way Madness Lies

The Asylum and Beyond
Mike Jay
Thames & Hudson, 2016. 256 pp.



ably not, according to *Bedlam*, as Mike Jay, one of the exhibition's two curators, implies in *This Way Madness Lies*, his illuminating, generously illustrated book that accompanies the exhibition. In the 21st century, as much as in the 17th century, writes Jay, “physicians, apothecaries, astrologers, preachers and folk healers competed with remedies that ranged from gentle herbs to powerful poisons, from horoscopes to exorcisms to cranial surgery.”

The exhibition's linking thread is the history of London's Bethlem hospital, originally founded in the 13th century as a priory dedicated to St. Mary of Bethlehem. By the time of Shakespeare in the late 16th century, Bethlem had ceased to be a peaceful cloister and was filled with cell blocks. Its atmosphere was crowded and noisy—hence its popular name, *Bedlam*, among the London public, who were permitted to visit and observe the inmates at the “madhouse” until 1770.

Although Bethlem survived London's Great Fire in 1666, it moved to a new site at Moor-

A precursor to the modern practice of “Care in the Community.” Mentally ill boarders have lived alongside locals in Geel, Belgium, for centuries.

fields, where a palatial building designed by Robert Hooke was built in 1676. After being condemned for its scandalously inhumane conditions, it moved again in 1815 to a new building in south London, which today houses the Imperial War Museum. Finally, in 1930, it relocated to a semirural estate on the outskirts of the city at Beckenham, where it continues as a respected National Health Service hospital, still dedicated to mental illness.

In advance of the 1815 move, James Tilly Matthews, a tea merchant who had been incarcerated at Bethlem after publicly accusing members of the British government of treason, came up with a set of architectural drawings for the new facility and detailed proposals for its reform. Matthews's plans, which are on display in the exhibition, included spacious grounds where the inmates could work as gardeners rather than being confined indoors—in some cases shackled—with nothing to do. With a new regime of therapeutic harmony between inmates and wardens, he argued, recovery rates would naturally rise. But the medical world was not willing to take advice from a “lunatic,” and Matthews's prescient redesign was rejected.

The reform of “madhouses” into more compassionate “asylums” took place during the 19th century in Britain, France, and some other parts of Europe. In the 20th century, art therapy became important. One of several compelling films in the exhibition, *Abandoned Goods* by Pia Borg and Edward Lawrenson, reveals the art produced by inmates of the Netherne Asylum under the pioneering encouragement of Edward Adamson in the 1940s. Many of these works were lost when the asylum closed in 1993; the remainder were abandoned in another hospital, but almost all of them—more than 5500 paintings, drawings, sculptures, and ceramics—were eventually relocated to the Adamson Collection at the Wellcome Library.

In postwar Britain, mental asylums were increasingly felt to be outmoded relics of the Victorian period and were closed for redevelopment. But are their current substitutes—today's psychiatric hospitals for those who are wholly incapable of looking after themselves, along with sedated “care in the community” for the rest—a definite improvement? The evidence offered by *Bedlam* is hardly reassuring. ■

REFERENCES

1. Letter from Vincent van Gogh to Theo van Gogh, Auvers-sur-Oise, 10 July 1890; www.webexhibits.org/vangogh/letter/21/648.htm.

10.1126/science.aah4751

The reviewer is the author of *Sudden Genius? The Gradual Path to Creative Breakthroughs*, Oxford University Press, 2010. Email: andrew@andrew-robinson.org

GENETIC ENGINEERING

The mythology of CRISPR

An optimistic outlook on gene editing seeks to reconcile scientific progress with wisdom from the humanities

By George J. Annas

The new CRISPR (clustered regularly interspaced short palindromic repeats) genome-editing technology has already spawned a series of start-ups, a major patent dispute, international meetings on ways to regulate it (or not), controversial articles (1), and a nascent discussion of using it to make a “better baby.” In *Modern Prometheus*, science writer and sometime genetics researcher Jim Kozubek covers all of these topics, but with a goal of conveying more than just the story of CRISPR. Writing “in the spirit of Shelley, Keats and Nietzsche,” Kozubek seeks “to show that something is at stake that is more real than our science.”

Modern Prometheus references the subtitle of Mary Shelley’s *Frankenstein*, which cogently tells the story of a scientist who is incapable of controlling his creation: a humanoid life-form brought into being through artificial means. Prometheus—the mythological Greek Titan—brought useful arts to humankind but could not prevent his brother’s wife, Pandora, from opening a present from the vengeful Zeus. Pandora unleashed Zeus’ “gifts,” including sickness, insanity, old age, vice, and passion.

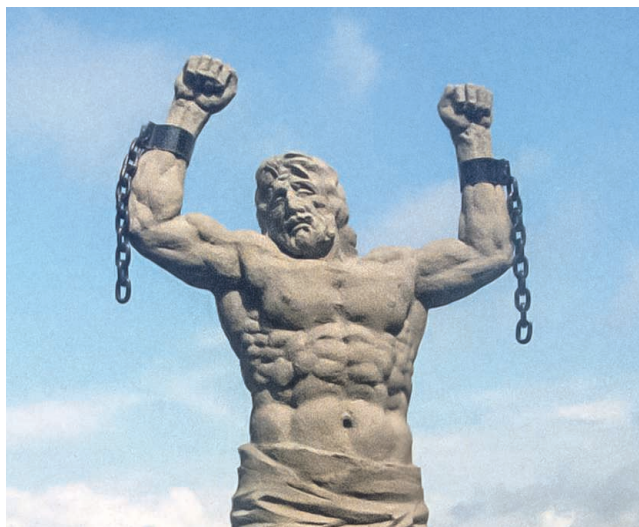
Hubris and overreaching led to Prometheus’ fall, and overreaching remains a danger to today’s researchers. Kozubek quotes George Church, who observed that “many classic Greek heroes were invulnerable, except to self-inflicted wounds.”

The biotech industry tends to look at life’s unwanted gifts as problems to be solved, rather than as fundamental characteristics of the human condition. In this context, CRISPR is seen as simply a useful new tool, rather than as a potential new danger to humanity.

But the core challenge that CRISPR presents to the world is not which biotech start-up can make the most money from

it or who will get the patent. Rather, it is what the new technology means to the human species. Is it a technology that alters our understanding of humanity and opens the door to a neo-eugenics agenda that could threaten the survival of the species? If so, global, democratically based oversight is in order. Or is it, as many scientists quoted in this book argue, just another medical technology that cannot be stopped and should be regulated, if at all, like any new drug or device?

Although scientists alone cannot answer these questions, they have made at least



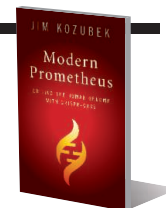
Like the “gifts” Pandora unleashed into the world, cheap, easy-to-use gene editing technologies will likely be difficult to contain, cautions Jim Kozubek.

two noteworthy attempts to do so. The first was the 1975 Asilomar conference, which sought to determine how to respond to the potential dangers of recombinant DNA technology. The second is ongoing and includes the December 2015 National Academy of Sciences meeting in Washington, D.C., which attempted to outline the implications of CRISPR. Both, I think, are evidence in support of the idea that scientists tend to believe that scientific progress is always good and that whatever dangers “progress” poses can best be managed by scientists themselves. This view represents what Kozubek describes as the containment myth, often illustrated in literature by the creation of “a rogue genetically engineered species, such as in *The Androm-*

Modern Prometheus
Editing the Human Genome
with CRISPR-CAS9

Jim Kozubek

Cambridge University Press,
2016. 452 pp.



eda Strain, The Stand or Jurassic Park.”

Kozubek labors valiantly to synthesize science and the humanities but, at least at times, underestimates the changes that have occurred since both cultures adopted market values. These include radical amplification in commercialization, public relations, public-private funding, and presentation.

The scientists who appear in the book sometimes seem to speak in sound bites and the overpromising language of advertising, and venture capitalists and lawyers are seen as competent to opine on science.

Kozubek, for example, seems to accept unquestioningly the optimistic pronouncement that we are “entering a revolution so profound we might reset the calendars to begin in 1953,” as asserted by a biotech investor with billions at stake in the success of synthetic biology.

The utopian libertarian view of our future that emerges is at least partially a result of the author’s oversampling of scientists from the Harvard/MIT/Kendall Square area. (Kozubek worked as a staff scientist at Brigham and Women’s Hospital from 2013 to 2016.) There are, nonetheless, enough opinions among the 40 scientists and other experts whom the author interviewed that readers will find many to agree with and certainly some to disagree with.

It is too soon to write a history of CRISPR. Kozubek nonetheless gives the general reader a solid introduction to the current state of affairs, as seen by its creators and those who are using it in research and commerce. His reporting confirms that there is no existing democratic global governance mechanism capable of regulating gene editing and that commerce-driven self-regulation is likely to treat potential benefits as certainties and potential harms as speculative. The lack of any meaningful species-level oversight is problematic and potentially dangerous. ■

REFERENCES

1. E. Lander, *Cell* **164**, 18 (2016).

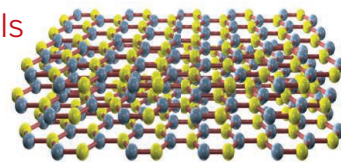
10.1126/science.aai7691

The reviewer is director of the Center for Health Law, Ethics, and Human Rights, Boston University School of Public Health, Boston, MA 02118, USA. Email: annasgj@bu.edu

RESEARCH

Van der Waals materials for nanophotonics

Basov et al., p. 195



IN SCIENCE JOURNALS

Edited by **Caroline Ash**

FOREST ECOLOGY

Global biodiversity and productivity

The relationship between biodiversity and ecosystem productivity has been explored in detail in herbaceous vegetation, but patterns in forests are far less well understood. Liang *et al.* have amassed a global forest data set from >770,000 sample plots in 44 countries. A positive and consistent relationship can be discerned between tree diversity and ecosystem productivity at landscape, country, and ecoregion scales. On average, a 10% loss in biodiversity leads to a 3% loss in productivity. This means that the economic value of maintaining biodiversity for the sake of global forest productivity is more than fivefold greater than global conservation costs. —AMS

Science, this issue p. 196

Loss of forest
diversity leads to a
loss of productivity.

SOLAR CELLS

Improving the stability of perovskite solar cells

Inorganic-organic perovskite solar cells have poor long-term stability because ultraviolet light and humidity degrade these materials. Bella *et al.* show that coating the cells with a water-proof fluorinated polymer that contains pigments to absorb ultraviolet light and re-emit it in the visible range can boost cell efficiency and limit photodegradation. The performance and stability of inorganic-organic perovskite solar cells are also limited by the size of the cations required for forming a correct lattice. Saliba *et al.* show that the rubidium cation, which is too small to form a perovskite by itself, can form a lattice with cesium and organic cations. Solar cells based on these materials have efficiencies exceeding

20% for over 500 hours if given environmental protection by a polymer coating. —PDS

Science, this issue pp. 203 and 206

VACCINES

A DNA vaccine candidate for Zika

The ongoing Zika epidemic in the Americas and the Caribbean urgently needs a protective vaccine. Two DNA vaccines composed of the genes that encode the structural premembrane and envelope proteins of Zika virus have been tested in monkeys. Dowd *et al.* show that two doses of vaccine given intramuscularly completely protected 17 of 18 animals against Zika virus challenge. A single low dose of vaccine was not protective but did reduce viral loads. Protection correlated with serum antibody neutralizing activity. Phase I clinical trials

testing these vaccines are already ongoing. —KLM

Science, this issue p. 237

PALEOBIOLOGY

The platypus's sixth sense cost it its teeth

The platypus, *Ornithorhynchus anatinus*, has an electromechanical sensory apparatus in its bill. The sixth sense endowed by its remarkable bill allows the platypus to detect prey in murky

waters with its eyes closed. Using comparative morphology and imaging techniques, Asahara *et al.* mapped the enlarged infraorbital canal that contains all the nerves and vessels that supply the bill. It seems that the evolution of this anatomical arrangement has limited space for the roots of teeth in modern platypuses. Platypuses can still "chew" their prey with horny pads. —SN

Sci. Adv. 10.1126/sciadv.1601329 (2016).



Platypuses use an electrical sixth sense to seek prey.

SIGNAL TRANSDUCTION

A function for multisite phosphorylation

Many transcription factors are regulated by phosphorylation on multiple residues. Mylona *et al.* analyzed multisite phosphorylation in the transcription factor Elk-1 and showed that it may protect against excessive activation (see the Perspective by Whitmarsh and Davis). Phosphorylation by the kinase ERK2 occurred at eight sites, but the sites were phosphorylated at different rates. Those that were phosphorylated more quickly promoted transcriptional activation. Those that were phosphorylated more slowly dampened excessive activation by ERK2s without needing a phosphatase or any other negative regulatory component. —LBR

Science, this issue p. 233;
see also p. 179

PROTEIN EVOLUTION

Phosphorylation and fungal evolution

Phosphorylation after transcription modifies the activity of proteins. To understand how phosphorylation sites have evolved, Studer *et al.* studied a range of fungal species (see the Perspective by Matalon *et al.*). Only a few sites were apparently present in the common ancestor of all 18 species investigated. Evolutionary age appeared to predict the potential functional importance of specific conserved phosphosites. —LMZ

Science, this issue p. 229;
see also p. 176

HIV-1 THERAPY

Antibodies sustain viral control

For many infected individuals, antiretroviral therapy (ART) means that an HIV-1 diagnosis is no longer a death sentence. But the virus persists in treated individuals, and complying with the intense drug regimen to keep virus loads

down can be challenging for patients. Seeking an alternative, Byraredy *et al.* treated ART-suppressed monkeys with antibodies targeting $\alpha 4\beta 7$ integrin. When ART was halted in the antibody-treated animals, viral loads stayed undetectable, and normal CD4 T cell counts were maintained for over 9 months—and persisted—even after stopping the antibody therapy. —KLM

Science, this issue p. 197

BIOPHYSICS

Two roads diverged in a yellow photolyase

Photolyase enzymes repair DNA that has been damaged by ultraviolet sunlight. The repair process begins when blue light absorption by a cofactor drives an electron transfer step. Zhang *et al.* applied ultrafast absorption spectroscopy to study the dynamics of this step. A bifurcation in the electron transfer pathway favors a direct tunneling mechanism in the prokaryotic enzymes and a two-step hopping mechanism in the eukaryotic variety. This difference explains the higher repair quantum yield seen in prokaryotes. —JSY

Science, this issue p. 209

SICKLE CELL DISEASE

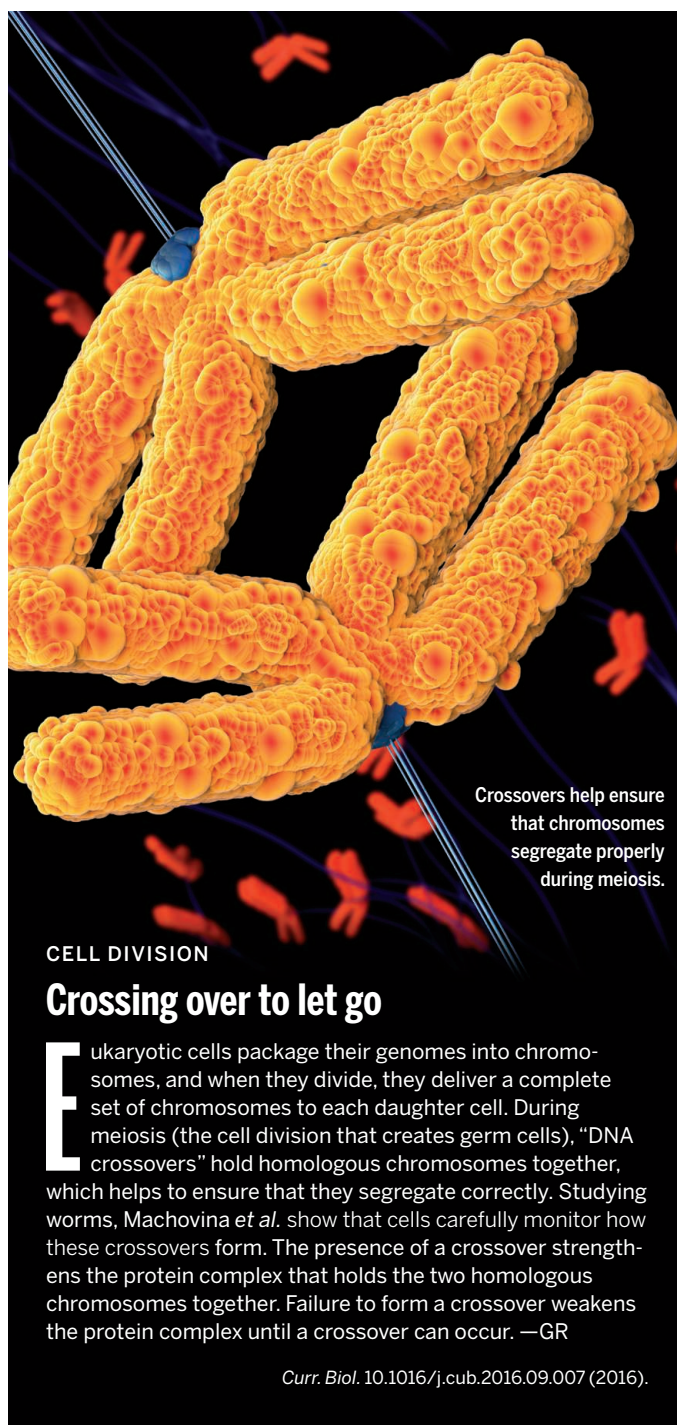
Hammering out the sickle cell mutation

Sickle cell disease is a genetic disorder caused by a mutation in one of the hemoglobin genes. This causes deformation of red blood cells and results in occlusion of blood vessels, severe pain, and progressive organ injury. To correct the mutation that causes this disease, De Witt *et al.* modified hematopoietic stem cells from sickle cell disease patients by using a CRISPR-Cas9 gene editing approach. The corrected cells successfully engrafted in a mouse and produced enough normal hemoglobin to indicate a potential clinical benefit in ameliorating sickle cell disease. —YN

Sci. Transl. Med. **8**, 360ra134 (2016).

IN OTHER JOURNALS

Edited by **Kristen Mueller**
and **Jesse Smith**



Crossovers help ensure that chromosomes segregate properly during meiosis.

CELL DIVISION

Crossing over to let go

Eukaryotic cells package their genomes into chromosomes, and when they divide, they deliver a complete set of chromosomes to each daughter cell. During meiosis (the cell division that creates germ cells), “DNA crossovers” hold homologous chromosomes together, which helps to ensure that they segregate correctly. Studying worms, Machovina *et al.* show that cells carefully monitor how these crossovers form. The presence of a crossover strengthens the protein complex that holds the two homologous chromosomes together. Failure to form a crossover weakens the protein complex until a crossover can occur. —GR

Curr. Biol. 10.1016/j.cub.2016.09.007 (2016).

BRAIN RESEARCH

Encoding false memories

A unique human ability is the use of concepts that confer meaning in an abstract way. Despite the importance of conceptual knowledge for human cognition,

scientists know little about the underlying neural mechanisms and structures. To better understand this process, Chadwick *et al.* scanned people’s brains while they performed tasks known to cause false memories in a statistically predictable manner.

ALSO IN SCIENCE JOURNALS

Edited by Caroline Ash

QUANTUM MATERIALS

A layered approach for nanophotonics

Nanophotonics aims to combine the speed of optics with the small size scale of electronics for ultrahigh-speed technology. However, several order differences in length scale have to be bridged. Basov *et al.* review how van der Waal materials, which are two-dimensional layered structures, can span such length-scale differences. The wide range of materials available, as well as their broad range of optical and electronic properties, offer opportunities to make devices with desirable optoelectronic functionality. —ISO

Science, this issue p. 195

POLITICAL SCIENCE

A consensus in Europe about asylum seekers

Violent conflicts between groups often generate large numbers of noncombatant refugees. Bansak *et al.* surveyed western European attitudes toward such asylum seekers. They found that voters favor applicants who will contribute to the recipient country's economy, who have suffered severe physical or mental distress rather than economic hardship, and who are Christian rather than Muslim. These preferences are similar across countries and independent of the voters' personal characteristics. —GJC

Science, this issue p. 217

GLOBAL CLIMATE CHANGE

An impactful event

Glassy silica spherules have been found in marine sediments from three sites across a wide area off the Atlantic coast of the United States, near the stratigraphic level of the Paleocene-Eocene boundary. The characteristics of these specimens are consistent with those of microtektites associated with extraterrestrial impact events. This discovery by Schaller *et al.* is evidence of an impact event at the time of the Paleocene-Eocene Thermal Maximum, a period during which global temperatures increased rapidly and the carbon cycle was substantially perturbed. —HJS

Science, this issue p. 225

MICROBIAL PHYSIOLOGY

Microbes make methane from coal

Methane associated with coal beds is an important global resource of natural gas. Much of the methane in coal comes from microbial methanogenesis. Mayumi *et al.* characterized a strain of *Methermicoccus shengliensis* that, unexpectedly, is capable of making methane from the dozens of methoxylated aromatic compounds found in a variety of coal types (see the Perspective by Welte). Isotope tracer experiments showed that this organism could also incorporate carbon dioxide into methane. —NW

Science, this issue p. 222;
see also p. 184

INFLUENZA

Migration of influenza in wild birds

Virus surveillance in wild birds could offer an early warning system that, combined with adequate farm hygiene, would lead to effective influenza control in poultry units. The Global Consortium for H5N8 and Related Influenza Viruses found that the H5 segment common to the highly pathogenic avian influenza viruses readily reassorts with other influenza viruses (see the Perspective by Russell). H5 is thus a continual source of new pathogenic variants. These data also show that the H5N8 virus that recently caused serious outbreaks in European and North American poultry farms came from migrant ducks, swans, and geese that meet at their Arctic breeding grounds. Because the virus is so infectious, culling wild birds is not an effective control measure. —CA

Science, this issue p. 213;
see also p. 174

CLIMATE CHANGE

The negative emissions gamble

Scenarios for how global warming can be kept below 2°C rely heavily on the large-scale use of technologies that remove carbon from the atmosphere. They are attractive to policymakers because they reduce the perceived need for reductions in carbon emissions in the short term. In a Perspective, Anderson and Peters argue that it may

not be possible or advisable to deploy these technologies at the scale required. For example, bioenergy with carbon capture and storage is seen as particularly promising, yet it would require vast areas of land that would then no longer be available for food production or for wildlife. By relying on these speculative technologies, humanity could miss a crucial window of opportunity for directly mitigating climate change. —JFU

Science, this issue p. 182

VASCULAR BIOLOGY

Relaxing in response to pressure

Small-diameter arteries link main arteries to capillary beds that feed tissues and organs. Persistent constriction of these arteries may generate high blood pressure (hypertension). Khavandi *et al.* (see also Hill and Braun) found that arterial constriction initiated the production of reactive oxygen species that oxidized and activated the kinase PKG, which opens a potassium channel that induces blood vessel relaxation. These results may explain why some drugs that generate reactive oxygen species are effective in treating hypertension. —WW

Sci. Signal. **9**, ra100 and fs15 (2016).

REVIEW SUMMARY

QUANTUM MATERIALS

Polaritons in van der Waals materials

D. N. Basov,* M. M. Fogler, F. J. García de Abajo

BACKGROUND: Light trapped at the nanoscale, deep below the optical wavelength, exhibits an increase in the associated electric field strength, which results in enhanced light-matter interaction. This leads to strong nonlinearities, large photonic forces, and enhanced emission and absorption probabilities. A practical approach toward nanoscale light trapping and manipulation is offered by interfaces separating media with permittivities of opposite signs. Such interfaces sustain hybrid light-matter modes involving collective oscillations of polarization charges in matter, hence the term polaritons. Surface plasmon polaritons, supported by electrons in metals, constitute a most-studied prominent example. Yet there are many other varieties of polaritons, including those formed by atomic vibrations in polar insulators, excitons in semiconductors, Cooper pairs in superconductors, and spin resonances in (anti) ferromagnets. Together, they span a broad region of the electromagnetic spectrum, ranging from microwave to ultraviolet wavelengths. We discuss polaritons in van der Waals (vdW) materials: layered systems in which individual atomic planes are bonded by weak vdW attraction (see the figure). This class of quantum materials includes graphene and other two-dimensional

crystals. In artificial structures assembled from dissimilar vdW atomic layers, polaritons associated with different constituents can interact to produce unique optical effects by design.

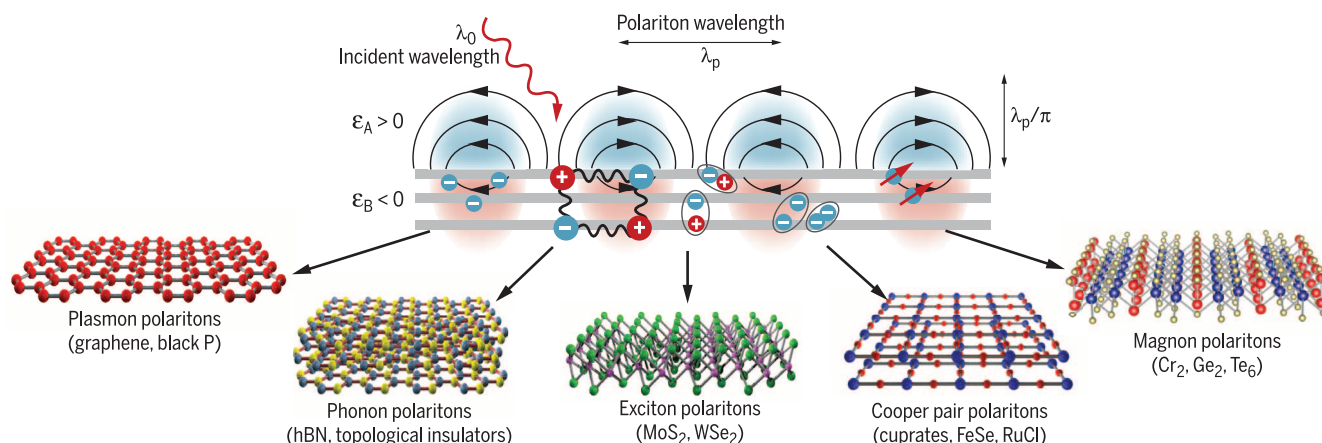
ADVANCES: vdW materials host a full suite of different polaritonic modes with the highest degree of confinement among all known materials. Advanced near-field imaging methods allow the polaritonic waves to be launched and visualized as they travel along vdW layers or through multilayered heterostructures. Spectroscopic and nano-imaging experiments have identified multiple routes toward manipulation of nano-optical phenomena endowed by polaritons. A virtue of polaritons in

vdW systems is their electrical tunability. Furthermore, in heterostructures assembled from dissimilar vdW layers, different brands of polaritons interact with each other, thus enabling unparalleled control of polaritonic response at the level of single atomic planes. New optoelectronic device concepts aimed at the detection, harvesting, emission, propagation, and modulation of light are becoming feasible as a result of combined synthesis, nanofabrication, and modeling of vdW systems. The extreme anisotropy of vdW systems leading to opposite signs of the

in-plane and out-of-plane permittivities of the same layered crystal enables efficient polaritonic waveguides, which are instrumental for subdiffractional focusing and imaging. In addition to near-field optical probes facilitating nanoimaging, coupling to polaritons can be accomplished via electrical excitation and nonlinear wave mixing.

OUTLOOK: Potential outcomes of polariton exploration in vdW heterostructures go beyond nano-optical technologies. In particular, images of polaritonic standing and traveling waves contain rich insights into quantum phenomena occurring in the host material supporting polaritons. This line of inquiry into fundamental physics through polaritonic observations constitutes an approach toward optics-based materials research. In particular, the strong spatial confinement exhibited by vdW polaritons involves large optical-field gradients—or equivalently, large momenta—which allows regions of the dispersion relations of electrons, phonons, and other condensed-matter excitations to be accessed beyond what is currently possible with conventional optics. Additionally, polaritons created by short and intense laser pulses add femtosecond resolution to the study of these phenomena. Alongside future advances in the understanding of the physics and interactions of vdW polaritons, solutions to application challenges may be anticipated in areas such as loss compensation, nanoscale lasing, quantum optics, and nanomanipulation. The field of vdW polaritonics is ripe for exploring genuinely unique physical scenarios and exploiting these new phenomena in technology. ■

The list of author affiliations is available in the full article online.
*Corresponding author. Email: db3056@columbia.edu
Cite this article as D. N. Basov *et al.*, *Science* 354, aag1992 (2016). DOI: 10.1126/science.aag1992



Polaritons in van der Waals (vdW) materials. Polaritons—a hybrid of light-matter oscillations—can originate in different physical phenomena: conduction electrons in graphene and topological insulators (surface plasmon polaritons), infrared-active phonons in boron nitride (phonon polaritons), excitons in dichalcogenide materials (exciton polaritons), superfluidity in FeSe- and Cu-based superconductors with high critical temperature T_c (Cooper-pair polaritons), and magnetic resonances (magnon polaritons). The family of vdW materials supports all of these polaritons. The matter oscillation component results in negative permittivity ($\epsilon_B < 0$) of the polaritonic material, giving rise to optical-field confinement at the interface with a positive-permittivity ($\epsilon_A > 0$) environment. vdW polaritons exhibit strong confinement, as defined by the ratio of incident light wavelength λ_0 to polariton wavelength λ_p .

REVIEW

QUANTUM MATERIALS

Polaritons in van der Waals materials

D. N. Basov,^{1,2*} M. M. Fogler,¹ F. J. García de Abajo^{3,4}

van der Waals (vdW) materials consist of individual atomic planes bonded by weak vdW attraction. They display nearly all optical phenomena found in solids, including plasmonic oscillations of free electrons characteristic of metals, light emission/lasing and excitons encountered in semiconductors, and intense phonon resonances typical of insulators. These phenomena are embodied in confined light-matter hybrid modes termed polaritons—excitations of polarizable media, which are classified according to the origin of the polarization. The most studied varieties are plasmon, phonon, and exciton polaritons. In vdW materials, polaritons exhibit extraordinary properties that are directly affected by dimensionality and topology, as revealed by state-of-the-art imaging of polaritonic waves. vdW heterostructures provide unprecedented control over the polaritonic response, enabling new quantum phenomena and nanophotonics applications.

Atomically thin two-dimensional (2D) crystalline layers constitute the elemental building blocks of van der Waals (vdW) materials. Exfoliated atomic layers are structurally robust and amenable to assembly to produce complex heterostructures. These materials support a variety of polaritons associated with oscillations of conduction electrons, phonons, and excitons, as well as their hybrids (e.g., plasmon-phonon polaritons). A number of vdW materials display extraordinary quantum phenomena: high-critical temperature (T_c) superconductivity, exotic magnetism, topologically protected states, strong Coulomb interactions, and non-Fermi-liquid behavior. All of these properties permeate the polaritonic response of vdW systems.

In the ongoing quest for exploration of polaritons, scanning optical near-field imaging (Fig. 1) has had an exceptional impact. This technique uses the sharp tip of an atomic force microscope (AFM) as an optical antenna (1, 2), allowing one to detect how incident light of free-space wavelength λ_0 is scattered at the apex of the tip in the proximity of the studied specimen (Fig. 1A). The obtained signal is governed by the local electric field of the polariton wave launched by the tip, rendering nanometer spatial resolution as the tip is raster-scanned over the sample. The principal characteristics of polaritons, including wavelength λ_p , confinement ratio λ_0/λ_p , and quality factor Q (Table 1), reveal that vdW polaritons are simultaneously compact and long-lived. The polariton wavelength can often be tuned with various methods, of which electrical gating is of paramount importance. These characteristics render vdW polaritons comple-

mentary and sometimes superior to those observed in more conventional materials (3, 4).

A major challenge of polariton imaging and spectroscopy stems from the large momentum mismatch with free-space photons. However, experimentalists are becoming increasingly adept at overcoming this difficulty. Figure 2 displays various coupling schemes. Coherent launchers (Fig. 2, A to C) have relatively small coupling cross sections, although they can be enhanced through optical antennas, including AFM tips (Fig. 2C) and metal bars or disks (5). Incoherent launchers (Fig. 2, D to F) can reach order-unity efficiency; in particular, electron beams (Fig. 2D) eventually will enable an impressive combination of energy and space resolution (6).

Primer on polaritons

Polariton dispersion in thin layers

When the sample thickness d is much smaller than the wavelength λ_p of polaritons, only the in-plane optical response of the material is important. In this thin-film limit, one finds

$$\lambda_p = \frac{2\pi}{k_p} = 4\pi^2 \operatorname{Im} \left\{ \frac{\sigma}{\omega \epsilon_a} \right\}, \quad d \ll \lambda_p \quad (1)$$

where ϵ_a is the permittivity of the environment, σ is the in-plane conductivity, ω is the frequency, and k_p is the in-plane polariton wave vector. The field of the polariton wave decreases exponentially away from the interface over a characteristic distance $\sim \lambda_p/2\pi$. It is common to describe σ in Eq. 1 as the sum

$$\sigma(\omega) = \frac{i}{\pi} \frac{S_f}{\omega + i\tau_f^{-1}} + \frac{i}{\pi} \frac{\omega S_b}{\omega^2 - \omega_b^2 + i\omega\tau_f^{-1}} \quad (2)$$

The first (Drude) and the second (Lorentz) terms represent the contribution of free (f) and bound (b) charges, respectively. The latter can also account for optical phonons. Different vdW mate-

rials can be modeled with a suitable choice of parameters in Eq. 2: the spectral weights S_f and S_b , the exciton/phonon frequency ω_b , and the phenomenological relaxation times τ_f and τ_b (related to Q in Table 1 by $\tau = Q/\omega$).

The spectral weights in Eq. 2, and therefore the polariton wavelengths of vdW materials, are often tunable. In graphene, S_f scales with the Fermi energy E_F according to $S_f \sim (e/\hbar)^2 E_F$ (where e is the charge on the electron and \hbar is the Planck constant divided by 2π) (7); the value of S_f can be controlled via electrical gating, doping, and photo-excitation. In insulators, where $S_b \sim (e^2/\hbar)f\omega_b$, the dimensionless parameter f scales linearly with the number N of atomic layers. In particular, $f_{ph} \sim N\sqrt{m/M} \ll 1$ for optical phonons and $f_{ex} \sim N(D/ea_{ex})^2$ for excitons. Here, m , M , a_{ex} , and D are the electron mass, the atomic mass, the exciton Bohr radius, and the exciton transition dipole, respectively. In superconductors, the total Drude weight is constant but is split between normal- and super-current components, with a relative weight depending on temperature. When applied to graphene, Eqs. 1 and 2 readily explain why the surface plasmon polariton (SPP) confinement ratio $\lambda_0/\lambda_p = (\epsilon_a/\alpha)(\hbar\omega/2E_F) \gg 1$ can be extraordinarily high (8): λ_0/λ_p scales with the inverse of the fine-structure constant $\alpha \approx 1/137$. However, a stronger confinement is accompanied by larger damping rate τ_f^{-1} [which also increases with ω (9, 10)].

Polariton dispersion in slabs and heterostructures

For highly confined polaritons (or thicker samples), the condition $\lambda_p \gg d$ may not hold, so the polariton dispersion becomes more intricate (Fig. 3). Both the in- and out-of-plane responses need to be considered, and it is more convenient to use the permittivity tensor, whose in-plane component ϵ_{\parallel} relates to $\sigma(\omega)$ as $\epsilon_{\parallel} = 1 + (4\pi i\sigma/\omega d)$, whereas the out-of-plane component ϵ_{\perp} may differ from ϵ_{\parallel} in both magnitude and sign because of the strong anisotropy of vdW materials (Fig. 3, E and F). Additional complications arise if the sample is a heterostructure made of dissimilar vdW materials (metals, insulators, or semiconductors). These more complex dispersions can be dissected into simpler elements (11, 12) as in Fig. 3, A to G.

SPPs are supported by materials that possess mobile charges: metals, doped semiconductors, and superconductors. We find three types of electromagnetic modes in these materials (Fig. 3A): two in the bulk (photon and plasmon) and one confined at the surface (lower curve, representing the TM-polarized SPP). The transverse upper branch also starts at frequency ω_p and disperses upward at higher wave vector k . This behavior results from level repulsion between the photon (dashed line in Fig. 3A) and the zero-frequency (Drude) resonance of the conductor. The high- k SPP is often referred to as a surface plasmon (SP). Its dispersion asymptotically approaches $\omega_{SP} = \omega_p/\sqrt{2}$.

The SPPs at the surfaces of a thin conducting film of thickness $d \ll c/\omega_p$ split into two branches of opposite symmetry. The lower,

¹Department of Physics, University of California, San Diego, CA, USA. ²Department of Physics, Columbia University, New York, NY, USA. ³Institut de Ciències Fotòniques, Barcelona Institute of Science and Technology, 08860 Castelldefels (Barcelona), Spain. ⁴Institució Catalana de Recerca i Estudis Avançats, 08010 Barcelona, Spain.

*Corresponding author. Email: db3056@columbia.edu

Table 1. Characteristics of polaritons in vdW materials. Tunability methods marked with asterisks indicate already demonstrated results. All experimental entries are obtained under ambient conditions, except for Cooper-pair plasmons at $T = 5$ K. SPP, surface plasmon polariton; DE, dielectric environment; N/A, not available.							
Polariton types (materials)	Image	Energy range (meV)	λ_p (nm)	max λ_o/λ_p	max Q	Tunability methods	References
Dirac SPP (graphene)	Fig. 1A	<1000	50 to 450	220	40	Gating,* doping,* photoexcitation,* DE*	(10, 20, 21, 100)
Edge SPP (graphene)	Fig. 1B	<1000	50 to 200	200	10	Gating,* doping,* photoexcitation, DE*	(64, 65)
One-dimensional SSP (carbon nanotubes)	Fig. 1C	<200		100 to 1000	26	Conducting channels,* DE	(30)
Superlattice SPP (graphene/hBN moiré superlattices)	Fig. 1D	<1000	50 to 250	220	4	Gating, doping,* photoexcitation	(24, 101)
Hyperbolic plasmon-phonon polaritons (graphene/hBN)	Fig. 1E	90 to 110 (type I), 170 to 200 (type II)	630 to 750	37	15	Gating,* doping,* photoexcitation	(18, 60)
Hyperbolic plasmon-phonon polaritons [Bi ₂ Se ₃ , (Bi,Sb) ₂ Te ₃]	N/A	8 to 20				Gating,* doping,* photoexcitation	(93)
Exciton polariton (WSe ₂)	Fig. 1F	1400 to 1600	>300	3	5	Crystal thickness,* DE	(45)
Hyperbolic phonon polariton (h-BN)	Fig. 1G	90 to 110 (type I), 170 to 200 (type II)	200 to 1000	50	200	Crystal thickness,* DE*	(17, 82, 102–104)
Topological SPP: Bi ₂ Se ₃ , (BiSb) ₂ Te ₃	N/A	<200	7 to 5000	900	3	Gating, doping*	(105, 106)
Cooper-pair and Josephson plasmon polaritons (cuprate high- T_c superconductors)	N/A	<40	9000 to 13,000	3	4	Doping, crystal thickness,* DE*	(89, 90, 107, 108)
Anisotropic SPP (black phosphorus)	N/A	<60 ($k \parallel \Gamma$ -X), <40 ($k \parallel \Gamma$ -Y)					(109)

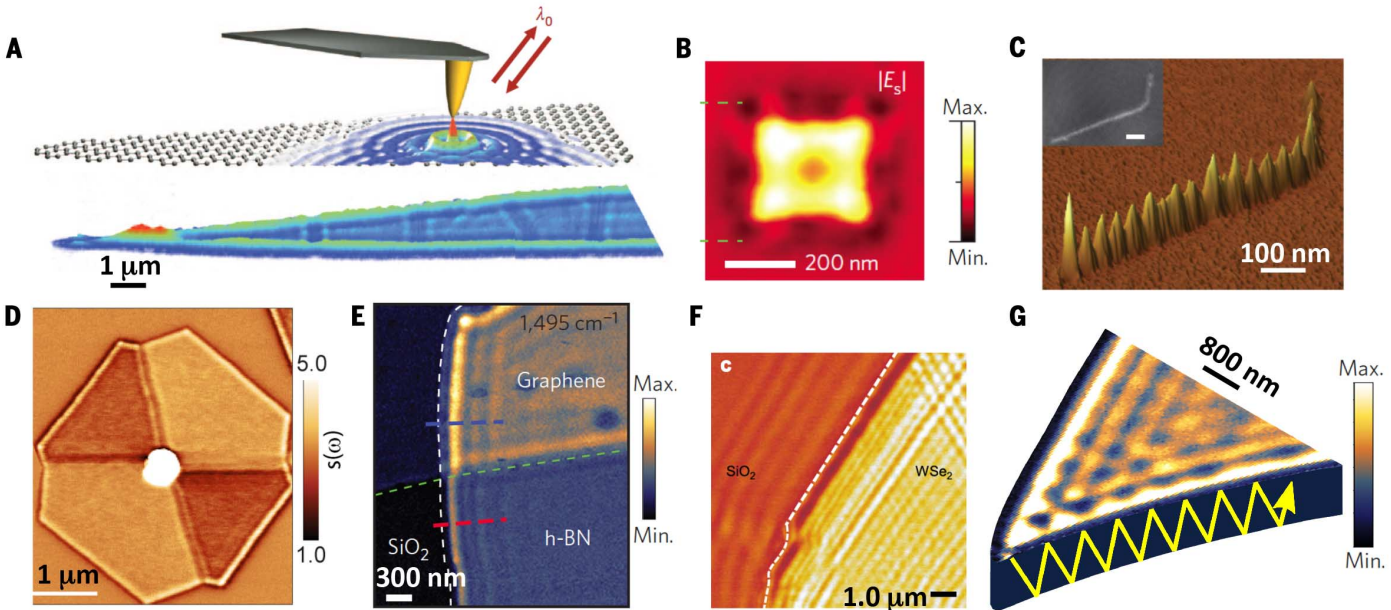


Fig. 1. Polaritons in vdW materials visualized through near-field nanoimaging. (A) Dirac plasmons in graphene (20, 21). [Reproduced from (20)] (B) Edge plasmons at the boundary of a graphene nanoresonator (64, 65). [Reproduced, with permission, from (65)] (C) One-dimensional plasmons in a carbon nanotube (30). [Reproduced, with permission, from (30)] (D) Superlattice plasmons in graphene–h-BN moiré superlattices (24). [Reproduced from (24)] (E) Hybrid plasmon-phonon polaritons in graphene on h-BN (60). [Reproduced from (60)] (F) Exciton polaritons (45) in WSe₂. [Reproduced, with permission, from (45)] (G) Hyperbolic phonon polaritons in a h-BN slab (102), propagating as guided waves (schematic line).

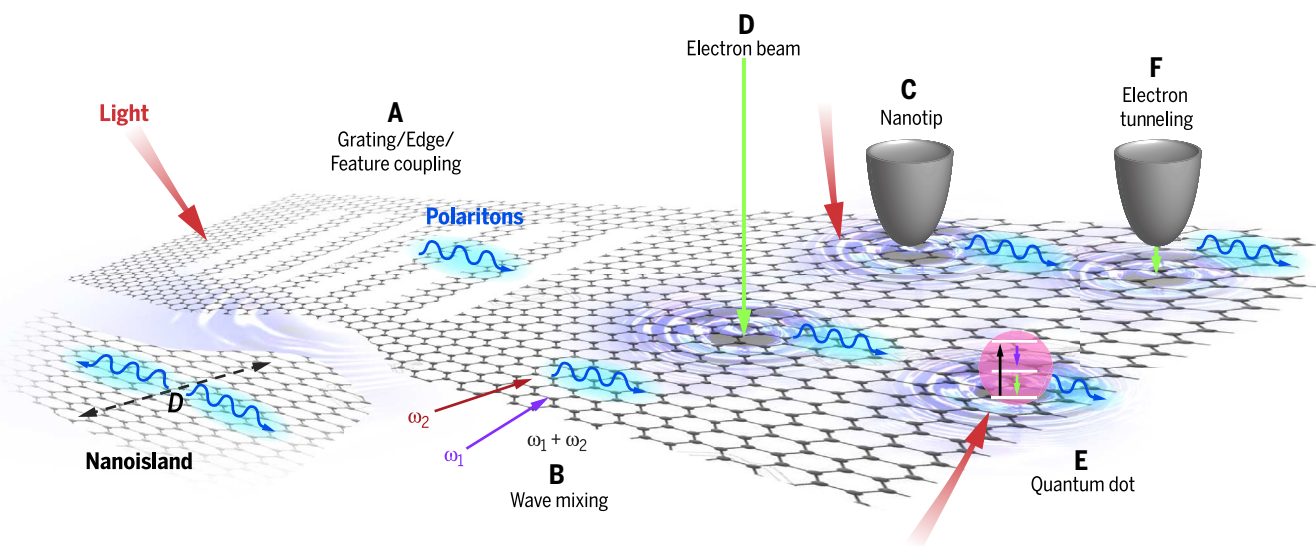


Fig. 2. Launching and visualizing polaritons. (A to F) Excitation and probing of vdW polaritons (blue arrows) can be achieved using (A) periodic structures (110–112), (B) nonlinear wave mixing (95), (C) antenna-like nanotips (20, 21), (D) electron beams (113), (E) quantum dots and localized emitters (114, 115), and (F) electron tunneling (116). Polaritons produced by processes shown in (A) to (C) maintain phase coherence with respect to the external

illumination, in contrast to mechanisms shown in (D) to (F), which are inelastic. A variant of (A) has been proposed that relies on surface acoustic wave modulation (117, 118). Sample edges (64, 65) also provide additional momentum to mediate light-polariton coupling. Localized polaritons confined to nanoislands can be resonantly excited by incident light. Radiative outcoupling of polaritons can be visualized by reversing the arrows in (A) to (C).

symmetric branch corresponds to the thin-film plasmons (Eq. 1 and Fig. 3B). For $k \gg 1/d$, both of these branches are localized to the film surfaces and are nearly degenerate. A set of guided waves above the bulk plasmon frequency ω_p may also exist between the light lines of vacuum and the material (tilted dashed lines in Fig. 3B) for films with high-frequency permittivity larger than unity.

Phonon and exciton polaritons in dielectrics

A typical bulk dielectric exhibits three modes: two transverse optical branches of phonon polaritons (PhPs) ω_{TO} , generated by hybridization of a photon (dashed line in Fig. 3C) and a TO phonon; and one longitudinal phonon ω_{LO} , analogous to the bulk plasmon in a metal. In a semi-infinite dielectric, a surface phonon polariton (SPhP) emerges inside the bulk stop band $\omega_{TO} < \omega < \omega_{LO}$. In thin slabs (Fig. 3D), the PhP branches split into guided modes while the SPhP generates symmetric and antisymmetric modes similar to SPPs in metal films. The mode structure of exciton polaritons in semiconductors is similar to that of phonon polaritons in dielectrics, except that the role of ω_{TO} is played by the exciton energy and the dispersion at large momenta is quadratic: $\omega(k) = \omega_{TO} + (\hbar k^2/2m_{ex})$, where m_{ex} is the exciton mass. The ω_{LO} - ω_{TO} gap in excitonic systems is referred to as the Rabi splitting.

Hyperbolic media and waveguide modes

Hyperbolic materials exhibit permittivities of opposite signs along different directions. In particular, type II hyperbolic materials possess

positive $\epsilon_{||}$ and negative ϵ_{\perp} . In anisotropic polar dielectrics, this regime may be realized within stop bands. Hyperbolicity leads to birefringence, with the dispersion relations of the ordinary and extraordinary rays given by $\omega^2/c^2 = (k_{||}^2 + k_{\perp}^2)/\epsilon_{\perp}$ and $\omega^2/c^2 = (k_{||}^2/\epsilon_{||}) + (k_{\perp}^2/\epsilon_{\perp})$, respectively. The extraordinary rays have peculiar isofrequency open surfaces, shaped as single-sheet hyperboloids (13–15). When projected on the ω - k_{\perp} plane, the hyperboloids fill a continuous region (orange fringes in Fig. 3E). The transverse $k_{||}$ and axial k_{\perp} momenta of these extraordinary polaritons can be very large, being limited only by the atomic structure of the material.

Polaritons can only propagate at angles θ or $\pi - \theta$ with respect to the optical axis satisfying the relation $\tan \theta = |\epsilon_{\perp}/\epsilon_{||}|^{1/2}$. This implies that the polariton can be focused into narrow beams that do not spread laterally as they propagate through the material (see below). A thin slab with surfaces normal to the optical axis supports weakly confined surface modes that evolve into the principal branch of the guided waves as k increases (Fig. 3F). This is accompanied by numerous higher-order branches (Fig. 3F) that arise from splitting of the extraordinary ray continuum in Fig. 3E. The group velocity can be negative in a hyperbolic material, as demonstrated by direct imaging (16, 17). Hyperbolic electrodynamics is ubiquitous in vdW materials and originates not only in the phonon modes (Fig. 3, E and F) but also in a highly anisotropic electronic response.

Plasmon-phonon polaritons are more complex modes involving the hybridization of the corresponding elemental excitations in heterostructures. For example, in graphene supported

by hexagonal boron nitride (h-BN) (18, 60) (Fig. 3E), the hyperbolic guided waves (13–15) appear in the two bands marked type I and type II. Outside these bands, one finds SPP and SP branches similar to those in Fig. 3B. The slope of the SP dispersion—the group velocity v_g —is much smaller than c : The light cone is nearly vertical (and hence invisible) in Fig. 3G. Additionally, v_g nearly everywhere exceeds the Fermi velocity and the plasmon does not overlap the electron-hole pair continuum (green region in Fig. 3G), so Landau damping is prevented.

New physics revealed by polaritonic observations

Polaritons in vdW materials provide unique opportunities for exploring electronic phenomena and lattice dynamics. In particular, polaritonic images grant us access into regions of the dispersion relations of various excitations beyond what is attainable with conventional optics.

Interactions and many-body effects

The decay rate and wavelength of plasmonic and polaritonic waves (Fig. 1) are determined by the complex optical conductivity $\sigma(k, \omega)$ of the medium that supports these waves. It is thus possible to reconstruct $\sigma(k, \omega)$ from polaritonic images, which contain information on both electronic and lattice dynamics (10, 19–21). Specifically, the periodicity of plasmonic waves in graphene (Fig. 1A) is determined by the imaginary part of the conductivity, whereas the rate at which these waves decay into the interior of the samples is governed by $\text{Re } \sigma/\text{Im } \sigma$. The plasmon propagation length $\sim (\text{Im } \sigma/\text{Re } \sigma)\lambda_p$ has been shown to reach $\sim 1 \mu\text{m}$ (i.e., tens of plasmon wavelengths) in

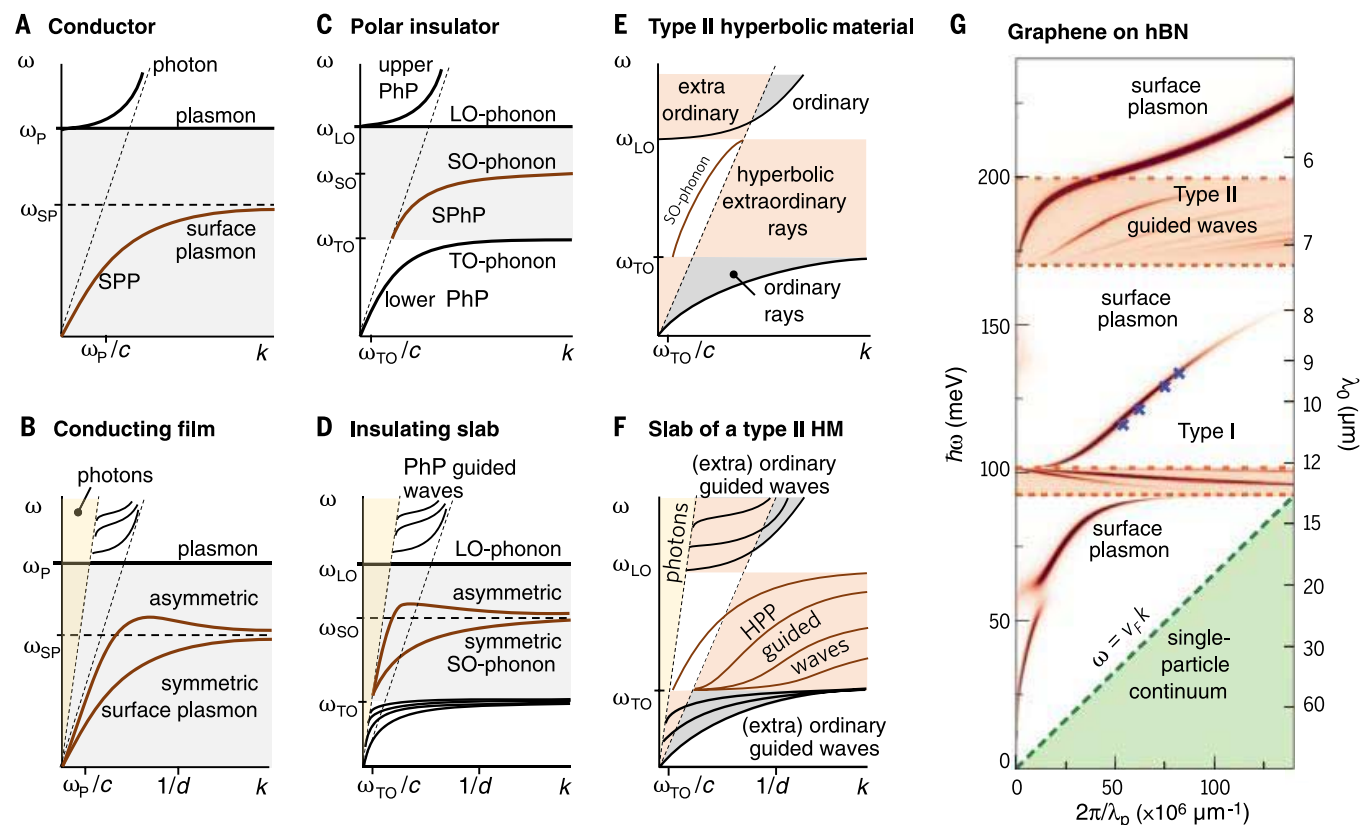


Fig. 3. Polariton dispersions. (A) Bulk conductors (metals or doped semiconductors). (B) Thin conducting films. (C) Isotropic polar dielectrics. (D) Thin polar dielectric slabs. (E) Type II hyperbolic materials. (F) Thin slab of a type II hyperbolic material with its optical axis normal to the surfaces. (G) Graphene–h-BN heterostructures (10). The horizontal axis is the transverse wave vector in (E) and the 3D bulk or in-plane wave vector in the other plots, depending on the mode. [Adapted from (10)]

high-mobility encapsulated graphene (10, 19). The corresponding lifetime, ~ 500 fs, is only weakly dependent on gate voltage or probing photon frequency from the terahertz to mid-infrared regimes (22). This result is consistent with the dominant role of acoustic phonons in scattering processes (9), a conjecture further supported by theoretical analysis of the ω and k dependence of the plasmon scattering rate $\tau^{-1} = (\text{Re } \sigma / \text{Im } \sigma) \omega$ (Fig. 4A). Data on interactions among electrons, phonons, and plasmons in other vdW systems are fragmentary, but implications of these interfacial effects may be quite spectacular. For example, coupling between electrons in monolayer FeSe and phonons in SrTiO₃ appears as a viable mechanism for high-temperature superconductivity in FeSe/SrTiO₃ heterostructures (23).

Polaritonic probe of the electronic structure and inhomogeneities

Equations 1 and 2 establish that images of polaritonic waves in a given medium encode the optical conductivity, and hence the fundamental information about intraband, interband, and excitonic effects within that medium. For example, the analysis of plasmonic reflections and standing waves has been used to decipher the electronic structure of moiré superlattices

formed at the interface of slightly mismatched hexagonal lattices of graphene and h-BN (24). Moiré patterns are periodic superlattice structures that appear when two crystals with a small lattice mismatch are superimposed. Moiré superlattices reveal the energy gap in the otherwise gapless electronic structure of graphene and therefore modify the conductivity $\sigma(k, \omega)$. The boundary between plain and superlattice graphene is thus associated with an abrupt change of the electronic conductivity—a property that prompts plasmonic reflections (Fig. 1D). The magnitude of the moiré-induced energy gap is inferred from a systematic analysis of these plasmonic patterns collected at different wavelengths for specimens with different doping. Plasmonic reflections also occur at other forms of electronic discontinuities, including grain boundaries in extended graphene films (25, 26), stacking domains (Fig. 4C) in bilayer graphene (27), and nanometer-scale local gates (28, 29). In particular, a carbon nanotube (CNT) gate acts as a perturbation produced by a line of charge, which introduces 1D-bound states in an adjacent graphene layer. In a related context, plasmons imaged in CNTs (Fig. 1C) are found to exhibit approximately doping- and frequency-independent (quantized) group velocity, which is a consequence of the 1D nature of these materials (30). We note

that 1D phonon polaritons are also observed in BN nanotubes (31).

Polaritons far and away from equilibrium

When subjected to photoexcitation by short and intense optical pulses, vdW polaritons can radically change their properties (32). Hyperspectral near-field imaging of graphene under intense optical pumping (19) (Fig. 4B) uncovers the emergence of mid-infrared plasmons in a specimen that shows no such modes in equilibrium because of its low Drude spectral weight S_f (Eq. 1). This effect is driven by thermal smearing of conduction electrons, which produces a boost in $S_f \propto k_B T$ (where k_B is the Boltzmann constant); the electron temperatures can be as high as $T = 5000$ K (33). Ultrafast heating of electrons and plasmons may realize a regime in which the dynamics of an approximately equal number of electrons and holes in graphene resembles the behavior of viscous liquids described by relativistic hydrodynamics (34, 35). Several theoretical works have discussed plasmon amplification in vdW materials (36, 37) under photoexcitation, followed by a recent experimental report (38). Apart from probing inherent nonlinearities of the materials (39), an experimental implementation of these ideas may uncover pathways for mitigating or eliminating

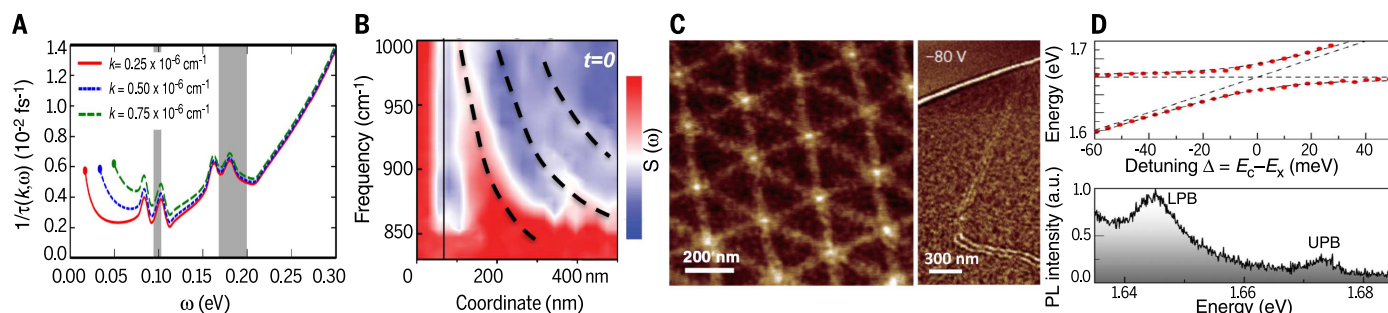


Fig. 4. Spectroscopy and imaging of polaritons enable a new line of inquiry into the fundamental physics of the media supporting polaritonic behavior. (A) Scattering rate $\tau^{-1}(k, \omega)$ for Dirac plasmons in monolayer graphene calculated (9) for three selected values of the in-plane wave vector k . Shaded areas correspond to stop bands. [Reproduced, with permission, from (9)] (B) Photoexcitation of semi-infinite monolayer graphene with intense femto-second pulses increases electronic temperature and enhances the spectral weight available for surface plasmons. Hyperspectral images (19) of the photoinduced change in the scattering amplitude $\Delta S(\omega, x)$ reveal the dispersion

of photoinduced plasmons (red traces). A vertical line indicates the edge of the graphene sample. Dashed lines are theoretical fits. [Reproduced from (19)] (C) Nano-infrared contrast produced by plasmonic reflections at topological domain boundaries in bilayer graphene (27). [Reproduced, with permission, from (27)] (D) Exciton-photon coupling in a MoSe_2 double quantum-well heterostructure showing an anticrossing between the neutral exciton and discrete cavity modes at 4.2 K. Top: A fit to the peak position as a function of detuning yields a Rabi splitting of 29 meV. Bottom: The upper and lower polariton branches (UPB and LPB) are well resolved spectrally (43). [Reproduced from (43)]

electronic losses in the plasmonic or polaritonic response. An alternative route for loss compensation consists of fulfilling the optical gain condition $\text{Re } \sigma(\omega) < 0$ by means of population inversion, an effect recently demonstrated (40) in the frequency range of excitonic transitions in WS_2 .

High-temperature exciton polaritons

Atomically thin transition metal dichalcogenides (TMDs), including MoS_2 and MoSe_2 , exhibit strong many-body effects due to their high effective carrier masses and low dielectric permittivities. Monolayers of TMDs are direct-gap semiconductors that host excitons with binding energies from 0.4 to 0.9 eV (41, 42). When integrated in an optical cavity, TMDs may form exciton polaritons, provided that the cavity-enhanced exciton-photon coupling (i.e., the Rabi frequency) exceeds the exciton decay rate (on the order of tens of meV). A realization of this regime was recently reported in a MoSe_2 -based heterostructure (Fig. 4D) at 4.2 K (43) with a Rabi frequency of 29 meV and a clearly resolved avoided crossing of exciton and photon dispersions. Similar results were obtained for MoS_2 (44). The lower- k part of the exciton polariton-guided waves (Fig. 1F) has been imaged in thin WSe_2 crystals under ambient conditions (45), in a regime where these propagating modes have a dominant photon character (Fig. 1F).

A challenge for future nanoimaging experiments is to probe the strongly confined, large- k part of the exciton polariton branches. The exciton and exciton polariton propagation lengths are expected to be greatly enhanced if they form condensates, which are also predicted to occur in TMDs near room temperature (46), more than one order of magnitude higher than in conventional inorganic semiconductors. The interaction of exciton polariton condensates with a two-dimensional electron system of vdW materials may enable a new pathway toward high-temperature superconductivity (47, 48). Diverse polaritonic phenomena of excitonic origin may also be anticipated in

CNTs, in view of the strong excitonic dipole activity of these 1D systems (49, 50).

Spatial dispersion

Nonlocal effects in the conductivity become relevant when the polariton wavelength is comparable with the Fermi wavelength λ_F . These phenomena remain largely unexplored in vdW materials. Nonlocal effects are typically investigated using momentum-resolved methods such as electron energy-loss spectroscopy, but they appear to be within reach for nano-optics techniques in view of the large values of λ_F in vdW layers. Nano-imaging and nanospectroscopy experiments allow one to determine the nonlocal conductivity (10, 51) $\sigma(k_p, \omega)$. Future nano-infrared measurements may provide additional insight into other momentum-dependent electronic phenomena (52).

Topological polaritonics

Topological order and Berry phases are playing a prominent role in the understanding of electronic properties of vdW solids such as chirality and anomalous Hall conductivity. These intriguing properties have implications in photonics and polaritonics (53, 54). For example, in gapped (bilayer) graphene or TMDs, the anomalous Hall conductivities of the two valleys cancel each other in equilibrium. This cancellation can be removed through pumping with circularly polarized light, leading to a chiral polaritonic response (55, 56). Among many fascinating predictions exploring the roles of topology and chirality in polariton propagation, we mention those of chiral edge modes of plasmonic and excitonic origin (57). Recent observations of edge plasmons in graphene nanoribbons (Fig. 1B) fulfill the preconditions for exploring topological properties via polaritons.

Tailoring polaritonic characteristics specific to vdW materials

Stacking

Restacking of exfoliated and/or epitaxial vdW layers yields vertical heterostructures in which

electromagnetic coupling between polaritonic modes of proximal planes gives rise to new optical properties beyond those of the individual constituents. For example, mid-infrared plasmons in graphene hybridize with phonon polaritons of an underlying polar substrate (18, 51, 58, 59). Hyperbolic polaritons observed in graphene-h-BN stacks (60) inherit electrostatic tunability from graphene and long propagation lengths from phonons in h-BN. Changes in electronic structure produced by interlayer interaction can further give rise to modified polaritonic response—for example, in rotationally aligned graphene-h-BN stacks, where the formation of long-period moiré superlattices modifies the dispersion and lifetime of composite plasmon polaritons (24). Finally, chiral twisted stacks may exhibit optical gyrotropy (61, 62).

Nanostructuring

Nanostructuring is commonly used to produce systems with reduced dimensionality, including stripes, discs, and nanocones of h-BN (63). Both artificial and natural boundaries of vdW samples harbor 1D polaritonic edge modes that reveal a dispersion distinct from that of “bulk” polaritons in the interior of vdW crystals (64, 65). Similarly, 1D modes are likely to occur at domain walls, lateral Josephson junctions, and p-n junctions.

Controls

Unlike conventional plasmonic media, vdW materials are amenable to active tuning of their polaritonic properties via chemical doping and gating. Graphene is a paramount example of this tunability. Additionally, doping of vdW semiconductors such as black phosphorus (66) affects the interplay between spectrally overlapping intra- and interband responses, which has an impact on their hyperbolic behavior (67). Persistent switching of optical properties can be realized in vdW/ferroelectric multilayers and by manipulating defects in h-BN layers (68). Optical pumping provides a mechanism of ultrafast control

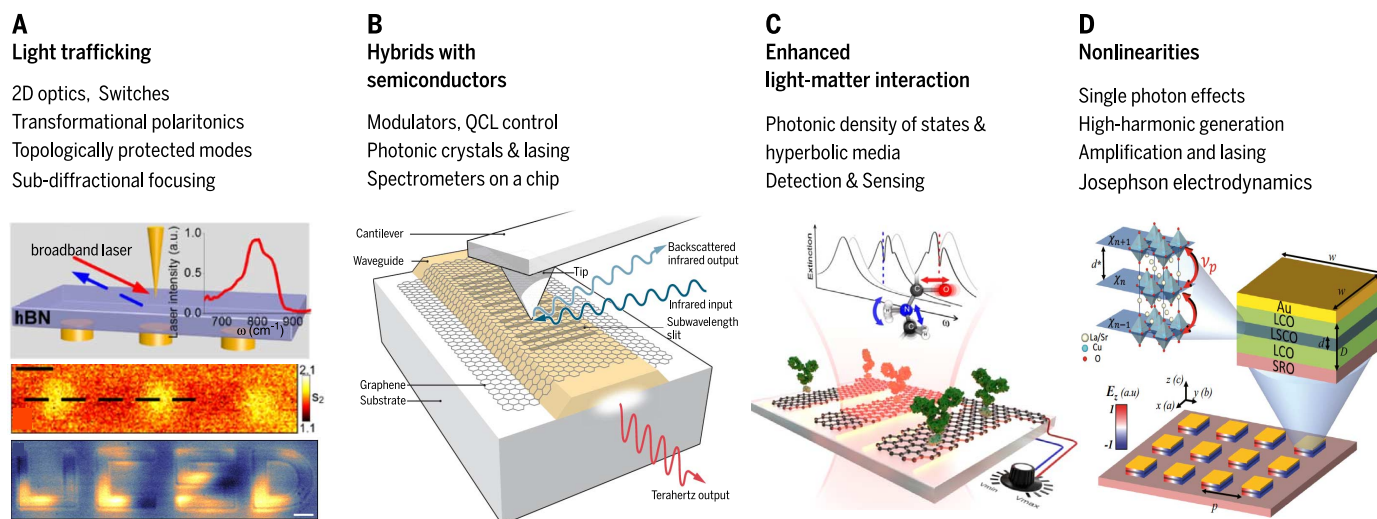


Fig. 5. Impending applications and future opportunities. (A) Subdiffractive focusing via phonon polaritons in h-BN (16, 82). Top: Au discs are deposited on the bottom surface of a h-BN slab. Middle: Image obtained on the top surface of the slab using a broadband source centered at $\lambda_0 = 12.5 \mu\text{m}$; scale bar, 500 nm. Bottom: Image of a pattern showing subdiffractive features, acquired with $\lambda_0 = 6 \mu\text{m}$; scale bar, 1 μm . [Reproduced from (16, 82)] (B) Schematics of a quantum-cascade laser (QCL) with emission controlled by plasmons in the top graphene layer (77, 78). [Reproduced from (78)] (C) Resonant absorption in graphene plasmonic strips for spectroscopic fingerprinting (83). [Reproduced from (83)] (D) Proposed structure for investigating cavity electrodynamic of Josephson plasmons (98). LCO, La_2CuO_4 ; LSCO, $\text{La}_{2-x}\text{Sr}_x\text{CuO}_4$; SRO, SrRuO_3 . [Reproduced, with permission, from (98)]

(40, 69, 70). Also, both strain and photoexcitation with circularly polarized light lift the valley degeneracy in vdW materials such as bilayer graphene and TMDs (71), enabling one to explore valley-selective phenomena. An expanding list of polaritonic “control knobs” includes population inversion (40), n- and p-type doping of graphene upon photoexcitation (69), magnetic fields applied to graphene (72), and strain engineering of excitons in WSe_2 (73).

Impending applications

The unusual optical properties displayed by vdW materials offer exciting opportunities for technological applications (74).

Light trafficking

Polariton nanoimaging experiments in vdW materials (Fig. 1) revealed that these ultracompact light-matter modes are capable of carrying optical signals over many micrometers in some cases. Furthermore, the propagation, reflection, and refraction of polaritons can be readily controlled by heterostructuring or through stimuli such as electrical gating (20, 21). Thus it is feasible to implement transformational polaritonics (75), polaritonic transistors, and integrated nanophotonic circuits using vdW systems. In heterostructures combining chiral and hyperbolic layers, it may be possible to produce polaritons topologically protected from backscattering, which could lead to protected unidirectional propagation and robustness against disorder (53, 76).

Electro-optical modulators

Integration of vdW materials with semiconductor photonics is equally appealing. Early demonstrations (Fig. 5B) include quantum-cascade lasers with tunable emission characteristics (77, 78)

and electrically controlled modulators (79–81). The extreme reduction of the polariton wavelength in vdW materials should enable the design of ultrascale spectrometers on a chip, with spectral resolution achieved through using different structures with polaritonic resonances covering a dense and broad set of frequencies.

Subdiffractive focusing and imaging

Compact but mobile phonon polaritons have already been used for subwavelength focusing and imaging (Fig. 5A), taking advantage of the hyperbolic dispersion of h-BN (16, 82). These properties could find application in detector arrays and lithographic imprinting at unprecedentedly small scales.

Optical sensing

Part of the success of metal-based plasmonics lies in its application to sensing, down to single molecules. This is made possible by exploiting the large concentration of electromagnetic energy associated with these optical modes. vdW polaritons produce even higher levels of field confinement than traditional plasmonic metals and therefore hold great potential for sensing. In particular, graphene-enabled ultrasensitive detection has recently been demonstrated for biological (83) and inorganic (84) molecules (Fig. 5C).

Light emission, amplification, and lasing

Spontaneous emission from a light-emitting device can be improved by coupling the radiated energy to polaritons (2, 85). This effect is particularly pronounced at the interface with hyperbolic media, where the photon density of states is greatly enhanced (13–15). The substantial field enhancement can also be used for efficient heat transfer at the nanoscale. Additionally, the low

saturation threshold of graphene has been exploited in fast mode-locked lasers (86), and polaritons in WSe_2 have recently been harnessed to implement an ultralow-threshold nanocavity laser (87).

Looking into the future

Polaritons in correlated van der Waals materials

Among the spectacular polaritonic effects intrinsic to vdW crystals, we highlight the Josephson plasmon originating from Cooper-pair tunneling between CuO_2 planes in layered cuprate high- T_c superconductors (88). Propagating and non-equilibrium Josephson plasmons are expected to provide insights (89, 90) into the unconventional superconductivity of these materials. Furthermore, the natural hyperbolic behaviors of cuprates, topological insulators (14, 91–93), and other anisotropic vdW compounds are yet to be exploited for imaging and focusing in a fashion similar to what has been done for h-BN (Fig. 5A).

Quantum and nonlinear optics with vdW polaritons

Decoherence is arguably the most serious impediment for a wide adoption of quantum technologies. The extreme concentration of electromagnetic energy associated with single polariton states in vdW materials can increase quantum interaction with neighboring optical emitters. Thus, it may be possible to reach the single-photon strong-coupling regime under ambient conditions, accompanied by nonlinearities down to the single-photon level (94). Notably, vdW materials exhibit unprecedented levels of nonlinearity, as revealed by wave-mixing experiments (95) as well as by harmonic-generation measurements (96), which are predicted to be boosted

by polaritonic field enhancement (97). Further explorations of nonlinear effects in vdW high- T_c superconductors may enable manipulation of the superconducting order parameter and phase coherence under nonequilibrium conditions (98). Strongly confined plasmonic modes in vdW materials may lead to increased rates of high-order multipolar transitions, two-plasmon spontaneous emission, and spin-flip transitions (99).

The study of polaritons in vdW materials is a vibrant area of research at the vanguard of physics, materials science, and engineering. Heterostructuring of atomic vdW layers, in conjunction with the inherent sensitivity of this class of materials to external stimuli, has uncovered opportunities for on-demand photonic and polaritonic characteristics. Novel visualization techniques have revealed the rich physics of vdW layers encoded in observed images of polaritonic waves. Nanoscale near-field imaging of polaritons is emerging as an experimental method providing new insights into quantum phenomena not attainable with conventional spectroscopies. Given the omnipresence of polaritons in condensed-matter systems, we anticipate this line of inquiry to continue to unfold novel effects in other classes of quantum materials.

REFERENCES AND NOTES

- J. M. Atkin, S. Berweger, A. C. Jones, M. B. Raschke, Nano-optical imaging and spectroscopy of order, phases, and domains in complex solids. *Adv. Phys.* **61**, 745–842 (2012). doi: [10.1080/00018732.2012.737982](https://doi.org/10.1080/00018732.2012.737982)
- J. A. Schuller *et al.*, Plasmonics for extreme light concentration and manipulation. *Nat. Mater.* **9**, 193–204 (2010). doi: [10.1038/nmat2630](https://doi.org/10.1038/nmat2630); pmid: [20168343](https://pubmed.ncbi.nlm.nih.gov/20168343/)
- G. V. Naik, V. M. Shalae, A. Boltasseva, Alternative plasmonic materials: Beyond gold and silver. *Adv. Mater.* **25**, 3264–3294 (2013). doi: [10.1002/adma.201205076](https://doi.org/10.1002/adma.201205076)
- A. Boltasseva, H. A. Atwater, Low-loss plasmonic metamaterials. *Science* **331**, 290–291 (2011). doi: [10.1126/science.1198258](https://doi.org/10.1126/science.1198258); pmid: [21252335](https://pubmed.ncbi.nlm.nih.gov/21252335/)
- P. Alonso-González *et al.*, Controlling graphene plasmons with resonant metal antennas and spatial conductivity patterns. *Science* **344**, 1369–1373 (2014). doi: [10.1126/science.1253202](https://doi.org/10.1126/science.1253202); pmid: [24855026](https://pubmed.ncbi.nlm.nih.gov/24855026/)
- F. J. García de Abajo, Optical excitations in electron microscopy. *Rev. Mod. Phys.* **82**, 209–275 (2010). doi: [10.1103/RevModPhys.82.209](https://doi.org/10.1103/RevModPhys.82.209)
- S. Das Sarma, S. Adam, E. H. Hwang, E. Rossi, Electronic transport in two-dimensional graphene. *Rev. Mod. Phys.* **83**, 407–470 (2011). doi: [10.1103/RevModPhys.83.407](https://doi.org/10.1103/RevModPhys.83.407)
- M. Jablan, H. Buljan, M. Soljačić, Plasmonics in graphene at infrared frequencies. *Phys. Rev. B* **80**, 245435 (2009). doi: [10.1103/PhysRevB.80.245435](https://doi.org/10.1103/PhysRevB.80.245435)
- A. Principi *et al.*, Plasmon losses due to electron-phonon scattering: The case of graphene encapsulated in hexagonal boron nitride. *Phys. Rev. B* **90**, 165408 (2014). doi: [10.1103/PhysRevB.90.165408](https://doi.org/10.1103/PhysRevB.90.165408)
- A. Woessner *et al.*, Highly confined low-loss plasmons in graphene-boron nitride heterostructures. *Nat. Mater.* **14**, 421–425 (2015). doi: [10.1038/nmat4169](https://doi.org/10.1038/nmat4169); pmid: [25532073](https://pubmed.ncbi.nlm.nih.gov/25532073/)
- A. V. Zayats, I. I. Smolyaninov, A. A. Maradudin, Nano-optics of surface plasmon polaritons. *Phys. Rep.* **408**, 131–314 (2005). doi: [10.1016/j.physrep.2004.11.001](https://doi.org/10.1016/j.physrep.2004.11.001)
- J. D. Caldwell *et al.*, Low-loss, infrared and terahertz nanophotonics using surface phonon polaritons. *Nanophotonics* **4**, 44 (2015). doi: [10.1515/nanoph-2014-0003](https://doi.org/10.1515/nanoph-2014-0003)
- A. Poddubny, I. Iorsh, P. Belov, Y. Kivshar, Hyperbolic metamaterials. *Nat. Photonics* **7**, 948–957 (2013). doi: [10.1038/nphoton.2013.243](https://doi.org/10.1038/nphoton.2013.243)
- J. Sun, N. M. Litchinitser, J. Zhou, Indefinite by nature: From ultraviolet to terahertz. *ACS Photonics* **1**, 293–303 (2014). doi: [10.1021/ph4000983](https://doi.org/10.1021/ph4000983)
- J. Kim *et al.*, Improving the radiative decay rate for dye molecules with hyperbolic metamaterials. *Opt. Express* **20**, 8100–8116 (2012). doi: [10.1364/OE.20.008100](https://doi.org/10.1364/OE.20.008100); pmid: [22453481](https://pubmed.ncbi.nlm.nih.gov/22453481/)
- S. Dai *et al.*, Subdiffractive focusing and guiding of polaritonic rays in a natural hyperbolic material. *Nat. Commun.* **6**, 6963 (2015). doi: [10.1038/ncomms7963](https://doi.org/10.1038/ncomms7963); pmid: [25902364](https://pubmed.ncbi.nlm.nih.gov/25902364/)
- E. Yoxall *et al.*, Direct observation of ultraslow hyperbolic polariton propagation with negative phase velocity. *Nat. Photonics* **9**, 674–678 (2015). doi: [10.1038/nphoton.2015.166](https://doi.org/10.1038/nphoton.2015.166)
- V. W. Brar *et al.*, Hybrid surface-phonon-plasmon polariton modes in graphene/monolayer h-BN heterostructures. *Nano Lett.* **14**, 3876–3880 (2014). doi: [10.1021/nl501096g](https://doi.org/10.1021/nl501096g); pmid: [24874205](https://pubmed.ncbi.nlm.nih.gov/24874205/)
- G. X. Ni *et al.*, Ultrafast optical switching of infrared plasmon polaritons in high-mobility graphene. *Nat. Photonics* **10**, 244–247 (2016). doi: [10.1038/nphoton.2016.45](https://doi.org/10.1038/nphoton.2016.45)
- J. Chen *et al.*, Optical nano-imaging of gate-tunable graphene plasmons. *Nature* **487**, 77–81 (2012). doi: [10.1038/nature11254](https://doi.org/10.1038/nature11254); pmid: [22722861](https://pubmed.ncbi.nlm.nih.gov/22722861/)
- Z. Fei *et al.*, Gate-tuning of graphene plasmons revealed by infrared nano-imaging. *Nature* **487**, 82–85 (2012). doi: [10.1038/nature11253](https://doi.org/10.1038/nature11253); pmid: [22722866](https://pubmed.ncbi.nlm.nih.gov/22722866/)
- P. Alonso-Gonzalez *et al.*, <http://arxiv.org/abs/1601.05753> (2016).
- J. J. Lee *et al.*, Interfacial mode coupling as the origin of the enhancement of T_c in FeSe films on SrTiO_3 . *Nature* **515**, 245–248 (2014). doi: [10.1038/nature13894](https://doi.org/10.1038/nature13894); pmid: [25391962](https://pubmed.ncbi.nlm.nih.gov/25391962/)
- G. X. Ni *et al.*, Plasmons in graphene moiré superlattices. *Nat. Mater.* **14**, 1217–1222 (2015). doi: [10.1038/nmat4425](https://doi.org/10.1038/nmat4425); pmid: [26413987](https://pubmed.ncbi.nlm.nih.gov/26413987/)
- Z. Fei *et al.*, Electronic and plasmonic phenomena at graphene grain boundaries. *Nat. Nanotechnol.* **8**, 821–825 (2013). doi: [10.1038/nnano.2013.197](https://doi.org/10.1038/nnano.2013.197); pmid: [24122082](https://pubmed.ncbi.nlm.nih.gov/24122082/)
- J. Chen *et al.*, Strong plasmon reflection at nanometer-size gaps in monolayer graphene on SiC. *Nano Lett.* **13**, 6210–6215 (2013). doi: [10.1021/nl403622t](https://doi.org/10.1021/nl403622t); pmid: [24188400](https://pubmed.ncbi.nlm.nih.gov/24188400/)
- L. Jiang *et al.*, Soliton-dependent plasmon reflection at bilayer graphene domain walls. *Nat. Mater.* **15**, 840–844 (2016). doi: [10.1038/nmat4653](https://doi.org/10.1038/nmat4653)
- A. Woessner *et al.*, Near-field photocurrent nanoscopy on bare and encapsulated graphene. *Nat. Commun.* **7**, 10783 (2016). doi: [10.1038/ncomms10783](https://doi.org/10.1038/ncomms10783); pmid: [26916951](https://pubmed.ncbi.nlm.nih.gov/26916951/)
- B.-Y. Jiang *et al.*, Tunable plasmonic reflection by bound 1D electron states in a 2D Dirac metal. *Phys. Rev. Lett.* **117**, 086801 (2016). doi: [10.1103/PhysRevLett.117.086801](https://doi.org/10.1103/PhysRevLett.117.086801)
- Z. Shi *et al.*, Observation of a Luttinger-liquid plasmon in metallic single-walled carbon nanotubes. *Nat. Photonics* **9**, 515–519 (2015). doi: [10.1038/nphoton.2015.123](https://doi.org/10.1038/nphoton.2015.123)
- X. G. Xu, A. E. Tanur, G. C. Walker, Phase controlled homodyne infrared near-field microscopy and spectroscopy reveal inhomogeneity within and among individual boron nitride nanotubes. *J. Phys. Chem.* **117**, 3348–3354 (2013). doi: [10.1021/jp4008784](https://doi.org/10.1021/jp4008784)
- F. J. García de Abajo, Graphene nanophotonics: Challenges and opportunities. *ACS Photonics* **1**, 135–152 (2014). doi: [10.1021/ph400147y](https://doi.org/10.1021/ph400147y)
- M. Wagner *et al.*, Ultrafast and nanoscale plasmonic phenomena in exfoliated graphene revealed by infrared pump-probe nanoscopy. *Nano Lett.* **14**, 894–900 (2014). doi: [10.1021/nl4042577](https://doi.org/10.1021/nl4042577); pmid: [24479682](https://pubmed.ncbi.nlm.nih.gov/24479682/)
- D. A. Bandurin *et al.*, Negative local resistance caused by viscous electron backflow in graphene. *Science* **351**, 1055–1058 (2016). doi: [10.1126/science.aad0201](https://doi.org/10.1126/science.aad0201); pmid: [26912363](https://pubmed.ncbi.nlm.nih.gov/26912363/)
- J. Cossino *et al.*, Observation of the Dirac fluid and the breakdown of the Wiedemann-Franz law in graphene. *Science* **351**, 1058–1061 (2016). doi: [10.1126/science.aad0343](https://doi.org/10.1126/science.aad0343); pmid: [26912362](https://pubmed.ncbi.nlm.nih.gov/26912362/)
- F. F. Rana, Graphene terahertz plasmon oscillators. *IEEE Trans. Nanotechnol.* **7**, 91–99 (2008). doi: [10.1109/NTANO.2007.910334](https://doi.org/10.1109/NTANO.2007.910334)
- Z. Sun, D. N. Basov, M. M. Fogler, Adiabatic amplification of plasmons and demons in 2D systems. *Phys. Rev. Lett.* **117**, 076805 (2016). doi: [10.1103/PhysRevLett.117.076805](https://doi.org/10.1103/PhysRevLett.117.076805)
- S. Rajasekaran *et al.*, Parametric amplification of a superconducting plasma wave. *Nat. Phys.* **10**, 1038/NPhys3819 (2016). doi: [10.1038/NPhys3819](https://doi.org/10.1038/NPhys3819)
- J. B. Khurgin, Graphene—A rather ordinary nonlinear optical material. *Appl. Phys. Lett.* **104**, 161116 (2014). doi: [10.1063/1.4873704](https://doi.org/10.1063/1.4873704)
- A. Chernikov, C. Ruppert, H. M. Hill, A. F. Rigosi, T. F. Heinz, Population inversion and giant bandgap renormalization in atomically thin WS_2 layers. *Nat. Photonics* **9**, 466–470 (2015). doi: [10.1038/nphoton.2015.104](https://doi.org/10.1038/nphoton.2015.104)
- F. Xia, H. Wang, D. Xiao, M. Dubey, A. Ramasubramaniam, Two-dimensional material nanophotonics. *Nat. Photonics* **8**, 899–907 (2014). doi: [10.1038/nphoton.2014.271](https://doi.org/10.1038/nphoton.2014.271)
- K. F. Mak, C. Lee, J. Hone, J. Shan, T. F. Heinz, Atomically thin MoS_2 : A new direct-gap semiconductor. *Phys. Rev. Lett.* **105**, 136805 (2010). doi: [10.1103/PhysRevLett.105.136805](https://doi.org/10.1103/PhysRevLett.105.136805); pmid: [21230799](https://pubmed.ncbi.nlm.nih.gov/21230799/)
- S. Dufferwiel *et al.*, Exciton-polaritons in van der Waals heterostructures embedded in tunable microcavities. *Nat. Commun.* **6**, 8579 (2015). doi: [10.1038/ncomms9579](https://doi.org/10.1038/ncomms9579)
- X. Liu *et al.*, Strong light-matter coupling in two-dimensional atomic crystals. *Nat. Photonics* **9**, 30–34 (2015). doi: [10.1038/nphoton.2014.304](https://doi.org/10.1038/nphoton.2014.304)
- Z. Fei *et al.*, Nano-optical imaging of WS_2 waveguide modes revealing light-exciton interactions. *Phys. Rev. B* **94**, 081402(R) (2016). doi: [10.1103/PhysRevB.94.081402](https://doi.org/10.1103/PhysRevB.94.081402)
- M. M. Fogler, L. V. Butov, K. S. Novoselov, High-temperature superfluidity with indirect excitons in van der Waals heterostructures. *Nat. Commun.* **5**, 4555 (2014). doi: [10.1038/ncomms5555](https://doi.org/10.1038/ncomms5555); pmid: [25065343](https://pubmed.ncbi.nlm.nih.gov/25065343/)
- F. P. Laussy, A. V. Kavokin, I. A. Shelykh, Exciton polariton mediated superconductivity. *Phys. Rev. Lett.* **104**, 106402 (2010). doi: [10.1103/PhysRevLett.104.106402](https://doi.org/10.1103/PhysRevLett.104.106402)
- O. Cotlet, S. Zeytinoglu, M. Sigrist, E. Demler, A. Imamoglu, Superconductivity and other collective phenomena in a hybrid Bose-Fermi mixture formed by a polariton condensate and an electron system in two dimensions. *Phys. Rev. B* **93**, 054510 (2016). doi: [10.1103/PhysRevB.93.054510](https://doi.org/10.1103/PhysRevB.93.054510)
- F. Wang, G. Dukovic, L. E. Brus, T. F. Heinz, The optical resonances in carbon nanotubes arise from excitons. *Science* **308**, 838–841 (2005). doi: [10.1126/science.1110265](https://doi.org/10.1126/science.1110265); pmid: [15879212](https://pubmed.ncbi.nlm.nih.gov/15879212/)
- I. V. Bondarev, L. M. Woods, K. Tatur, Strong exciton-plasmon coupling in semiconducting carbon nanotubes. *Phys. Rev. B* **80**, 085407 (2009). doi: [10.1103/PhysRevB.80.085407](https://doi.org/10.1103/PhysRevB.80.085407)
- Z. Fei *et al.*, Infrared nanoscopy of Dirac plasmons at the graphene- SiO_2 interface. *Nano Lett.* **11**, 4701–4705 (2011). doi: [10.1021/nl202362d](https://doi.org/10.1021/nl202362d); pmid: [21972938](https://pubmed.ncbi.nlm.nih.gov/21972938/)
- J. P. Carbotte, J. P. F. LeBlanc, E. J. Nicol, Emergence of plasmaronic structure in the near-field optical response of graphene. *Phys. Rev. B* **85**, 201411(R) (2012). doi: [10.1103/PhysRevB.85.201411](https://doi.org/10.1103/PhysRevB.85.201411)
- L. Lu, J. D. Joannopoulos, M. Soljačić, Topological photonics. *Nat. Photonics* **8**, 821–829 (2014). doi: [10.1038/nphoton.2014.248](https://doi.org/10.1038/nphoton.2014.248)
- K. Y. Bliokh, F. J. Rodríguez-Fortuño, F. Nori, A. V. Zayats, Spin-orbit interactions of light. *Nat. Photonics* **9**, 796–808 (2015). doi: [10.1038/nphoton.2015.201](https://doi.org/10.1038/nphoton.2015.201)
- J. C. W. Song, M. S. Rudner, Chiral plasmons without magnetic field. *Proc. Natl. Acad. Sci. U.S.A.* **113**, 4658–4663 (2016). doi: [10.1073/pnas.1519086113](https://doi.org/10.1073/pnas.1519086113); pmid: [27071090](https://pubmed.ncbi.nlm.nih.gov/27071090/)
- A. Kumar *et al.*, Chiral plasmon in gapped Dirac systems. *Phys. Rev. B* **93**, 041413(R) (2016). doi: [10.1103/PhysRevB.93.041413](https://doi.org/10.1103/PhysRevB.93.041413)
- T. Karzig, C.-E. Bardyn, N. H. Lindner, G. Refael, Topological polaritons. *Phys. Rev. X* **5**, 031001 (2015). doi: [10.1103/PhysRevX.5.031001](https://doi.org/10.1103/PhysRevX.5.031001)
- A. Kumar, T. Low, K. H. Fung, P. Avouris, N. X. Fang, Tunable light-matter interaction and the role of hyperbolicity in graphene-hBN system. *Nano Lett.* **15**, 3172–3180 (2015). doi: [10.1021/acs.nanolett.5b01191](https://doi.org/10.1021/acs.nanolett.5b01191); pmid: [25897983](https://pubmed.ncbi.nlm.nih.gov/25897983/)
- J. D. Caldwell *et al.*, Atomic-scale photonic hybrids for mid-infrared and terahertz nanophotonics. *Nat. Nanotechnol.* **11**, 9–15 (2016). doi: [10.1038/nnano.2015.305](https://doi.org/10.1038/nnano.2015.305)
- S. Dai *et al.*, Graphene on hexagonal boron nitride as a tunable hyperbolic metamaterial. *Nat. Nanotechnol.* **10**, 682–686 (2015). doi: [10.1038/nnano.2015.131](https://doi.org/10.1038/nnano.2015.131); pmid: [26098228](https://pubmed.ncbi.nlm.nih.gov/26098228/)
- C.-J. Kim *et al.*, Chiral atomically thin films. *Nat. Nanotechnol.* **11**, 520–524 (2016). doi: [10.1038/nnano.2016.3](https://doi.org/10.1038/nnano.2016.3); pmid: [26900756](https://pubmed.ncbi.nlm.nih.gov/26900756/)
- P.-C. Yeh *et al.*, Direct measurement of the tunable electronic structure of bilayer MoS_2 by interlayer twist. *Nano Lett.* **16**, 953–959 (2016). doi: [10.1021/acs.nanolett.5b03883](https://doi.org/10.1021/acs.nanolett.5b03883); pmid: [26760447](https://pubmed.ncbi.nlm.nih.gov/26760447/)
- A. J. Giles *et al.*, Imaging of anomalous internal reflections of hyperbolic phonon-polaritons in hexagonal boron nitride. *Nano Lett.* **16**, 3858–3865 (2016). doi: [10.1021/acs.nanolett.6b01341](https://doi.org/10.1021/acs.nanolett.6b01341)
- Z. Fei *et al.*, Edge and surface plasmons in graphene nanoribbons. *Nano Lett.* **15**, 8271–8276 (2015). doi: [10.1021/acs.nanolett.5b03834](https://doi.org/10.1021/acs.nanolett.5b03834); pmid: [26571096](https://pubmed.ncbi.nlm.nih.gov/26571096/)

65. A. Y. Nikitin *et al.*, Real-space mapping of tailored sheet and edge plasmons in graphene nanoresonators. *Nat. Photonics* **10**, 239–243 (2016). doi: [10.1038/nphoton.2016.44](#)
66. S. Gamage *et al.*, Nanoscopy of black phosphorus degradation. *Adv. Mater. Interfaces* **10**, 1600121 (2016). doi: [10.1002/admi.201600121](#)
67. A. Nemilentsau, T. Low, G. Hanson, Anisotropic 2D materials for tunable hyperbolic plasmonics. *Phys. Rev. Lett.* **116**, 066804 (2016). doi: [10.1103/PhysRevLett.116.066804](#); pmid: [26919007](#)
68. J. Velasco Jr. *et al.*, Nanoscale control of rewritable doping patterns in pristine graphene/boron nitride heterostructures. *Nano Lett.* **16**, 1620–1625 (2016). doi: [10.1021/acs.nanolett.5b04441](#); pmid: [26852622](#)
69. Z. Fang *et al.*, Plasmon-induced doping of graphene. *ACS Nano* **6**, 10222–10228 (2012). doi: [10.1021/nn304028b](#); pmid: [22998468](#)
70. F. H. L. Koppens *et al.*, Photodetectors based on graphene, other two-dimensional materials and hybrid systems. *Nat. Nanotechnol.* **9**, 780–793 (2014). doi: [10.1038/nnano.2014.215](#); pmid: [25286273](#)
71. X. Xu, W. Yao, D. Xiao, T. F. Heinz, Spin and pseudospins in layered transition metal dichalcogenides. *Nat. Phys.* **10**, 343–350 (2014). doi: [10.1038/nphys2942](#)
72. I. Crassee *et al.*, Intrinsic terahertz plasmons and magnetoplasmons in large scale monolayer graphene. *Nano Lett.* **12**, 2470–2474 (2012). doi: [10.1021/nl300572y](#); pmid: [22519967](#)
73. K.-D. Park *et al.*, Hybrid tip-enhanced nanospectroscopy and nanoimaging of monolayer WSe₂ with local strain control. *Nano Lett.* **16**, 2621–2627 (2016). doi: [10.1021/acs.nanolett.6b00238](#)
74. P. Bharadwaj, L. Novotny, Optoelectronics in Flatland. *Opt. Photon. News* **26**, 24 (2015). doi: [10.1364/OPN.26.7.000024](#)
75. A. Vakil, N. Engheta, Transformation optics using graphene. *Science* **332**, 1291–1294 (2011). doi: [10.1126/science.1202691](#); pmid: [21659598](#)
76. W. Gao *et al.*, Topological photonic phase in chiral hyperbolic metamaterials. *Phys. Rev. Lett.* **114**, 037402 (2015). doi: [10.1103/PhysRevLett.114.037402](#); pmid: [25659022](#)
77. S. Chakraborty *et al.*, Gain modulation by graphene plasmons in aperiodic lattice lasers. *Science* **351**, 246–248 (2016). doi: [10.1126/science.aad2930](#); pmid: [26816373](#)
78. M. Polini, Tuning terahertz lasers via graphene plasmons. *Science* **351**, 229–231 (2016). doi: [10.1126/science.aad7995](#); pmid: [26816365](#)
79. Z. Fang *et al.*, Gated tunability and hybridization of localized plasmons in nanostructured graphene. *ACS Nano* **7**, 2388–2395 (2013). doi: [10.1021/nn3055835](#); pmid: [23390960](#)
80. M. Liu *et al.*, A graphene-based broadband optical modulator. *Nature* **474**, 64–67 (2011). doi: [10.1038/nature10067](#); pmid: [21552277](#)
81. C. T. Phare, Y.-H. D. Lee, J. Cardenas, M. Lipson, Graphene electro-optic modulator with 30 GHz bandwidth. *Nat. Photonics* **9**, 511–514 (2015). doi: [10.1038/nphoton.2015.122](#)
82. P. Li *et al.*, Hyperbolic phonon-polaritons in boron nitride for near-field optical imaging and focusing. *Nat. Commun.* **6**, 7507 (2015). doi: [10.1038/ncomms8507](#); pmid: [26112474](#)
83. D. Rodrigo *et al.*, Mid-infrared plasmonic biosensing with graphene. *Science* **349**, 165–168 (2015). doi: [10.1126/science.aab2051](#); pmid: [26160941](#)
84. D. B. Farmer, P. Avouris, Y. Li, T. F. Heinz, S.-J. Han, Ultrasensitive plasmonic detection of molecules with graphene. *ACS Photonics* **3**, 553–557 (2016). doi: [10.1021/acsp Photonics.6b00143](#)
85. J. B. Khurgin, G. Sun, R. A. Soref, Enhancement of luminescence efficiency using surface plasmon polaritons: Figures of merit. *J. Opt. Soc. Am. B* **24**, 1968 (2007). doi: [10.1364/JOSAB.24.001968](#)
86. T. Hasan *et al.*, Nanotube-polymer composites for ultrafast photonics. *Adv. Mater.* **21**, 3874–3899 (2009). doi: [10.1002/adma.200901122](#)
87. S. Wu *et al.*, Monolayer semiconductor nanocavity lasers with ultralow thresholds. *Nature* **520**, 69–72 (2015). doi: [10.1038/nature14290](#); pmid: [25778703](#)
88. D. N. Basov, T. Timusk, Electrodynamics of high-T_c superconductors. *Rev. Mod. Phys.* **77**, 721–779 (2005). doi: [10.1103/RevModPhys.77.721](#)
89. H. T. Stinson *et al.*, Infrared nanospectroscopy and imaging of collective superfluid excitations in anisotropic superconductors. *Phys. Rev. B* **90**, 014502 (2014). doi: [10.1103/PhysRevB.90.014502](#)
90. A. Tsiatmas, V. A. Fedotov, F. J. García de Abajo, N. I. Zheludev, Low-loss terahertz superconducting plasmonics. *New J. Phys.* **14**, 115006 (2012). doi: [10.1088/1367-2630/14/11/115006](#)
91. E. E. Narimanov, A. V. Kildishev, Metamaterials: Naturally hyperbolic. *Nat. Photonics* **9**, 214–216 (2015). doi: [10.1038/nphoton.2015.56](#)
92. J. B. Khurgin, Two-dimensional exciton-polariton—light guiding by transition metal dichalcogenide monolayers. *Optica* **2**, 740 (2015). doi: [10.1364/OPTICA.2.000740](#)
93. J.-S. Wu, D. N. Basov, M. M. Fogler, Topological insulators are tunable waveguides for hyperbolic polaritons. *Phys. Rev. B* **92**, 205430 (2015). doi: [10.1103/PhysRevB.92.205430](#)
94. M. Gullans, D. E. Chang, F. H. L. Koppens, F. J. García de Abajo, M. D. Lukin, Single-photon nonlinear optics with graphene plasmons. *Phys. Rev. Lett.* **111**, 247401 (2013). doi: [10.1103/PhysRevLett.111.247401](#); pmid: [24483697](#)
95. T. J. Constant, S. M. Hornett, D. E. Chang, E. Hendry, All-optical generation of surface plasmons in graphene. *Nat. Phys.* **12**, 124–127 (2016). doi: [10.1038/nphys3545](#)
96. X. Yin *et al.*, Edge nonlinear optics on a MoS₂ atomic monolayer. *Science* **344**, 488–490 (2014). doi: [10.1126/science.1250564](#); pmid: [24786072](#)
97. J. D. Cox, F. Javier García de Abajo, Electrically tunable nonlinear plasmonics in graphene nanoislands. *Nat. Commun.* **5**, 5725 (2014). doi: [10.1038/ncomms5725](#); pmid: [25500534](#)
98. Y. Laplace, S. Fernandez-Pena, S. Gariglio, J. M. Triscone, A. Cavalleri, Proposed cavity Josephson plasmonics with complex-oxide heterostructures. *Phys. Rev. B* **93**, 075152 (2016). doi: [10.1103/PhysRevB.93.075152](#)
99. N. Rivera, I. Kaminer, B. Zhen, J. D. Joannopoulos, M. Soljačić, Shrinking light to allow forbidden transitions on the atomic scale. *Science* **353**, 263–269 (2016). doi: [10.1126/science.1250564](#); pmid: [24786072](#)
100. J. A. Gerber, S. Berweger, B. T. O'Callahan, M. B. Raschke, Phase-resolved surface plasmon interferometry of graphene. *Phys. Rev. Lett.* **113**, 055502 (2014). doi: [10.1103/PhysRevLett.113.055502](#); pmid: [25126927](#)
101. A. Tomadin, F. Guinea, M. Polini, Generation and morphing of plasmons in graphene superlattices. *Phys. Rev. B* **90**, 161406(R) (2014). doi: [10.1103/PhysRevB.90.161406](#)
102. S. Dai *et al.*, Tunable phonon polaritons in atomically thin van der Waals crystals of boron nitride. *Science* **343**, 1125–1129 (2014). doi: [10.1126/science.1246833](#); pmid: [24604197](#)
103. J. D. Caldwell *et al.*, Sub-diffractive volume-confined polaritons in the natural hyperbolic material hexagonal boron nitride. *Nat. Commun.* **5**, 5221 (2014). doi: [10.1038/ncomms5221](#); pmid: [25323633](#)
104. Z. Shi *et al.*, Amplitude- and phase-resolved nanospectral imaging of phonon polaritons in hexagonal boron nitride. *ACS Photonics* **2**, 790–796 (2015). doi: [10.1021/acsp Photonics.5b00007](#)
105. A. Politano *et al.*, Interplay of surface and Dirac plasmons in topological insulators: The case of Bi₂Se₃. *Phys. Rev. Lett.* **115**, 216802 (2015). doi: [10.1103/PhysRevLett.115.216802](#); pmid: [26636863](#)
106. A. Kogar *et al.*, Surface collective modes in the topological insulators Bi₂Se₃ and Bi_{0.5}Sb_{1.5}Te₃. *Phys. Rev. Lett.* **115**, 257402 (2015). doi: [10.1103/PhysRevLett.115.257402](#); pmid: [26722943](#)
107. V. A. Golick *et al.*, Surface Josephson plasma waves in layered superconductors above the plasma frequency: Evidence for a negative index of refraction. *Phys. Rev. Lett.* **104**, 187003 (2010). doi: [10.1103/PhysRevLett.104.187003](#); pmid: [20482202](#)
108. F. J. Dunmore, D. Z. Liu, H. D. Drew, S. Das Sarma, Observation of below-gap plasmon excitations in superconducting YBa₂Cu₃O₇ films. *Phys. Rev. B* **52**, R731(R) (1995). doi: [10.1103/PhysRevB.52.R731](#); pmid: [9980738](#)
109. T. Low *et al.*, Plasmons and screening in monolayer and multilayer black phosphorus. *Phys. Rev. Lett.* **113**, 106802 (2014). doi: [10.1103/PhysRevLett.113.106802](#); pmid: [25238376](#)
110. H. Yan *et al.*, Damping pathways of mid-infrared plasmons in graphene nanostructures. *Nat. Photonics* **7**, 394–399 (2013). doi: [10.1038/nphoton.2013.57](#)
111. L. Ju *et al.*, Graphene plasmonics for tunable terahertz metamaterials. *Nat. Nanotechnol.* **6**, 630–634 (2011). doi: [10.1038/nnano.2011.146](#); pmid: [21892164](#)
112. M. Autore *et al.*, Plasmon-phonon interactions in topological insulator microrings. *Adv. Opt. Mater.* **3**, 1257–1263 (2015). doi: [10.1002/adom.201400513](#)
113. F. J. García de Abajo, Multiple excitation of confined graphene plasmons by single free electrons. *ACS Nano* **7**, 11409–11419 (2013). doi: [10.1021/nn405367e](#); pmid: [24219514](#)
114. F. H. L. Koppens, D. E. Chang, F. J. García de Abajo, Graphene plasmonics: A platform for strong light-matter interactions. *Nano Lett.* **11**, 3370–3377 (2011). doi: [10.1021/nl201771h](#); pmid: [21766812](#)
115. A. Yu. Nikitin, F. Guinea, F. J. García-Vidal, L. Martín-Moreno, Fields radiated by a nanoemitter in a graphene sheet. *Phys. Rev. B* **84**, 195446 (2011). doi: [10.1103/PhysRevB.84.195446](#)
116. R. Beams, P. Bharadwaj, L. Novotny, Electroluminescence from graphene excited by electron tunneling. *Nanotechnology* **25**, 055206 (2014). doi: [10.1088/0957-4848/25/5/055206](#); pmid: [24407020](#)
117. J. Schiefele, J. Pedrós, F. Sols, F. Calle, F. Guinea, Coupling light into graphene plasmons through surface acoustic waves. *Phys. Rev. Lett.* **111**, 237405 (2013). doi: [10.1103/PhysRevLett.111.237405](#); pmid: [24476304](#)
118. M. Farhat, S. Guenneau, H. Bagci, Exciting graphene surface plasmon polaritons through light and sound interplay. *Phys. Rev. Lett.* **111**, 237404 (2013). doi: [10.1103/PhysRevLett.111.237404](#)

ACKNOWLEDGMENTS

Supported by Office of Naval Research grant N00014-15-1-2671, Air Force Office of Scientific Research grant FA9550-15-1-0478, and U.S. Department of Energy grants DE-FG02-00ER45799, DOE-DE-SC0012592, and DE-SC0012375. D.N.B. is an investigator in quantum materials funded by the Gordon and Betty Moore Foundation's EPIQS Initiative through grant GBMF4533. F.J.G.d.A. is supported by Ministerio de Economía y Competitividad (Spain) grants MAT2014-59096-P and SEV-2015-0522 and by European Commission grants CNECT-ICT-604391 and FP7-ICT-2013-613024-GRASP.

10.1126/science.aag1992

RESEARCH ARTICLE SUMMARY

FOREST ECOLOGY

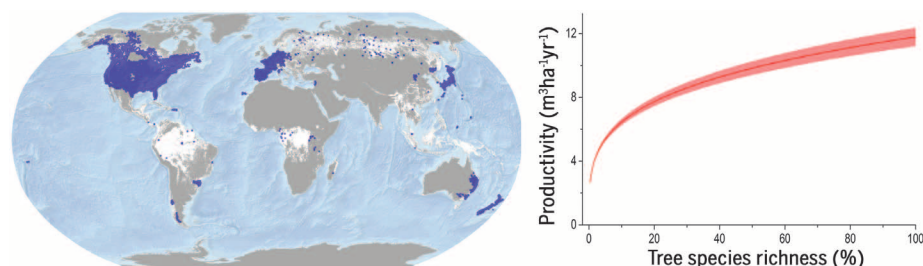
Positive biodiversity-productivity relationship predominant in global forests

Jingjing Liang,* Thomas W. Crowther, Nicolas Picard, Susan Wiser, Mo Zhou, Giorgio Alberti, Ernst-Detlef Schulze, A. David McGuire, Fabio Bozzato, Hans Pretzsch, Sergio de-Miguel, Alain Paquette, Bruno Hérault, Michael Scherer-Lorenzen, Christopher B. Barrett, Henry B. Glick, Geerten M. Hengeveld, Gert-Jan Nabuurs, Sebastian Pfautsch, Helder Viana, Alexander C. Vibrans, Christian Ammer, Peter Schall, David Verbyla, Nadja Tchebakova, Markus Fischer, James V. Watson, Han Y. H. Chen, Xiangdong Lei, Mart-Jan Schelhaas, Huicui Lu, Damiano Gianelle, Elena I. Parfenova, Christian Salas, Eungul Lee, Boknam Lee, Hyun Seok Kim, Helge Bruelheide, David A. Coomes, Daniel Piotto, Terry Sunderland, Bernhard Schmid, Sylvie Gourlet-Fleury, Bonaventure Sonké, Rebecca Tavani, Jun Zhu, Susanne Brandl, Jordi Vayreda, Fumiaki Kitahara, Eric B. Searle, Victor J. Neldner, Michael R. Ngugi, Christopher Baraloto, Lorenzo Frizzera, Radomir Balazy, Jacek Oleksyn, Tomasz Zawila-Niedzwiecki, Olivier Bouriaud, Filippo Bussotti, Leena Finér, Bogdan Jaroszewicz, Tommaso Jucker, Fernando Valladares, Andrzej M. Jagodzinski, Pablo L. Peri, Christelle Gonmadje, William Marthy, Timothy O'Brien, Emanuel H. Martin, Andrew R. Marshall, Francesco Rovero, Robert Bitariho, Pascal A. Niklaus, Patricia Alvarez-Loayza, Nurdin Chamuya, Renato Valencia, Frédéric Mortier, Verginia Wortel, Nestor L. Engone-Obiang, Leandro V. Ferreira, David E. Odeke, Rodolfo M. Vasquez, Simon L. Lewis, Peter B. Reich

INTRODUCTION: The biodiversity-productivity relationship (BPR; the effect of biodiversity on ecosystem productivity) is foundational to our understanding of the global extinction crisis and its impacts on the functioning of natural ecosystems. The BPR has been a prominent research topic within ecology in recent decades, but it is only recently that we have begun to develop a global perspective.

RATIONALE: Forests are the most important global repositories of terrestrial biodiversity, but deforestation, forest degradation, climate change, and other factors are threatening

approximately one half of tree species worldwide. Although there have been substantial efforts to strengthen the preservation and sustainable use of forest biodiversity throughout the globe, the consequences of this diversity loss pose a major uncertainty for ongoing international forest management and conservation efforts. The forest BPR represents a critical missing link for accurate valuation of global biodiversity and successful integration of biological conservation and socioeconomic development. Until now, there have been limited tree-based diversity experiments, and the forest BPR has only been explored within regional-



Global effect of tree species diversity on forest productivity. Ground-sourced data from 777,126 global forest biodiversity permanent sample plots (dark blue dots, left), which cover a substantial portion of the global forest extent (white), reveal a consistent positive and concave-down biodiversity-productivity relationship across forests worldwide (red line with pink bands representing 95% confidence interval, right).

scale observational studies. Thus, the strength and spatial variability of this relationship remains unexplored at a global scale.

RESULTS: We explored the effect of tree species richness on tree volume productivity at the global scale using repeated forest inventories from 777,126 permanent sample plots in 44 countries containing more than 30 million trees from 8737 species spanning most of the global terrestrial biomes. Our findings reveal a

ON OUR WEBSITE

Read the full article at <http://dx.doi.org/10.1126/science.aaf8957>

consistent positive concave-down effect of biodiversity on forest productivity across the world, showing that a continued biodiversity loss would result in an accelerating decline in forest productivity worldwide.

The BPR shows considerable geospatial variation across the world. The same percentage of biodiversity loss would lead to a greater relative (that is, percentage) productivity decline in the boreal forests of North America, Northeastern Europe, Central Siberia, East Asia, and scattered regions of South-central Africa and South-central Asia. In the Amazon, West and Southeastern Africa, Southern China, Myanmar, Nepal, and the Malay Archipelago, however, the same percentage of biodiversity loss would lead to greater absolute productivity decline.

CONCLUSION: Our findings highlight the negative effect of biodiversity loss on forest productivity and the potential benefits from the transition of monocultures to mixed-species stands in forestry practices. The BPR we discover across forest ecosystems worldwide corresponds well with recent theoretical advances, as well as with experimental and observational studies on forest and nonforest ecosystems. On the basis of this relationship, the ongoing species loss in forest ecosystems worldwide could substantially reduce forest productivity and thereby forest carbon absorption rate to compromise the global forest carbon sink. We further estimate that the economic value of biodiversity in maintaining commercial forest productivity alone is \$166 billion to \$490 billion per year. Although representing only a small percentage of the total value of biodiversity, this value is two to six times as much as it would cost to effectively implement conservation globally. These results highlight the necessity to reassess biodiversity valuation and the potential benefits of integrating and promoting biological conservation in forest resource management and forestry practices worldwide. ■

The list of author affiliations is available in the full article online.

*Corresponding author. Email: albeca.liang@gmail.com
Cite this article as J. Liang et al., *Science* 354, aaf8957 (2016). DOI: 10.1126/science.aaf8957

RESEARCH ARTICLE

FOREST ECOLOGY

Positive biodiversity-productivity relationship predominant in global forests

Jingjing Liang,^{1*} Thomas W. Crowther,^{2,3†} Nicolas Picard,⁴ Susan Wiser,⁵ Mo Zhou,¹ Giorgio Alberti,⁶ Ernst-Detlef Schulze,⁷ A. David McGuire,⁸ Fabio Bozzato,⁹ Hans Pretzsch,¹⁰ Sergio de-Miguel,^{11,12} Alain Paquette,¹³ Bruno Hérault,¹⁴ Michael Scherer-Lorenzen,¹⁵ Christopher B. Barrett,¹⁶ Henry B. Glick,³ Geerten M. Hengeveld,^{17,18} Gert-Jan Nabuurs,^{17,19} Sebastian Pfautsch,²⁰ Helder Viana,^{21,22} Alexander C. Vibrans,²³ Christian Ammer,²⁴ Peter Schall,²⁴ David Verbyla,²⁵ Nadja Tchekakova,²⁶ Markus Fischer,^{27,28} James V. Watson,¹ Han Y. H. Chen,²⁹ Xiangdong Lei,³⁰ Mart-Jan Schelhaas,¹⁷ Huicui Lu,¹⁹ Damiano Gianelle,^{31,32} Elena I. Parfenova,²⁶ Christian Salas,³³ Eungul Lee,³⁴ Boknam Lee,³⁵ Hyun Seok Kim,^{35,36,37,38} Helge Bruelheide,^{39,40} David A. Coomes,⁴¹ Daniel Piotto,⁴² Terry Sunderland,^{43,44} Bernhard Schmid,⁴⁵ Sylvie Gourlet-Fleury,⁴⁶ Bonaventure Sonké,⁴⁷ Rebecca Tavani,⁴⁸ Jun Zhu,^{49,50} Susanne Brandt,^{10,51} Jordi Vayreda,^{52,53} Fumiaki Kitahara,⁵⁴ Eric B. Searle,²⁹ Victor J. Neldner,⁵⁵ Michael R. Ngugi,⁵⁵ Christopher Baraloto,^{56,57} Lorenzo Frizzera,³¹ Radomir Bałazy,⁵⁸ Jacek Oleksyn,^{59,60} Tomasz Zawila-Niedzwiecki,^{61,62} Olivier Bouriaud,^{63,64} Filippo Bussotti,⁶⁵ Leena Finér,⁶⁶ Bogdan Jaroszewicz,⁶⁷ Tommaso Jucker,⁴¹ Fernando Valladares,^{68,69} Andrzej M. Jagodzinski,^{59,70} Pablo L. Peri,^{71,72,73} Christelle Gonmadje,^{74,75} William Marthy,⁷⁶ Timothy O'Brien,⁷⁶ Emanuel H. Martin,⁷⁷ Andrew R. Marshall,^{78,79} Francesco Rovero,⁸⁰ Robert Bitariho,⁸¹ Pascal A. Niklaus,⁴⁵ Patricia Alvarez-Loayza,⁸² Nurdin Chamuya,⁸³ Renato Valencia,⁸⁴ Frédéric Mortier,⁴⁶ Verginia Wortel,⁸⁵ Nestor L. Engone-Obiang,⁸⁶ Leandro V. Ferreira,⁸⁷ David E. Odeke,⁸⁸ Rodolfo M. Vasquez,⁸⁹ Simon L. Lewis,^{90,91} Peter B. Reich^{20,60}

The biodiversity-productivity relationship (BPR) is foundational to our understanding of the global extinction crisis and its impacts on ecosystem functioning. Understanding BPR is critical for the accurate valuation and effective conservation of biodiversity. Using ground-sourced data from 777,126 permanent plots, spanning 44 countries and most terrestrial biomes, we reveal a globally consistent positive concave-down BPR, showing that continued biodiversity loss would result in an accelerating decline in forest productivity worldwide. The value of biodiversity in maintaining commercial forest productivity alone—US\$166 billion to 490 billion per year according to our estimation—is more than twice what it would cost to implement effective global conservation. This highlights the need for a worldwide reassessment of biodiversity values, forest management strategies, and conservation priorities.

The biodiversity-productivity relationship (BPR) has been a major ecological research focus over recent decades. The need to understand this relationship is becoming increasingly urgent in light of the global extinction crisis because species loss affects the functioning and services of natural ecosystems (1, 2). In response to an emerging body of evidence that suggests that the functioning of natural ecosystems may be substantially impaired by reductions in species richness (3–10), global environmental authorities, including the Intergovernmental Platform on Biodiversity and Ecosystem Services (IPBES) and United Nations Environment Programme (UNEP), have made substantial efforts to strengthen the preservation and sustainable use of biodiversity (2, 11). Successful international

collaboration, however, requires a systematic assessment of the value of biodiversity (11). Quantification of the global BPR is thus urgently needed to facilitate the accurate valuation of biodiversity (12), the forecast of future changes in ecosystem services worldwide (11), and the integration of biological conservation into international socioeconomic development strategies (13).

The evidence of a positive BPR stems primarily from studies of herbaceous plant communities (14). In contrast, the forest BPR has only been explored at the regional scale [(3, 4, 7, 15) and references therein] or within a limited number of tree-based experiments [(16, 17) and references therein], and it remains unclear whether these relationships hold across forest types. Forests are the most important global repositories of

terrestrial biodiversity (18), but deforestation, climate change, and other factors are threatening a considerable proportion (up to 50%) of tree species worldwide (19–21). The consequences of this diversity loss pose a critical uncertainty for ongoing international forest management and conservation efforts. Conversely, forest management that converts monocultures to mixed-species stands has often seen a substantial positive effect on productivity with other benefits (22–24). Although forest plantations are predicted to meet 50 to 75% of the demand for lumber by 2050 (25, 26), nearly all are still planted as monocultures, highlighting the potential of forest management in strengthening the conservation and sustainable use of biodiversity worldwide.

Here, we compiled in situ remeasurement data, most of which were taken at two consecutive inventories from the same localities, from 777,126 permanent sample plots [hereafter, global forest biodiversity (GFB) plots] across 44 countries and territories and 13 ecoregions to explore the forest BPR at a global scale (Fig. 1). GFB plots encompass forests of various origins (from naturally regenerated to planted) and successional stages (from stand initiation to old-growth). A total of more than 30 million trees across 8737 species were tallied and measured on two or more consecutive inventories from the GFB plots. Sampling intensity was greater in developed countries, where nationwide forest inventories have been fully or partially funded by governments. In most other countries, national forest inventories were lacking, and most ground-sourced data were collected by individuals and organizations (table S1).

On the basis of ground-sourced GFB data, we quantified BPR at the global scale using a data-driven ensemble learning approach (Materials and methods, Geospatial random forest). Our quantification of BPR involved characterizing the shape and strength of the dependency function through the elasticity of substitution (θ), which represents the degree to which species can substitute for each other in contributing to forest productivity; θ measures the marginal productivity—the change in productivity resulting from one unit decline of species richness—and reflects the strength of the effect of tree diversity on forest productivity, after accounting for climatic, soil, and plot-specific covariates. A higher θ corresponds to a greater decline in productivity due to one unit loss in biodiversity. The niche-efficiency (N-E) model (3) and several preceding studies (27–30) provide a framework for interpreting the elasticity of substitution and approximating BPR with a power function model:

$$P = \alpha \cdot f(\mathbf{X}) \cdot S^{\theta} \quad (1)$$

where P and S signify primary site productivity and tree species richness (observed on a 900-m² area basis on average) (Materials and methods), respectively; $f(\mathbf{X})$ is a function of a vector of control variables \mathbf{X} (selected from stand basal area and 14 climatic, soil, and topographic covariates); and α is a constant. This model is capable of representing a variety of potential patterns of

BPR. $0 < \theta < 1$ represents a positive and concave down pattern (a degressively increasing curve), which is consistent with the N-E model and preceding studies (3, 27–30), whereas other θ values can represent alternative BPR patterns, including decreasing ($\theta < 0$), linear ($\theta = 1$), convex ($\theta > 1$), or no effect ($\theta = 0$) (Fig. 2) (14, 31). The model (Eq. 1) was estimated by using the geospatial random forest technique based on GFB data and covariates acquired from ground-measured and remote-sensing data (Materials and methods).

We found that a positive BPR predominated in forests worldwide. Out of 10,000 randomly selected subsamples (each consisting of 500 GFB plots), 99.87% had a positive concave-down relationship with relative species richness ($0 < \theta < 1$), whereas only 0.13% show negative trends, and none was equal to zero or greater than or equal to 1 (Fig. 2). Overall, the global forest productivity increased with a declining rate from 2.7 to 11.8 $\text{m}^3 \text{ha}^{-1} \text{year}^{-1}$ as relative tree species richness increased from the minimum to the maximum

value, which corresponds to a θ value of 0.26 (Fig. 3A).

At the global scale, we mapped the magnitude of BPR (as expressed by θ) using geospatial random forest and universal kriging. By plotting values of θ onto a global map, we revealed considerable geospatial variation across the world (Fig. 3B). The highest θ (0.29 to 0.30) occurred in the boreal forests of North America, North-eastern Europe, Central Siberia, and East Asia and the sporadic tropical and subtropical forests of South-central Africa, South-central Asia, and the Malay Archipelago. In these areas of the highest elasticity of substitution (32), the same percentage of biodiversity loss would lead to a greater percentage of reduction in forest productivity (Fig. 4A). In terms of absolute productivity, the same percentage of biodiversity loss would lead to the greatest productivity decline in the Amazon; West Africa's Gulf of Guinea; South-eastern Africa, including Madagascar; Southern China; Myanmar; Nepal; and the Malay Archi-

pelago (Fig. 4B). Because of a relatively narrow range of the elasticity of substitution (32) estimated from the global-level analysis (0.2 to 0.3), the regions of the greatest productivity decline under the same percentage of biodiversity loss largely matched the regions of the greatest productivity (fig. S1). Globally, a 10% decrease in tree species richness (from 100 to 90%) would cause a 2 to 3% decline in productivity, and with a decrease in tree species richness to one (Materials and methods, Economic analysis), this decline in forest productivity would be 26 to 66% even if other things, such as the total number of trees and forest stocking, remained the same (fig. S4).

Discussion

Our global analysis provides strong and consistent evidence that productivity of forests would decrease at an accelerating rate with the loss of biodiversity. The positive concave-down pattern we discovered across forest ecosystems worldwide corresponds well with recent theoretical advances

- ¹School of Natural Resources, West Virginia University, Morgantown, WV 26505, USA. ²Netherlands Institute of Ecology, Droevendaalsesteeg 10, 6708 PB Wageningen, Netherlands. ³Yale School of Forestry and Environmental Studies, Yale University, 195 Prospect Street, New Haven, CT 06511, USA. ⁴Forestry Department, Food and Agriculture Organization of the United Nations, Rome, Italy. ⁵Landcare Research, Lincoln 7640, New Zealand. ⁶Department of Agri-Food, Animal and Environmental Sciences, University of Udine via delle Scienze 206, Udine 33100, Italy. ⁷Max-Planck Institut für Biogeochemie, Hans-Knoell-Strasse 10, 07745 Jena, Germany. ⁸U.S. Geological Survey, Alaska Cooperative Fish and Wildlife Research Unit, University of Alaska Fairbanks, Fairbanks, AK 99775, USA. ⁹Architecture and Environment Department, Italcementi Group, 24100 Bergamo, Italy. ¹⁰Institute of Forest Growth and Yield Science, School of Life Sciences Weihenstephan, Technical University of Munich (TUM), Hans-Carl-von-Carlowitz-Platz 2, 85354 Freising, Germany. ¹¹Departament de Producció Vegetal i Ciència Forestal, Universitat de Lleida-Agrotecnic Center (UdL-Agrotecnic), Avinguda Rovira Roure, 191, E-25198 Lleida, Spain. ¹²Centre Tecnològic Forestal de Catalunya (CTFC), Carretera De St. Llorenç de Morunys, km. 2, E-25280 Solsona, Spain. ¹³Centre d'étude de la forêt (CEF), Université du Québec à Montréal, Montréal, QC H3C 3P8, Canada. ¹⁴Centre de Coopération Internationale en la Recherche Agronomique pour le Développement (CIRAD), UMR Joint Research Unit Ecology of Guianan Forests (EcoFoG) AgroParisTech, CNRS, INRA, Université des Antilles, Université de la Guyane, Kourou, French Guiana. ¹⁵University of Freiburg, Faculty of Biology, Geobotany, D-79104 Freiburg, Germany. ¹⁶Charles H. Dyson School of Applied Economics and Management, Cornell University, Ithaca, NY 14853, USA. ¹⁷Wageningen University and Research (Alterra), Team Vegetation, Forest and Landscape Ecology–6700 AA, Netherlands. ¹⁸Forest and Nature Conservation Policy Group, Wageningen University and Research, 6700 AA Wageningen, Netherlands. ¹⁹Forest Ecology and Forest Management Group, Wageningen University, 6700 AA Wageningen UR, Netherlands. ²⁰Hawkesbury Institute for the Environment, Western Sydney University, Richmond NSW 2753, Australia. ²¹Center for Studies in Education, Technologies and Health (CI&DETS) Research Centre/Departamento de Ecologia e Agricultura Sustentável (DEAS)–Escola Superior Agrária de Viseu (ESAV), Polytechnic Institute of Viseu, Portugal. ²²Centre for the Research and Technology of Agro-Environmental and Biological Sciences, (CITAB), University of Trás-os-Montes and Alto Douro (UTAD), Quinta de Prados, 5000-801 Vila Real, Portugal. ²³Departamento de Engenharia Florestal, Universidade Regional de Blumenau, Rua São Paulo, 3250, 89030-000 Blumenau-Santa Catarina, Brazil. ²⁴Department of Silviculture and Forest Ecology of the Temperate Zones, Georg-August University Göttingen, Büsgenweg 1, D-37077 Göttingen, Germany. ²⁵School of Natural Resources and Extension, University of Alaska Fairbanks, Fairbanks, AK 99709, USA. ²⁶V. N. Sukachev Institute of Forests, Siberian Branch, Russian Academy of Sciences, Academgorodok, 50/28, 660036 Krasnoyarsk, Russia. ²⁷Institute of Plant Sciences, Botanical Garden, and Oeschger Centre for Climate Change Research, University of Bern, 3013 Bern, Switzerland. ²⁸Senckenberg Gesellschaft für Naturforschung, Biodiversity and Climate Research Centre (BIK-F), 60325 Frankfurt, Germany. ²⁹Faculty of Natural Resources Management, Lakehead University, Thunder Bay, ON P7B 5E1 Canada. ³⁰Research Institute of Forest Resource Information Techniques, Chinese Academy of Forestry, Beijing 100091, China. ³¹Sustainable Agro-Ecosystems and Bioresources Department, Research and Innovation Centre - Fondazione Edmund Mach, Via E. Mach 1, 38010-S. Michele all'Adige (TN), Italy. ³²Foxlab Joint CNR–Fondazione Edmund Mach Initiative, Via E. Mach 1, 38010 - S. Michele all'Adige (TN), Italy. ³³Departamento de Ciencias Forestales, Universidad de La Frontera, Temuco, Chile. ³⁴Department of Geology and Geography, West Virginia University, Morgantown, WV 26506, USA. ³⁵Research Institute of Agriculture and Life Sciences, Seoul National University, Seoul, Republic of Korea. ³⁶Department of Forest Sciences, Seoul National University, Seoul 151-921, Republic of Korea. ³⁷Interdisciplinary Program in Agricultural and Forest Meteorology, Seoul National University, Seoul 151-744, Republic of Korea. ³⁸National Center for AgroMeteorology, Seoul National University, Seoul 151-744, Republic of Korea. ³⁹Institute of Biology/Geobotany and Botanical Garden, Martin Luther University Halle-Wittenberg, Am Kirchtor 1, 06108 Halle (Saale), Germany. ⁴⁰German Centre for Integrative Biodiversity Research (iDiv) Halle-Jena-Leipzig, Deutscher Platz 5e, 04103 Leipzig, Germany. ⁴¹Forest Ecology and Conservation, Department of Plant Sciences, University of Cambridge, Cambridge CB2 3EA, UK. ⁴²Universidade Federal do Sul da Bahia, Ferradas, Itabuna 45613-204, Brazil. ⁴³Sustainable Landscapes and Food Systems, Centre for International Forestry Research, Bogor, Indonesia. ⁴⁴School of Marine and Environmental Studies, James Cook University, Australia. ⁴⁵Institute of Evolutionary Biology and Environmental Studies, University of Zurich, CH-8057 Zurich, Switzerland. ⁴⁶UPR F&S Montpellier, 34398, France. ⁴⁷Plant Systematic and Ecology Laboratory, Department of Biology, Higher Teachers' Training College, University of Yaounde I, Post Office Box 047 Yaounde, Cameroon. ⁴⁸Forestry Department, Food and Agriculture Organization of the United Nations, Rome 00153, Italy. ⁴⁹Department of Statistics, University of Wisconsin–Madison, Madison, WI 53706, USA. ⁵⁰Department of Entomology, University of Wisconsin–Madison, Madison, WI 53706, USA. ⁵¹Bavarian State Institute of Forestry, Hans-Carl-von-Carlowitz-Platz 1, Freising 85354, Germany. ⁵²Center for Ecological Research and Forestry Applications (CREAF), Cerdanyola del Vallès 08193, Spain. ⁵³Universitat Autònoma Barcelona, Cerdanyola del Vallès 08193, Spain. ⁵⁴Shikoku Research Center, Forestry and Forest Products Research Institute, Kochi 780-8077, Japan. ⁵⁵Ecological Sciences Unit at Queensland Herbarium, Department of Science, Information Technology and Innovation, Queensland Government, Toowoong, Qld, 4066, Australia. ⁵⁶International Center for Tropical Botany, Department of Biological Sciences, Florida International University, Miami, FL 33199, USA. ⁵⁷INRA, UMR EcoFoG, Kourou, French Guiana. ⁵⁸Forest Research Institute, Sekonci Stary Braci Lesnej 3 Street, 05-090 Raszyn, Poland. ⁵⁹Institute of Dendrology, Polish Academy of Sciences, Parkowa 5, PL-62-035 Kornik, Poland. ⁶⁰Department of Forest Resources, University of Minnesota, St. Paul, MN 55108, USA. ⁶¹Warsaw University of Life Sciences (SGGW), Faculty of Forestry, ul. Nowoursynowska 159, 02-776 Warszawa, Poland. ⁶²Polish State Forests, ul. Grojecka 127, 02-124 Warszawa, Poland. ⁶³Forestry Faculty, University Stefan Cel Mare of Suceava, 13 Strada Universitatii, 720229 Suceava, Romania. ⁶⁴Institutul National de Cercetare-Dezvoltare in Silvicultura, 128 Bd Eroilor, 077190 Voluntari, Romania. ⁶⁵Department of Agri-Food Production and Environmental Science, University of Florence, P. le Cascine 28, 51044 Florence, Italy. ⁶⁶Natural Resources Institute Finland, 80101 Joensuu, Finland. ⁶⁷Białowieża Geobotanical Station, Faculty of Biology, University of Warsaw, Sportowa 19, 17-230 Białowieża, Poland. ⁶⁸Museo Nacional de Ciencias Naturales, Consejo Superior de Investigaciones Científicas, Serrano 115 dpdo, E-28006 Madrid, Spain. ⁶⁹Universidad Rey Juan Carlos, Mostoles, Madrid, Spain. ⁷⁰Poznan University of Life Sciences, Department of Game Management and Forest Protection, Wojska Polskiego 71c, PL-60-625 Poznan, Poland. ⁷¹Consejo Nacional de Investigaciones Científicas y Técnicas (CONICET), Rivadavia 1917 (1033) Ciudad de Buenos Aires, Buenos Aires, Argentina. ⁷²Instituto Nacional de Tecnología Agropecuaria (INTA) Estación Experimental Agropecuaria (EEA) Santa Cruz, Mahatma Gandhi 1322 (9400) Río Gallegos, Santa Cruz, Argentina. ⁷³Universidad Nacional de la Patagonia Austral (UNPA), Lisandro de la Torre 1070 (9400) Río Gallegos, Santa Cruz, Argentina. ⁷⁴Department of Plant Ecology, Faculty of Sciences, University of Yaounde I, Post Office Box 812, Yaounde, Cameroon. ⁷⁵National Herbarium, Post Office Box 1601, Yaounde, Cameroon. ⁷⁶Wildlife Conservation Society, Bronx, NY 10460, USA. ⁷⁷College of African Wildlife Management, Department of Wildlife Management, Post Office Box 3031, Moshi, Tanzania. ⁷⁸Environment Department, University of York, Heslington, York, YO10 5NG, UK. ⁷⁹Flamingo Land, Malton, North Yorkshire, YO10 6UX. ⁸⁰Tropical Biodiversity Section, MUSE-Museo delle Scienze, Trento, Italy. ⁸¹Institute of Tropical Forest Conservation, Kabale, Uganda. ⁸²Center for Tropical Conservation, Durham, NC 27705, USA. ⁸³Ministry of Natural Resources and Tourism, Forestry and Beekeeping Division, Dar es Salaam, Tanzania. ⁸⁴Escuela de Ciencias Biológicas, Pontificia Universidad Católica del Ecuador, Apartado 1701-2184, Quito, Ecuador. ⁸⁵Forest Management Department, Centre for Agricultural Research in Suriname (CELOS), Paramaribo, Suriname. ⁸⁶Institut de Recherche en Ecologie Tropicale, Institut de Recherche en Ecologie Tropicale (IRET)/Centre National de la Recherche Scientifique et Technologique (CENAREST), B. P. 13354, Libreville, Gabon. ⁸⁷Museu Paraense Emilio Goeldi, Coordenacao de Botânica, Belem, PA, Brazil. ⁸⁸National Forest Authority, Kampala, Uganda. ⁸⁹Prolongación Bolognesi Mz-E-6, Oxapampa Pasco, Peru. ⁹⁰Department of Geography, University College London, UK. ⁹¹School of Geography, University of Leeds, UK.

*Corresponding author. Email: albeca.liang@gmail.com †Present address: Netherlands Institute of Ecology, Droevendaalsesteeg 10, 6708 PB Wageningen, Netherlands.

in BPR (3, 28–30), as well as with experimental (27) and observational (14) studies on forest and nonforest ecosystems. The elasticity of substitution (32) estimated in this study (ranged between 0.2 and 0.3) largely overlaps the range of values of the same exponent term (0.1 to 0.5) from previous theoretical and experimental studies [(10) and references therein]. Furthermore, our findings are consistent with the global estimates of the biodiversity-dependent ecosystem service debt under distinct assumptions (10) and with recent reports of the diminishing marginal benefits of adding a species as species richness increases, based on long-term forest experiments dating back to 1870 [(15, 33) and references therein].

Our analysis relied on stands ranging from unmanaged to extensively managed forests—managed forests with low operating and invest-

ment costs per unit area. Conditions of natural forests would not be comparable with intensively managed forests, because timber production in the latter systems often focuses on a single or limited number of highly productive tree species. Intensively managed forests, where saturated resources can weaken the effects of niche efficiency (3), are shown in some studies (34, 35) to have higher productivity than that of natural diverse forests of the same climate and site conditions (fig. S3). In contrast, other studies (6, 22–24) compared diverse stands with monocultures at the same level of management intensity and found that the positive effects of species diversity on tree productivity and other ecosystem services are applicable to intensively managed forests. As such, there is still an unresolved debate on the BPR of intensively managed forests. Nevertheless,

because intensively managed forests only account for a minor (<7%) portion of global forests (18), our estimated BPR would be minimally affected by such manipulations and thus should reflect the inherent processes governing the vast majority of global forest ecosystems.

We focused on the effect of biodiversity on ecosystem productivity. Recent studies on the opposite causal direction [productivity-biodiversity relationship (14, 36, 37)] suggest that there may be a potential two-way causality between biodiversity and productivity. It is admittedly difficult to use correlative data to detect and attribute causal effects. Fortunately, substantial progress has been made to tease the BPR causal relationship from other potentially confounding environmental variables (14, 38, 39), and this study made considerable efforts to account for these otherwise

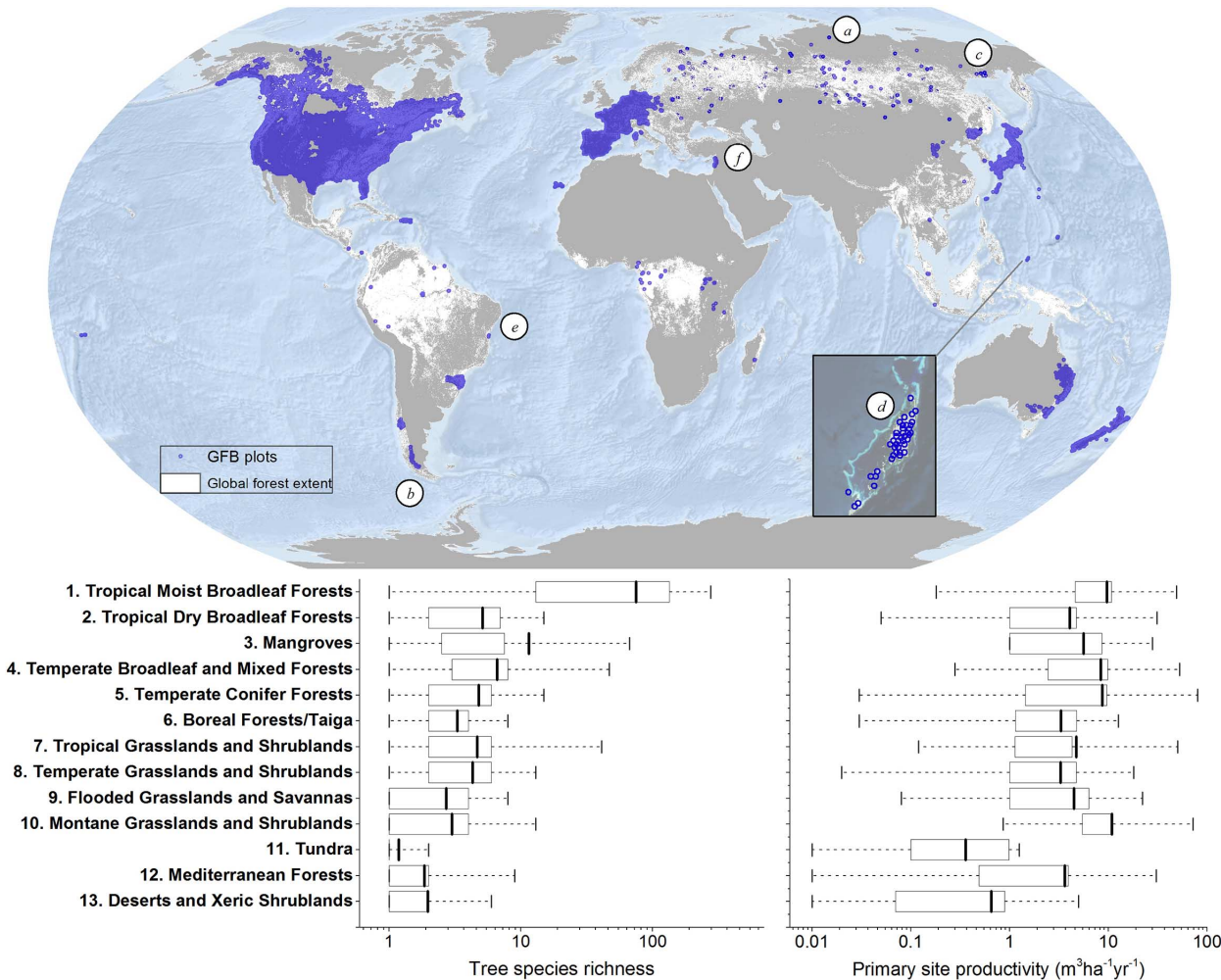


Fig. 1. GFB ground-sourced data were collected from in situ remeasurement of 777,126 permanent sample plots consisting of more than 30 million trees across 8737 species. GFB plots extend across 13 ecoregions [vertical axis, delineated by the World Wildlife Fund where extensive forests occur within all the ecoregions (72)], and 44 countries and territories. Ecoregions are named for their dominant vegetation types, but all contain some forested areas. GFB plots cover a substantial portion of the global forest extent (white), including some of the most distinct forest conditions: (a) the northernmost (73°N, Central Siberia, Russia),

(b) southernmost (52°S, Patagonia, Argentina), (c) coldest (−17°C annual mean temperature, Oimyakon, Russia), (d) warmest (28°C annual mean temperature, Palau, United States), and (e) most diverse (405 tree species on the 1-ha plot, Bahia, Brazil). Plots in war-torn regions [such as (f)] were assigned fuzzed coordinates to protect the identity of the plots and collaborators. The box plots show the mean and interquartile range of tree species richness and primary site productivity (both on a common logarithmic scale) derived from ground-measured tree- and plot-level records. The complete list of species is presented in table S2.

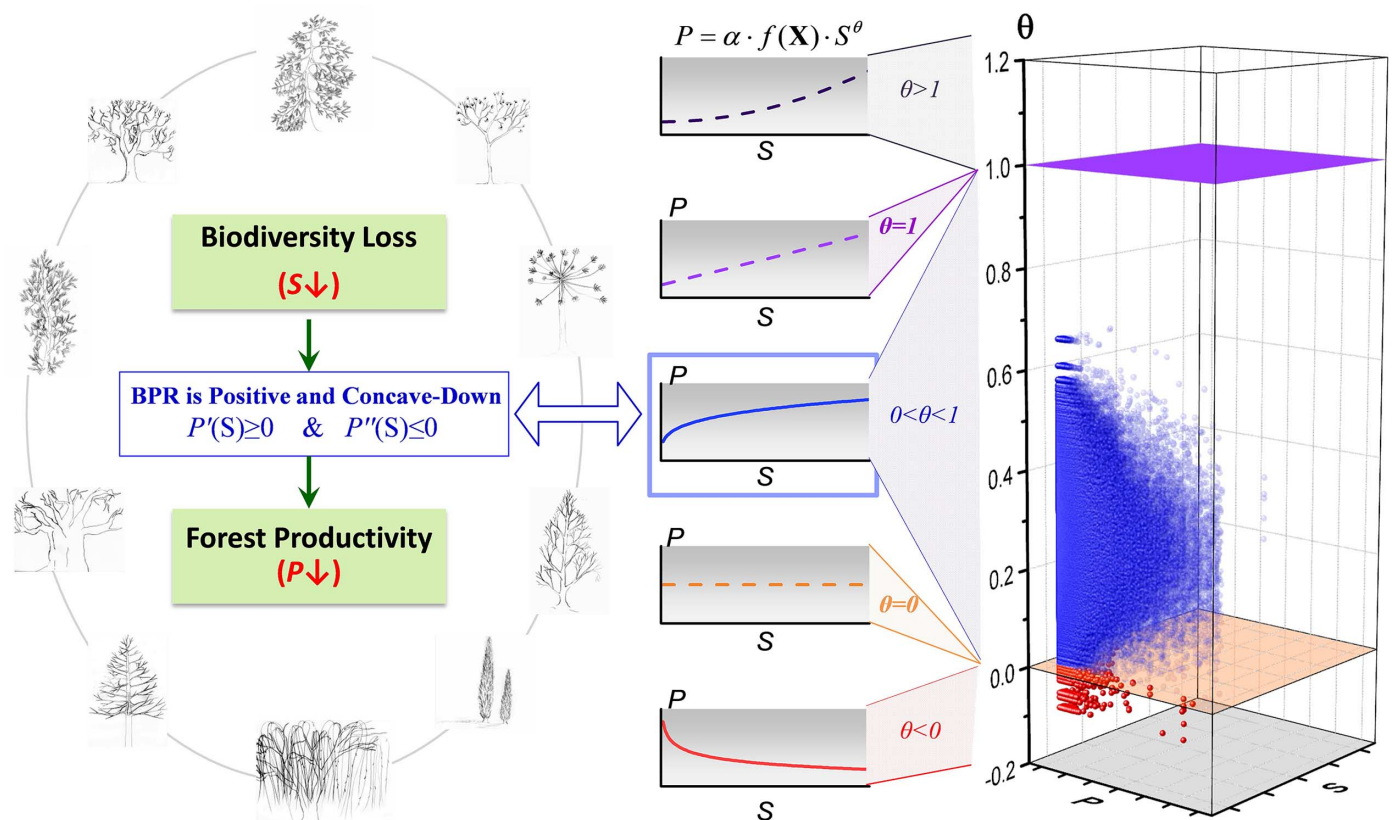


Fig. 2. Theoretical positive and concave-down biodiversity–productivity relationship supported by empirical evidence drawn from the GFB data. (Left) The diagram demonstrates that under the theoretical positive and concave-down (monotonically and degressively increasing) BPR (3, 27, 28), loss in tree species richness may reduce forest productivity (73). **(Middle)** Functional curves represent different BPR under different values of elasticity of substitution (θ). θ values

between 0 and 1 correspond to the positive and concave-down BPR (blue curve). **(Right)** The three-dimensional scatter plot shows θ values we estimated from observed productivity (P), species richness (S), and other covariates. Out of 5,000,000 estimates of θ (mean = 0.26, SD = 0.09), 4,993,500 fell between 0 and 1 (blue), whereas only 6500 were negative (red), and none was equal to zero or greater than or equal to 1; the positive and concave-down BPR was supported by 99.9% of our estimates.

potentially confounding environmental covariates in assessing likely causal effects of biodiversity on productivity.

Because taxonomic diversity indirectly incorporates functional, phylogenetic, and genomic diversity, our results that focus on tree species richness are likely applicable to these other elements of biodiversity, all of which have been found to influence plant productivity (7). Our straightforward analysis makes clear the taxonomic contribution to forest ecosystem productivity and functioning, and the importance of preserving species diversity to biological conservation and forest management.

Our findings highlight the necessity to reassess biodiversity valuation and reevaluate forest management strategies and conservation priorities in forests worldwide. In terms of global carbon cycle and climate change, the value of biodiversity may be considerable. On the basis of our global-scale analyses (Fig. 4), the ongoing species loss in forest ecosystems worldwide (1, 21) could substantially reduce forest productivity and thereby forest carbon absorption rate, which would in turn compromise the global forest carbon sink (40). We further estimate that the economic value of biodiversity in maintaining commercial forest pro-

ductivity is \$166 billion to \$490 billion per year (1.66×10^{11} to 4.90×10^{11} year⁻¹ in 2015 US\$) (Materials and methods, Economics analysis). By itself, this estimate does not account for other values of forest biodiversity (including potential values for climate regulation, habitat, water flow regulation, and genetic resources), and represents only a small percentage of the total value of biodiversity (41, 42). However, this value is already between two to six times the total estimated cost that would be necessary if we were to effectively conserve all terrestrial ecosystems at a global scale [\$76.1 billion per year (43)]. The high benefit-to-cost ratio underlines the importance of conserving biodiversity for forestry and forest resource management.

Amid the struggle to combat biodiversity loss, the relationship between biological conservation and poverty is gaining increasing global attention (13, 44), especially with respect to rural areas where livelihoods depend most directly on ecosystem products. Given the substantial geographic overlaps between severe, multifaceted poverty and key areas of global biodiversity (45), the loss of species in these areas has the potential to exacerbate local poverty by diminishing forest productivity and related ecosystem services (44). For example, in tropical and subtropical regions,

many areas of high elasticity of substitution (32) overlapped with biodiversity hotspots (46), including Eastern Himalaya and Nepal, Mountains of Southwest China, Eastern Afrotropical, Madrean pine-oak woodlands, Tropical Andes, and Cerrado. For these areas, only a few species of commercial value are targeted by logging. As such, the risk of losing species through deforestation would far exceed the risk through harvesting (47). Deforestation and other anthropogenic drivers of biodiversity loss in these biodiversity hotspots are likely to have considerable impacts on the productivity of forest ecosystems, with the potential to exacerbate local poverty. Furthermore, the greater uncertainty in our results for the developing countries (Fig. 5) reflects the well-documented geographic bias in forest sampling, including repeated measurements, and reiterates the need for strong commitments toward improving sampling in the poorest regions of the world.

Our findings reflect the combined strength of large-scale integration and synthesis of ecological data and modern machine learning methods to increase our understanding of the global forest system. Such approaches are essential for generating global insights into the consequences of biodiversity loss and the potential benefits of

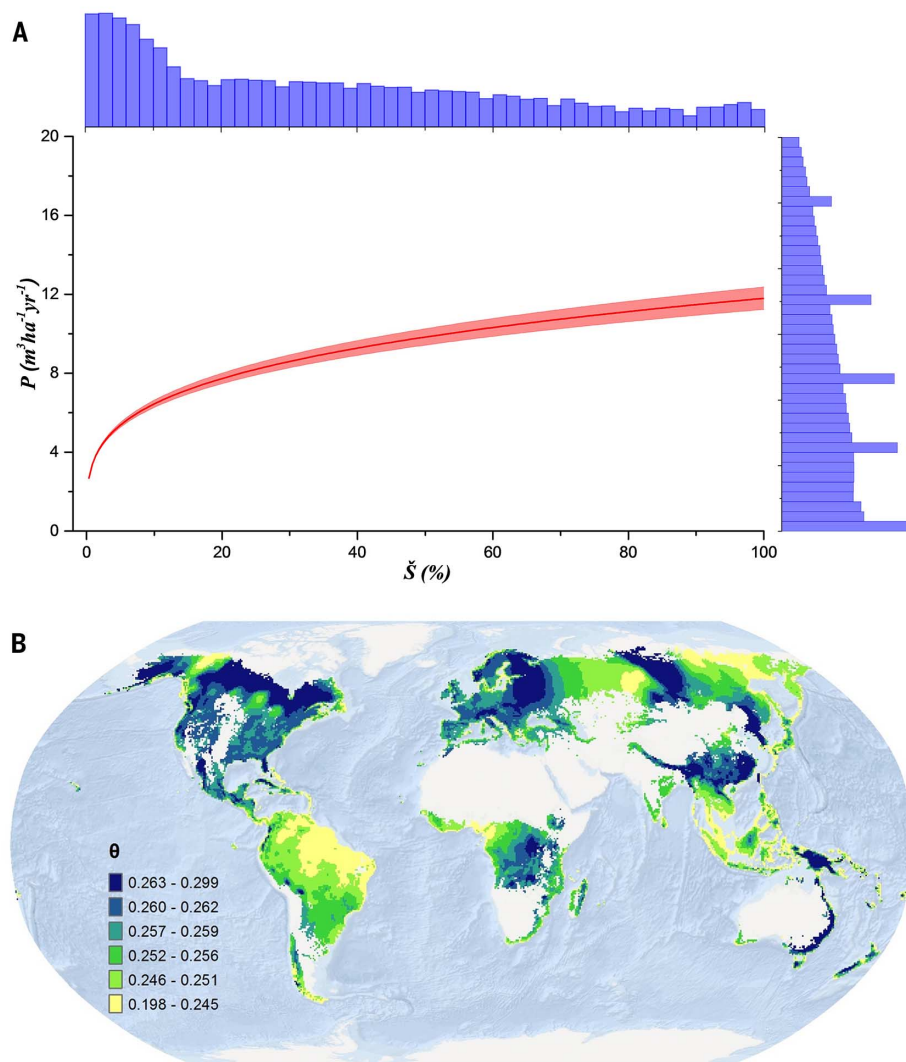


Fig. 3. The estimated global effect of biodiversity on forest productivity was positive and concave-down, and revealed considerable geospatial variation across forest ecosystems worldwide. (A) Global effect of biodiversity on forest productivity (red line with pink bands representing 95% confidence interval) corresponds to a global average elasticity of substitution (θ) value of 0.26, with climatic, soil, and other plot covariates being accounted for and kept constant at sample mean.

Relative species richness (\tilde{S}) is in the horizontal axis, and productivity (P , $\text{m}^3 \text{ha}^{-1} \text{year}^{-1}$) is in the vertical axis (histograms of the two variables on top and right in the logarithm scale). **(B)** θ represents the strength of the effect of tree diversity on forest productivity. Spatially explicit values of θ were estimated by using universal kriging (Materials and methods) across the current global forest extent (effect sizes of the estimates are shown in Fig. 5), whereas blank terrestrial areas were nonforested.

integrating and promoting biological conservation in forest resource management and forestry practices—a common goal already shared by intergovernmental organizations such as the Montréal and Helsinki Process Working Groups. These findings should facilitate efforts to accurately forecast future changes in ecosystem services worldwide, which is a primary goal of IPBES (11), and provide baseline information necessary to establish international conservation objectives, including the United Nations Convention on Biological Diversity Aichi targets, the United Nations Framework Convention on Climate Change REDD+ goal, and the United Nations Convention to Combat Desertification land degradation neutrality goal. The success of these goals relies on the under-

standing of the intrinsic link between biodiversity and forest productivity.

Materials and methods

Data collection and standardization

Our current study used ground-sourced forest measurement data from 45 forest inventories collected from 44 countries and territories (Fig. 1 and table S1). The measurements were collected in the field from predesignated sample area units, i.e., Global Forest Biodiversity permanent sample plots (hereafter, GFB plots). For the calculation of primary site productivity, GFB plots can be categorized into two tiers. Plots designated as “Tier 1” have been measured at two or more points in time with a minimum time interval between mea-

surements of two years or more (global mean time interval is 9 years, see Table 1). “Tier 2” plots were only measured once, and primary site productivity can be estimated from known stand age or dendrochronological records. Overall, our study was based on 777,126 GFB plots, of which 597,179 (77%) were Tier 1, and 179,798 (23%) were Tier 2. GFB plots primarily measured natural forests ranging from unmanaged to extensively managed forests, i.e., managed forests with low operating and investment costs per unit area. Intensively managed forests with harvests exceeding 50 percent of the stocking volume were excluded from this study. GFB plots represent forests of various origins (from naturally regenerated to planted) and successional stages (from stand initiation to old-growth).

Table 1. Definition, unit, and summary statistics of key variables.

Variable	Definition	Unit	Mean	Standard deviation	Source	Nominal resolution
Response variables						
P	Primary forest productivity measured in periodic annual increment in stem volume (PAI)	$\text{m}^3 \text{ha}^{-1} \text{year}^{-1}$	7.57	14.52	Author-generated from ground-measured data	
Plot attributes						
S	Tree species richness, the number of live tree species observed on the plot	unitless	5.79	8.64	ground-measured	
A	Plot size, area of the sample plot	ha	0.04	0.12	ground-measured	
Y	Elapsed time between two consecutive inventories	year	8.63	11.62	ground-measured	
G	Basal area, total cross-sectional area of live trees measured at 1.3 to 1.4 m above ground	$\text{m}^2 \text{ha}^{-1}$	19.00	18.94	Author-generated from ground-measured data	
E	Plot elevation	m	469.30	565.92	G/SRTM (74)	
I_1	Indicator of plot tier $I_1 = 1$ if a plot was Tier-2, $I_1 = 0$ if otherwise	unitless	0.23	0.42	Author-generated from ground-measured data	
I_2	Indicator of plot size $I_2 = 1$ when $0.01 \leq ps < 0.05$, $I_2 = 2$ when $0.05 \leq ps < 0.15$, $I_2 = 3$ when $0.15 \leq ps < 0.50$, $I_2 = 4$ when $0.50 \leq ps < 1.00$, where ps was plot size (hectares)	unitless	1.43	0.80	Author-generated from ground-measured data	
Climatic covariates						
T_1	Annual mean temperature	0.1°C	108.4	55.92	WorldClim v.1 (75)	1 km^2
T_2	Isothermality	unitless index*100	35.43	7.05	WorldClim v.1	1 km^2
T_3	Temperature seasonality	Std.(0.001°C)	7786.00	2092.39	WorldClim v.1	1 km^2
C_1	Annual precipitation	mm	1020.00	388.35	WorldClim v.1	1 km^2
C_2	Precipitation seasonality (coefficient of variation)	unitless%	27.54	16.38	WorldClim v.1	1 km^2
C_3	Precipitation of warmest quarter	mm	282.00	120.88	WorldClim v.1	1 km^2
PET	Global Potential Evapotranspiration	mm year^{-1}	1063.43	271.80	CGIAR-CSI (76)	1 km^2
IAA	Indexed Annual Aridity	unitless index* 10^{-4}	9915.09	4512.99	CGIAR-CSI	1 km^2
Soil covariates						
O_1	Bulk density	g cm^{-3}	0.70	0.57	WISE30sec v.1 (77)	1 km^2
O_2	pH measured in water	unitless	3.72	2.80	WISE30sec v.1	1 km^2
O_3	Electrical conductivity	dS m^{-1}	0.44	0.76	WISE30sec v.1	1 km^2
O_4	C/N ratio	unitless	9.64	7.78	WISE30sec v.1	1 km^2
O_5	Total nitrogen	g kg^{-1}	2.71	4.62	WISE30sec v.1	1 km^2
Geographic coordinates and classification						
x	Longitude in WGS84 datum	degree				
y	Latitude in WGS84 datum	degree				
Ecoregion	Ecoregion defined by World Wildlife Fund (78)					

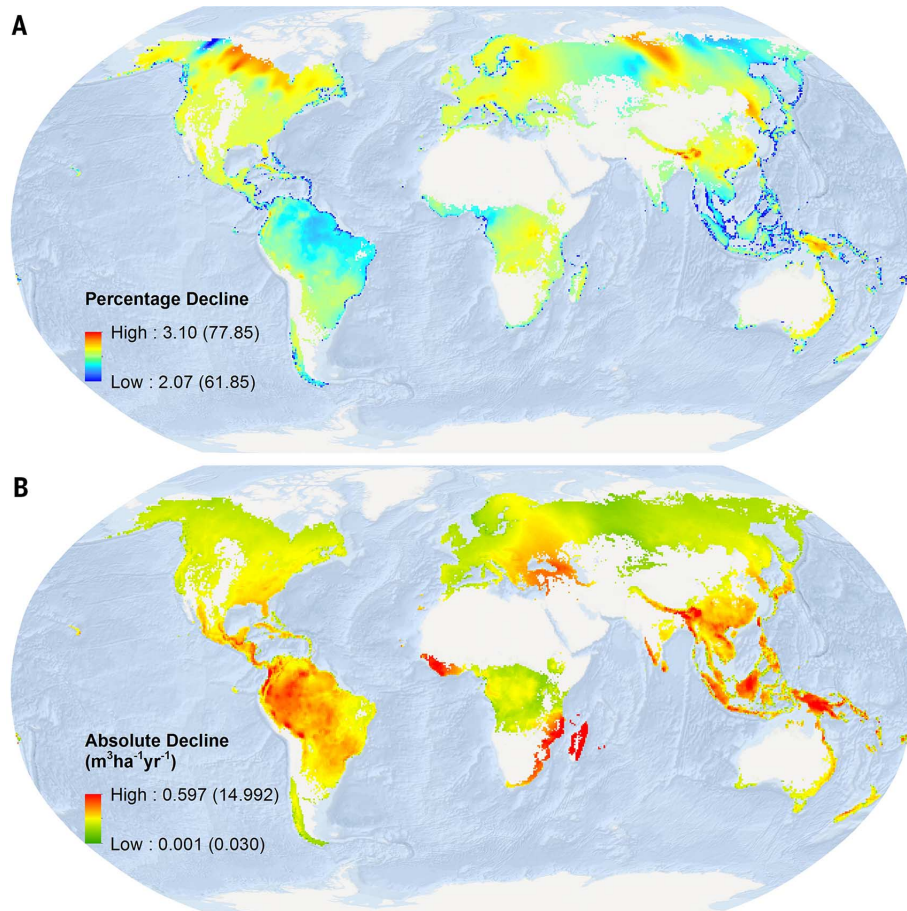


Fig. 4. Estimated percentage and absolute decline in forest productivity under 10 and 99% decline in current tree species richness (values in parentheses correspond to 99%), holding all the other terms constant. (A) Percent decline in productivity was calculated according to the general BPR model (Eq. 1) and estimated worldwide spatially explicit values of the elasticity of substitution (Fig. 3B). **(B)** Absolute decline in productivity was derived from the estimated elasticity of substitution (Fig. 3B) and estimates of global forest productivity (fig. S1). The first 10% reduction in tree species richness would lead to a 0.001 to 0.597 m³ ha⁻¹ year⁻¹ decline in periodic annual increment, which accounts for 2 to 3% of current forest productivity. The raster data are displayed in 50-km resolution with a 3 SD stretch.

For each GFB plot, we derived three key attributes from measurements of individual trees—tree species richness (S), stand basal area (G), and primary site productivity (P). Because for each of all the GFB plot samples, S and P were derived from the measurements of the same trees, the sampling issues commonly associated with biodiversity estimation (48) had little influence on the S – P relationship (i.e., BPR) in this study.

Species richness, S , represents the number of different tree species alive at the time of inventory within the perimeter of a GFB plot with an average size of approximately 900 m². Ninety-five percent of all plots fall between 100 and 1,100 m² in size. To minimize the species-area effect (49), we studied the BPR here using a geospatial random forest model in which observations from nearby GFB plots would be more influential than plots that are farther apart (see §Geospatial random forest). Because nearby plots are most likely from the same forest inventory data set, and there was no or little variation of plot area within each data set, the BPR derived from this model largely reflected patterns under the same plot area basis.

To investigate the potential effects of plot size on our results, we plotted the estimated elasticity of substitution (θ) against plot size, and found that the scatter plot was normally distributed with no discernible pattern (fig. S2). In addition, the fact that the plot size indicator I_2 had the second lowest (0.8%) importance score (50) among all the covariates (Fig. 6) further supports that the influence of plot size variation in this study was negligible.

Across all the GFB plots, there were 8,737 species in 1,862 genera and 231 families, and S values ranged from 1 to 405 per plot. We verified all the species names against 60 taxonomic databases, including NCBI, GRIN Taxonomy for Plants, Tropicos–Missouri Botanical Garden, and the International Plant Names Index, using the ‘taxize’ package in R (51). Out of 8737 species recorded in the GFB database, 7425 had verified taxonomic information with a matching score (51) of 0.988 or higher, whereas 1312 species names partially matched existing taxonomic databases with a matching score between 0.50 and 0.75, indicating that these species may have not been

documented in the 60 taxonomic databases. To facilitate inter-biome comparison, we further developed relative species richness (\tilde{S}), a continuous percentage score converted from species richness (S) and the maximal species richness of a set of sample plots (S^*) using

$$\tilde{S} = \frac{S}{S^*} \quad (2)$$

Stand basal area (G , in m² ha⁻¹) represents the total cross-sectional area of live trees per unit sample area. G was calculated from individual tree diameter-at-breast-height (dbh , in cm):

$$G = 0.000079 \cdot \sum_i dbh_i^2 \cdot \kappa_i \quad (3)$$

where κ_i denotes the conversion factor (ha⁻¹) of the i th tree, *viz.* the number of trees per ha represented by that individual. G is a key biotic factor of forest productivity as it represents stand density—often used as a surrogate for resource acquisition (through leaf area) and stand

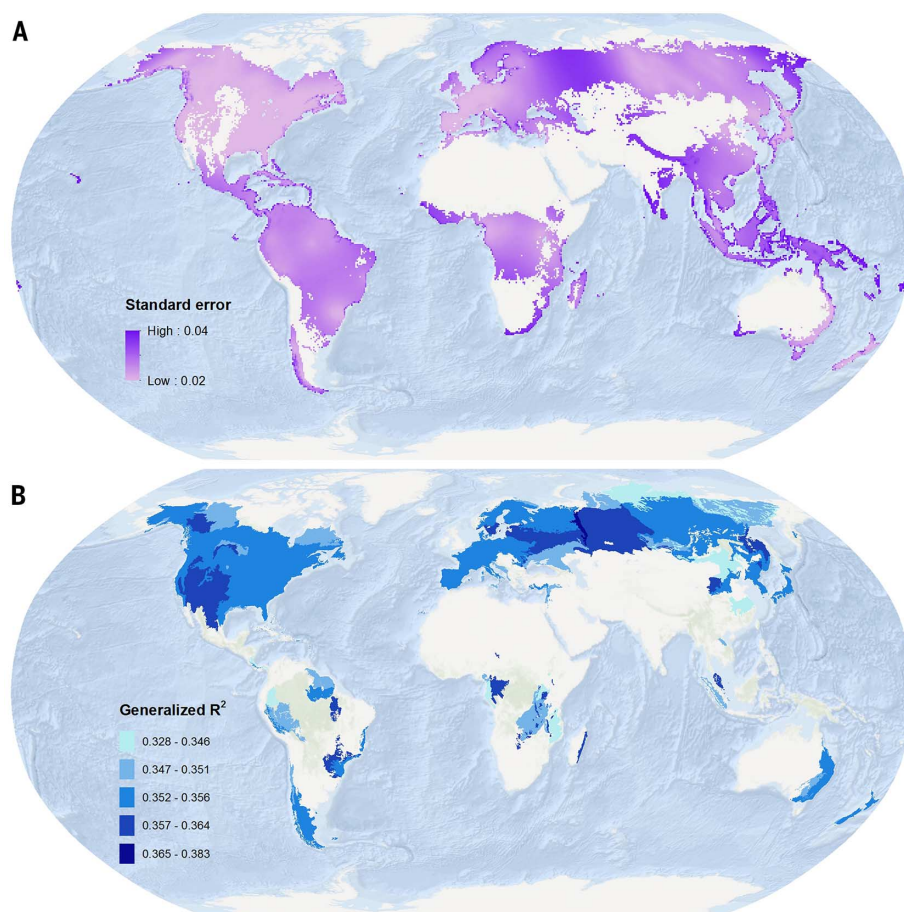


Fig. 5. Standard error and generalized R^2 of the spatially explicit estimates of elasticity of substitution (θ) across the current global forest extent in relation to \hat{S} . (A) Standard error increased as a location was farther from those sampled. (B) The generalized R^2 values were derived with a geostatistical nonlinear mixed-effects model for GFB sample locations, and thus (B) only covers a subset of the current global forest extent.

competition (52). Accounting for basal area as a covariate mitigated the artifact of different minimum dbh across inventories, and the artifact of different plot sizes.

Primary site productivity (P , in $\text{m}^3 \text{ha}^{-1} \text{yr}^{-1}$) was measured as tree volume productivity in terms of periodic annual increment (PAI) calculated from the sum of individual tree stem volume (V , in m^3)

$$P = \frac{\sum_{i,2} V_{i,2} \cdot \kappa_i - \sum_{i,1} V_{i,1} \cdot \kappa_i + M}{Y} \quad (4)$$

where $V_{i,1}$ and $V_{i,2}$ (in m^3) represent total stem volume of the i th tree at the time of the first inventory and the second inventory, respectively. M denotes total removal of trees (including mortality, harvest, and thinning) in stem volume (in $\text{m}^3 \text{ha}^{-1}$). Y represents the time interval (in years) between two consecutive inventories. P accounted for mortality, ingrowth (i.e., recruitment between two inventories), and volume growth. Stem volume values were predominantly calculated using region- and species-specific allometric equations based on dbh and other tree- and plot-level attributes (Table 1). For the regions lacking an allometric equation, we approximated

stem volume at the stand level from basal area, total tree height, and stand form factors (53). In case of missing tree height values from the ground measurement, we acquired alternative measures from a global 1-km forest canopy height database (54). For Tier 2 plots that lacked re-measurement, P was measured in mean annual increment (MAI) based on total stand volume and stand age (52), or tree radial growth measured from increment cores. Since the traditional MAI metric does not account for mortality, we calculated P by adding to MAI the annual mortality based on regional-specific forest turnover rates (55). The small and insignificant correlation coefficient between P and the indicator of plot tier (I_1), together with the negligible variable importance of I_1 (1.8%, Fig. 6), indicate that PAI and MAI were generally consistent, such that MAI could be a good proxy of PAI in our study. Although MAI and PAI have considerable uncertainty in any given stand, it is difficult to see how systematic bias across diversity gradients could occur on a scale sufficient to influence the results shown here.

P , although only representing a fraction of total forest net primary production, has been an important and widely used measure of forest pro-

ductivity, because it reflects the dominant aboveground biomass component and the long-lived biomass pool in most forest ecosystems (56). Additionally, although other measures of productivity (e.g., net ecosystem exchange processed to derive gross and net primary production; direct measures of aboveground net primary production including all components; and remotely sensed estimates of LAI and greenness coupled with models) all have their advantages and disadvantages, none would be feasible at a similar scale and resolution as in this study.

To account for abiotic factors that may influence primary site productivity, we compiled 14 geospatial covariates based on biological relevance and spatial resolution (Fig. 6). These covariates, derived from satellite-based remote sensing and ground-based survey data, can be grouped into three categories: climatic, soil, and topographic (Table 1). We preprocessed all geospatial covariates using ArcMap 10.3 (57) and R 2.15.3 (58). All covariates were extracted to point locations of GFB plots, with a nominal resolution of 1 km^2 .

Geospatial random forest

We developed geospatial random forest—a data-driven ensemble learning approach—to characterize

the biodiversity–productivity relationship (BPR), and to map BPR in terms of elasticity of substitution (31) on all sample sites across the world. This approach was developed to overcome two major challenges that arose from the size and complexity of GFB data without assuming any underlying BPR patterns or data distribution. First, we need to account for broad-scale differences in vegetation types, but global classification and mapping of homogeneous vegetation types is lacking (59); and secondly, correlations and trends that naturally occur through space (60) can be significant and influential in forest ecosystems (61). Geostatistical models (62) have been developed to address the spatial autocorrelation, but the size of the GFB data set far exceeds the computational constraints of most geostatistical software.

Geospatial random forest integrated conventional random forest (50) and a geostatistical nonlinear mixed-effects model (63) to estimate BPR across the world based on GFB plot data and their spatial dependence. The underlying model had the following form

$$\log P_{ij}(\mathbf{u}) = \theta_i \cdot \log \tilde{S}_{ij}(\mathbf{u}) + \boldsymbol{\alpha}_i \cdot \mathbf{X}_{ij}(\mathbf{u}) + e_{ij}(\mathbf{u}), \mathbf{u} \in \mathcal{D} \subset \mathcal{R}^2, \quad (5)$$

where $\log P_{ij}(\mathbf{u})$ and $\log \tilde{S}_{ij}(\mathbf{u})$ represent natural logarithm of productivity and relative species richness (calculated from actual species richness and the maximal species richness of the training set) of plot i in the j th training set at point locations \mathbf{u} , respectively. The model was derived from the niche–efficiency model, and θ corresponds to the elasticity of substitution (31). $\boldsymbol{\alpha}_i \cdot \mathbf{X}_{ij}(\mathbf{u}) = \alpha_{i0} + \alpha_{i1}x_{ij1} + \dots + \alpha_{in}x_{ijn}$ represents n covariates and their coefficients (Fig. 6 and Table 1).

To account for potential spatial autocorrelation, which can bias tests of significance due to the violation of independence assumption and is especially problematic in large-scale forest ecosystem studies (60, 61), we incorporated a spherical variogram model (62) into the residual term $e_{ij}(\mathbf{u})$. The underlying geostatistical assumption was that across the world BPR is a second-order stationary process—a common geographical phenomenon in which neighboring points are more similar to each other than they are to points that are more distant (64). In our study, we found strong evidence for this gradient (Fig. 7), indicating that observations from nearby GFB plots would be more influential than plots that are farther away. The positive spherical semivariance curves estimated from a large number of bootstrapping iterations indicated that spatial dependence increased as plots became closer together.

The aforementioned geostatistical nonlinear mixed-effects model was integrated into random forest analysis (50) by means of model selection and estimation. In the model selection process, random forest was employed to assess the contribution of each of the candidate variables to the dependent variable $\log P_{ij}(\mathbf{u})$, in terms of the amount of increase in prediction error as one variable is permuted while all the others are kept constant. We

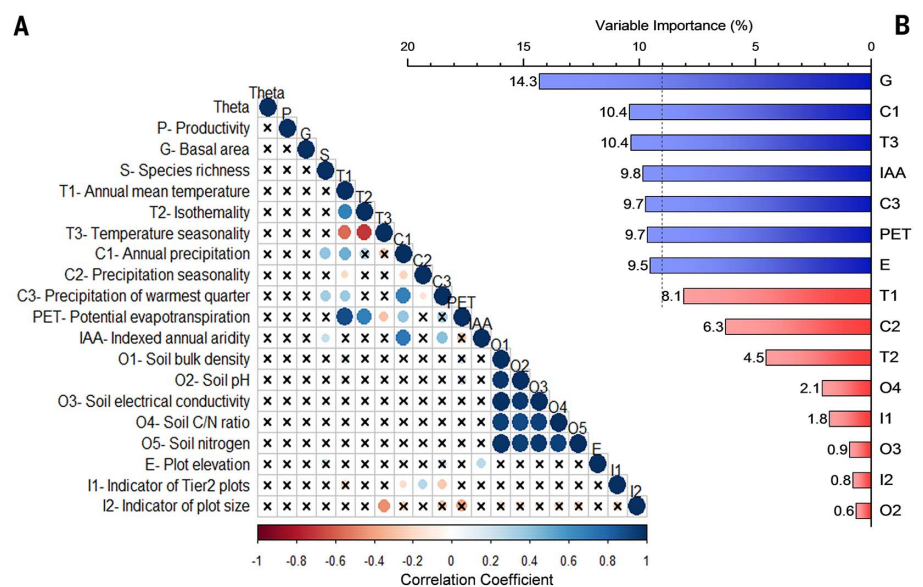


Fig. 6. Correlation matrix and importance values of potential variables for the geospatial random forest analysis. (A) There were a total of 15 candidate variables from three categories, namely plot attributes, climatic variables, and soil factors (a detailed description is provided in Table 1). Correlation coefficients between these variables were represented by sizes and colors of circles, and “x” marks coefficients not significant at $\alpha = 0.05$ level. (B) Variable importance (%) values were determined by the geospatial random forest (Materials and methods). Variables with importance values exceeding the 9% threshold line (blue) were selected as control variables in the final geospatial random forest models. Elasticity of substitution (coefficient), productivity (dependent variable), and species richness (key explanatory variable) were not ranked in the variable importance chart because they were not potential covariates.

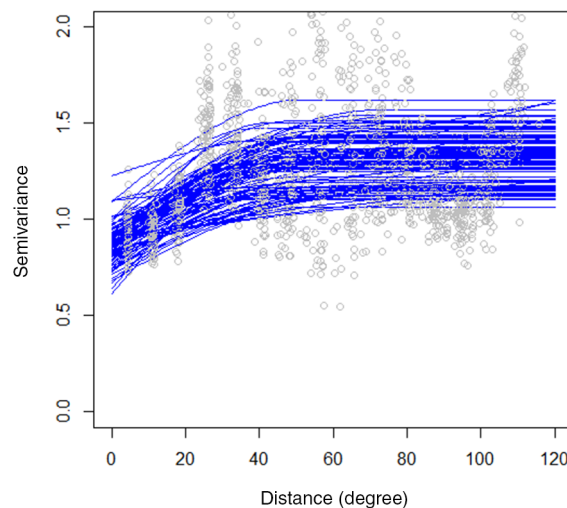


Fig. 7. Semivariance and estimated spherical variogram models (blue curves) obtained from geospatial random forest in relation to \tilde{S} . Gray circles, semivariance; blue curves, estimated spherical variogram models. There was a general trend that semivariance increased with distance; spatial dependence of θ weakened as the distance between any two GFB plots increased. The final spherical models had nugget = 0.8, range = 50 degrees, and sill = 1.3. To avoid identical distances, all plot coordinates were jittered by adding normally distributed random noises.

used the randomForest package (65) in R to obtain importance measures for all the covariates to guide our selection of the final variables in the geostatistical nonlinear mixed-effects model, $\mathbf{X}_{ij}(\mathbf{u})$. We selected stand basal area (G), temperature seasonality (T_3), annual precipitation (C_1), precipitation of the warmest quarter (C_3), potential evapotranspiration (PET), indexed annual aridity (IAA), and plot elevation (E) as control variables since their importance measures were greater than the 9 percent threshold (Fig. 6) preset to ensure

that the final variables accounted for over 60 percent of the total variable importance measures.

For geospatial random forest analysis of BPR, we first selected control variables based on the variable importance measures derived from random forests (50). We then evaluated the values of elasticity of substitution (32), which are expected to be real numbers greater than 0 and less than 1, against the alternatives, i.e., negative BPR (H_{01} : $\theta < 0$), no effect (H_{02} : $\theta = 0$), linear (H_{03} : $\theta = 1$), and convex positive BPR (H_{04} : $\theta > 1$). We

Table 2. Parameters of the global geospatial random forest model in 10,000 iterations of 500 randomly selected (with replacement) GFB plots. Mean and SE of all the parameters were estimated by using bootstrapping. Effect sizes were represented by the Akaike information criterion (AIC), Bayesian information criterion (BIC), and generalized R^2 ($G-R^2$). Const, constant.

	Coefficients												
	Loglik	AIC	BIC	$G-R^2$	const	θ	G	T3	C1	C3	PET	IAA	E
Mean	-761.41	1546.71	1597.08	0.354	3.816	0.2625243	0.014607	-0.000106	0.001604	0.001739	-0.002566	-0.000134	-0.000809
SE	0.54	1.10	1.13	0.001	0.011	0.0009512	0.000039	0.000001	0.000008	0.000008	0.000009	0.000001	0.000002
Iteration													
1	-756.89	1537.78	1588.35	0.259	4.299	0.067965	0.014971	-0.000100	0.002335	0.001528	-0.003019	-0.000185	-0.000639
2	-801.46	1626.91	1677.49	0.281	3.043	0.167478	0.018232	-0.000061	0.000982	0.002491	-0.001916	-0.000103	-0.000904
3	-768.71	1561.41	1611.99	0.357	5.266	0.299411	0.008571	-0.000145	0.002786	0.002798	-0.003775	-0.000258	-0.000728
4	-775.19	1574.37	1624.95	0.354	4.273	0.236135	0.016808	-0.000126	0.001837	0.003755	-0.003075	-0.000182	-0.000768
5	-767.66	1559.32	1609.89	0.248	2.258	0.166024	0.018491	-0.000051	0.000822	0.002707	-0.001575	-0.000078	-0.000553
6	-773.76	1571.52	1622.10	0.342	3.983	0.266962	0.018675	-0.000113	0.001372	0.001855	-0.002824	-0.000101	-0.000953
7	-770.26	1564.53	1615.10	0.421	4.691	0.353071	0.009602	-0.000127	0.002390	-0.001151	-0.003337	-0.000172	-0.000441
2911	-778.21	1580.43	1631.00	0.393	3.476	0.187229	0.020798	-0.000069	0.001826	0.001828	-0.002695	-0.000135	-0.000943
2912	-755.35	1534.71	1585.28	0.370	2.463	0.333485	0.013165	-0.000005	0.001749	0.000303	-0.002447	-0.000119	-0.000223
2913	-800.52	1625.03	1675.61	0.360	4.526	0.302214	0.021163	-0.000105	0.001860	0.001382	-0.003207	-0.000166	-0.000974
2914	-725.89	1475.78	1526.36	0.327	2.639	0.324987	0.013195	-0.000057	0.001322	0.000778	-0.001902	-0.000080	-0.000582
2915	-753.64	1531.28	1581.85	0.324	4.362	0.202992	0.014003	-0.000146	0.001746	0.002229	-0.002844	-0.000143	-0.000750
2916	-796.75	1617.50	1668.08	0.307	3.544	0.244332	0.010373	-0.000118	0.002086	0.002510	-0.002667	-0.000152	-0.000650
2917	-746.88	1517.77	1568.34	0.348	4.427	0.290416	0.008630	-0.000107	0.002203	-0.000314	-0.002770	-0.000155	-0.000945
9997	-775.08	1574.17	1624.74	0.313	1.589	0.193865	0.012525	-0.000056	-0.000589	0.000550	-0.000066	-0.000155	-0.000839
9998	-781.20	1586.40	1636.98	0.438	5.453	0.412750	0.014459	-0.000169	0.002346	0.002175	-0.003973	-0.000117	-0.000705
9999	-734.72	1493.43	1544.01	0.387	4.238	0.211103	0.013415	-0.000118	0.001896	0.002450	-0.002927	-0.000076	-0.000648
10000	-776.14	1576.28	1626.86	0.355	2.622	0.468073	0.015632	-0.000150	-0.000093	0.001151	-0.000756	-0.000019	-0.000842

examined all the coefficients by their statistical significance and effect sizes, using Akaike information criterion (AIC), Bayesian information criterion (BIC), and the generalized coefficient of determination (66).

Global analysis

For the global-scale analysis, we calibrated the nonlinear mixed-effects model parameters (θ and α 's) using training sets of 500 plots randomly selected (with replacement) from the GFB global dataset according to the bootstrap aggregating (bagging) algorithm. We calibrated a total of 10,000 models based on the bagging samples, using our own bootstrapping program and the nonlinear package nlme (63) of R, to calculate the means and standard errors of final model estimates (Table 2). This approach overcame computational limits by partitioning the GFB sample into smaller subsamples to enable the nonlinear estimation. The size of training sets was selected based on the convergence and effect size of the geospatial random forest models. In pilot simulations with increasing sizes of training sets (Fig. 8), the value of elasticity of substitution (32) fluctuated at the start until the convergence point at 500 plots. Generalized R^2 values declined as the size of training sets increased from 0 to 350 plots, and stabilized at around 0.35 as training set size increased further. Accordingly, we selected 500 as the size of the training sets for the final geospatial random forest analysis. Based on the estimated parameters of the global model (Table 2), we analyzed the effect of relative species

richness on global forest productivity with a sensitivity analysis by keeping all the other variables constant at their sample means for each ecoregion.

Mapping BPR across global forest ecosystems

For mapping purposes, we first estimated the current extent of global forests in several steps. We aggregated the "treecover2000" and "loss" data (67) from 30 m pixels to 30 arc-second pixels (~1 km) by calculating the respective means. The result was ~1 km pixels showing the percentage forest cover for the year 2000 and the percentage of this forest cover lost between 2000 and 2013, respectively. The aggregated forest cover loss was multiplied by the aggregated forest cover to produce a single raster value for each ~1 km pixel representing a percentage forest lost between 2000 and 2013. This multiplication was necessary since the initial loss values were relative to initial forest cover. Similarly, we estimated the percentage forest cover gain by aggregating the forest "gain" data (67) from 30 m to 30 arc-seconds while taking a mean. Then, this gain layer was multiplied by 1 minus the aggregated forest cover from the first step to produce a single value for each ~1 km pixel that signifies percentage forest gain from 2000–2013. This multiplication ensured that the gain could only occur in areas that were not already forested. Finally, the percentage forest cover for 2013 was computed by taking the aggregated data from the first step (year 2000) and subtracting the computed loss and adding the computed gain.

We mapped productivity P and elasticity of substitution (32) across the estimated current extent of global forests, here defined as areas with 50 percent or more forest cover. Because GFB ground plots represent approximately 40 percent of the forested areas, we used universal kriging (62) to estimate P and θ for the areas with no GFB sample coverage. The universal kriging models consisted of covariates specified in Fig. 6B and a spherical variogram model with parameters (i.e., nugget, range, and sill) specified in Fig. 7. We obtained the best linear unbiased estimators of P and θ and their standard error in relation to \hat{S} across the current global forest extent with the *gstat* package of R (68). By combining θ estimated from geospatial random forest and universal kriging, we produced the spatially continuous maps of the elasticity of substitution (Fig. 3B) and forest productivity (fig. S1) at a global scale. The effect sizes of the best linear unbiased estimator of θ (in terms of standard error and generalized R^2) are shown in Fig. 5. We further estimated percentage and absolute decline in worldwide forest productivity under two scenarios of loss in tree species richness— low (10% loss) and high (99% loss). These levels represent the productivity decline (in both percentage and absolute terms) if local species richness across the global forest extent would decrease to 90 and 1 percent of the current values, respectively. The percentage decline was calculated based on the general BPR model (Eq. 1) and estimated worldwide spatially explicit values of the elasticity of substitution (Fig. 3B).

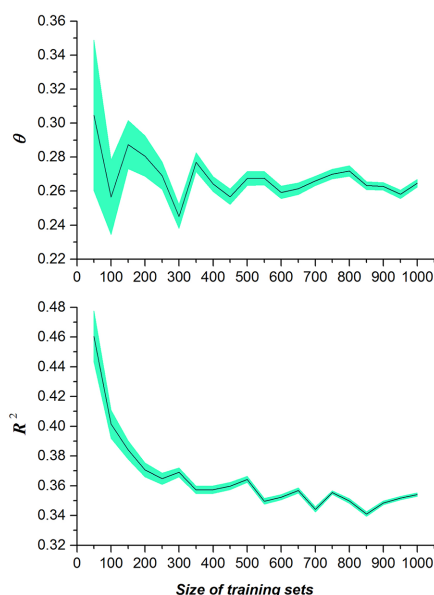


Fig. 8. Effect of the size of training sets used in the geospatial random forest on estimated elasticity of substitution (θ) and generalized R^2 in relation to \tilde{S} . Mean (solid line) and SE band (green area) were estimated with 100 randomly selected (with replacement) training sets for each of the 20 size values (between 50 and 1000 GFB plots, with an increment of 50).

The absolute decline was the product of the worldwide estimates of primary forest productivity (fig. S1) and the standardized percentage decline at the two levels of biodiversity loss (Fig. 4A).

Economic analysis

Estimates of the economic value-added from forests employ a range of methods. One prominent recent global valuation of ecosystem services (69) valued global forest production [in terms of ‘raw materials’ (including timber, fiber, biomass fuels, and fuelwood and charcoal)] provided by forests (table S1) (69) in 2011 at US\$ 649 billion (6.49×10^{11} , in constant 2007 dollars). Using an alternative method, the UN FAO (25, 26) estimates gross value-added in the formal forestry sector, a measure of the contribution of forestry, wood industry, and pulp and paper industry to the world’s economy, at US\$606 billion (6.06×10^{11} , in constant 2011 dollars). Because these two reasonably comparable values are directly impacted by and proportional to forest productivity, we used them as bounds on our coarse estimate of the global economic value of commercial forest productivity, converted to constant 2015 US\$ based on the US consumer price indices (70, 71). As indicated by our global-scale analyses (Fig. 4A), a 10 percent decrease of tree species richness distributed evenly across the world (from 100% to 90%) would cause a 2.1 to 3.1 percent decline in productivity, which would equate to US\$13–23 billion per year (constant 2015 US\$). For the assessment of the value of biodiversity in main-

taining forest productivity, a drop in species richness from the current level to one species would lead to 26–66% reduction in commercial forest productivity in the biomes that contribute substantially to global commercial forestry (fig. S4), equivalent to 166–490 billion US\$ per year (1.66×10^{11} to 4.90×10^{11} , constant 2015 US\$, calculated by multiplying the foregoing economic value-added from FAO and the other study by 26 and 66%, respectively.) Therefore, we estimated that the economic value of biodiversity in maintaining commercial forest productivity worldwide would be 166 billion to 490 billion US\$ per year.

We held the total number of trees, global forest area and stocking, and other factors constant to estimate the value of productivity loss solely due to a decline in tree species richness. As such, these estimates did not include the value of land converted from forest and losses due to associated fauna and flora decline or forest habitat reduction. This estimate only reflects the value of biodiversity in maintaining commercial forest productivity that contributes directly to forestry, wood industry, and pulp and paper industry, and does not account for other values of biodiversity, including potential values for climate regulation, habitat, water flow regulation, genetic resources, etc. The total global value of biodiversity could exceed this estimate by orders of magnitudes (41, 42).

REFERENCES AND NOTES

1. S. Naeem, J. E. Duffy, E. Zavaleta, The functions of biological diversity in an age of extinction. *Science* **336**, 1401–1406 (2012). doi: [10.1126/science.1215855](https://doi.org/10.1126/science.1215855); pmid: 22700920
2. Millennium Ecosystem Assessment, “Ecosystems and Human Well-being: Biodiversity Synthesis” (World Resources Institute, 2005)
3. J. Liang, M. Zhou, P. C. Tobin, A. D. McGuire, P. B. Reich, Biodiversity influences plant productivity through niche-efficiency. *Proc. Natl. Acad. Sci. U.S.A.* **112**, 5738–5743 (2015). doi: [10.1073/pnas.1409853112](https://doi.org/10.1073/pnas.1409853112); pmid: 25901325
4. M. Scherer-Lorenzen, in *Forests and Global Change*, D. Burslem, D. Coomes, W. Simonson, Eds. (Cambridge Univ. Press, 2014), pp. 195–238.
5. B. J. Cardinale et al., Biodiversity loss and its impact on humanity. *Nature* **486**, 59–67 (2012). doi: [10.1038/nature11148](https://doi.org/10.1038/nature11148); pmid: 22678280
6. Y. Zhang, H. Y. H. Chen, P. B. Reich, Forest productivity increases with evenness, species richness and trait variation: A global meta-analysis. *J. Ecol.* **100**, 742–749 (2012). doi: [10.1111/j.1365-2745.2011.01944.x](https://doi.org/10.1111/j.1365-2745.2011.01944.x)
7. A. Paquette, C. Messier, The effect of biodiversity on tree productivity: From temperate to boreal forests. *Glob. Ecol. Biogeogr.* **20**, 170–180 (2011). doi: [10.1111/j.1466-8238.2010.00592.x](https://doi.org/10.1111/j.1466-8238.2010.00592.x)
8. P. Ruiz-Benito et al., Diversity increases carbon storage and tree productivity in Spanish forests. *Glob. Ecol. Biogeogr.* **23**, 311–322 (2014). doi: [10.1111/geb.12126](https://doi.org/10.1111/geb.12126)
9. F. van der Plas et al., Biotic homogenization can decrease landscape-scale forest multifunctionality. *Proc. Natl. Acad. Sci. U.S.A.* **113**, 3557–3562 (2016). doi: [10.1073/pnas.1517903113](https://doi.org/10.1073/pnas.1517903113); pmid: 26979952
10. F. Isbell, D. Tilman, S. Polasky, M. Loreau, The biodiversity-dependent ecosystem service debt. *Ecol. Lett.* **18**, 119–134 (2015). doi: [10.1111/ele.12393](https://doi.org/10.1111/ele.12393); pmid: 25430966
11. S. Diaz et al., The IPBES Conceptual Framework—Connecting nature and people. *Curr. Op. Environ. Sust.* **14**, 1–16 (2015). doi: [10.1016/j.cosust.2014.11.002](https://doi.org/10.1016/j.cosust.2014.11.002)
12. United Nations, vol. COP 10 Decision X/2 (Nagoya, Japan, 2010).
13. W. M. Adams et al., Biodiversity conservation and the eradication of poverty. *Science* **306**, 1146–1149 (2004). doi: [10.1126/science.1097920](https://doi.org/10.1126/science.1097920); pmid: 15539593
14. J. B. Grace et al., Integrative modelling reveals mechanisms linking productivity and plant species richness. *Nature* **529**, 390–393 (2016). doi: [10.1038/nature16524](https://doi.org/10.1038/nature16524); pmid: 26760203
15. D. I. Forrester, H. Pretzsch, Tamm Review: On the strength of evidence when comparing ecosystem functions of mixtures with monocultures. *For. Ecol. Manage.* **356**, 41–53 (2015). doi: [10.1016/j.foreco.2015.08.016](https://doi.org/10.1016/j.foreco.2015.08.016)
16. C. M. Tobner et al., Functional identity is the main driver of diversity effects in young tree communities. *Ecol. Lett.* **19**, 638–647 (2016). doi: [10.1111/ele.12600](https://doi.org/10.1111/ele.12600); pmid: 27072428
17. K. Verheyen et al., Contributions of a global network of tree diversity experiments to sustainable forest plantations. *Ambio* **45**, 29–41 (2016). doi: [10.1007/s13280-015-0685-1](https://doi.org/10.1007/s13280-015-0685-1); pmid: 26264716
18. FAO, “Global Forest Resources Assessment 2015—How are the world’s forests changing?” (Food and Agriculture Organization of the United Nations, 2015).
19. H. Ter Steege et al., Estimating the global conservation status of more than 15,000 Amazonian tree species. *Science Advances* **1**, e1500936 (2015). doi: [10.1126/sciadv.1500936](https://doi.org/10.1126/sciadv.1500936); pmid: 26702442
20. R. Fleming, N. Brown, J. Jenik, P. Kahumbu, J. Plesnik, in *UNEP Year Book 2011*, United Nations Environment Program, Ed. (UNEP, Nairobi, Kenya, 2011), pp. 46–59.
21. International Union for Conservation of Nature (IUCN), *IUCN Red List Categories and Criteria: Version 3.1. Version 2011.1* (Gland, Switzerland and Cambridge, ed. 2, 2012), vol. iv, p. 32.
22. H. Pretzsch, G. Schütze, Transgressive overyielding in mixed compared with pure stands of Norway spruce and European beech in Central Europe: Evidence on stand level and explanation on individual tree level. *Eur. J. For. Res.* **128**, 183–204 (2009). doi: [10.1007/s10342-008-0215-9](https://doi.org/10.1007/s10342-008-0215-9)
23. A. Bravo-Oviedo et al., European Mixed Forests: Definition and research perspectives. *For. Syst.* **23**, 518–533 (2014).
24. K. B. Hulvey et al., Benefits of tree mixes in carbon plantings. *Nature Clim. Change* **3**, 869–874 (2013). doi: [10.1038/nclimate1862](https://doi.org/10.1038/nclimate1862)
25. FAO, “Contribution of the forestry sector to national economies, 1990–2011” (Food and Agriculture Organization of the United Nations, 2014).
26. Value-added has been adjusted for inflation and is expressed in USD at 2011 prices and exchange rates.
27. B. J. Cardinale et al., The functional role of producer diversity in ecosystems. *Am. J. Bot.* **98**, 572–592 (2011). doi: [10.3732/ajb.1000364](https://doi.org/10.3732/ajb.1000364); pmid: 21613148
28. P. B. Reich et al., Impacts of biodiversity loss escalate through time as redundancy fades. *Science* **336**, 589–592 (2012). doi: [10.1126/science.1217909](https://doi.org/10.1126/science.1217909); pmid: 22556253
29. M. Loreau, A. Hector, Partitioning selection and complementarity in biodiversity experiments. *Nature* **412**, 72–76 (2001). doi: [10.1038/35083573](https://doi.org/10.1038/35083573); pmid: 11452308
30. D. Tilman, C. L. Lehman, K. T. Thomson, Plant diversity and ecosystem productivity: Theoretical considerations. *Proc. Natl. Acad. Sci. U.S.A.* **94**, 1857–1861 (1997). doi: [10.1073/pnas.94.5.1857](https://doi.org/10.1073/pnas.94.5.1857); pmid: 11038606
31. H. Y. H. Chen, K. Klinka, Aboveground productivity of western hemlock and western redcedar mixed-species stands in southern coastal British Columbia. *For. Ecol. Manage.* **184**, 55–64 (2003). doi: [10.1016/S0378-1127\(03\)00148-8](https://doi.org/10.1016/S0378-1127(03)00148-8)
32. The elasticity of substitution (θ), which represents the degree to which species can substitute for each other in contributing to stand productivity, reflects the strength of the effect of biodiversity on ecosystem productivity, after accounting for climatic, soil, and other environmental and local covariates.
33. H. Pretzsch et al., Growth and yield of mixed versus pure stands of Scots pine (*Pinus sylvestris* L.) and European beech (*Fagus sylvatica* L.) analysed along a productivity gradient through Europe. *Eur. J. For. Res.* **134**, 927–947 (2015). doi: [10.1007/s10342-015-0900-4](https://doi.org/10.1007/s10342-015-0900-4)
34. E. D. Schulze et al., Opinion paper: Forest management and biodiversity. *Web Ecol.* **14**, 3–10 (2014). doi: [10.5194/we-14-3-2014](https://doi.org/10.5194/we-14-3-2014)
35. R. Waring et al., Why is the productivity of Douglas-fir higher in New Zealand than in its native range in the Pacific Northwest, USA? *For. Ecol. Manage.* **255**, 4040–4046 (2008). doi: [10.1016/j.foreco.2008.03.049](https://doi.org/10.1016/j.foreco.2008.03.049)
36. J. Liang, J. V. Watson, M. Zhou, X. Lei, Effects of productivity on biodiversity in forest ecosystems across the United States and China. *Conserv. Biol.* **30**, 308–317 (2016). doi: [10.1111/cobi.12636](https://doi.org/10.1111/cobi.12636); pmid: 26954431
37. L. H. Fraser et al., Worldwide evidence of a unimodal relationship between productivity and plant species richness. *Science* **349**, 302–305 (2015). doi: [10.1126/science.1258916](https://doi.org/10.1126/science.1258916); pmid: 26185249
38. M. Loreau, Biodiversity and ecosystem functioning: A mechanistic model. *Proc. Natl. Acad. Sci. U.S.A.* **95**, 5632–5636 (1998). doi: [10.1073/pnas.95.10.5632](https://doi.org/10.1073/pnas.95.10.5632); pmid: 9576935

39. F. Isbell *et al.*, Nutrient enrichment, biodiversity loss, and consequent declines in ecosystem productivity. *Proc. Natl. Acad. Sci. U.S.A.* **110**, 11911–11916 (2013). doi: [10.1073/pnas.1310880110](https://doi.org/10.1073/pnas.1310880110); pmid: [23818582](https://pubmed.ncbi.nlm.nih.gov/23818582/)
40. C. Le Quéré *et al.*, Global carbon budget 2015. *Earth Syst. Sci. Data* **7**, 349–396 (2015). doi: [10.5194/essd-7-349-2015](https://doi.org/10.5194/essd-7-349-2015)
41. A. Hector, R. Bagchi, Biodiversity and ecosystem multifunctionality. *Nature* **448**, 188–190 (2007). doi: [10.1038/nature05947](https://doi.org/10.1038/nature05947); pmid: [17625564](https://pubmed.ncbi.nlm.nih.gov/17625564/)
42. L. Gamfeldt *et al.*, Higher levels of multiple ecosystem services are found in forests with more tree species. *Nat. Commun.* **4**, 1340 (2013). doi: [10.1038/ncomms2328](https://doi.org/10.1038/ncomms2328); pmid: [23299890](https://pubmed.ncbi.nlm.nih.gov/23299890/)
43. D. P. McCarthy *et al.*, Financial costs of meeting global biodiversity conservation targets: Current spending and unmet needs. *Science* **338**, 946–949 (2012). doi: [10.1126/science.1229803](https://doi.org/10.1126/science.1229803); pmid: [23065904](https://pubmed.ncbi.nlm.nih.gov/23065904/)
44. C. B. Barrett, A. J. Travis, P. Dasgupta, On biodiversity conservation and poverty traps. *Proc. Natl. Acad. Sci. U.S.A.* **108**, 13907–13912 (2011). doi: [10.1073/pnas.1011521108](https://doi.org/10.1073/pnas.1011521108); pmid: [21873176](https://pubmed.ncbi.nlm.nih.gov/21873176/)
45. B. Fisher, T. Christopher, Poverty and biodiversity: Measuring the overlap of human poverty and the biodiversity hotspots. *Ecol. Econ.* **62**, 93–101 (2007). doi: [10.1016/j.ecolecon.2006.05.020](https://doi.org/10.1016/j.ecolecon.2006.05.020)
46. N. Myers, R. A. Mittermeier, C. G. Mittermeier, G. A. B. da Fonseca, J. Kent, Biodiversity hotspots for conservation priorities. *Nature* **403**, 853–858 (2000). doi: [10.1038/35002501](https://doi.org/10.1038/35002501); pmid: [10706275](https://pubmed.ncbi.nlm.nih.gov/10706275/)
47. S. Gourlet-Fleury, J.-M. Guehl, O. Laroussinie, *Ecology and Management of a Neotropical Rainforest: Lessons Drawn from Paracou, A Long-Term Experimental Research Site in French Guiana* (Elsevier, 2004).
48. J. C. Tipper, Rarefaction and rarefaction—The use and abuse of a method in paleoecology. *Paleobiology* **5**, 423–434 (1979). doi: [10.1017/S0094837300016924](https://doi.org/10.1017/S0094837300016924)
49. M. L. Rosenzweig, *Species Diversity in Space and Time* (Cambridge Univ. Press, 1995).
50. L. Breiman, Random forests. *Mach. Learn.* **45**, 5–32 (2001). doi: [10.1023/A:1010933404324](https://doi.org/10.1023/A:1010933404324)
51. S. A. Chamberlain, E. Szöcs, taxize: Taxonomic search and retrieval in R. *F1000Res.* **2**, 191 (2013).pmid: [24555091](https://pubmed.ncbi.nlm.nih.gov/24555091/)
52. B. Husch, T. W. Beers, J. A. Kershaw Jr., *Forest Mensuration* (John Wiley & Sons, ed. 4, 2003).
53. M. G. R. Cannell, Woody biomass of forest stands. *For. Ecol. Manage.* **8**, 299–312 (1984). doi: [10.1016/0378-1127\(84\)90062-8](https://doi.org/10.1016/0378-1127(84)90062-8)
54. M. Simard, N. Pinto, J. B. Fisher, A. Baccini, Mapping forest canopy height globally with spaceborne lidar. *J. Geophys. Res.* **116**, G04021 (2011). doi: [10.1029/2011JG001708](https://doi.org/10.1029/2011JG001708)
55. N. L. Stephenson, P. J. Mantgem, Forest turnover rates follow global and regional patterns of productivity. *Ecol. Lett.* **8**, 524–531 (2005). doi: [10.1111/j.1461-0248.2005.00746.x](https://doi.org/10.1111/j.1461-0248.2005.00746.x); pmid: [21352456](https://pubmed.ncbi.nlm.nih.gov/21352456/)
56. D. A. Clark *et al.*, Measuring net primary production in forests: Concepts and field methods. *Ecol. Appl.* **11**, 356–370 (2001). doi: [10.1890/1051-0761\(2001\)011\[0356:MNPPIF\]2.0.CO;2](https://doi.org/10.1890/1051-0761(2001)011[0356:MNPPIF]2.0.CO;2)
57. ESRI, “Release 10.3 of Desktop, ESRI ArcGIS” (Environmental Systems Research Institute, 2014)
58. R Core Team, “R: A language and environment for statistical computing” (R Foundation for Statistical Computing, Vienna, 2013)
59. A. Di Gregorio, L. J. Jansen, “Land Cover Classification System (LCCS): classification concepts and user manual” (FAO, Department of Natural Resources and Environment, 2000)
60. P. Legendre, Spatial autocorrelation: Trouble or new paradigm? *Ecology* **74**, 1659–1673 (1993). doi: [10.2307/1939924](https://doi.org/10.2307/1939924)
61. J. Liang, Mapping large-scale forest dynamics: A geospatial approach. *Landscape Ecol.* **27**, 1091–1108 (2012). doi: [10.1007/s10980-012-9767-7](https://doi.org/10.1007/s10980-012-9767-7)
62. N. A. C. Cressie, *Statistics for Spatial Data* (J. Wiley, 1993).
63. J. Pinheiro, D. Bates, S. DebRoy, D. Sarkar, R Development Core Team, *nlme: Linear and Nonlinear Mixed Effects Models* (2011), vol. R package version 3.1-101.
64. P. Legendre, N. L. Oden, R. R. Sokal, A. Vaudor, J. Kim, Approximate analysis of variance of spatially autocorrelated regional data. *J. Classif.* **7**, 53–75 (1990). doi: [10.1007/BF01889703](https://doi.org/10.1007/BF01889703)
65. A. Liaw, M. Wiener, Classification and regression by randomForest. *R News* **2**, 18–22 (2002).
66. L. Magee, R^2 measures based on Wald and likelihood ratio joint significance tests. *Am. Stat.* **44**, 250–253 (1990).
67. M. C. Hansen *et al.*, High-resolution global maps of 21st-century forest cover change. *Science* **342**, 850–853 (2013). doi: [10.1126/science.1244693](https://doi.org/10.1126/science.1244693); pmid: [24233722](https://pubmed.ncbi.nlm.nih.gov/24233722/)
68. E. J. Pebesma, Multivariable geostatistics in S: The gstat package. *Comput. Geosci.* **30**, 683–691 (2004). doi: [10.1016/j.comgeo.2004.03.012](https://doi.org/10.1016/j.comgeo.2004.03.012)
69. R. Costanza *et al.*, Changes in the global value of ecosystem services. *Glob. Environ. Change* **26**, 152–158 (2014). doi: [10.1016/j.gloenvcha.2014.04.002](https://doi.org/10.1016/j.gloenvcha.2014.04.002)
70. BLS, in *BLS Handbook of Methods*. (U.S. Department of Labor, Washington, DC, 2015).
71. We used the online CPI calculator; <http://data.bls.gov/cgi-bin/cpicalc.pl>.
72. T. W. Crowther *et al.*, Mapping tree density at a global scale. *Nature* **525**, 201–205 (2015). doi: [10.1038/nature14967](https://doi.org/10.1038/nature14967); pmid: [26331545](https://pubmed.ncbi.nlm.nih.gov/26331545/)
73. The tree drawings in Fig. 2 were based on actual species from the GFB plots. The scientific names of these species are (clockwise from the top) *Abies nebrodensis*, *Handroanthus albus*, *Araucaria angustifolia*, *Magnolia sinica*, *Cupressus sempervirens*, *Salix babylonica*, *Liriodendron tulipifera*, *Adansonia grandidieri*, *Torreya taxifolia*, and *Quercus mongolica*. Five of these 10 species (*A. nebrodensis*, *A. angustifolia*, *M. sinica*, *A. grandidieri*, and *T. taxifolia*) are listed as endangered or critically endangered species in the IUCN Red List. Hand drawings were made by R. K. Watson.
74. Elevation consists mostly of ground-measured data, and the missing values were replaced with the highest-resolution topographic data generated from NASA’s Shuttle Radar Topography Mission (SRTM).
75. R. J. Hijmans, S. E. Cameron, J. L. Parra, P. G. Jones, A. Jarvis, Very high resolution interpolated climate surfaces for global land areas. *Int. J. Climatol.* **25**, 1965–1978 (2005). doi: [10.1002/joc.1276](https://doi.org/10.1002/joc.1276)
76. A. Trabucco, R. J. Zomer, in *CGIAR Consortium for Spatial Information* (CGIAR, 2009).
77. N. Batjes, “World soil property estimates for broad-scale modelling (WISE30sec)” (ISRIC-World Soil Information, 2015).
78. D. M. Olson, E. Dinerstein, The Global 200: Priority ecoregions for global conservation. *Ann. Mo. Bot. Gard.* **89**, 199–224 (2002).

ACKNOWLEDGMENTS

We are grateful to all the people and agencies that helped in collection, compilation, and coordination of the field data, including but not limited to T. Malone, J. Crowe, M. Sutton, J. Lovett, P. Munishi, M. Rautiainen, staff members from the Seoul National University Forest, and all persons who made the two Spanish Forest Inventories possible, especially the main coordinators, R. Villaseca (IFN2) and J. A. Villanueva (IFN3). This work was supported in part by West Virginia University under the United States Department of Agriculture (USDA) McIntire-Stennis Funds WVA00104 and WVA00105; U.S. National Science Foundation (NSF) Long-Term Ecological Research Program at Cedar Creek (DEB-1234162); the University of Minnesota Department of Forest Resources and Institute on the Environment; the Architecture and Environment Department of Italcementi Group, Bergamo (Italy); a Marie Skłodowska Curie fellowship; Polish National Science Center grant 2011/02/A/N9/00108; the French L’Agence Nationale de la Recherche (ANR) (Centre d’Étude de la Biodiversité Amazonienne: ANR-10-LABX-0025); the General Directory of State Forest National Holding DB; General Directorate of State Forests, Warsaw, Poland (Research Projects 1/07 and OR/2717/3/11); the 12th Five-Year Science and Technology Support Project (grant 2012BAD22B02) of China; the U.S. Geological Survey and the Bonanza Creek Long Term Ecological Research Program funded by NSF and the U.S. Forest Service (any use of trade, firm, or product names is for descriptive purposes only and does not imply endorsement by the U.S. government); National Research Foundation of Korea (grant NRF-2015R1C1A1A02037721), Korea Forest Service (grants S111215L020110, S211315L020120 and S111415L080120) and Promising-Pioneering Researcher Program through Seoul National University (SNU) in 2015; Core funding for Crown Research Institutes from the New Zealand Ministry of Business, Innovation and Employment’s Science and Innovation Group; the Deutsche Forschungsgemeinschaft (DFG) Priority Program 1374 Biodiversity Exploratories; Chilean research grants Fondo Nacional de Desarrollo Científico y Tecnológico (FONDECYT) 1151495 and 11110270; Natural Sciences and Engineering Research Council of Canada (grant RGPIN-2014-04181); Brazilian Research grants CNPq 312075/2013 and FAPESP 2013/TR441 supporting Santa Catarina State Forest Inventory (IFFSC); the General Directorate of State Forests, Warsaw, Poland; the Bavarian State Ministry for Nutrition, Agriculture, and Forestry project W07; the Bavarian State Forest Enterprise (Bayerische Staatsforsten AöR); German

Science Foundation for project PR 292/12-1; the European Union for funding the COST Action FP1206 EuMIXFOR; FEDER/COMPETE/POCI under Project POCI-01-0145-FEDER-006958 and FCT—Portuguese Foundation for Science and Technology under the project UID/AGR/04033/2013; Swiss National Science Foundation grant 310030B_147092; the EU H2020 PEGASUS project (no 633814), EU H2020 Simwood project (no 613762); and the European Union’s Horizon 2020 research and innovation program within the framework of the MultiFUNGtionality Marie Skłodowska-Curie Individual Fellowship (IF-EF) under grant agreement 655815. The expeditions in Cameroon to collect the data were partly funded by a grant from the Royal Society and the Natural Environment Research Council (UK) to Simon L. Lewis. Pontificia Universidad Católica del Ecuador offered working facilities and reduced station fees to implement the census protocol in Yasuni National Park. We thank the following agencies and organization for providing the data: USDA Forest Service; School of Natural Resources and Agricultural Sciences, University of Alaska Fairbanks; the Ministère des Forêts, de la Faune et des Parcs du Québec (Canada); the Alberta Department of Agriculture and Forestry, the Saskatchewan Ministry of the Environment, and Manitoba Conservation and Water Stewardship (Canada); the National Vegetation Survey Databank (New Zealand); Italian and Friuli Venezia Giulia Forest Services (Italy); Bavarian State Forest Enterprise (Bayerische Staatsforsten AöR) and the Thünen Institute of Forest Ecosystems (Germany); Queensland Herbarium (Australia); Forestry Commission of New South Wales (Australia); Instituto de Conservação da Natureza e das Florestas (Portugal). M’Baiki data were made possible and provided by the ARF Project (Appui la Recherche Forestière) and its partners: AFD (Agence Française de Développement), CIRAD (Centre de Coopération Internationale en Recherche Agronomique pour le Développement), ICRA (Institut Centrafricain de Recherche Agronomique), MEDDEFCP (Ministère de l’Environnement, du Développement Durable des Eaux, Forêts, Chasse et Pêche), SCAC/MAE (Service de Coopération et d’Actions Culturelles, Ministère des Affaires Étrangères), SCAD (Société Centrafricaine de Déroulage), and the University of Bangui. All TEAM data were provided by the Tropical Ecology Assessment and Monitoring (TEAM) Network—a collaboration between Conservation International, the Smithsonian Institute, and the Wildlife Conservation Society—and partially funded by these institutions: the Gordon and Betty Moore Foundation, the Valuing the Arc Project (Leverhulme Trust), and other donors. The Exploratory plots of FunDivEUROPE received funding from the European Union Seventh Framework Programme (FP7/2007-2013) under grant agreement 265171. The Chinese Comparative Study Plots (CSPs) were established in the framework of BEF-China, funded by the German Research Foundation (DFG FOR891); The Gabon data set was provided by the Institut de Recherche en Ecologie Tropicale (IRET)/Centre National de la Recherche Scientifique et Technologique (CENAREST); Dutch inventory data collection was done with the help of Probos, Silve, Bureau van Nierop and Wim Daamen, financed by the Dutch Ministry of Economic Affairs. Data collection in Middle Eastern countries was supported by the Spanish Agency for International Development Cooperation [Agencia Española de Cooperación Internacional para el Desarrollo (AECID)] and Fundación Biodiversidad, in cooperation with the governments of Syria and Lebanon. We are grateful to the Polish State Forest Holding for the data collected in the project “Establishment of a forest information system covering the area of the Sudetes and the West Beskids with respect to the forest condition monitoring and assessment” financed by the General Directory of State Forest National Holding. We thank two reviewers who provided constructive and helpful comments to help us further improve this paper. The data used in this manuscript are summarized in the supplementary materials (tables S1 and S2). All data needed to replicate these results are available at <https://figshare.com> and www.gbifinitiative.org. New Zealand data (doi:10.7931/V13W29) are available from S.W. under a materials agreement with the National Vegetation Survey Databank managed by Landcare Research, New Zealand. Access to Poland data needs additional permission from Polish State Forest National Holding, as provided to T.Z.-N.

SUPPLEMENTARY MATERIALS

www.sciencemag.org/content/354/6309/aaf8957/suppl/DC1
Figs. S1 to S4
Tables S1 to S2
References (79–134)

6 May 2016; accepted 22 August 2016
10.1126/science.aaf8957

RESEARCH ARTICLE

HIV-1 THERAPY

Sustained virologic control in SIV⁺ macaques after antiretroviral and $\alpha_4\beta_7$ antibody therapy

Siddappa N. Byreddy,^{1*} James Arthos,^{2*} Claudia Cicala,^{2*} Francois Villinger,^{1,3†} Kristina T. Ortiz,¹ Dawn Little,¹ Neil Sidell,⁴ Maureen A. Kane,⁵ Jianshi Yu,⁵ Jace W. Jones,⁵ Philip J. Santangelo,⁶ Chiara Zurla,⁶ Lyle R. McKinnon,^{7§} Kelly B. Arnold,⁸ Caroline E. Woody,⁸ Lutz Walter,⁹ Christian Roos,⁹ Angela Noll,⁹ Donald Van Ryk,² Katija Jelacic,² Raffaello Cimbrotto,¹⁰ Sanjeev Gumber,³ Michelle D. Reid,¹ Volkan Adsay,¹ Praveen K. Amancha,³ Ann E. Mayne,¹ Tristram G. Parslow,¹ Anthony S. Fauci,² Aftab A. Ansari^{1||}

Antiretroviral drug therapy (ART) effectively suppresses replication of both the immunodeficiency viruses, human (HIV) and simian (SIV); however, virus rebounds soon after ART is withdrawn. SIV-infected monkeys were treated with a 90-day course of ART initiated at 5 weeks post infection followed at 9 weeks post infection by infusions of a primatized monoclonal antibody against the $\alpha_4\beta_7$ integrin administered every 3 weeks until week 32. These animals subsequently maintained low to undetectable viral loads and normal CD4⁺ T cell counts in plasma and gastrointestinal tissues for more than 9 months, even after all treatment was withdrawn. This combination therapy allows macaques to effectively control viremia and reconstitute their immune systems without a need for further therapy.

Profound and durable suppression of HIV by antiretroviral therapy (ART) represents a major accomplishment in HIV-AIDS research. However, HIV persists in patients despite long-term ART therapy such that, once ART is withdrawn, virus invariably rebounds. Lifetime ART treatment is associated with toxicity (1), residual chronic inflammation, and the accelerated onset of diseases associated with aging (2, 3).

High levels of viral replication in gastrointestinal tissues (GITs) during acute infection lead to severe depletion of local CD4⁺ T cells (4), damage to the gut epithelium, and the rapid formation of persistent viral reservoirs. Generalized immune dysfunction and chronic immune activation follow. Even when administered days after infection, ART fails to fully reverse these insults (5). We reasoned that preventing HIV-susceptible cells from accessing GITs might reduce damage to the gut and the mucosal immune system in a way that would allow immune mechanisms to effectively control infection.

A principal pathway that CD4⁺ T cells use to traffic into GITs involves an interaction between integrin $\alpha_4\beta_7$, expressed on CD4⁺ T cells, with mucosal vascular addressin cell adhesion molecule 1 (MAdCAM-1), expressed primarily on high endothelial venules within GITs (6, 7). CD4⁺ T cells that express high levels of the $\alpha_4\beta_7$ integrin ($\alpha_4\beta_7^{\text{hi}}$) are preferential targets of HIV and simian immunodeficiency virus (SIV) during acute infection (8–12). In order to disrupt trafficking of $\alpha_4\beta_7^{\text{hi}}$ CD4⁺ T cells into GITs, we developed a recombinant rhesus monoclonal antibody against the heterodimeric form of $\alpha_4\beta_7$ ($\alpha_4\beta_7$ mAb) that blocks $\alpha_4\beta_7$ binding to MAdCAM (13–15).

Administration of $\alpha_4\beta_7$ mAb before and during repeated low-dose intravaginal SIV challenge of rhesus macaques (RMs) leads to significant protection from transmission (13). In treated animals that became infected, GIT CD4⁺ T cells were preserved and GIT proviral DNA was reduced,

and thus, virus-mediated damage to GITs was minimized.

Because ART provides only partial protection to GITs (5, 14), we considered the possibility that adding $\alpha_4\beta_7$ mAb might improve this protection. To this end, we conducted a study in genetically characterized (table S1, A to D) SIV-infected RMs that combined a 90-day course of ART, beginning 5 weeks post-infection with a series of eight infusions of $\alpha_4\beta_7$ mAb. This treatment strategy included five phases as outlined in fig. S1. In phase I (weeks 1 to 5), 18 RMs were infected intravenously with a 200 median tissue culture infectious dose (TCID₅₀) of SIVmac239. After 5 weeks, all 18 animals began a 90-day daily regimen of ART (phase II). During phase III (weeks 9 to 18), 11 animals received $\alpha_4\beta_7$ mAb once every 3 weeks (eight infusions total); 7 animals received nonspecific rhesus immunoglobulin G (IgG). During phase IV (weeks 18 to 32), ART was withdrawn, and $\alpha_4\beta_7$ mAb–IgG treatment was continued. In phase V (weeks 32 to 50), all treatment was terminated. Three out of 11 $\alpha_4\beta_7$ mAb-treated animals developed antibodies against the $\alpha_4\beta_7$ mAb (fig. S2) and were excluded from further analysis.

ART + $\alpha_4\beta_7$ mAb controls plasma and gut viral loads

All 15 animals showed similar peaks in viremia around weeks 2 to 3 ($\sim 2.9 \times 10^6$ copies/ml), and they all fully suppressed viremia by 3 weeks after ART initiation. The two groups developed divergent viral load (VL) patterns after ART was withdrawn (phase IV). In all seven IgG-treated animals, viremia rebounded to high levels ($\sim 10^6$ copies/ml) within 2 weeks and maintained those levels out to week 50 (Fig. 1B). In contrast, two out of eight $\alpha_4\beta_7$ mAb-treated animals never rebounded, and the remaining six out of eight rebounded but then regained control of viremia within 4 weeks (Fig. 1A). Virologic control was robust in all eight $\alpha_4\beta_7$ mAb-treated animals, with either complete control or transient low-level blips of viremia. The difference in viremia between the two groups after discontinuation of ART was significant ($P < 0.0001$) (Fig. 1C). Virologic control in all eight $\alpha_4\beta_7$ mAb-treated animals persisted to week 81 (fig. S3), although the last infusion of $\alpha_4\beta_7$ mAb (half-life of ~ 11.4 days) was administered at week 32 (13).

Both treatment groups showed similar levels of proviral DNA in GITs during phases I and II. Immediately after cessation of ART, all monkeys showed increases in proviral DNA. High levels (20 to 40 copies/ng DNA) persisted in the seven IgG-treated animals until week 50 (Fig. 1E). In contrast, in all eight $\alpha_4\beta_7$ mAb-treated macaques, proviral DNA decreased to levels at or below the level of detection by week 30 (Fig. 1D). The difference in the geometric means of the two groups (Fig. 1F) during phases IV and V was significant ($P < 0.0001$). Undetectable proviral DNA loads in all eight $\alpha_4\beta_7$ mAb-treated macaques persisted well after the final infusion of $\alpha_4\beta_7$ mAb (week 32). Thus, combining $\alpha_4\beta_7$ mAb therapy with short-term ART promoted persistent systemic and

¹Department of Pathology and Laboratory Medicine, Emory University School of Medicine, Atlanta, GA 30322, USA.

²Laboratory of Immunoregulation, NIAID, NIH, Bethesda, MD 20892, USA. ³Division of Pathology, The Yerkes National Primate Center of Emory University, Atlanta, GA 30329, USA.

⁴Department of Obstetrics and Gynecology, Emory University School of Medicine, Atlanta, GA 30322, USA. ⁵Department of Pharmaceutical Sciences, School of Pharmacy, University of Maryland, Baltimore, MD 21201, USA. ⁶Wallace H. Coulter Department of Biomedical Engineering, Georgia Institute of Technology and Emory University, Atlanta, GA 30680, USA.

⁷Centre for the AIDS Program of Research in South Africa (CAPRISA), Durban, South Africa. ⁸Department of Biomedical Engineering, University of Michigan, Ann Arbor, MI 48109, USA. ⁹Primate Genetics Laboratory, German Primate Center, Leibniz Institute for Primate Research, Göttingen, Germany.

¹⁰Division of Rheumatology, Johns Hopkins School of Medicine, Baltimore, MD 21201, USA.

*These authors contributed equally to the planning and performance of this study. †Present address: Department of Pharmacology and Experimental Neuroscience, University of Nebraska Medical Center, Omaha, NE 68198, USA. ‡Present address: Office of the Director, New Iberia Research Center, University of Louisiana at Lafayette, New Iberia, LA 70560, USA. §Present address: Department of Medical Microbiology, University of Manitoba, Winnipeg, Canada. ||Corresponding author. Email: pathaa@emory.edu

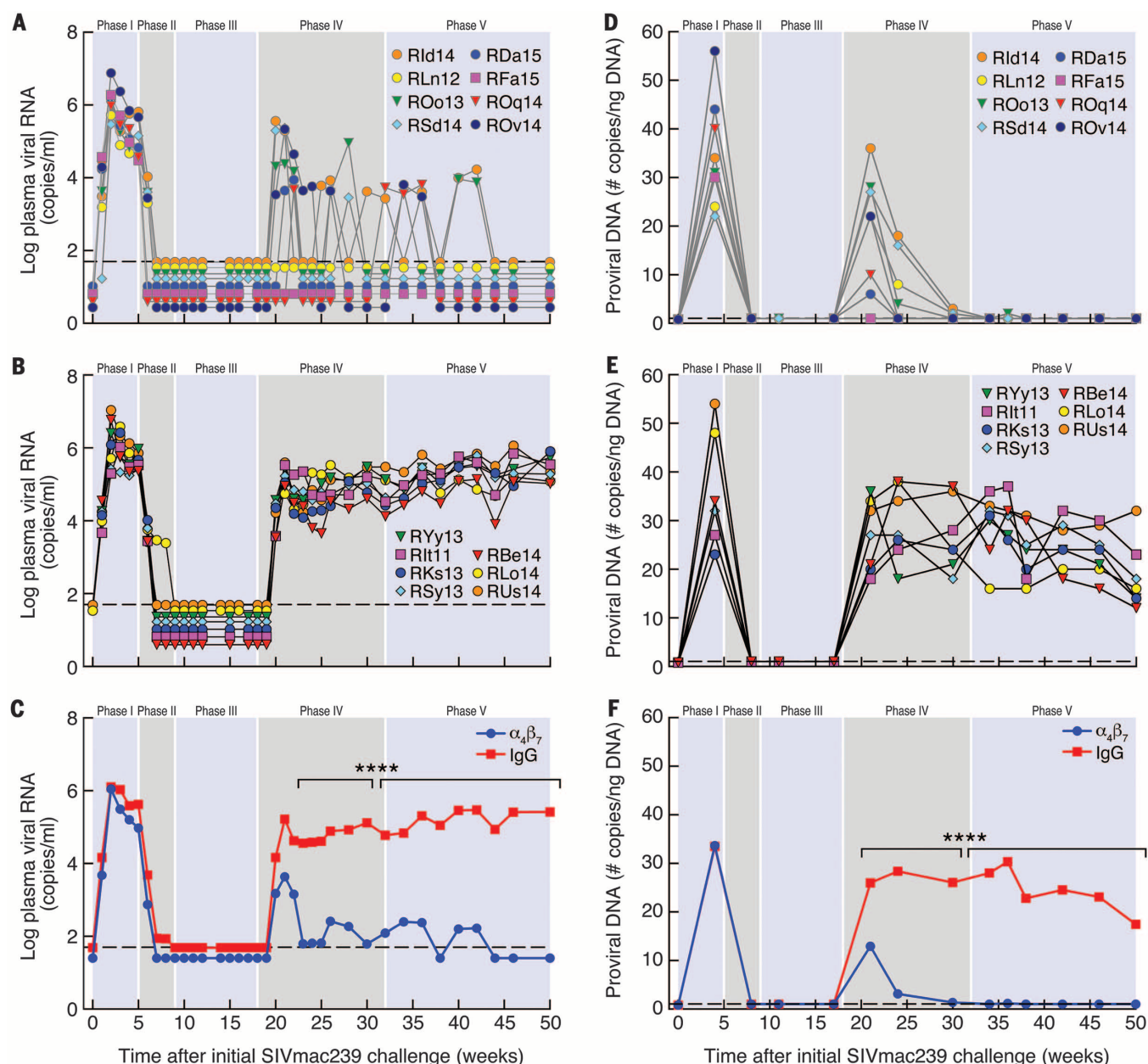


Fig. 1. Control of plasma and GIT viral loads. Plasma viral loads from (A) eight monkeys receiving ART + $\alpha_4\beta_7$ mAb and (B) seven monkeys receiving ART + IgG are reported as log₁₀ number of viral copies/ml of plasma. (C) Geometric means for plasma viral loads of monkeys treated with ART + $\alpha_4\beta_7$ mAb (blue) or IgG (red). GIT proviral DNA loads for (D) eight monkeys receiving ART + $\alpha_4\beta_7$ mAb and (E) seven monkeys receiving IgG are

reported as the number of copies of proviral DNA/ng of total DNA. (F) Geometric means for GIT proviral loads of monkeys treated with ART + $\alpha_4\beta_7$ mAb (blue) or IgG (red). The shaded areas in each graph demarcate the five phases of the study. Code names of individual monkeys are shown in each graph. *P* values were determined using analysis of covariance (ANCOVA) (*****P* < 0.0001).

mucosal virologic control following discontinuation of all therapy.

Rebound of CD4⁺ T cell subsets

Blood and GIT mononuclear cells isolated from each phase of the study were analyzed by flow cytometry (table S2, A to C). During phase I, the absolute numbers of blood total CD4⁺ T cells and subsets showed a sharp decline (Fig. 2, A to D). After the first administration of $\alpha_4\beta_7$ mAb (phase III), CD4 values diverged. The $\alpha_4\beta_7$ mAb-treated

animals, but not controls, showed marked increases in total CD4⁺ T cells and, notably, in the effector memory (EM) CD4⁺ T cell subset (>four-fold increase, *P* < 0.0001) (Fig. 2D). These increases were sustained after discontinuation of the $\alpha_4\beta_7$ mAb treatment (phase V). By week 50, total CD4⁺ T cell numbers approached preinfection levels.

Acute HIV-1 and SIV infections are characterized by a rapid depletion of CD4⁺ T cells in GITs (4, 15–18). Therefore, we evaluated the fate of GIT CD4⁺ T cells (Fig. 2, E to H), with values expressed

as the percent of CD4⁺ T cells within the gated population of CD45⁺ cells. We observed a sharp decline in total CD4⁺ T cells during the acute phase in both groups with CD45⁺/CD4⁺ T cells reaching their nadir by the end of phase I (Fig. 2E). In phase III, the CD4⁺ T cell profile of the two treatment groups diverged. The relative frequency of CD45⁺/CD4⁺ cells in the $\alpha_4\beta_7$ mAb-treated animals gradually increased through phase V (*P* < 0.0001). CD4⁺ T cell subsets showed an apparent recovery of both T central memory (CM)

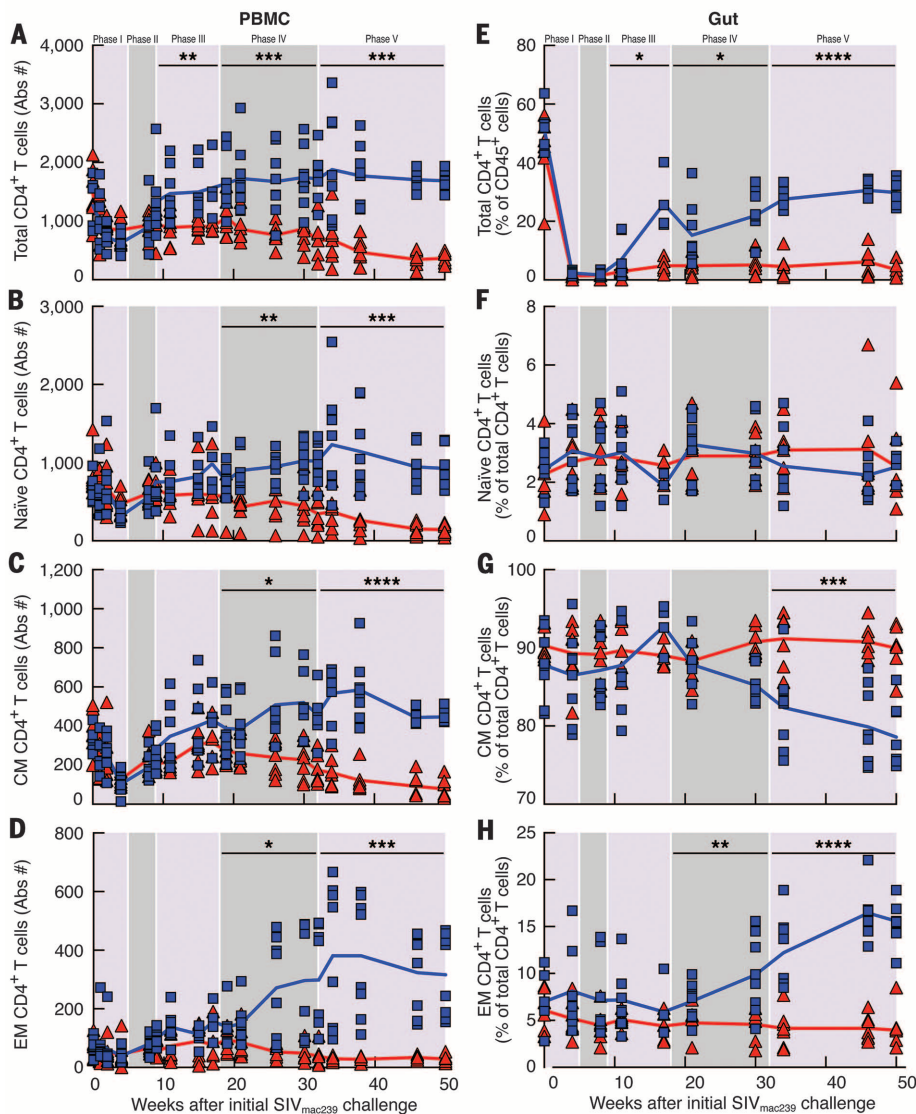


Fig. 2. Kinetic changes in CD4⁺ T cell subsets. Kinetic changes in the absolute number of circulating CD4⁺ T cells in (A) PBMCs and subsets, (B) naïve CD4⁺ T cells, (C) T central memory (T_{CM}) CD4⁺ T cells, and (D) T effector memory (T_{EM}) CD4⁺ T cells. α4β7 mAb-treated monkeys (blue) and IgG-treated animals (red). Frequencies in GITs of (E) total CD4⁺ T cells expressed as the percentage of the gated population of CD45⁺ cells, (F) naïve CD4⁺ T cells, (G) T_{CM} CD4⁺ T cells, and (H) T_{EM} CD4⁺ T cells. The frequencies of CD4⁺ T cell subsets in GITs were calculated as the percentage of total CD4⁺ T cells in the same sample. *P* values were determined using the multiple *t* test (**P* < 0.05; ***P* < 0.01; ****P* < 0.001; *****P* < 0.0001).

and T EM cells in the α4β7 mAb-treated animals, with the EM recovering at a faster rate (Fig. 2, G and H). The relative proportion of naïve CD4⁺ T cells remained constant through phase V (Fig. 2F). The quality of this recovery was well reflected by increases in the frequencies of T helper 17 (T_H17) and T helper 22 (T_H22) subsets of CD4⁺ T cells in both GITs and blood (fig. S4) (19). Consistent with these results, immunohistological analysis of GIT sections after week 50 revealed abundant CD4⁺ T cells in α4β7 mAb-treated animals but not in controls (fig. S5).

To better understand the repopulation of gut tissues with CD4⁺ T cells, we used a newly developed antibody-targeted positron emission tomog-

raphy (immuno-PET) combined with the computed tomography (CT) imaging technique (20). Around week 50 (phase V), four macaques from each treatment group were imaged with a ⁶⁴Cu-labeled F(ab')₂ antibody against CD4. Although we had originally hypothesized that α4β7 mAb would inhibit CD4⁺ T cell trafficking to GITs, we instead observed repopulation of CD4⁺ cells in a wide variety of immune tissues, including GITs (Fig. 3). This result suggests that the protective effect of α4β7 mAb in minimizing GIT viral load early in infection (Fig. 1, D to F) facilitated the repopulation of CD4⁺ cells throughout the systemic and mucosal immune systems. It is unclear whether the reconstitution of these immune sites resulted from the control of vi-

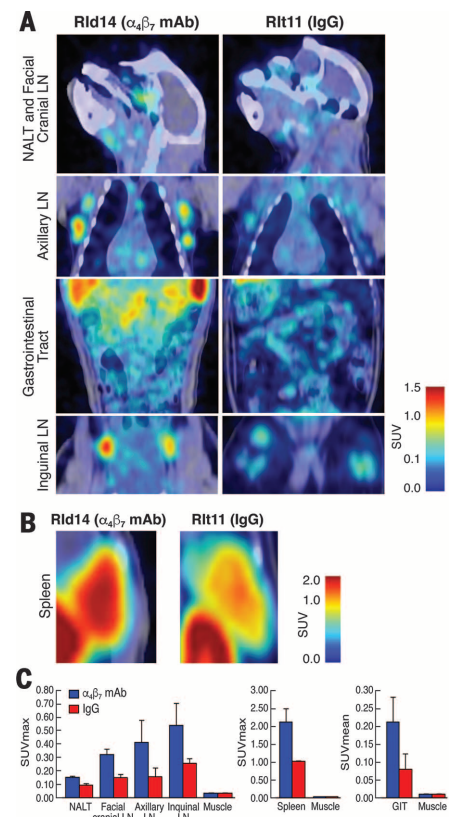


Fig. 3. Immuno-PET-CT analysis confirms the preservation of CD4⁺ cells. PET-CT image analysis of four IgG- and four α4β7 mAb-treated monkeys with ⁶⁴Cu-labeled anti-CD4 F(ab')₂ mAb around week 50 post infection. (A) Representative images of the nasal-associated lymphoid tissues (NALTs), facial cranial lymph nodes (LN), axillary LN, GI tract, and inguinal LN from a monkey receiving α4β7 mAb (Rld14) (left) and a monkey receiving IgG (Rlt11) (right). (B) Images of spleen from α4β7 mAb-treated (Rld14) (left) and IgG-treated (Rlt11) (right). (C) Average (means ± SD) signals obtained from four α4β7 mAb-treated and four IgG-treated animals for NALTs, facial cranial LN, axillary LN, inguinal LN, GITs, and muscle. Values shown are SUVmax [density of highest signal obtained within a region of interest (ROI)] for all tissues except GITs, where SUVmean is reported (mean of signals within an ROI).

remia, whether these immune competent components contributed to virologic control, or both.

Phenotypic analysis of NK cells and other cell lineages

Total natural killer (NK) cells in blood remained similar in both groups during phases I to IV (Fig. 4) and decreased during phase V but only in the IgG-treated group (Fig. 4A). We observed a decrease in the cytolytic subset (NKG2a⁺/CD8⁺/CD16⁺/CD56⁺) during phase III and IV in the α4β7 mAb-treated group, followed by an increase during phase V (Fig. 4B). Cytokine-synthesizing NK cells (NKG2a⁺/CD8⁺/CD16⁺/CD56⁺) increased during phase IV in α4β7 mAb-treated animals

(Fig. 4C). By week 50, these values approached baseline. A related pattern was observed in GITs. In the $\alpha_4\beta_7$ mAb-treated group, the proportion of the cytokine-synthesizing NK cell subset increased through phases IV and V (Fig. 4H), with corresponding decreases in the proportion of other NK cell subsets. These changes are noteworthy in two ways. First, among all NK cell subsets analyzed, $\alpha_4\beta_7$ expression is highest (~40%) on cytokine-synthesizing NK cells. Second, these increases coincided with the appearance of virologic control in phase IV. Frequencies of NKp44⁺ innate lymphoid cells (ILCs) decreased in both treatment groups as early as phase I (fig. S6), which is consistent with the loss of ILCs in acute HIV infection (27). However, we observed a sustained increase in the frequency of ILCs in gut biopsies in ART + $\alpha_4\beta_7$ mAb-treated animals beginning in phase III but not in controls. Note that vaccine-induced ILCs have been correlated with protection from SIV infection (22). Other cell lineages (CD8⁺ T cells, B cells, and plasmacytoid and myeloid dendritic cells) were analyzed (figs. S7 and S8), as were activation markers on CD4⁺CD8⁺ T and NK cells (figs. S9 to S11). Although differences were noted, further studies will be required to inform the impact of those differences.

Identification of signature plasma cytokines

Results presented above suggest that virologic control was immune mediated. To this end, we analyzed a panel of 20 immune or inflammatory markers (table S3) in plasma samples. To identify signatures for each of the five phases of the study, we used a partial least square discriminant analysis (PLSDA). PLSDA models were created for the five study phases by using measurements from each sample and time point, and variable importance projection scores were used to omit markers that did not contribute to group differentiation. Cross-validation was used to assess model performance. In phases I and II, we found no distinction between treatment groups, with a high cross-validation error between models (0.28 and 0.21, respectively) (fig. S12, A and B). In phases III to V, distinct signatures differentiated the two treatment groups, with low cross-validation errors in each phase (0.09, 0.02, and 0, respectively) (Fig. 5A). The differentiating signature varied in each of these phases. One common feature of all three was a comparative increase in retinoic acid (RA) in the $\alpha_4\beta_7$ mAb-treatment group (Fig. 5B). The signature in phase III, when both groups were aviremic, included increases in interleukin-21 (IL-21), granulocyte-macrophage colony-stimulating factor, soluble CD14 (sCD14), interferon- α (IFN- α), as well as RA; however, IFN- γ and transforming growth factor- β (TGF- β) were reduced. In phases IV and V, $\alpha_4\beta_7$ mAb treatment was associated with increased IL-10 and RA, with comparative decreases of proinflammatory markers, including IL-1 β , IFN- γ -induced protein (IP-10), complement-reactive protein (CRP), the coagulation biomarker D-dimer, and two markers, sCD163 and intestinal

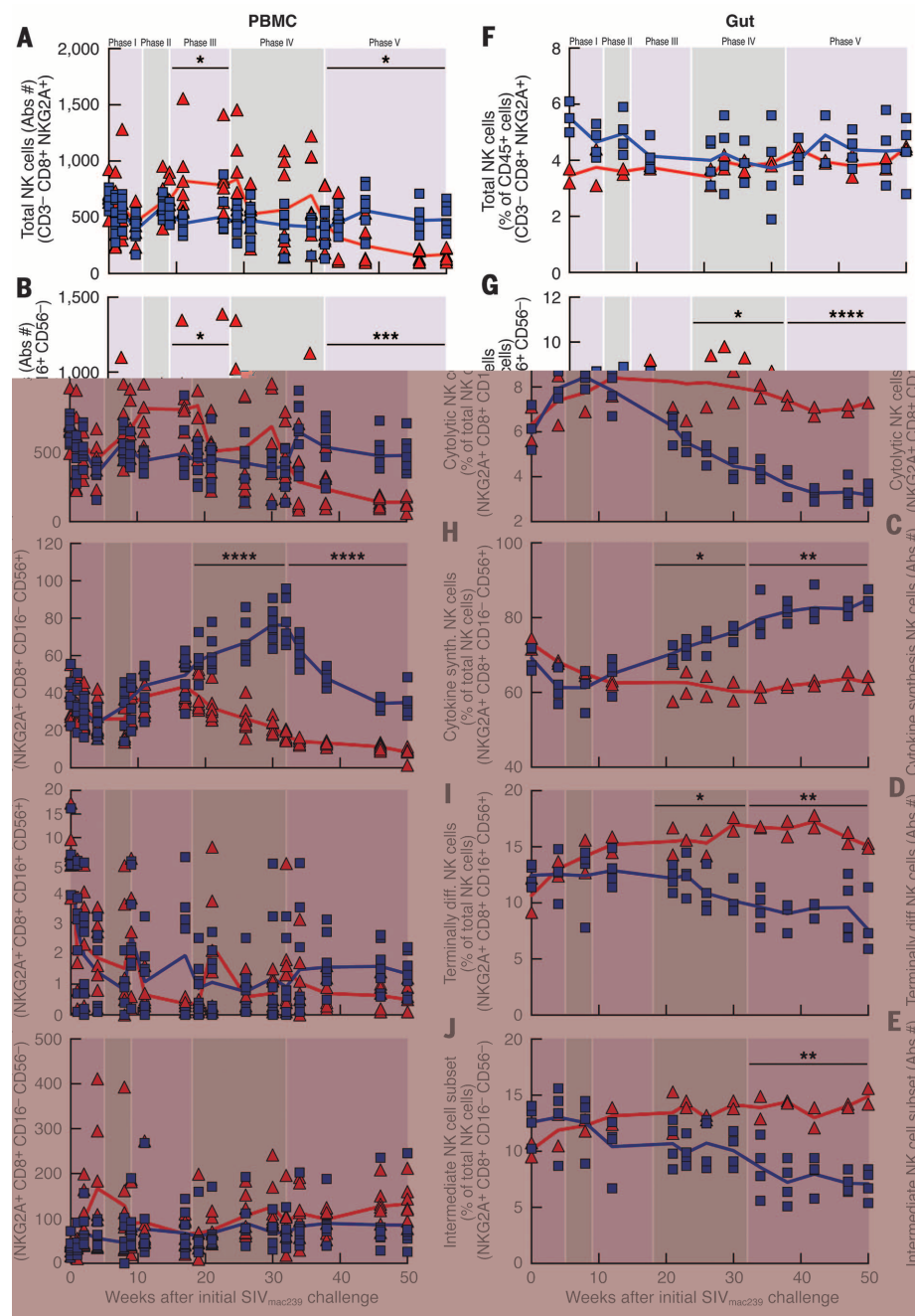


Fig. 4. Kinetic changes in the frequencies of NK cell subsets. The absolute numbers of circulating (A) total NK cells in PBMCs, (B) cytolytic NK cells, (C) cytokine-synthesizing NK cells, (D) terminally differentiated NK cells, and (E) intermediate NK cells. Monkeys treated with ART + $\alpha_4\beta_7$ mAb (blue) and the ART + rhesus IgG (red). Frequencies in GITs of (F) total NK cells as a percentage of CD45⁺ cells, (G) cytolytic NK cells, (H) cytokine synthesizing NK cells, (I) terminally differentiated NK cells, and (J) intermediate NK cells. The frequencies of NK cell subsets in GITs were calculated as the percentage of total NK cells in the same sample. *P* values were determined using the multiple *t* test (**P* < 0.05; ***P* < 0.01; ****P* < 0.001; *****P* < 0.0001).

fatty acid-binding protein (I-FABP), associated with gut permeability (Fig. 5A and fig. S13).

ART + $\alpha_4\beta_7$ mAb restores plasma retinoic acid levels

RA induces the expression of $\alpha_4\beta_7$ (23, 24) and also plays an essential role in gut homeostasis

(23, 25–27). Baseline RA levels decreased during acute infection in both groups (Fig. 5B). A similar response was observed in two uninfected monkeys afflicted with chronic diarrhea (fig. S14), suggesting that such declines are linked to gut inflammation. Of note, measurements taken on weeks 15, 17, and 19 (phase III) differentiated

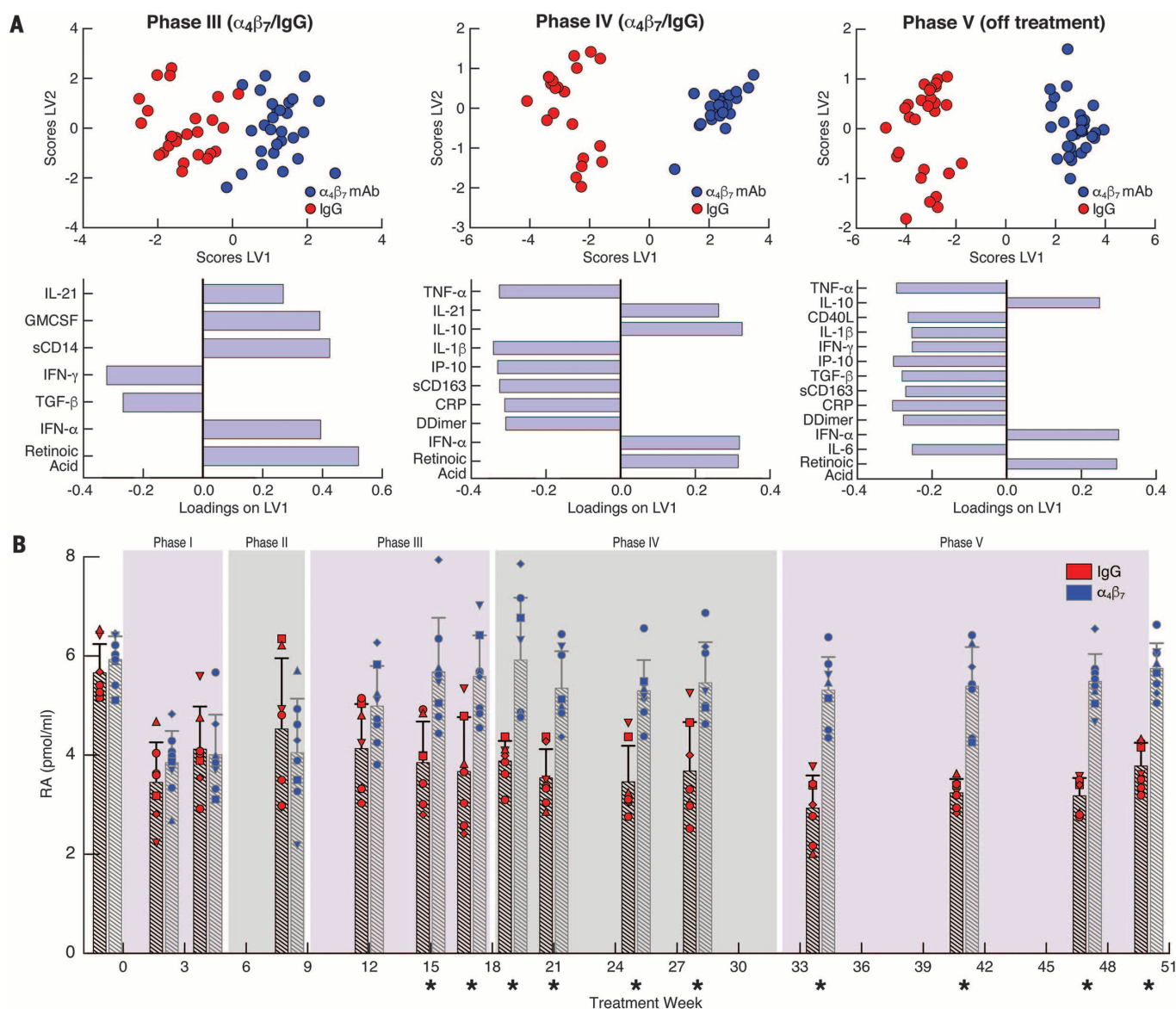


Fig. 5. Multivariate cytokine signatures and plasma levels of retinoic acid. (A) Separate PLSDA models for phases III (left), IV (middle), and V (right). Score plots of latent variable 1 (LV1) versus LV2 (top). Monkeys treated with $\alpha_4\beta_7$ mAb (blue) and IgG (red). Corresponding loadings plots (bottom) with the multivariate cytokine signatures for each phase. (B) Plasma levels (means \pm SD) of RA are displayed (pmol/ml) in the individual monkeys treated with $\alpha_4\beta_7$ mAb (blue) and IgG (red) through all five phases of the study (denotes unpaired *t* test, $*P < 0.003$).

the two groups, such that RA in the $\alpha_4\beta_7$ treatment group recovered to near-baseline levels. To understand whether these changes reflected the administration of $\alpha_4\beta_7$ mAb, independent of SIV infection, we treated two uninfected animals with $\alpha_4\beta_7$ mAb and observed no effect on serum RA (fig. S15). Indeed, we also observed a similar response in I-FABP levels in phase III (fig. S13). Finally, we carried out an exploratory analysis to identify additional biomarkers in phase III that might correlate with the degree of gut proviral DNA rebound in phase IV. Both positive and negative predictors of the magnitude of viral rebound in gut tissues were identified (fig. S16).

Induction of gp120 V2-specific antibody responses

Plasma and peripheral blood mononuclear cell (PBMC) samples were also screened for SIV-specific antibody responses and antibody-dependent cell-mediated cytotoxicity (ADCC). We found neither neutralizing antibodies nor differences in ADCC titers (fig. S17). In human and macaque vaccine trials, nonneutralizing antibodies directed against the second variable loop (V2) in Env glycoprotein 120 (gp120) correlated with reduced risk of acquisition (28, 29). We therefore characterized the specificity of the antibody responses by performing Pepscan enzyme-linked immunosorbent assay (ELISA) of sera from five animals in each

group against linear peptides spanning the entire gp120 subunit (fig. S18). Serum samples from weeks 30 to 36 showed that five out of five $\alpha_4\beta_7$ mAb-treated macaques reacted, to varying levels, with two overlapping V2 peptides (peptides 26 and 27). None of the IgG-treated controls reacted to both of these peptides (two animals reacted to one peptide). We found no other consistent difference in epitope-specific reactivity between the two groups. We then evaluated antibody responses using a more sensitive surface plasmon resonance (SPR) assay. Sera from all 15 animals through the five treatment phases were reacted with both SIV gp120 and an SIV cyclic V2 peptide. Sera from both treatment

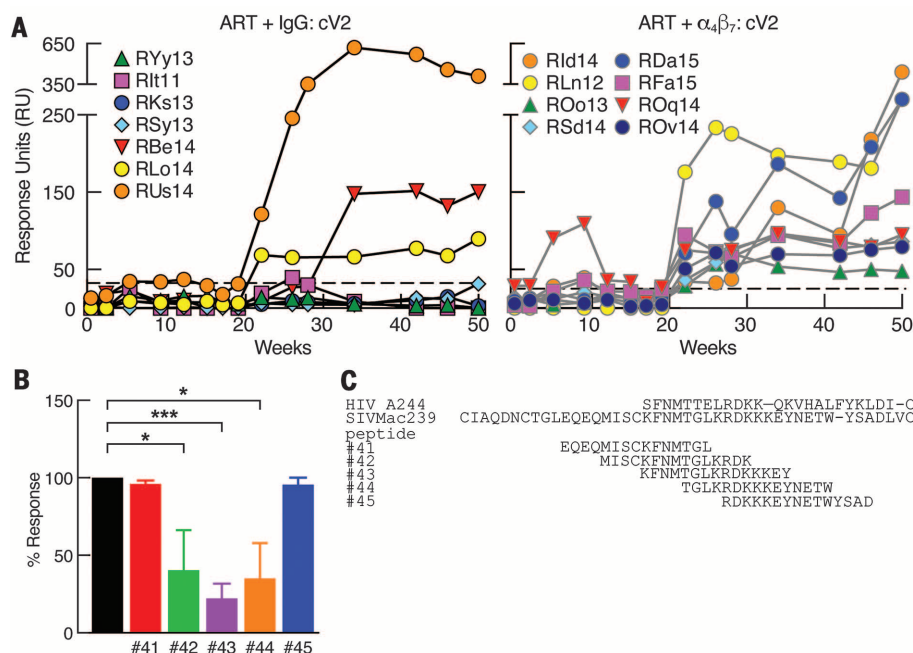


Fig. 6. Characterization of the anti-SIV gp120 V2 antibody response. (A) Reactivity (response units, RU) of sera from individual animals in the groups treated with ART + IgG (top left) and ART + $\alpha_4\beta_7$ mAb (top right) against a cyclic V2 peptide (cV2). The dashed line represents the cut-off value for positive reactivity. (B) Serum reactivity (percent response, means \pm SD) against cV2 of four ART + $\alpha_4\beta_7$ mAb-treated animals in the presence of overlapping V2 peptides (41 to 45), or in the absence of any competing peptide (black bar), defined as 100% response. Asterisk (*) represents the level of significance (* P < 0.05; *** P < 0.001, paired t test for each condition, compared with the no-peptide control). (C) Alignment of the SIV V2 overlapping peptides 41 to 45 with the V2 region of SIVmac239 and the corresponding region of HIV A244 gp120. Single-letter abbreviations for the amino acid residues are as follows: A, Ala; C, Cys; D, Asp; E, Glu; F, Phe; G, Gly; H, His; I, Ile; K, Lys; L, Leu; M, Met; N, Asn; P, Pro; Q, Gln; R, Arg; S, Ser; T, Thr; V, Val; W, Trp; and Y, Tyr. * P < 0.001.

groups showed similar reactivity to gp120 (mean values) (fig. S19). However, the two treatment groups differed in their reactivity to V2. Whereas eight out of eight $\alpha_4\beta_7$ mAb-treated animals showed persistent reactivity to V2, only three out of seven IgG-treated animals reacted to V2 (Fig. 6A). We then fine-mapped this reactivity by competing serum reactivity from all eight animals with overlapping 15mer peptides spanning V2 (Fig. 6B). A peptide corresponding to the sequence KFNMTGLKRDKKKEY (see Fig. 6 legend) reduced serum reactivity by ~80%. Alignment of this sequence with an HIV Thai clade A/E V2 sequence indicates that it recognizes the same region identified in a sieving analysis for immune correlates of reduced risk in the RV144 vaccine trial (Fig. 6C) (30). These data indicate that $\alpha_4\beta_7$ mAb treatment promotes V2 antibody responses by an undefined mechanism.

Discussion

Combining ART with $\alpha_4\beta_7$ mAb promoted prolonged virologic control (Fig. 1 and fig. S3) and the restoration of CD4⁺ T cells. Control persisted long after $\alpha_4\beta_7$ mAb treatment was terminated. It was not associated with neutralizing antibody or classical cell-mediated immune responses (figs. S20 to S24) but instead with reduced damage to GITs. The precise mechanism(s) by which ART +

$\alpha_4\beta_7$ mAb therapy promoted virologic control remains to be defined. However, we identified a series of correlates that individually or in combination may have contributed to that control. These include the recovery of T_H17 and T_H22 subsets of CD4⁺ T cells, significant increases in cytokine-synthesizing NK cells and NKp44⁺ ILCs, skewing of the antibody response toward the gp120 V2 domain, distinguishing plasma biomarkers in phase III followed by signatures associated with reduced gut damage and inflammation in phases IV and V, and the recovery of RA levels. RA is a key regulator of gut immune responses (31, 32) but it also inhibits fibrosis (33).

Vedolizumab, the humanized analog of $\alpha_4\beta_7$ mAb is believed to reduce trafficking of $\alpha_4\beta_7$ -expressing CD4⁺ T cells to GITs. This is the basis for its use in the treatment of inflammatory bowel disease (IBD) (34). Yet, paradoxically, in this study $\alpha_4\beta_7$ mAb promoted the repopulation of GITs with CD4⁺ T cells. Future studies are needed to address the phenotype and functionality of these cells. Such information may help us better understand both the virologic control we are observing and the mechanism of action of drugs like vedolizumab. Vedolizumab belongs to a class of therapeutic agents that are currently in various stages of development for the treatment of IBD (34, 35). It may be possible

to use these drugs as adjunctive agents in the treatment of HIV infection.

REFERENCES AND NOTES

1. J. Saison, L. Cotte, C. Chidiac, T. Ferry, *BMJ Case Rep.* **2012** (mar08 1), bcr1020114905 (2012).
2. A. H. Warriner, G. A. Burkholder, E. T. Overton, *Infect. Dis. Clin. North Am.* **28**, 457–476 (2014).
3. L. Barrett, K. R. Fowke, M. D. Grant, *AIDS Rev.* **14**, 159–167 (2012).
4. R. S. Veazey et al., *Science* **280**, 427–431 (1998).
5. J. Ananworanich, K. Dubé, N. Chomont, *Curr. Opin. HIV AIDS* **10**, 18–28 (2015).
6. M. Briskin et al., *Am. J. Pathol.* **151**, 97–110 (1997).
7. D. J. Erle et al., *J. Immunol.* **153**, 517–528 (1994).
8. M. Kader et al., *Mucosal Immunol.* **2**, 439–449 (2009).
9. X. Wang et al., *Mucosal Immunol.* **2**, 518–526 (2009).
10. C. Cicala et al., *Proc. Natl. Acad. Sci. U.S.A.* **106**, 20877–20882 (2009).
11. X. Lu et al., *Cell. Mol. Immunol.* **10**, 1038/cmi.2015.60 (2015).
12. E. Martinelli et al., *J. Acquir. Immune Defic. Syndr.* **64**, 325–331 (2013).
13. S. N. Byrreddy et al., *Nat. Med.* **20**, 1397–1400 (2014).
14. M. Guadalupe et al., *J. Virol.* **77**, 11708–11717 (2003).
15. J. M. Brechley, D. C. Douek, *Mucosal Immunol.* **1**, 23–30 (2008).
16. Q. Li et al., *Nature* **434**, 1148–1152 (2005).
17. J. J. Mattapallil et al., *Nature* **434**, 1093–1097 (2005).
18. S. Mehandru et al., *J. Virol.* **81**, 599–612 (2007).
19. H. Xu, X. Wang, R. S. Veazey, *J. AIDS Clin. Res.* **5**, 302 (2014).
20. P. J. Santangelo et al., *Nat. Methods* **12**, 427–432 (2015).
21. H. N. Kløverpris et al., *Immunity* **44**, 391–405 (2016).
22. M. Vaccari et al., *Nat. Med.* **22**, 762–770 (2016).
23. M. Iwata et al., *Immunity* **21**, 527–538 (2004).
24. A. C. Ross, *Am. J. Clin. Nutr.* **96**, 1166S–1172S (2012).
25. W. Agace, *Immunol. Lett.* **128**, 21–23 (2010).
26. S. Sirisinha, *Asian Pac. J. Allergy Immunol.* **33**, 71–89 (2015).
27. R. Zeng et al., *Mucosal Immunol.* **6**, 847–856 (2013).
28. R. Gottardo et al., *PLOS ONE* **8**, e75665 (2013).
29. P. Pegu et al., *J. Virol.* **87**, 1708–1719 (2013).
30. M. Rolland et al., *Nature* **490**, 417–420 (2012).
31. Y. Guo, C. Brown, C. Ortiz, R. J. Noelle, *Physiol. Rev.* **95**, 125–148 (2015).
32. J. A. Hall, J. R. Grainger, S. P. Spencer, Y. Belkaid, *Immunity* **35**, 13–22 (2011).
33. R. Xiao et al., *J. Dermatol.* **38**, 345–353 (2011).
34. M. Jovani, S. Danese, *Curr. Drug Targets* **14**, 1433–1443 (2013).
35. Vedolizumab, FDA Advisory Committee Recommendations Approval of Vedolizumab (Drugs.com, 2013); www.drugs.com/nda/vedolizumab_131209.html.

ACKNOWLEDGMENTS

The authors are deeply grateful to the veterinary staff of the Yerkes National Primate Center, particularly S. Ehrent, C. Souder, and the staff of the Research Services. We thank K. Reimann for making the primatized mAbs for our studies. We also thank M. Rao and K. Peachman for the SIV reagents used for the antibody characterization studies, K. Rogers for FcRγ and TRIM5α sequencing, R. Gelezunias and D. Hazuda for providing the antiretroviral drugs, and A. Weddle and J. Weddle for preparation of all graphics. The data presented in this manuscript are tabulated in the main paper and in the supplementary materials. J.A., C.C., and A.S.F. are inventors on patent no. 20160075786 held by the National Institute of Allergy and Infectious Diseases (NIAID), NIH, that covers the use of antagonists of the interaction between HIV gp120 and $\alpha_4\beta_7$ integrin. The work performed herein was supported by NIAID-NIH R01 AI098628, R01 AI111907, R01 HD077260, U.S. Food and Drug Administration U01FD005266, the Intramural Program of the NIAID, NIH, Bethesda, MD, and the base grant to the Yerkes National Primate Research Center of Emory University NIH-ORIP-OD-510D-11132. Additional support was provided by the University of Maryland School of Pharmacy Mass Spectrometry Center (SOP1841-1QB2014). J.A., C.C., and A.S.F. are inventors in the patent and patent application 20160075786 submitted by the NIAID. The authors declare no competing financial interest.

SUPPLEMENTARY MATERIALS

www.sciencemag.org/content/354/6309/197/suppl/DC1
Materials and Methods
Supplementary Text
Figs. S1 to S24
Tables S1 to S3
References (36–51)

12 May 2016; accepted 9 September 2016
10.1126/science.aag1276

REPORTS

SOLAR CELLS

Improving efficiency and stability of perovskite solar cells with photocurable fluoropolymers

Federico Bella,^{1,*†} Gianmarco Griffini,^{2,*†} Juan-Pablo Correa-Baena,^{3†} Guido Saracco,⁴ Michael Grätzel,⁵ Anders Hagfeldt,^{3,*} Stefano Turri,² Claudio Gerbaldi¹

Organometal halide perovskite solar cells have demonstrated high conversion efficiency but poor long-term stability against ultraviolet irradiation and water. We show that rapid light-induced free-radical polymerization at ambient temperature produces multifunctional fluorinated photopolymer coatings that confer luminescent and easy-cleaning features on the front side of the devices, while concurrently forming a strongly hydrophobic barrier toward environmental moisture on the back contact side. The luminescent photopolymers re-emit ultraviolet light in the visible range, boosting perovskite solar cells efficiency to nearly 19% under standard illumination. Coated devices reproducibly retain their full functional performance during prolonged operation, even after a series of severe aging tests carried out for more than 6 months.

Photovoltaic devices made with organometal halide perovskites [perovskite solar cells (PSCs)] have achieved certified power conversion efficiencies (PCEs) as high as 22.1% (1–9). Reliable device operation will require achieving long-term stability (10–12), in which PSCs suffer from two types of stresses that severely limit their operation, namely degradation from atmospheric exposure and electrical stresses (polarization). The latter is represented by a hysteresis loop in current-voltage measurement under light and is caused by ionic motion in the perovskite material that can be overcome largely by using appropriate contacts (13) or modifying morphology (14). However, the stability of PSCs in humid environments, where photochemical and thermal stresses also are typically encountered, have presented an unsurmountable challenge to date (11, 12).

Several strategies to improve the stability of PSCs have been proposed. Device encapsulation, where hydrophobic polymer layers may substantially limit the permeation of atmospheric mois-

ture (15, 16), is not suitable for protecting the device against photochemical and thermal stresses during outdoor functioning. Replacement (or pro-

tection) of the organic components with metal oxides—e.g., a chromium oxide-chromium ($\text{Cr}_2\text{O}_3/\text{Cr}$) interlayer protecting the metal contacts from reactions with the perovskite material—has recently been proposed, as well as the fabrication of solar cells with all-solution-processed metal oxide charge transport layers (17–19). However, these strategies [and others, such as the perovskite crystal cross-linking with alkylphosphonic acid ω -ammonium chlorides (20) or the introduction of porous carbon layers (21, 22)] affect only the air stability of the solar cells. With regard to ultraviolet (UV)-light stability, cesium bromide has been recently proposed as an interfacial modifier between the electron collection layer and the perovskite absorber layer, but resistance to moisture or high temperatures remains to be demonstrated (23).

We propose the use of multifunctional photopolymers as a comprehensive promising solution to PSC instability. A luminescent downshifting (LDS) fluoropolymeric layer is rapidly photogenerated on the front side of the device (i.e., the glass side), as detailed in section 1 in the supplementary materials (24). The coating prevents the UV portion of the incident solar spectrum from negatively interacting with the PSC stack by converting it into visible light (Fig. 1A) and also increases the photocurrent by 6%. Devices can achieve PCEs approaching 19% without affecting the chemistry as well as the electronic properties of both the photoactive and the buffer layers.

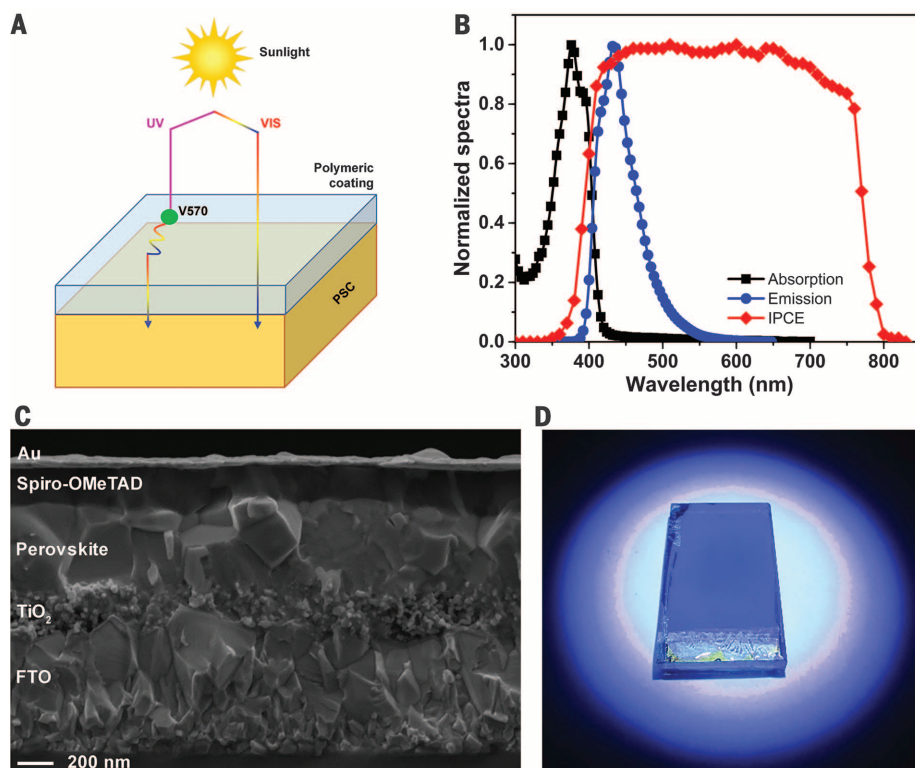


Fig. 1. LDS-PSC integrated system. (A) Scheme of the UV-coating operating principle. (B) Normalized absorption and emission spectra of V570-doped UV coating compared with the IPCE response of the PSC devices under study. (C) Cross-sectional field-emission scanning electron microscopy image of the PSC device before coating deposition. (D) Digital photograph of a PSC bearing the UV coating when exposed to UV light.

¹Group for Applied Materials and Electrochemistry (GAME Lab), CHENERGY Group, Department of Applied Science and Technology (DISAT), Politecnico di Torino, Corso Duca degli Abruzzi 24, 10129, Torino, Italy. ²Department of Chemistry, Materials and Chemical Engineering "Giulio Natta," Politecnico di Milano, Piazza Leonardo da Vinci 32, 20133, Milano, Italy.

³Laboratory of Photomolecular Science, Institute of Chemical Sciences and Engineering, Ecole Polytechnique Fédérale de Lausanne (EPFL), Chemin des Alambics, Station 3, 1015, Lausanne, Switzerland. ⁴Center for Sustainable Futures @PoliTO, Istituto Italiano di Tecnologia, Corso Trento 21, 10129, Torino, Italy. ⁵Laboratory of Photonics and Interfaces, Institut des Sciences et Ingénierie Chimiques, Ecole Polytechnique Fédérale de Lausanne (EPFL), Station 3, 1015, Lausanne, Switzerland.

*Corresponding author. Email: federico.bella@polito.it (F.B.); gianmarco.griffini@polimi.it (G.G.); anders.hagfeldt@epfl.ch (A.H.)

†These authors contributed equally to this work.

With regard to atmospheric humidity tolerance, a strongly hydrophobic photopolymer is grown on the back contact side. This additional layer behaves as an efficient barrier toward water permeation within the solar cell stack. The resulting devices demonstrated unrivaled stability in terms of PCEs during a 180-day (4320 hours) aging test carried out under different atmospheric conditions and in the presence of various photochemical external stresses. The same devices were also exposed to real outdoor conditions for more than 3 months (2160 hours), successfully demonstrating their exceptional tolerance to dust, soil, and heavy rain on the external glass surface. Finally, the low-surface-energy fluorinated LDS layer makes the front electrode easily cleanable in real outdoor conditions.

The precursor material used for the LDS coatings is based on a combination of a UV-curable chloro-trifluoro-ethylene vinyl ether fluoropolymer binder and a dimethacrylic perfluoropolyether oligomer. The materials react upon UV-light exposure to give a fully cross-linked coating (full characterization of the coating material is presented in sections 2 to 4 in the supplementary materials) (25). To impart the LDS functionality to this fluoropolymeric coating (referred to as UV coating hereafter), a luminescent species was added to the precursor formulation in different amounts. The fluorescent organic dye Lumogen F Violet 570 by BASF (referred to hereafter as V570; see inset of fig. S2D) was selected as a luminophore given its commercial availability and favorable optical properties (i.e., high absorption coefficient and fluorescence quantum yield) (26). In addition, this particular class of dyes is characterized by relatively good solubility in the polymer to avoid aggregation-induced quenching and easy processability in polymers (26).

The optical properties of the V570-doped fluoropolymeric coating are well matched with the spectral response of the PSC devices that we used (Fig. 1B). In particular, the absorption spectrum of the LDS material peaks in the short-wavelength region where the PSC device exhibits a minimum incident photon-to-current conversion efficiency (IPCE) [$\lambda_{\text{max}}(\text{abs}) = 377 \text{ nm}$]. As a result of the fluorescence process (Fig. 1D), the re-emitted photons are red-shifted to a region where the IPCE of the device is maximum.

We tested these films on devices composed of a typical stack of fluorine-doped tin oxide (FTO)/compact-TiO₂/mesoporous-TiO₂/mixed perovskite/spiro-OMeTAD/gold (Fig. 1C). The compact-TiO₂ and thin mesoporous-TiO₂ layers are used as the electron selective materials, whereas the perovskite capping layer absorbs most of the light and transports the charges. Spiro-OMeTAD is used as the hole selective layer. In this study, a Pb-based “mixed” perovskite containing a mix of cations and halides (formamidinium iodide:PbI₂:methylammonium bromide:PbBr₂ = 1.0:1.1:0.20:0.22) is used, as described in our recent publications (27, 28) and detailed in the experimental section. Thin films of liquid, light-curable reactive mixtures (precursors of the fluoropolymeric layer) with different amounts of V570 were spin-coated on the

front side of the devices. Then, the as-cast wet fluoropolymeric precursor was UV-irradiated for 30 s under a nitrogen atmosphere to cure a layer $\sim 5 \mu\text{m}$ in thickness.

The photovoltaic response of the resulting PSCs at increasing V570 concentration is shown in Table 1, where the efficiency-boosting effect of the LDS coatings on device performance can be noted for V570 loadings in the range of 1 to 2 weight % (wt %). The short-circuit photocurrent density (J_{sc}) increased from 19.20 to 20.31 mA cm^{-2} when 2 wt % of V570 was introduced in the fluorinated coating, thus leading to a 6% increase in J_{sc} (and also in PCE). At higher fluorophore loadings ($>2 \text{ wt } \%$), the photocurrent density started to decrease, likely because a greater amount of fluorescent species can reasonably increase the probability for an emitted photon to be reabsorbed by another adjacent fluorophore molecule within the polymeric layer, given the partial overlap between absorption and emission bands of V570 (Fig. 1B and fig. S1D). For V570 loadings exceeding 3 wt %, the J_{sc} values were further lowered.

To confirm the beneficial effects of the LDS coatings on the photocurrent generated upon illumination, IPCE curves were recorded (Fig. 2A). The luminescent species introduced in the

polymeric architecture effectively converted the near-UV region of the solar spectrum (Fig. 2B) into lower-energy photons of wavelengths well matching the absorption spectrum of the perovskite layer.

These PSCs have relatively moderate but highly reproducible efficiencies ($\sim 15.5\%$). We also investigated the LDS effect with more efficient devices (PCE $> 17\%$) by incorporating an optimized LDS coating (i.e., fluorophore concentration of 2 wt %). The increase in PCE from 17.31 to 18.67% resulted from a $\sim 5\%$ enhancement in photocurrent (J_{sc} increased from 21.96 to 23.23 mA cm^{-2}). Given the correlation between J_{sc} and V570 content (Table 1) and the broadening of the IPCE curve in the UV region (see Fig. 2B), we can exclude that such photocurrent enhancement is caused by a mere antireflective effect produced by the LDS layer (as also confirmed by the poorer performance observed on the undoped LDS system). Conversely, the downshifting phenomenon consistently explains the measured trends. The integration of the product of the AM1.5G photon flux with the IPCE spectrum (Fig. 3B) yielded predicted J_{sc} values equal to 21.09 and 22.13 mA cm^{-2} for the uncoated and coated devices, respectively; the mismatch with respect to the values inferred

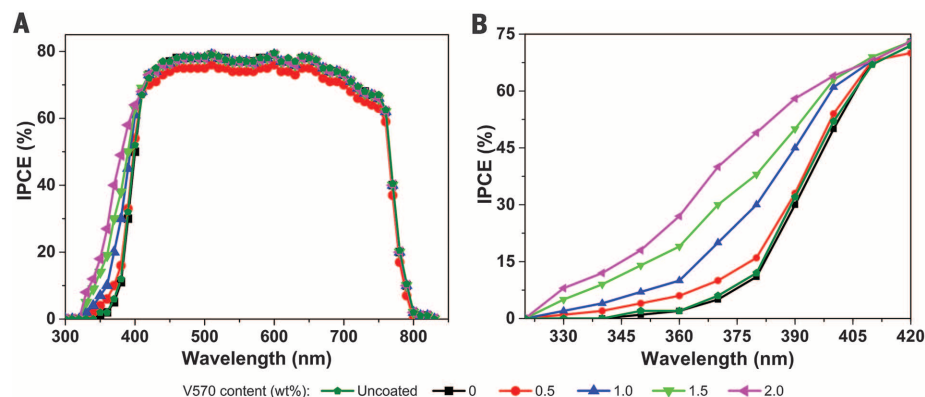


Fig. 2. IPCE curves for PSCs. (A) Cells were coated with the LDS fluoropolymeric layer loaded with different amounts (0 to 2 wt %) of V570. (B) Detail of IPCE curves for illumination below 420 nm. Mask area = 0.16 cm^2 .

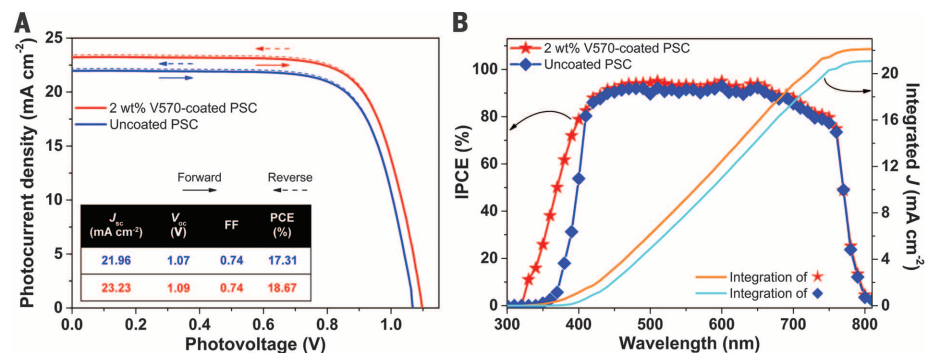


Fig. 3. Photovoltaic characterization of the best device. (A) J - V curves (1 Sun, AM1.5G, 5 mV s^{-1}) for a highly efficient PSC before and after coating with the optimized LDS fluoropolymeric layer (2 wt % V570). Dotted lines represent the reverse scan. (B) IPCE curves of the same PSCs. The integration of the product of the AM1.5G photon flux with the IPCE spectrum is also shown for coated and uncoated devices.

from the photocurrent density versus voltage (J - V) curves (Fig. 3A) was equal to $\approx 1 \text{ mA cm}^{-2}$, consistent with other recent reports in the PSC field (21, 29, 30). The excellent quality of the fabricated PSCs is reflected in the negligible hysteresis phenomenon observed in the J - V curves of our high-efficiency devices (Fig. 3A, dotted lines), consistent with recent reports (14).

We investigated whether these luminescent polymeric coatings (with 2 wt % loading) can enhance device stability on a long-term basis by carrying out three aging studies under markedly different conditions. In the first aging test, uncoated devices and front-coated ones (five solar cells for each condition) were studied for an overall period of 6 months. In the first 3 months, the devices were kept in an Ar-filled dry glove box and continuously irradiated (8 hours per

day) with a UV optical fiber having a 5 mW cm^{-2} intensity. This value simulates well the 5% contribution given by UV light (280 to 400 nm) to the overall solar spectral irradiance on Earth (1000 W m^{-2} , AM1.5G) based on the Standard Reference Solar Spectra (ASTM G-173-03). The uncoated devices (black curve) in this UV-induced aging test (Fig. 4A) lost 30% of their initial efficiency after 1 week of exposure and failed after 1 month; conversely, all five front-coated cells (red curve) demonstrated excellent stability under the same conditions, retaining 98% of their initial PCE after 3 months.

After this period, the solar cells were taken out of the Ar-filled glove box and placed inside a quartz chamber, where they were exposed to constant relative humidity (RH) (50%), and the aging test was allowed to proceed in the same UV irra-

diation conditions described above. Figure 4A shows that, immediately after the modification of the aging conditions, front-coated cells (red curve) showed a sharp decrease in efficiency, resulting in an 82% decrease of their initial efficiency at the end of the second quarter of the aging test. Such a rapid decay was attributed to the amount of moisture present in the aging chamber that progressively infiltrated the PSC stack from the back contact side, thus causing the gradual hydrolysis of the perovskite layer. The effects of degradation were easily detectable by simple visual inspection, as a progressive yellowing of the mixed-perovskite layer upon 50% RH exposure was observed (see inset of Fig. 4A).

With the aim of stabilizing our devices in terms of photochemical resistance, as well as moisture tolerance, a fluoropolymeric light-curable coating was deposited also on the back contact side (front/back-coated device configuration). The same formulation used in the LDS experiment was used for back-coating the PSC devices, except that no luminescent dye was used. The use of such fluoropolymeric layer on top of the PSC stack is expected to efficiently combat water permeation through the top back contact toward the perovskite layer as a result of the highly hydrophobic character of the coating (see section 3 in the supplementary materials) (25). In addition, the cross-linked nature of the fluoropolymeric UV coating entails a lower free volume than typical non-cross-linked polymeric systems and should therefore enhance the long-term durability of PSCs (31, 32).

Figure 4A shows the aging test performed onto front/back-coated PSCs (blue curve), i.e., devices bearing the luminescent coating on the front side and the moisture-resistant one on the back contact side. All of the five devices maintained an excellent stability (98%) in the aging conditions resulting from the combined effects

Table 1. Photovoltaic parameters of PSCs coated with the fluoropolymeric layer laden with different amounts (0 to 3 wt %) of V570. Average values for uncoated devices are also shown for comparison purposes. Each experimental condition was reproduced five times on different devices; solar cells were tested under 1 Sun, AM1.5G, at a scan rate of 5 mV s^{-1} and with a mask area of 0.16 cm^2 . In addition to the J_{sc} trend described in the text, a slight variation of V_{oc} (open-circuit voltage) values can also be appreciated, scaling logarithmically with J_{sc} in accordance with the photodiode equation—i.e., $V_{oc} = kTq^{-1} \ln(J_{sc}J_0^{-1} + 1)$. FF, fill factor.

V570 (wt %)	J_{sc} (mA cm^{-2})	V_{oc} (V)	FF	PCE (%)	Δ PCE (%)
Uncoated	19.20 ± 0.05	1.120 ± 0.003	0.72 ± 0.01	15.48	0
0	18.14 ± 0.05	1.108 ± 0.003	0.72 ± 0.01	14.47	-6.52
0.5	18.52 ± 0.04	1.111 ± 0.002	0.73 ± 0.01	15.02	-3.54
1	19.37 ± 0.06	1.123 ± 0.003	0.72 ± 0.01	15.66	+0.89
1.5	19.90 ± 0.05	1.133 ± 0.003	0.72 ± 0.01	16.23	+3.65
2	20.31 ± 0.04	1.142 ± 0.002	0.73 ± 0.01	16.93	+5.78
2.5	20.20 ± 0.06	1.137 ± 0.003	0.72 ± 0.01	16.54	+5.21
3	20.11 ± 0.08	1.134 ± 0.004	0.73 ± 0.01	16.65	+4.74

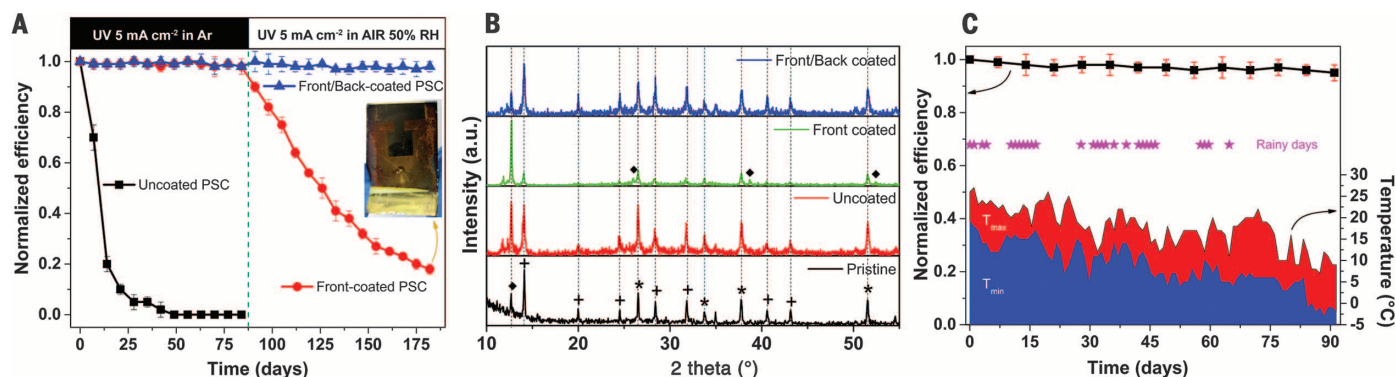


Fig. 4. Aging of LDS-PSC integrated system. (A) Results of the aging test on the three series of PSCs: uncoated, front-coated (i.e., luminescent fluorinated coating on the front side), and front/back-coated (i.e., front side coated with the luminescent fluorophore and back contact coated with the moisture-resistant fluoropolymeric layer). During the first 3 months, PSCs were kept under Ar atmosphere and in the next 3 months under air at 50% RH, in both cases under continuous UV irradiation. PCE was measured once a week. A digital photograph of a front-coated solar cell at the end of the test is also shown. Further details are given in fig. S1A and section 5 in the supplementary

materials. (B) XRD patterns of both uncoated and (front and front/back) coated PSC devices after the 6 months aging test. For comparison purposes, the XRD pattern of the pristine uncoated PSC system is also shown. Asterisks, crosses, and diamonds denote the main signals ascribed to FTO, perovskite, and PbI_2 , respectively. (C) Results of the aging test on front/back-coated devices left for three months on the terrace of the Politecnico di Torino building in Turin (Italy), thus experiencing real outdoor operating conditions. PCE was measured once a week. Further details are given in fig. S1B and section 7 in the supplementary materials.

of photochemical and environmental stresses. X-ray diffraction (XRD) (Fig. 4B) analysis showed that performance degradation corresponded to the decomposition of the crystalline perovskite material into PbI_2 , which was not observed for the fully coated devices (see section 6 in the supplementary materials).

Given the stabilizing effect of the fluoropolymeric coating applied on both sides of the cells, a second aging test was designed to verify the stability of the front/back-coated PSCs under real outdoor atmospheric conditions, where temperature variations, precipitation phenomena, and pollution are typically encountered. A batch of five cells was exposed on the terrace of the Politecnico di Torino building in Turin ($45^\circ 06' \text{N}$, $7^\circ 66' \text{E}$), located in northwest Italy, in a humid subtropical climate zone from October to December 2015. The PSCs were subjected to highly variable climatic conditions, as outdoor temperatures ranged from -3° to $+27^\circ \text{C}$, and 27 out of 92 days were characterized by heavy rain and storms (33), as shown in Fig. 4C. The front/back-coated PSCs exhibited long-term stability retaining 95% of their initial efficiency after this test by (i) protecting the perovskite from UV radiation, converting it into exploitable visible photons; (ii) acting as a moisture barrier, thus preventing hydrolytic phenomena of the perovskite material; and (iii) keeping the front electrode clean by means of the easy-cleaning characteristics of this fluorinated polymer. Similar results were found for outdoor tests performed during Summer 2016, and the data collected are available in section 7 in the supplementary materials.

To demonstrate the water resistance of the photopolymerized fluorinated coatings, we kept five solar cells for 1 month in a closed chamber in the presence of a beaker containing boiling water (95% RH, fig. SIC), and the photovoltaic response was evaluated once a week. After 1 month, four of the five cells withstood the strong aging conditions and remarkably retained $96 \pm 2\%$ of their initial PCE. Only one device lost 95% of its initial efficiency after the first week. After inspection, we found a small area on the back side of the solar cell not thoroughly coated by the fluoropolymeric layer. The nonhomogeneous deposition of the coating caused a gradual hydrolysis of the underlying perovskite layer. We also dipped the front/back-coated devices into water. After 1 day of immersion, no changes in their photovoltaic performance were observed.

REFERENCES AND NOTES

- H. S. Kim *et al.*, *Sci. Rep.* **2**, 591 (2012).
- M. M. Lee, J. Teuscher, T. Miyasaka, T. N. Murakami, H. J. Snaith, *Science* **338**, 643–647 (2012).
- H. Zhou *et al.*, *Science* **345**, 542–546 (2014).
- M. Liu, M. B. Johnston, H. J. Snaith, *Nature* **501**, 395–398 (2013).
- J. Burschka *et al.*, *Nature* **499**, 316–319 (2013).
- National Center for Photovoltaics (NCPV) at the National Renewable Energy Laboratory (NREL); <http://www.nrel.gov/ncpv> (accessed July 2016).
- N. G. Park, *Mater. Today* **18**, 65–72 (2015).
- J. Seo, J. H. Noh, S. I. Seok, *Acc. Chem. Res.* **49**, 562–572 (2016).
- H. S. Jung, N. G. Park, *Small* **11**, 10–25 (2015).
- T. A. Berhe *et al.*, *Energy Environ. Sci.* **9**, 323–356 (2016).
- Y. Rong, L. Liu, A. Mei, X. Li, H. Han, *Adv. Energy Mater.* **5**, 1501066 (2015).
- T. Leijtens *et al.*, *Adv. Energy Mater.* **5**, 1500963 (2015).
- J. P. Correa Baena *et al.*, *Energy Environ. Sci.* **8**, 2928–2934 (2015).
- J. P. Correa-Baena *et al.*, *Adv. Mater.* **28**, 5031–5037 (2016).
- H. C. Weerasinghe, Y. Dkhissi, A. D. Scully, R. A. Caruso, Y. B. Cheng, *Nano Energy* **18**, 118–125 (2015).
- I. Hwang, I. Jeong, J. Lee, M. J. Ko, K. Yong, *ACS Appl. Mater. Interfaces* **7**, 17330–17336 (2015).
- M. Kaltenbrunner *et al.*, *Nat. Mater.* **14**, 1032–1039 (2015).
- J. You *et al.*, *Nat. Nanotechnol.* **11**, 75–81 (2016).
- K. Domanski *et al.*, *ACS Nano* **10**, 6306–6314 (2016).
- X. Li *et al.*, *Nat. Chem.* **7**, 703–711 (2015).
- A. Mei *et al.*, *Science* **345**, 295–298 (2014).
- L. Zhang *et al.*, *J. Mater. Chem. A* **3**, 9165–9170 (2015).
- W. Li *et al.*, *Energy Environ. Sci.* **9**, 490–498 (2016).
- Materials and methods are available as supplementary materials on Science Online.
- F. Bella *et al.*, *Adv. Funct. Mater.* **26**, 1127–1137 (2016).
- L. R. Wilson, B. S. Richards, *Appl. Opt.* **48**, 212–220 (2009).
- D. Bi *et al.*, *Sci. Adv.* **2**, e1501170 (2016).
- F. Giordano *et al.*, *Nat. Commun.* **7**, 10379 (2016).
- D. Liu, T. L. Kelly, *Nat. Photonics* **8**, 133–138 (2014).
- J.-H. Im, I.-H. Jang, N. Pellet, M. Grätzel, N.-G. Park, *Nat. Nanotechnol.* **9**, 927–932 (2014).
- G. Griffini, M. Levi, S. Turri, *Sol. Energy Mater. Sol. Cells* **118**, 36–42 (2013).
- G. Griffini, M. Levi, S. Turri, *Prog. Org. Coat.* **77**, 528–536 (2014).
- II Meteo; <http://www.ilmeteo.it/meteo/Torino> (accessed September 2016).

ACKNOWLEDGMENTS

Authors from EPFL thank the Swiss National Science Foundation, the NRP 70 “Energy Turnaround,” the 9th call proposal 906 (CONNECT PV), SNF-NanoTera, and the Swiss Federal Office of Energy (SYNERGY) for financial support. All data used in this study are included in the main text and in the supplementary materials.

SUPPLEMENTARY MATERIALS

www.sciencemag.org/content/354/6309/203/suppl/DC1
Materials and Methods
Supplementary Text Sections 1 to 7
Figs. S1 to S8
References (34–40)

21 June 2016; accepted 20 September 2016
Published online 29 September 2016
10.1126/science.aah4046

SOLAR CELLS

Incorporation of rubidium cations into perovskite solar cells improves photovoltaic performance

Michael Saliba,^{1,*†} Taisuke Matsui,^{1,2†} Konrad Domanski,^{1†} Ji-Youn Seo,¹ Amita Ummadisingu,¹ Shaik M. Zakeeruddin,¹ Juan-Pablo Correa-Baena,³ Wolfgang R. Tress,¹ Antonio Abate,¹ Anders Hagfeldt,³ Michael Grätzel^{1,*}

All of the cations currently used in perovskite solar cells abide by the tolerance factor for incorporation into the lattice. We show that the small and oxidation-stable rubidium cation (Rb^+) can be embedded into a “cation cascade” to create perovskite materials with excellent material properties. We achieved stabilized efficiencies of up to 21.6% (average value, 20.2%) on small areas (and a stabilized 19.0% on a cell 0.5 square centimeters in area) as well as an electroluminescence of 3.8%. The open-circuit voltage of 1.24 volts at a band gap of 1.63 electron volts leads to a loss in potential of 0.39 volts, versus 0.4 volts for commercial silicon cells. Polymer-coated cells maintained 95% of their initial performance at 85°C for 500 hours under full illumination and maximum power point tracking.

Low-cost perovskite solar cells (PSCs) have achieved certified power conversion efficiencies (PCEs) of 22.1% (1). The organic-inorganic perovskites used for photovoltaics (PV) have an AMX_3 formula that comprises a monovalent cation, A [cesium Cs^+ , methylammonium (MA) CH_3NH_3^+ , or formamidinium (FA) $\text{CH}_3(\text{NH}_2)_2^+$; a divalent metal, M (Pb^{2+} or Sn^{2+});

and an anion, X (Cl^- , Br^- , or I^-). The highest-efficiency perovskites are Pb-based with mixed MA/FA cations and Br/I halides (2–4). Recently, Cs was used to explore more complex cation combinations: Cs/MA, Cs/FA, and Cs/MA/FA (5–9). These perovskite formulations exhibit unexpected properties. For example, Cs/FA mixtures suppress halide segregation, enabling band gaps for perovskite/silicon tandems (10). The Cs/MA/FA-based solar cells are more reproducible and thermally stable than MA/FA mixtures (9).

In general, increasing the perovskite complexity is motivated by the need to improve stability by adding more inorganic elements and increasing the entropy of mixing, which can stabilize ordinarily unstable materials (such as the “yellow,” non-photoactive phase of FAPbI_3 that can be avoided by using small amounts of the otherwise unstable

¹Laboratory of Photonics and Interfaces, École Polytechnique Fédérale de Lausanne, Station 6, CH-1015 Lausanne, Switzerland. ²Advanced Research Division, Materials Research Laboratory, Panasonic Corporation, 1006 Kadoma, Kadoma City, Osaka 571-8501, Japan. ³Laboratory of Photomolecular Science, École Polytechnique Fédérale de Lausanne, Station 6, CH-1015 Lausanne, Switzerland.

*Corresponding author. Email: michael.saliba@epfl.ch (M.S.); michael.gratzel@epfl.ch (M.G.) †These authors contributed equally to this work.

of photochemical and environmental stresses. X-ray diffraction (XRD) (Fig. 4B) analysis showed that performance degradation corresponded to the decomposition of the crystalline perovskite material into PbI_2 , which was not observed for the fully coated devices (see section 6 in the supplementary materials).

Given the stabilizing effect of the fluoropolymeric coating applied on both sides of the cells, a second aging test was designed to verify the stability of the front/back-coated PSCs under real outdoor atmospheric conditions, where temperature variations, precipitation phenomena, and pollution are typically encountered. A batch of five cells was exposed on the terrace of the Politecnico di Torino building in Turin ($45^\circ 06' \text{N}$, $7^\circ 66' \text{E}$), located in northwest Italy, in a humid subtropical climate zone from October to December 2015. The PSCs were subjected to highly variable climatic conditions, as outdoor temperatures ranged from -3° to $+27^\circ \text{C}$, and 27 out of 92 days were characterized by heavy rain and storms (33), as shown in Fig. 4C. The front/back-coated PSCs exhibited long-term stability retaining 95% of their initial efficiency after this test by (i) protecting the perovskite from UV radiation, converting it into exploitable visible photons; (ii) acting as a moisture barrier, thus preventing hydrolytic phenomena of the perovskite material; and (iii) keeping the front electrode clean by means of the easy-cleaning characteristics of this fluorinated polymer. Similar results were found for outdoor tests performed during Summer 2016, and the data collected are available in section 7 in the supplementary materials.

To demonstrate the water resistance of the photopolymerized fluorinated coatings, we kept five solar cells for 1 month in a closed chamber in the presence of a beaker containing boiling water (95% RH, fig. SIC), and the photovoltaic response was evaluated once a week. After 1 month, four of the five cells withstood the strong aging conditions and remarkably retained $96 \pm 2\%$ of their initial PCE. Only one device lost 95% of its initial efficiency after the first week. After inspection, we found a small area on the back side of the solar cell not thoroughly coated by the fluoropolymeric layer. The nonhomogeneous deposition of the coating caused a gradual hydrolysis of the underlying perovskite layer. We also dipped the front/back-coated devices into water. After 1 day of immersion, no changes in their photovoltaic performance were observed.

REFERENCES AND NOTES

- H. S. Kim et al., *Sci. Rep.* **2**, 591 (2012).
- M. M. Lee, J. Teuscher, T. Miyasaka, T. N. Murakami, H. J. Snaith, *Science* **338**, 643–647 (2012).
- H. Zhou et al., *Science* **345**, 542–546 (2014).
- M. Liu, M. B. Johnston, H. J. Snaith, *Nature* **501**, 395–398 (2013).
- J. Burschka et al., *Nature* **499**, 316–319 (2013).
- National Center for Photovoltaics (NCPV) at the National Renewable Energy Laboratory (NREL); <http://www.nrel.gov/ncpv> (accessed July 2016).
- N. G. Park, *Mater. Today* **18**, 65–72 (2015).
- J. Seo, J. H. Noh, S. I. Seok, *Acc. Chem. Res.* **49**, 562–572 (2016).
- H. S. Jung, N. G. Park, *Small* **11**, 10–25 (2015).
- T. A. Berhe et al., *Energy Environ. Sci.* **9**, 323–356 (2016).
- Y. Rong, L. Liu, A. Mei, X. Li, H. Han, *Adv. Energy Mater.* **5**, 1501066 (2015).
- T. Leijtens et al., *Adv. Energy Mater.* **5**, 1500963 (2015).
- J. P. Correa Baena et al., *Energy Environ. Sci.* **8**, 2928–2934 (2015).
- J. P. Correa-Baena et al., *Adv. Mater.* **28**, 5031–5037 (2016).
- H. C. Weerasinghe, Y. Dkhissi, A. D. Scully, R. A. Caruso, Y. B. Cheng, *Nano Energy* **18**, 118–125 (2015).
- I. Hwang, I. Jeong, J. Lee, M. J. Ko, K. Yong, *ACS Appl. Mater. Interfaces* **7**, 17330–17336 (2015).
- M. Kaltenbrunner et al., *Nat. Mater.* **14**, 1032–1039 (2015).
- J. You et al., *Nat. Nanotechnol.* **11**, 75–81 (2016).
- K. Domanski et al., *ACS Nano* **10**, 6306–6314 (2016).
- X. Li et al., *Nat. Chem.* **7**, 703–711 (2015).
- A. Mei et al., *Science* **345**, 295–298 (2014).
- L. Zhang et al., *J. Mater. Chem. A* **3**, 9165–9170 (2015).
- W. Li et al., *Energy Environ. Sci.* **9**, 490–498 (2016).
- Materials and methods are available as supplementary materials on Science Online.
- F. Bella et al., *Adv. Funct. Mater.* **26**, 1127–1137 (2016).
- L. R. Wilson, B. S. Richards, *Appl. Opt.* **48**, 212–220 (2009).
- D. Bi et al., *Sci. Adv.* **2**, e1501170 (2016).
- F. Giordano et al., *Nat. Commun.* **7**, 10379 (2016).
- D. Liu, T. L. Kelly, *Nat. Photonics* **8**, 133–138 (2014).
- J.-H. Im, I.-H. Jang, N. Pellet, M. Grätzel, N.-G. Park, *Nat. Nanotechnol.* **9**, 927–932 (2014).
- G. Griffini, M. Levi, S. Turri, *Sol. Energy Mater. Sol. Cells* **118**, 36–42 (2013).
- G. Griffini, M. Levi, S. Turri, *Prog. Org. Coat.* **77**, 528–536 (2014).
- II Meteo; <http://www.ilmeteo.it/meteo/Torino> (accessed September 2016).

ACKNOWLEDGMENTS

Authors from EPFL thank the Swiss National Science Foundation, the NRP 70 “Energy Turnaround,” the 9th call proposal 906 (CONNECT PV), SNF-NanoTera, and the Swiss Federal Office of Energy (SYNERGY) for financial support. All data used in this study are included in the main text and in the supplementary materials.

SUPPLEMENTARY MATERIALS

www.sciencemag.org/content/354/6309/203/suppl/DC1
Materials and Methods
Supplementary Text Sections 1 to 7
Figs. S1 to S8
References (34–40)

21 June 2016; accepted 20 September 2016
Published online 29 September 2016
10.1126/science.aah4046

SOLAR CELLS

Incorporation of rubidium cations into perovskite solar cells improves photovoltaic performance

Michael Saliba,^{1,*†} Taisuke Matsui,^{1,2†} Konrad Domanski,^{1†} Ji-Youn Seo,¹ Amita Ummadisingu,¹ Shaik M. Zakeeruddin,¹ Juan-Pablo Correa-Baena,³ Wolfgang R. Tress,¹ Antonio Abate,¹ Anders Hagfeldt,³ Michael Grätzel^{1,*}

All of the cations currently used in perovskite solar cells abide by the tolerance factor for incorporation into the lattice. We show that the small and oxidation-stable rubidium cation (Rb^+) can be embedded into a “cation cascade” to create perovskite materials with excellent material properties. We achieved stabilized efficiencies of up to 21.6% (average value, 20.2%) on small areas (and a stabilized 19.0% on a cell 0.5 square centimeters in area) as well as an electroluminescence of 3.8%. The open-circuit voltage of 1.24 volts at a band gap of 1.63 electron volts leads to a loss in potential of 0.39 volts, versus 0.4 volts for commercial silicon cells. Polymer-coated cells maintained 95% of their initial performance at 85°C for 500 hours under full illumination and maximum power point tracking.

Low-cost perovskite solar cells (PSCs) have achieved certified power conversion efficiencies (PCEs) of 22.1% (1). The organic-inorganic perovskites used for photovoltaics (PV) have an AMX_3 formula that comprises a monovalent cation, A [cesium Cs^+ , methylammonium (MA) CH_3NH_3^+ , or formamidinium (FA) $\text{CH}_3(\text{NH}_2)_2^+$; a divalent metal, M (Pb^{2+} or Sn^{2+});

and an anion, X (Cl^- , Br^- , or I^-). The highest-efficiency perovskites are Pb-based with mixed MA/FA cations and Br/I halides (2–4). Recently, Cs was used to explore more complex cation combinations: Cs/MA, Cs/FA, and Cs/MA/FA (5–9). These perovskite formulations exhibit unexpected properties. For example, Cs/FA mixtures suppress halide segregation, enabling band gaps for perovskite/silicon tandems (10). The Cs/MA/FA-based solar cells are more reproducible and thermally stable than MA/FA mixtures (9).

In general, increasing the perovskite complexity is motivated by the need to improve stability by adding more inorganic elements and increasing the entropy of mixing, which can stabilize ordinarily unstable materials (such as the “yellow,” non-photoactive phase of FAPbI_3 that can be avoided by using small amounts of the otherwise unstable

¹Laboratory of Photonics and Interfaces, École Polytechnique Fédérale de Lausanne, Station 6, CH-1015 Lausanne, Switzerland. ²Advanced Research Division, Materials Research Laboratory, Panasonic Corporation, 1006 Kadoma, Kadoma City, Osaka 571-8501, Japan. ³Laboratory of Photomolecular Science, École Polytechnique Fédérale de Lausanne, Station 6, CH-1015 Lausanne, Switzerland.

*Corresponding author. Email: michael.saliba@epfl.ch (M.S.); michael.gratzel@epfl.ch (M.G.) †These authors contributed equally to this work.

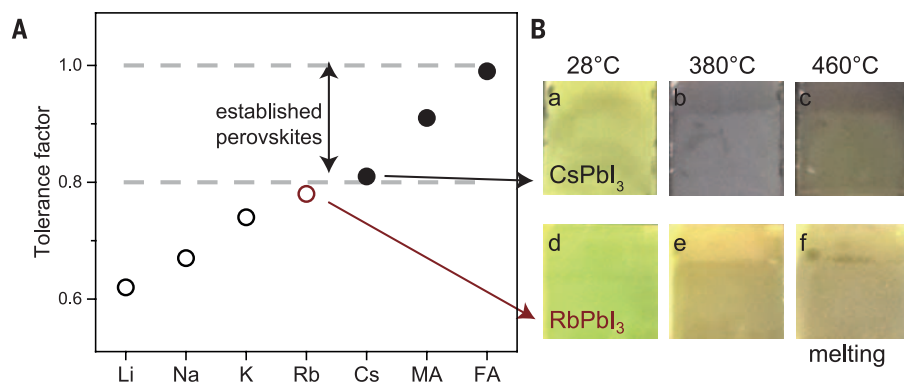


Fig. 1. Tolerance factor and perovskites at different temperatures. (A) Tolerance factor of APbI₃ perovskite with the oxidation-stable A (Li, Na, K, Rb, or Cs) and MA or FA (see table S1 for detailed calculations and ionic radii). Empirically, perovskites with a tolerance factor between 0.8 and 1.0 (dashed lines) show a photoactive black phase (solid circles) as opposed to nonphotoactive phases (open circles). Rb (red open circle) is very close to this limit, making it a candidate for integration into the perovskite lattice. (B) CsPbI₃ [(a) to (c)] and RbPbI₃ [(d) to (f)] at 28°, 380°, or 460°C. Irreversible melting for both compounds occurs at 460°C. RbPbI₃ never shows a black phase.

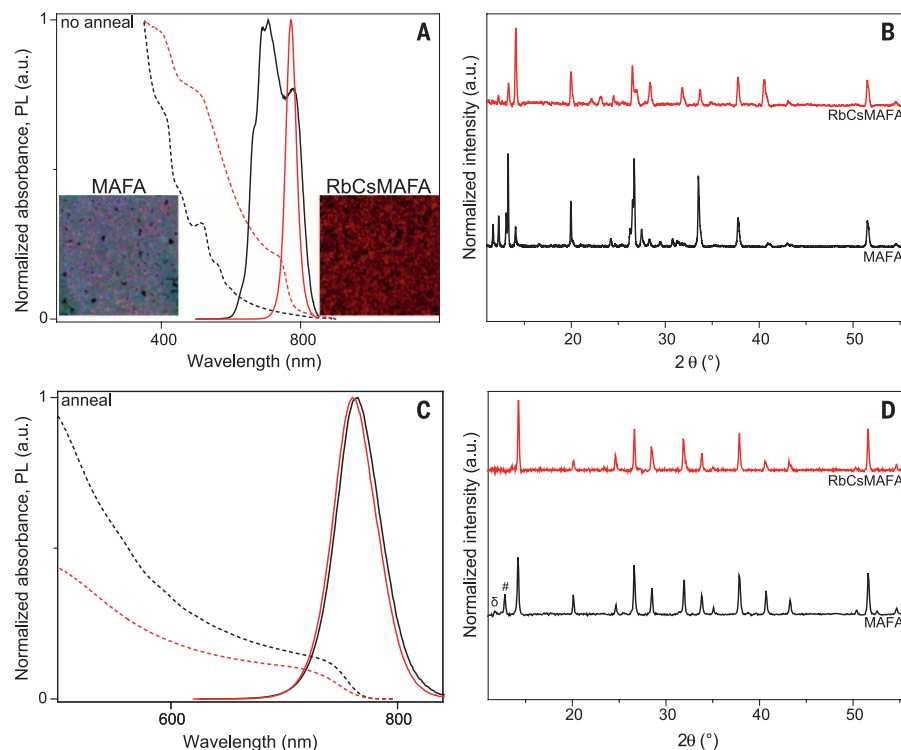


Fig. 2. Characterization of unannealed and annealed films. (A) UV-vis (dashed lines) and PL (solid lines) of unannealed MAFA (black) and RbCsMAFA (red) films. The inset images show fluorescence microscopy measurements (image size $\sim 26 \mu\text{m} \times 26 \mu\text{m}$) of MAFA and RbCsMAFA films. Each image is an overlay of three emission ranges sampled from 640 to 650 nm (assigned as green), 680 to 690 nm (blue), and 725 to 735 nm (red). The colors were chosen to ensure easily discernible features. (B) XRD data of the unannealed MAFA and RbCsMAFA films. (C) UV-vis (dashed lines) and PL (solid lines) of MAFA (black) and RbCsMAFA (red) films annealed at 100°C for 1 hour. (D) XRD data of the annealed MAFA and RbCsMAFA films. The PbI₂ and yellow-phase peaks are denoted as # and δ, respectively.

CsPbI₃ (6, 7). However, all combinations of Cs, MA, and FA cations were selected because each individually forms a photoactive perovskite “black” phase (11–13).

Further progress requires exploration of a wider circle of cations. Unfortunately, most monovalent cations are mismatched to sustain a photoactive APbI₃ perovskite with an appropriate Goldschmidt

tolerance factor [$t = (r_A + r_1)/\sqrt{2} (r_{\text{Pb}} + r_1)$, where r is ionic radius] between 0.8 and 1.0 (14, 15), rendering almost all elemental cations too small for consideration. We illustrate this point in Fig. 1A, which shows tolerance factor calculations for the alkali metals (Li, Na, K, Rb, Cs) as well as MA and FA (see table S1 for numeric values and ionic radii). We selected specifically the alkali metals that are oxidation-stable monovalent cations, as these would have a stability advantage over oxidation-prone Pb/Sn mixtures that have distorted material electronic properties (16).

The tolerance factor shows that only CsPbI₃, MAPbI₃, and FAPbI₃ fall into the range of “established perovskites” with a black phase. Li, Na, and K are clearly outside of the range, whereas RbPbI₃ only misses by a small margin. The ionic radii of Cs and Rb are 167 pm and 152 pm, respectively. This small difference still has a large impact, with RbPbI₃ and CsPbI₃ drawing the demarcation line between photoactive black perovskite and photoinactive yellow nonperovskite phases. As shown by heating CsPbI₃ and RbPbI₃ films at different temperatures (Fig. 1B), both films are yellow at 28°C; upon heating to 380°C, only CsPbI₃ turns black, whereas RbPbI₃ remains yellow. At 460°C, both films start melting irreversibly, without RbPbI₃ ever showing a black phase; this is consistent with the observations of Trots and Myagkota (17). Thus, only CsPbI₃ has a black phase, which explains why Rb has so far not been used for PSCs despite its desirable oxidation stability.

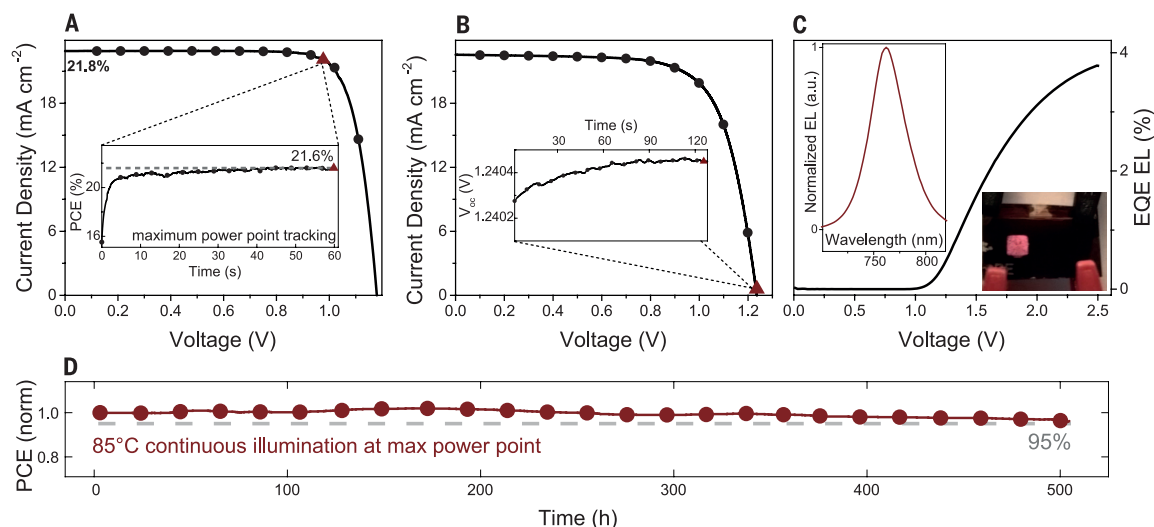
In this work, we propose embedding Rb⁺, only slightly smaller than Cs⁺, into a photoactive perovskite phase using multiple A-cation formulations. We retain FA as the majority cation because of the beneficial, red-shifted band gap. We identify four previously unexplored combinations: RbFA, RbCsFA, RbMAFA, and RbCsMAFA. In (18) and figs. S1 to S3, following the antisolvent approach pioneered by Jeon *et al.* (2), we present device data on a glass/fluorine-doped tin oxide/compact TiO₂/mesoporous TiO₂/perovskite/spiro-OMeTAD [2,2',7,7'-tetrakis(*N,N*-di-*p*-methoxyphenylamine)-9,9'-spirobifluorene]/Au architecture. [See fig. S4A for a cross-sectional scanning electron microscopy (SEM) image and fig. S4C for an image of typical devices.] All preparation details are given in (18). We use the nomenclature of RbFA, RbCsFA, RbMAFA, and RbCsMAFA to denote the entire perovskite compounds at the optimized values found in (18) (usually achieved with an addition of 5 to 10% Rb).

Reasonable device performances were reached with RbFA (14%), RbCsFA (19.3%), RbMAFA (19.2%) [comparable to CsFA (20%)], and CsMAFA (19.2%), as shown in figs. S1 to S3 (measured on a device area of 0.16 cm²). Thus, Rb can stabilize the black phase of FA perovskite and be integrated into PSCs, despite not being suitable as a pure RbPbI₃ compound. Surprisingly, RbCsMAFA (with 5% Rb; fig. S3) resulted in PCEs of 20.6%, with an open-circuit voltage V_{oc} of 1186 mV (18). Hence, we focus below on RbCsMAFA to substantiate the impact of the Rb⁺ integration approach for PSCs.

We investigated the starting condition of the crystallization process for the RbCsMAFA compound

Fig. 3. Efficiency, open-circuit voltage, electroluminescence, and high-temperature stability of the best-performing RbCsMAFA solar cell. (A) Current density–voltage (*J*-*V*) curve, taken at 10 mV s⁻¹ scan rate, of the solar cell with 21.8% efficiency (V_{oc} = 1180 mV, J_{sc} = 22.8 mA cm⁻², and FF = 81%). The forward and reverse scan is shown in table S2. The inset shows the scan rate–independent MPP tracking for 60 s, resulting in a stabilized

efficiency of 21.6% at 977 mV and 22.1 mA cm⁻² (displayed as triangles in the *J*-*V* and MPP scans). (B) *J*-*V* curve of the highest- V_{oc} device. The inset shows the V_{oc} over 120 s, resulting in 1240 mV (displayed as the red triangles in the *J*-*V* and V_{oc} scans). (C) EQE electroluminescence (EL) as a function of voltage. The left inset shows the corresponding EL spectrum over wavelength. The right inset shows a solar cell (device size ~1.4 cm × 2.8 cm) with two active areas. The left area is operated as an LED displaying a clearly



upon annealing at 100°C, which is needed to fully crystallize the perovskite films. In Fig. 2A, we present the ultraviolet-visible (UV-vis) and photoluminescence (PL) data of the unannealed MAFA and RbCsMAFA films. Whereas MAFA showed several PL peaks with maxima ranging from 670 to 790 nm, the RbCsMAFA film had a narrow peak at 770 nm attributable to perovskite. The insets in Fig. 2A are fluorescence microscopy maps of the surface of the unannealed films, showing that the MAFA films comprise various emissive species that force the preannealed film to crystallize with inhomogeneous starting conditions. However, the RbCsMAFA films were emissive in a narrow range and began to crystallize from more homogeneous conditions. Thus, the addition of the inorganic cations enforced a crystallization that starts with a photoactive perovskite phase (near the final emission after annealing) instead of a mixture of varying emissions that need to converge toward the final emission (see Fig. 2C). These results are consistent with the high reproducibility and lack of yellow phase in the RbCsMAFA films.

Furthermore, we collected the corresponding x-ray diffraction (XRD) data of the unannealed films (Fig. 2B) that showed a pronounced perovskite peak for RbCsMAFA as compared to MAFA films. In Fig. 2, C and D, we show analogous data after annealing, including UV-vis, PL, and XRD data, that reveal a RbCsMAFA band gap of ~1.63 eV (slightly blue-shifted relative to MAFA at ~1.62 eV) containing neither a PbI₂ nor a yellow-phase peak. The low-angle perovskite peaks for MAFA and RbCsMAFA occur at 14.17° and 14.25°, respectively, revealing that Rb indeed modified the crystal lattice. In figs. S5 and S6, we show XRD data of

RbMAFA perovskite where we increased the concentration of Rb. We observed, similar to CsMAFA (9), that the Pb excess and the yellow-phase impurities of MAFA perovskite disappeared when Rb was added. For Rb₅MAFA, there was a shift to wider angles for the perovskite peak. Moreover, in figs. S7 and S8, we show a series of RbCsMAFA perovskite with an increased amount of Rb together with a RbPbI₃ reference. We observed that the perovskite peak shifted to wider angles for Rb₅CsMAFA as well as further suppression of the residual PbI₂ (12.7°) and yellow-phase peak (11.7°) of FA-based perovskite. As more Rb was added, we noted the appearance of a second peak at 13.4° and a double peak at 10.1° that coincide with the peaks for the pure yellow-phase RbPbI₃, indicating phase segregation at higher Rb concentrations. This is in good agreement with previous work where a phase segregation was also observed as more and more Cs was added to FA-based perovskite (8).

In addition, top-view scanning electron microscopy (SEM) images revealed large crystals in the RbCsMAFA devices (fig. S9), which have been shown to be beneficial for the PV metrics (19). Energy-dispersive x-ray spectroscopy measurements (fig. S10) indicated the presence and distribution of Cs and Rb within the perovskite layer.

We collected statistical data on RbCsMAFA devices (with 12 CsMAFA and 17 RbCsMAFA devices measured at a scan rate of 10 mV s⁻¹, without preconditioning such as light soaking or long-term forward voltage biasing; see fig. S11) and observed superior performance relative to CsMAFA. Remarkably, the average V_{oc} increased from 1120 to 1158 mV and the fill factor (FF) increased from 0.75 to 0.78. In Fig. 3A, we show that the best-performing RbCsMAFA cell reached a stabilized

visible red emission even under ambient light. At the same time, the right area can be operated as a solar cell or a photodetector. (D) Thermal stability test of a perovskite solar cell. The device was aged for 500 hours at 85°C under continuous full illumination and MPP tracking in a nitrogen atmosphere (red curve, circles). This aging routine exceeds industry norms. During the light soaking at 85°C, the device retained 95% (dashed line) of its initial performance.

power output of 21.6% with FF of 81% and V_{oc} of 1180 mV. The measured short-circuit current density J_{sc} matched the incident photon to current efficiency (IPCE) measurement in fig. S12. We also achieved a stabilized PCE of 19.0% on a large-area 0.5-cm² device (see fig. S13).

To correctly determine the value of V_{oc} , we investigated RbCsMAFA devices with the active area being fully illuminated, held at room temperature, and under an inert nitrogen atmosphere. This setup permitted an accurate V_{oc} value without heating or degradation effects (from moisture, for example). In Fig. 3B, for one of our highest-performing devices, we measured an outstanding V_{oc} of 1240 mV, as confirmed by the inset tracking V_{oc} over time. The “loss in potential” (difference between V_{oc} and band gap) is only ~0.39 V, which is one of the lowest recorded for any PV material, implying very small nonradiative recombination losses (20). The high V_{oc} is particularly intriguing because this is the major parameter preventing PSCs from reaching their thermodynamic limit (J_{sc} and FF are already approaching their maximal values). Theoretically, in very pure, defect-free materials with only radiative recombination, the loss in potential can be as small as 0.23 V (band gap of 1 eV) to 0.3 V (band gap of 2 eV). In particular, silicon, the main industrial PV material, cannot approach this limit because of its indirect band gap and Auger recombination, exhibiting a loss in potential of ~0.4 V for the most efficient devices (20).

The nonradiative recombination losses were quantified by measuring the external electroluminescence quantum efficiency (EQE_{EL}), which is > 1% at a driving current that is equal to the short-circuit current (see Fig. 3C). This value is in the

same order of magnitude and thus consistent with a measured external PL quantum yield of 3.6% for RbCsMAFA (and 2.4% for CsMAFA). Following the approach in (21–25) [see also fig. S14 and (18)], we used the EQE_{EL} and the emission spectrum to predict a V_{oc} value of 1240 mV, confirming independently the value measured from the J - V curve.

Furthermore, for higher driving currents, the EQE_{EL} in Fig. 3C reaches 3.8%, making the solar cell one of the most efficient perovskite LEDs as well, emitting in the near-infrared/red spectral range (Fig. 3C, inset) (26–28). Movie S1 shows a RbCsMAFA device mounted in our custom-made device holder. As we tuned toward maximum emission and back, we observed bright EL in daylight. For comparison, for commercially available Si solar cells, $\text{EQE}_{\text{EL}} \approx 0.5\%$ (20). These values for our PSC devices indicate that all major sources of nonradiative recombination were strongly suppressed and that the material has very low bulk and surface defect density. We also investigated transport behavior by means of intensity-modulated photocurrent spectroscopy (IMPS); the findings suggest that the charge transport within the RbCsMAFA perovskite layer is substantially faster than in CsMAFA, which is already much more defect-free than MAFA (19) [see also fig. S15 and (18)].

Despite the high efficiencies and an outstanding EL, this Rb-containing perovskite material must be able to achieve high stability. This task is not trivial given the hygroscopic nature of perovskite films, phase instabilities, and light sensitivity (29). Interestingly, the Achilles' heel of PSCs is not necessarily the perovskite itself, but rather the commonly used spiro-OMeTAD hole transporter material that becomes permeable (at elevated temperature) to metal electrode diffusion into the perovskite, causing irreversible degradation (30, 31). This effect can be mitigated with buffer layers or by avoiding the use of metal electrodes (30–32). Alternatively, for the combined heat-light stress tests in this work, we found a thin layer of polytriarylamine polymer (PTAA) (see SEM image in fig. S4B) to work equally well (33). We imposed the above protocols simultaneously and aged devices for 500 hours at 85°C under continuous illumination with full intensity and maximum power point (MPP) tracking in a nitrogen atmosphere. This compounded stress test exceeds industrial standards (34). We show the result in Fig. 3D (red curve). The device started with >17% efficiency at room temperature before the aging protocol was applied (see fig. S16 for non-normalized values of PCE, FF, J_{sc} , V_{oc} , J_{MPP} , and V_{MPP}). During the 85°C step (in which V_{oc} is inevitably lowered), the device retained 95% of its initial performance.

REFERENCES AND NOTES

- National Renewable Energy Laboratory, Best Research-Cell Efficiencies chart; www.nrel.gov/ncpv/images/efficiency_chart.jpg.
- N. J. Jeon *et al.*, *Nature* **517**, 476–480 (2015).
- M. Saliba *et al.*, *Nat. Energy* **1**, 15017 (2016).
- X. Li *et al.*, *Science* **353**, 58–62 (2016).
- H. Choi *et al.*, *Nano Energy* **7**, 80–85 (2014).
- J. W. Lee *et al.*, *Adv. Energy Mater.* **5**, 1501310 (2015).
- C. Yi *et al.*, *Energy Environ. Sci.* **9**, 656–662 (2016).
- Z. Li *et al.*, *Chem. Mater.* **28**, 284–292 (2016).
- M. Saliba *et al.*, *Energy Environ. Sci.* **9**, 1989–1997 (2016).
- D. P. McMeekin *et al.*, *Science* **351**, 151–155 (2016).
- H. L. Wells, *Z. Anorg. Chem.* **3**, 195–210 (1893).
- D. Weber, *Z. Naturforsch. B* **33**, 1443 (1978).
- D. B. Mitzi, K. Liang, *J. Solid State Chem.* **134**, 376–381 (1997).
- G. Kieslich, S. J. Sun, A. K. Cheetham, *Chem. Sci.* **5**, 4712–4715 (2014).
- M. R. Filip, G. E. Eperon, H. J. Snaith, F. Giustino, *Nat. Commun.* **5**, 5757 (2014).
- F. Hao, C. C. Stoumpos, D. H. Cao, R. P. H. Chang, M. G. Kanatzidis, *Nat. Photonics* **8**, 489–494 (2014).
- D. M. Trops, S. V. Myagkota, *J. Phys. Chem. Solids* **69**, 2520–2526 (2008).
- See supplementary materials on Science Online.
- J. P. Correa-Baena *et al.*, *Adv. Mater.* **28**, 5031–5037 (2016).
- M. A. Green, *Prog. Photovolt. Res. Appl.* **20**, 472–476 (2012).
- K. Tvingstedt *et al.*, *Sci. Rep.* **4**, 6071 (2014).
- D. Bi *et al.*, *Sci. Advances* **2**, e1501170 (2016).
- U. Rau, *Phys. Rev. B* **76**, 085303 (2007).
- R. T. Ross, *J. Chem. Phys.* **46**, 4590 (1967).
- W. Tress *et al.*, *Adv. Energy Mater.* **5**, 1400812 (2015).
- H. Cho *et al.*, *Science* **350**, 1222–1225 (2015).
- L. Gil-Escrig *et al.*, *Chem. Commun.* **51**, 569–571 (2015).
- G. Li *et al.*, *Adv. Mater.* **28**, 3528–3534 (2016).
- N. H. Tiep, Z. L. Ku, H. J. Fan, *Adv. Energy Mater.* **6**, 1501420 (2016).
- K. Domanski *et al.*, *ACS Nano* **10**, 6306–6314 (2016).
- K. A. Bush *et al.*, *Adv. Mater.* **28**, 3937–3943 (2016).
- A. Mei *et al.*, *Science* **345**, 295–298 (2014).
- J. H. Heo *et al.*, *Nat. Photonics* **7**, 487 (2013).
- Y. G. Rong, L. F. Liu, A. Y. Mei, X. Li, H. W. Han, *Adv. Energy Mater.* **5**, 1501066 (2015).
- M.S. conceived, designed, and led the overall project; M.S., J.-Y.S., A.U., and J.-P.C.-B. conducted SEM, PL, and XRD experiments on the perovskite films; M.S. and W.R.T. performed EL and PL quantum yield experiments; A.U. conducted confocal laser scanning fluorescence microscopy for PL mapping; M.S., K.D., and W.R.T. conducted long-term aging tests on the devices; M.S., T.M., J.-P.C.-B., and A.A. prepared and characterized PV devices; A.H. participated in the supervision of the work; M.G. directed and supervised the research; M.S. wrote the first draft of the paper; and all authors contributed to the discussion and writing of the paper. Supported by the co-funded Marie Skłodowska Curie fellowship, H2020 grant agreement no. 665667 (M.S.); the European Union's Seventh Framework Programme for research, technological development, and demonstration under grant agreement no. 291771 (A.A.); the Swiss National Science Foundation, funding from the framework of Umbrella project (grant agreement nos. 407040-153952, 407040-153990, and 200021-157135/1); the NRP 70 "Energy Turnaround"; the 9th call proposal 906: CONNECT PV; and SNF-NanoTera and the Swiss Federal Office of Energy (SYNERGY). A.A. conducted IMPS experiments at the Adolphe Merkle Institute, Fribourg, Switzerland. M.G. and S.M.Z. thank the King Abdulaziz City for Science and Technology for financial support under a joint research project. All data are available in the main paper and supplement. M.S., T.M., K.D., J.-Y.S., S.M.Z., W.R.T., and M.G. are inventors on European Patent Application 1618056.7 submitted by École Polytechnique Fédérale de Lausanne and Panasonic Corporation that covers the perovskite compounds in this work.

SUPPLEMENTARY MATERIALS

www.sciencemag.org/content/354/6309/206/suppl/DC1
Materials and Methods
Supplementary Text
Figs. S1 to S16
Tables S1 and S2
Movie S1
References (35–41)

18 July 2016; accepted 8 September 2016
Published online 29 September 2016
10.1126/science.aah5557

BIOPHYSICS

Bifurcating electron-transfer pathways in DNA photolyases determine the repair quantum yield

Meng Zhang,¹ Lijuan Wang,¹ Shi Shu,¹ Aziz Sancar,² Dongping Zhong^{1*}

Photolyase is a blue-light-activated enzyme that repairs ultraviolet-induced DNA damage that occurs in the form of cyclobutane pyrimidine dimers (CPDs) and pyrimidine-pyrimidone (6-4) photoproducts. Previous studies on microbial photolyases have revealed an electron-tunneling pathway that is critical for the repair mechanism. In this study, we used femtosecond spectroscopy to deconvolute seven electron-transfer reactions in 10 elementary steps in all classes of CPD photolyases. We report a unified electron-transfer pathway through a conserved structural configuration that bifurcates to favor direct tunneling in prokaryotes and a two-step hopping mechanism in eukaryotes. Both bifurcation routes are operative, but their relative contributions, dictated by the reduction potentials of the flavin cofactor and the substrate, determine the overall quantum yield of repair.

Photolyases, which belong to the photolyase (PL)-cryptochrome (CRY) superfamily, use a fully reduced flavin (FADH^-) cofactor to repair sunlight-induced DNA lesions, including cyclobutane pyrimidine dimers (CPDs) and pyrimidine-pyrimidone (6-4) photoproducts (1–5). On the basis of sequence analyses, CPD photolyases are highly diversified and can be subdivided into three classes (I to III) (6–8),

as well as single-stranded DNA (ssDNA)-specific PLs (9) (Fig. 1A). Thus, the molecular repair

¹Department of Physics, Department of Chemistry and Biochemistry, and Programs of Biophysics, Chemical Physics, and Biochemistry, The Ohio State University, Columbus, OH 43210, USA. ²Department of Biochemistry and Biophysics, University of North Carolina School of Medicine, Chapel Hill, NC 27599, USA.

*Corresponding author. Email: zhong.28@osu.edu

of the intermediate T-T⁻ after the first C-C bond breakage, T⁻ after the second C-C cleavage, and the final product of repaired base T. The various dissections are shown in Fig. 3, D, F, and H, and fig. S4. Thus, we obtained the ultrafast electron hopping of FET3 in 6, 11, and 15 ps and the electron return after repair in 437, 2890, and 819 ps for AnPL, DmPL, and AtPL, respectively. Knowing the total QYs (Fig. 1C), we can also derive the second C-C cleavage in 87, 48, and 36 ps and the futile back electron transfer BET2 in 1138, 149, and 527 ps, respectively, for three PLs (table S1).

To recapitulate, we have identified 10 elementary steps in the repair reaction by DNA photolyase, including 7 ET steps, and measured their time scales in real time (table S1). Consequently, we can calculate the QY of each step that contributes to the total QY (table S2). In Fig. 4, A and B, we show the two resolved photocycles for class I AnPL and class II AtPL, respectively, with the corresponding reaction times of each step. For class I PL (Fig. 4A), the two systems we studied, AnPL and EcPL, show a dominant tunneling pathway with the highest QYs (table S2). For class II PL (Fig. 4B), the two systems studied here, DmPL and AtPL, adopt mainly a two-step hopping route, also with good repair efficiency. For other PLs [class III CcPL and ssDNA-specific AtPL (AtCRY3)], both tunneling and hopping channels are operative (table S1). These detailed dynamics and time scales for seven ET reactions involved in repair can be used to derive microscopic pictures of various reorganization energies; their relevant reduction potentials; and, thus, reaction driving forces (table S3) (21, 24, 25). We did not observe clear evidence for the possible flickering resonance for the initial electron bifurcation, as proposed recently in a theoretical study (26).

Figure 4C shows the repair QYs along the evolutionary path from the microbial class I to the eukaryotic class II PLs, with initial electron bifurcation into the tunneling route FET2 and the hopping path FET1 and their resulting QYs (QY2 and QY1). Clearly, the tunneling route in class I leads to a higher repair QY. With the decrease in the rates of tunneling, the hopping channel comes to dominate in class II PLs. Consequently, class II PLs can never reach the class I repair QY because the electron path at Ade⁻ also bifurcates into the repair channel to the CPD and the futile path back to the original ground state, both of which share similar hopping rates. The conserved active-site configuration and the folded flavin structure that occur as a result of evolution in the entire photolyase-cryptochrome superfamily (11–15, 27–30) are essential to ensure a unified electron-transfer mechanism through electron path bifurcation into two operative routes for all CPD photolyases.

REFERENCES AND NOTES

1. A. Sancar, *Chem. Rev.* **103**, 2203–2238 (2003).
2. C. Lin, T. Todo, *Genome Biol.* **6**, 220 (2005).
3. S. T. Kim, A. Sancar, C. Essenmacher, G. T. Babcock, *Proc. Natl. Acad. Sci. U.S.A.* **90**, 8023–8027 (1993).
4. D. E. Brash, *Trends Genet.* **13**, 410–414 (1997).
5. J. S. Taylor, *Acc. Chem. Res.* **27**, 76–82 (1994).
6. S. Kanai, R. Kikuno, H. Toh, H. Ryo, T. Todo, *J. Mol. Evol.* **45**, 535–548 (1997).
7. A. Sancar *et al.*, *Cold Spring Harb. Symp. Quant. Biol.* **65**, 157–172 (2000).
8. J. I. Lucas-Lledó, M. Lynch, *Mol. Biol. Evol.* **26**, 1143–1153 (2009).
9. D. Zhong, *Annu. Rev. Phys. Chem.* **66**, 691–715 (2015).
10. Z. Liu, L. Wang, D. Zhong, *Phys. Chem. Chem. Phys.* **17**, 11933–11949 (2015).
11. S. Kiontke *et al.*, *EMBO J.* **30**, 4437–4449 (2011).
12. K. Hitomi *et al.*, *J. Biol. Chem.* **287**, 12060–12069 (2012).
13. H. W. Park, S. T. Kim, A. Sancar, J. Deisenhofer, *Science* **268**, 1866–1872 (1995).
14. A. Mees *et al.*, *Science* **306**, 1789–1793 (2004).
15. Y. Huang *et al.*, *Proc. Natl. Acad. Sci. U.S.A.* **103**, 17701–17706 (2006).
16. Z. Liu *et al.*, *Proc. Natl. Acad. Sci. U.S.A.* **110**, 12972–12977 (2013).
17. C.-W. Chang *et al.*, *Proc. Natl. Acad. Sci. U.S.A.* **107**, 2914–2919 (2010).
18. Y. T. Kao, C. Saxena, L. Wang, A. Sancar, D. Zhong, *Proc. Natl. Acad. Sci. U.S.A.* **102**, 16128–16132 (2005).
19. Z. Liu *et al.*, *Proc. Natl. Acad. Sci. U.S.A.* **108**, 14831–14836 (2011).
20. C. Tan *et al.*, *Nat. Commun.* **6**, 7302 (2015).
21. Z. Liu *et al.*, *J. Am. Chem. Soc.* **134**, 8104–8114 (2012).
22. A. A. Hassanali, D. Zhong, S. J. Singer, *J. Phys. Chem. B* **115**, 3848–3859 (2011).
23. V. Thiagarajan, M. Byrdin, A. P. Eker, P. Müller, K. Brettel, *Proc. Natl. Acad. Sci. U.S.A.* **108**, 9402–9407 (2011).
24. H. Wang *et al.*, *Science* **316**, 747–750 (2007).
25. D. N. LeBard, V. Kapko, D. V. Matyushov, *J. Phys. Chem. B* **112**, 10322–10342 (2008).
26. Y. Zhang, C. Liu, A. Balaeff, S. S. Skourtis, D. N. Beratan, *Proc. Natl. Acad. Sci. U.S.A.* **111**, 10049–10054 (2014).
27. M. J. Maul *et al.*, *Angew. Chem. Int. Ed.* **47**, 10076–10080 (2008).
28. W. Xing *et al.*, *Nature* **496**, 64–68 (2013).
29. B. D. Zoltowski *et al.*, *Nature* **480**, 396–399 (2011).
30. C. A. Brautigam *et al.*, *Proc. Natl. Acad. Sci. U.S.A.* **101**, 12142–12147 (2004).

ACKNOWLEDGMENTS

We dedicate this paper to the memory of the “father of femtochemistry,” Ahmed H. Zewail, who passed away on 2 August 2016. D.Z. was trained as a student and later as a postdoctoral fellow in Dr. Zewail’s lab. We thank Y.-T. Kao, Z. Liu, X. Guo, C. Tan, Y. Qin, and N. Ozturk for help in the initial stages of this work. We also thank P. Houston for careful reading of the manuscript. This work was supported, in part, by NIH grants GM074813 and GM118332 to D.Z. and GM031082 to A.S. Additional data supporting the conclusions of this study are included in the supplementary materials.

SUPPLEMENTARY MATERIALS

www.sciencemag.org/content/354/6309/209/suppl/DC1
Materials and Methods
Figs. S1 to S4
Tables S1 to S4
References (31–36)

20 July 2016; accepted 15 September 2016
10.1126/science.aah6071

INFLUENZA

Role for migratory wild birds in the global spread of avian influenza H5N8

The Global Consortium for H5N8 and Related Influenza Viruses*†

Avian influenza viruses affect both poultry production and public health. A subtype H5N8 (clade 2.3.4.4) virus, following an outbreak in poultry in South Korea in January 2014, rapidly spread worldwide in 2014–2015. Our analysis of H5N8 viral sequences, epidemiological investigations, waterfowl migration, and poultry trade showed that long-distance migratory birds can play a major role in the global spread of avian influenza viruses. Further, we found that the hemagglutinin of clade 2.3.4.4 virus was remarkably promiscuous, creating reassortants with multiple neuraminidase subtypes. Improving our understanding of the circumpolar circulation of avian influenza viruses in migratory waterfowl will help to provide early warning of threats from avian influenza to poultry, and potentially human, health.

In 2014, highly pathogenic avian influenza (HPAI) virus of the subtype H5N8 caused disease outbreaks in poultry in Asia, Europe, and North America (1–3). Avian influenza viruses are a threat both to global poultry production and to public health; they have the potential to cause severe disease in people and to adapt to transmit efficiently in human populations (4). This was the first time since 2005 that a single subtype of HPAI virus had spread over such a large geographical area and the first time that a Eurasian HPAI virus had spread to

North America. The rapid global spread of HPAI H5N8 virus outbreaks raised the question of the routes by which the virus had been transmitted.

The segment encoding for the hemagglutinin (HA) surface protein of the HPAI H5N8 viruses is a descendant of the HPAI H5N1 virus (A/Goose/Guangdong/1/1996), first detected in China in 1996 (5). Since then, HPAI H5N1 viruses have become endemic in poultry populations in several countries. The H5 viruses have developed new characteristics by mutation and by reassortment with other avian influenza (AI) viruses, both in poultry and in wild birds. In 2005–2006, HPAI H5N1 spread from Asia to Europe, the Middle East, and Africa during the course of a few months. Although virus spread traditionally had been

*Corresponding author. Email: t.kuiken@erasmusmc.nl †All authors with their affiliations appear at the end of this paper.

attributed to transport of infected poultry, infected poultry products, or HPAI-virus-contaminated materials, several observations in the 2005–2006 epidemic suggested that wild birds also might have carried the virus to previously unaffected areas (6).

A HPAI H5N8 virus with genes from viruses of the influenza A (H5N1) A/Goose/Guangdong/1/1996 lineage was first detected in birds at live bird markets in China in 2010 (7). This HPAI H5N8 virus was a reassortant virus with the HA gene segment from HPAI H5N1 virus and other gene segments from multiple other AI viruses circulating in eastern China (7) and is now categorized as HPAI H5 virus clade 2.3.4.4 (7). This clade is unusually promiscuous and has been found in combination with six different neuraminidase (NA) segments, and multiple H5Nx viruses may be circulating at the same time and in the same region (8, 9). The propensity of HPAI H5 virus clade 2.3.4.4 to form novel subtypes capable of rapid, global spread is a major concern.

HPAI H5N8 virus caused a large avian influenza outbreak in poultry in South Korea in the winter of 2013–2014 and subsequently spread to Japan, North America, and Europe, causing outbreaks there between autumn 2014 and spring 2015 (table S1). However, it is not clear by which routes HPAI H5N8 virus spread so rapidly around the world. Although there have been reports on parts of these outbreaks (1, 2, 10) and speculation on possible routes of transmission (3), no comprehensive global analysis has yet been performed.

The goal of this study was to analyze the available genetic, epidemiological, and ornithological data for evidence of the relative contributions from poultry trade and from wild bird movements (3, 6) for the global spread of clade 2.3.4.4 during 2014–2015. For this purpose, we performed phylogeographic analysis of HPAI H5N8 viruses detected in wild birds and poultry from this global outbreak. In addition, we analyzed migration patterns of wild birds found infected with HPAI H5N8 virus, epidemiological investigations of HPAI H5N8 virus outbreaks, and poultry-trade records from countries where HPAI H5N8 virus was reported (11).

Initial phylogenetic analysis was performed using HA sequences from HPAI H5 clade 2.3.4.4 viruses of poultry and wild birds from around the world between 2004 and 2015, including subtypes H5N1, H5N2, H5N3, H5N5, H5N6, and H5N8. From 2004 to 2012, clade 2.3.4.4 viruses were circulating predominantly in Eastern Asia (China), with some transmission to Southeastern Asia (Fig. 1 and fig. S1). During this period, transmission involving domestic anseriforms (ducks and geese) appears to dominate, although some contribution from domestic galliforms (chickens and turkeys) and short-distance migratory wild birds (e.g., mallard ducks) is also evident (Fig. 1). Unlike H5 segments from other clades, which are mostly found as H5N1, the HPAI H5 segment of the clade 2.3.4.4 viruses reassorts frequently, acquiring NA segments from cocirculating low pathogenic avian influenza (LPAI) subtypes, including N5 (from 2006 to 2010), N2

(from 2008 to 2012), N8 (from 2010), and, more recently, N6 (from 2013) (8). To indicate the host species and regions in which the reassortments are thought to have occurred, a reassortment measure was calculated using the number of branches in the posterior set of phylogenetic trees for which the NA subtype changed while the host species and region traits remained the same (normalized by branch lengths). This measure suggests that most of the observed reassortants were generated in domestic anseriforms (fig. S2), and particularly domestic anseriforms in Eastern Asia (China) within the time period 2004 to 2012 (fig. S3).

The time to the most recent common ancestor (TMRCA) for the HA segment of all clade 2.3.4.4 HPAI H5N8 sequences was estimated as June 2010 [95% highest posterior density (HPD), January to October 2010]; the TMRCA for the corresponding NA segments was similar (September 2010; 95% HPD, April to December 2010). Clade 2.3.4.4 HA H5N8 sequences were found in two subclades (Fig. 1). The smaller and earlier subclade (a in Fig. 1) contained the first sequenced 2.3.4.4 HPAI H5N8 virus [A/Duck/Jiangsu/k1203/2010 (H5N8)]. The larger and more recent subclade (b in Fig. 1) contained sequences from outbreaks in South Korea and other countries included in this study and caused multiple HPAI outbreaks in 2014 and 2015 globally. The TMRCA of subclade b was September 2013 for both HA (95% HPD, July to November 2013) and NA (95% HPD, May to November 2013). Consistent with earlier findings (1, 10), the phylogeny indicates that HPAI H5N8 was introduced into South Korea by long-distance migrant wild birds that acquired it from the pool of HPAI H5 viruses circulating in domestic anseriforms in Eastern Asia (China), although we

formally cannot exclude the possibility that HPAI H5 viruses were circulating in unsampled locations (Fig. 1).

Distinct, well-supported clades were identified in South Korea, likely originating in the transmission of HPAI H5N8 viruses from long-distance migrants to other wild and domestic birds (10). One clade (c in Fig. 1) was ancestral to the European outbreak and another (d in Fig. 1) was ancestral to the North American outbreak. Again, we cannot exclude the possibility that viruses from these subclades were present in unsampled locations.

More detailed phylogenetic analyses, using only clade 2.3.4.4 H5N8 HA sequences with location coordinates (11), showed that the virus spread along two main long-distance migration routes: one from the east Asia coast/Korean peninsula, north to the Arctic coast of the Eurasian continent, then west to Europe; and the other north from the Korean peninsula, then east across the Bering Strait, and south along the northwest coast of the North American continent to Canada and the United States (Fig. 2 and movie S1). The reconstruction did not indicate any spread between Europe and North America. The TMRCA for European HA segments was August 2014 (95% HPD, July to October 2014), and September to October 2014 (95% HPD, August to November 2014) for the North American HA segments (table S2, a and b). Similar results were found from analysis of the NA segments (table S2, c and d). There were also four separate introductions into Japan, the first estimated around February 2014 (ancestral date of single virus A/Chicken/Kumamoto/1-7/2014), and then three more, all with TMRCA in October and November 2014. The sequences from one Japanese introduction were most closely related to sequences from Taiwan and those from

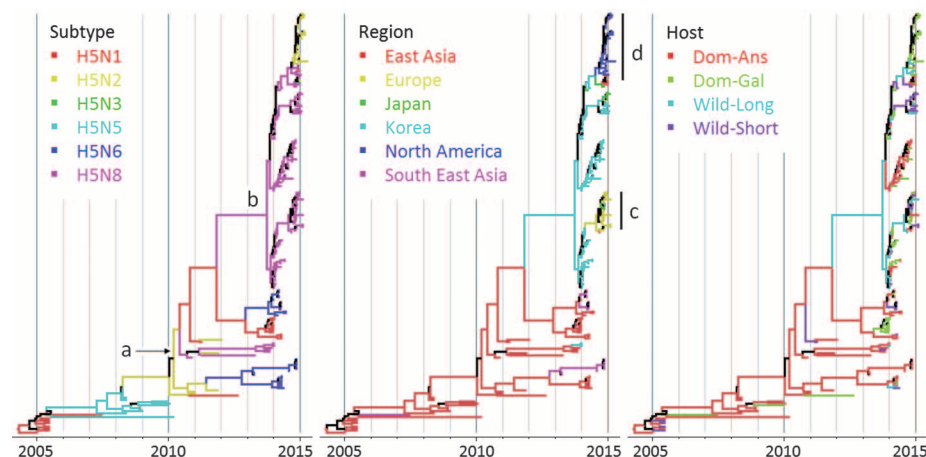


Fig. 1. Maximum clade credibility (MCC) time-scaled phylogenetic tree of multisubtype HA sequences colored by subtype, region, and host-type traits. The clades marked a and b contain H5N8 sequences, and c and d contain sequences from Europe and North America, respectively. The displayed MCC tree was obtained from a posterior set of trees inferred using the Bayesian Evolutionary Analysis Sampling Trees (BEAST) program (13) with the SRD06 nucleotide substitution model, uncorrelated relaxed clock model, and constant population size tree prior. The branches are colored according to the most probable ancestral trait, and ancestral traits were inferred by a symmetric (subtype and region) or asymmetric discrete trait model (host-type) upon the posterior tree set (14). Host types are Dom-Ans (red), domestic anseriform birds; Dom-Gal (green), domestic galliform birds; Wild-Long (blue), long-distance migratory wild birds; Wild-Short (purple), short-distance migratory wild birds.

another introduction to the Russian (A/Wigeon/Sakha/1/2014) and European sequences.

The phylogenetic data were also used to infer the ancestral host categories of the most recent common ancestor of the European and North American outbreak sequences, thus providing evidence for which host type had introduced the viruses into those areas (Fig. 3, figs. S4 and S5, and table S2). The most likely ancestral host category for the North American outbreak for both HA and NA segments was long-distance migrants (HA, 66%; NA, 84%). A similar result was obtained for Europe (HA, 66%; NA, 70%).

Several wild bird species with known HPAI H5N8 sequences were long-distance migrants at different stages of their migratory cycle, depending on time and place found (table S3): Five of the nine species found in South Korea in winter 2013–2014 were long-distance migrants at their wintering sites or on spring migration. Both in North America and Europe, two of the four species found in winter 2014–2015 were long-distance migrants at their wintering sites or on autumn migration (17) (tables S4 and S5 and fig. S6).

The April 2014 HPAI H5N8 virus outbreak in Japan had different characteristics from the later

outbreaks in North America and Europe. The Japan outbreak was the only one that was contemporaneous with the outbreak in South Korea, and no wild birds were found positive for HPAI H5N8 virus in Japan during that outbreak.

Qualitative analysis of data from outbreak investigations on affected poultry farms in North America, Europe, and Japan (17) (table S6) showed that the likelihood of virus introduction via contaminated water, feed, and poultry was negligible (Germany). Furthermore, no links between the outbreaks in one country and those in other countries could be attributed to personnel contacts or

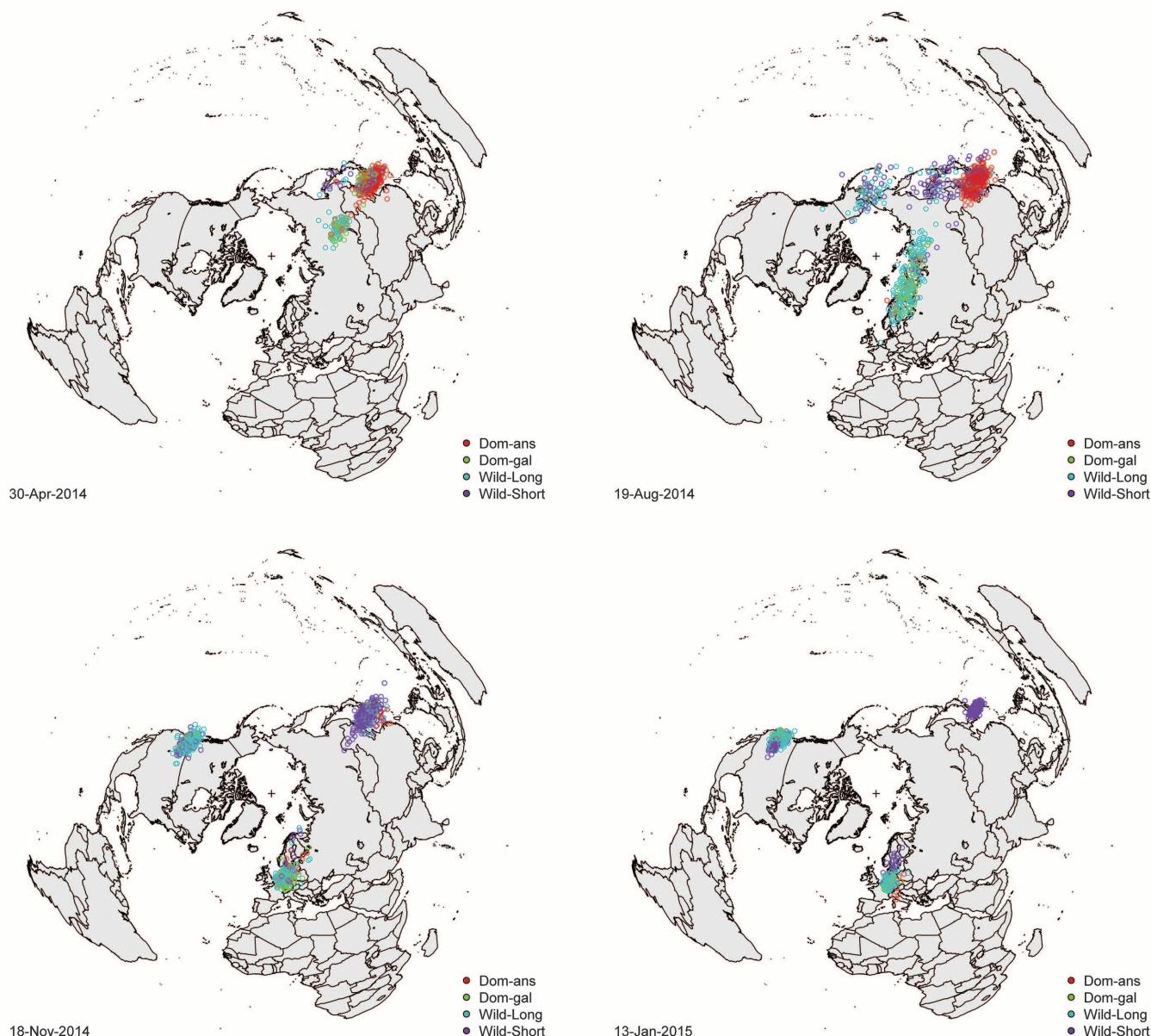


Fig. 2. Reconstruction of the transmission routes using phylogenetic data only from H5N8 HA sequences. At each time slice, the host-type and location coordinates on the branches of the posterior set of phylogenetic trees are inferred and plotted as a cloud of points. The host type was inferred by discrete trait model (as Fig. 1) (14), and the continuous location coordinates were inferred using a homogeneous Brownian motion diffusion model (15). The map projection used is the azimuthal equal areas projection, centered on the North Pole, which is marked with a + sign. Color key as for Fig. 1; see also movie S1.

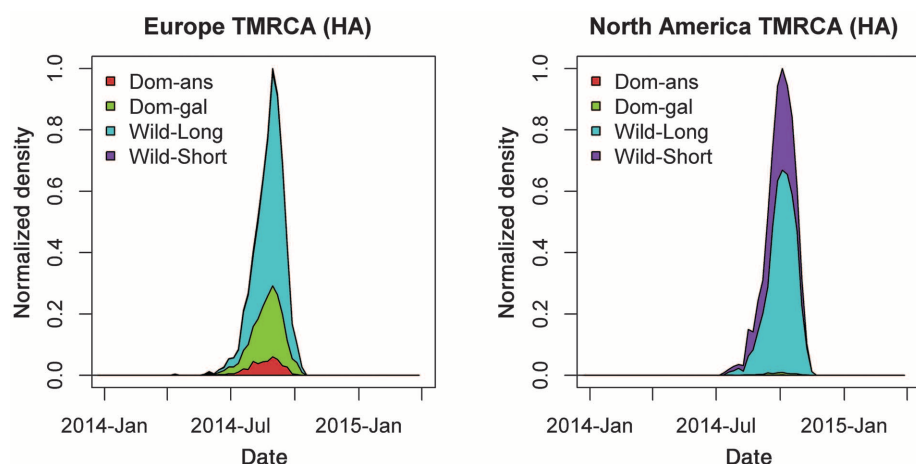


Fig. 3. Posterior distributions of TMRCA of HA sequences from Europe and North America with H5N8 subtype only, including host-type reconstructions, based upon a posterior set of phylogenetic trees generated as in Fig. 1. Color key as for Fig. 1.

trade of live animals, feed, or products of animal origin (Germany, Netherlands, United Kingdom, and Hungary). Many affected poultry farms were located in areas where wild waterfowl are abundant (Germany, Netherlands, United Kingdom, Italy, and Canada). Direct contact with infected wild birds (United States) or indirect contact with materials (e.g., bedding material, boots, and wheels of vehicles) contaminated with wild-bird feces was considered the most likely route of introduction into poultry holdings (United States, Germany, Netherlands, United Kingdom, and Italy). In some outbreaks, the source of infection was unknown or inconclusive (Japan and Hungary).

We reviewed data from the Food and Agriculture Organization of the United Nations (FAO) (12) for 2011 to 2013 on export and import of live domestic ducks and chickens of affected countries to estimate the risk of spread of HPAI virus from South Korea to other countries via the international poultry trade (table S7). Data on the export of live poultry from North Korea and Mongolia, also in East Asia, were not available from FAO. Although all countries (Japan, Canada, United States, Germany, Netherlands, United Kingdom, Italy, and Hungary) where HPAI H5N8 virus emerged between November 2014 and February 2015 imported live chickens and live domestic ducks in 2013, South Korea reported the export of a low number of live chickens and no export of live domestic ducks, although unreported cross-border trade cannot be excluded. Nevertheless, based on these data, it seems unlikely that international trade in live poultry played a major role in the long-distance spread of South Korean clade HPAI H5N8 virus in 2014–2015.

Our analysis, using four different sources of data, indicates that the main routes of large-scale geographical spread of HPAI H5N8 virus were most probably via long-distance flights of infected migratory wild birds, first in spring 2014 from South Korea or other unsampled locations in the

region to northern breeding grounds and then in autumn 2014 from these breeding grounds along migration routes to wintering sites in North America and Europe.

Recognition of a likely role of wild birds in the spread of HPAI reinforces the need to improve biosecurity on poultry farms and to exclude wild birds from the immediate vicinity of poultry farms. Culling wild birds and draining or disinfecting wetlands would not be effective because these viruses disseminate on rapid time scales over very large distances, making reactive interventions of this kind impractical and ineffective, as well as contravening commitments made by signatory countries to the Convention on Migratory Species and the Ramsar Convention on Wetlands.

The potential role of wild birds in the circumpolar circulation of influenza viruses does point to the need to increase our knowledge about the connectedness at the vast circumpolar (sub)arctic breeding areas between migratory waterfowl populations originating from different wintering areas. Surveillance of waterfowl at the crossroads of migratory flyways to wintering areas in Europe, Asia, and North America would inform epidemiological risk analysis and provide early warning of specific HPAI threats to poultry, and potentially human, health.

REFERENCES AND NOTES

1. Y.-J. Lee et al., *Emerg. Infect. Dis.* **20**, 1087–1089 (2014).
2. D.-H. Lee et al., *J. Virol.* **89**, 6521–6524 (2015).
3. J. H. Verhagen, S. Herfst, R. A. M. Fouchier, *Science* **347**, 616–617 (2015).
4. M. Richard, M. de Graaf, S. Herfst, *Future Virol.* **9**, 513–524 (2014).
5. X. Xu, N. J. Subbarao, N. J. Cox, Y. Guo, *Virology* **261**, 15–19 (1999).
6. B. Olsen et al., *Science* **312**, 384–388 (2006).
7. World Health Organization (WHO), Evolution of the influenza A(H5) haemagglutinin: WHO/OIE/FAO H5 Working Group reports a new clade designated 2.3.4.4 (2015); www.who.int/influenza/gisrs_laboratory/h5_nomenclature_clade2344/en/.
8. E. de Vries et al., *Emerg. Infect. Dis.* **21**, 842–846 (2015).
9. J. S. Hall, R. J. Dusek, E. Spackman, *Emerg. Infect. Dis.* **21**, 1251–1252 (2015).

10. S. C. Hill et al., *Infect. Genet. Evol.* **34**, 267–277 (2015).
11. Materials and methods are available as supplementary materials on Science Online.
12. Food and Agriculture Organization of the United Nations (FAO), FAOSTAT; <http://faostat3.fao.org>.
13. A. J. Drummond, M. A. Suchard, D. Xie, A. Rambaut, *Mol. Biol. Evol.* **29**, 1969–1973 (2012).
14. P. Lemey, A. Rambaut, A. J. Drummond, M. A. Suchard, *PLOS Comput. Biol.* **5**, e1000520 (2009).
15. P. Lemey, A. Rambaut, J. J. Welch, M. A. Suchard, *Mol. Biol. Evol.* **27**, 1877–1885 (2010).

ACKNOWLEDGMENTS

This study was financially supported by the European Commission H2020 program under contract number 643476 (www.compare-europe.eu) (to A.P., J.B., A.B., I.B., M.P.K., A.R., R.A.M.F., M.B., M.W., and T.K.), European Commission FP7 program under contract number 278433 (PREDEMICS) (to A.R.), the U. S. Geological Survey Ecosystems Mission Area (to H.S.I.), National Institutes of Health grant number 1R01AI101028-02A1 (to M.G.), United Kingdom Research Council Environmental and Social Ecology of Human Infectious Diseases UrbanZoo program (G1100783/1), Biotechnology and Biological Sciences Research Council (BBSRC) Zoonoses in Livestock in Kenya Zoolink (BB/L019019/1) programs (to T.P.R. and M.W.), CGIAR Research Programme on Agriculture for Nutrition and Health (A4NH) (to T.P.R.), Canadian Food Inspection Agency (to J.P.), Hungarian Academy of Sciences Lendület (Momentum) program (to K.B.) and the Wellcome Trust (grant number 093724/B/10/Z) (to M.W. and A.R.). S.J.L. is supported by the University of Edinburgh Chancellor's Fellowship scheme, the Roslin Institute BBSRC strategic program grant (BB/J004227/1), and the Centre of Expertise in Animal Disease Outbreaks (EPIC). We gratefully acknowledge the originating laboratories, where specimens were first obtained, and the submitting laboratories, where sequence data were generated and submitted to the EpiFlu Database of the Global Initiative on Sharing All Influenza Data (GISAID), on which this research is based. All contributors of data may be contacted directly via the GISAID website (<http://platform.gisaid.org>). The accession numbers (GenBank, GISAID, and/or workset identification numbers) of all genetic sequences used in this study are provided in table S9 and are accessible from the website of GISAID (<http://platform.gisaid.org>). We acknowledge Y. Berhane and T. Hisanaga for sequencing the Canadian virus isolates and G. Koch for his technical advice on the poultry outbreaks in the Netherlands. The funders had no role in study design, data collection and interpretation, or the decision to submit the work for publication. Any use of trade products or firm names is for descriptive purposes and does not imply endorsement by the U.S. government.

The Global Consortium for H5N8 and Related Influenza Viruses

Samantha J. Lycett,¹ Rogier Bodewes,² Anne Pohlmann,³ Jill Banks,⁴ Krisztián Bányai,⁵ Maciej F. Boni,^{6,7} Ruth Bouwstra,^{8,9} Andrew C. Breed,¹⁰ Ian H. Brown,⁴ Hualan Chen,¹¹ Ádám Dán,¹² Thomas J. Deliberto,¹³ Nguyen Diep,¹⁴ Marius Gilbert,^{14,15} Sarah Hill,¹⁶ Hon S. Ip,¹⁷ Chang Wen Ke,¹⁸ Hiroshi Kida,¹⁹ Mary Lea Killian,²⁰ Marion P. Koopmans,²¹ Jung-Hoon Kwon,²² Dong-Hun Lee,²³ Youn Jeong Lee,²⁴ Lu Lu,²⁵ Isabella Monne,²⁶ John Paskic,^{27,28} Oliver G. Pybus,¹⁶ Andrew Rambaut,²⁵ Timothy P. Robinson,²⁹ Yoshihiro Sakoda,³⁰ Siamak Zohari,³¹ Chang-Seon Song,²² David E. Swayne,²³ Mia Kim Torchetti,²⁰ Hsiang-Jung Tsai,³² Ron A. M. Fouchier,² Martin Beer,³ Mark Woolhouse,²⁵ Thijs Kuiken²¹

*These authors contributed equally to this work.

[†]These authors contributed equally to this work.

¹The Roslin Institute, University of Edinburgh, Edinburgh EH25 9RG, UK. ²Department of Farm Animal Health, Faculty of Veterinary Medicine, University of Utrecht, 3584 CL Utrecht, Netherlands. ³Institute of Diagnostic Virology, Friedrich Loeffler Institut, D-17493 Greifswald-Insel Riems, Germany. ⁴Virology Department, Animal and Plant Health Agency, Woodham Lane, Addlestone KT15 3NB, UK. ⁵Institute for Veterinary Medical Research, Centre for Agricultural Research, Hungarian Academy of Sciences, H1143 Budapest, Hungary. ⁶Centre for Tropical Medicine, Nuffield Department of Medicine, University of Oxford, Oxford OX3 7FZ, UK. ⁷Oxford University Clinical Research Unit, Wellcome Trust Major Overseas Programme, Ho Chi Minh City, Vietnam. ⁸Department of Virology, Central Veterinary Institute, Wageningen University and Research Centre, 8221 RA Lelystad, Netherlands. ⁹Animal Health Service, 7400 AA Deventer, Netherlands. ¹⁰Department of Epidemiological Sciences, Animal and Plant Health Agency, Woodham Lane, Addlestone KT15 3NB, UK. ¹¹Harbin Veterinary Research Institute,

Chinese Academy of Agricultural Sciences, 150001 Harbin, China.

¹²Veterinary Diagnostic Directorate, National Food Chain Safety Office, H1149 Budapest, Hungary. ¹³National Wildlife Research Center, Wildlife Services, US Department of Agriculture, Fort Collins, CO 80521, USA. ¹⁴Spatial Epidemiology Laboratory (SpELL), Université Libre de Bruxelles, B-1050 Brussels, Belgium. ¹⁵Fonds National de la Recherche Scientifique, B-1000 Brussels, Belgium. ¹⁶Department of Zoology, University of Oxford, Oxford OX1 3PS, UK. ¹⁷Wildlife Disease Diagnostic Laboratories Branch, National Wildlife Health Center, US Geological Survey, Madison, WI 53711, USA. ¹⁸Institute of Microbiology, Center for Diseases Control and Prevention of Guangdong Province, 511430 Guangzhou, China. ¹⁹Research Center for Zoonosis Control, Hokkaido University, Sapporo, Hokkaido 001-0020, Japan. ²⁰National Veterinary Services Laboratories, Veterinary Services, US Department of Agriculture, Ames, IA 50010, USA. ²¹Department of Viroscience, Erasmus

University Medical Center, 3015 CN Rotterdam, Netherlands.

²²Avian Disease Laboratory, College of Veterinary Medicine, Konkuk University, Seoul 143-701, Republic of Korea. ²³Southeast Poultry Research Laboratory, US Department of Agriculture, Athens, GA 30605, USA. ²⁴Avian Disease Division, Animal and Plant Quarantine Agency, Gimcheon, Republic of Korea. ²⁵Centre for Immunity, Infection and Evolution, University of Edinburgh, Edinburgh EH9 3FL, UK. ²⁶Research and Innovation Department, Istituto Zooprofilattico Sperimentale delle Venezie, 10-35020 Legnaro (Padova), Italy. ²⁷National Centre for Foreign Animal Disease, Canadian Food Inspection Agency, Winnipeg, MB R3E 3M4, Canada. ²⁸Canadian Food Inspection Agency, Guelph, ON N1G 4S9, Canada. ²⁹Livestock Systems and Environment (LSE), International Livestock Research Institute (ILRI), Post Office Box 30709, 00100 Nairobi, Kenya. ³⁰Graduate School of Veterinary Medicine, Hokkaido University, Sapporo, Hokkaido 060-0818, Japan.

³¹Department of Virology, Immunobiology and Parasitology, National Veterinary Institute, SE-751 89 Uppsala, Sweden.

³²Animal Health Research Institute, Council of Agriculture, New Taipei City 25158, Taiwan.

SUPPLEMENTARY MATERIALS

www.sciencemag.org/content/354/6309/213/suppl/DC1
Materials and Methods

Figs. S1 to S6

Tables S1 to S10

Movie S1

References (16–59)

21 April 2016; accepted 7 September 2016

10.1126/science.aaf8852

POLITICAL SCIENCE

How economic, humanitarian, and religious concerns shape European attitudes toward asylum seekers

Kirk Bansak,^{1,2*} Jens Hainmueller,^{1,2,3,*†} Dominik Hangartner^{2,4*}

What types of asylum seekers are Europeans willing to accept? We conducted a conjoint experiment asking 18,000 eligible voters in 15 European countries to evaluate 180,000 profiles of asylum seekers that randomly varied on nine attributes. Asylum seekers who have higher employability, have more consistent asylum testimonies and severe vulnerabilities, and are Christian rather than Muslim received the greatest public support. These results suggest that public preferences over asylum seekers are shaped by sociotropical evaluations of their potential economic contributions, humanitarian concerns about the deservingness of their claims, and anti-Muslim bias. These preferences are similar across respondents of different ages, education levels, incomes, and political ideologies, as well as across the surveyed countries. This public consensus on what types of asylum seekers to accept has important implications for theory and policy.

Europe currently faces the largest refugee crisis since the Second World War. In 2015, Europe received ~1.3 million new asylum claims (1), and many more people are expected to flee to Europe as conflicts in the Middle East and other regions linger on. The number of migrants trying to reach Europe via the Mediterranean Sea who have been reported missing or dead totaled 3771 in 2015 alone (2), and this number is likely to be higher in 2016 as asylum seekers embark on new and even more dangerous routes to Europe after the implementation of the refugee deal between the European Union and Turkey (3).

As more and more people flee war-torn countries and persecution, refugee-receiving democracies must confront a fundamental challenge: how to

honor international commitments—including treaties like the United Nations 1951 Refugee Convention—to process asylum claims and provide shelter to accepted refugees, while at the same time developing asylum policies that are supported by domestic voters.

There is considerable heterogeneity in the exposure of European countries to the asylum crisis (Fig. 1). Whereas some countries, like Germany and Sweden, process a large number of asylum applications per capita, others, like the United Kingdom and Czech Republic, share a comparatively small responsibility. Yet the migrant crisis has been so severe that it has resulted in political conflict and social tensions widely across Europe, including extreme right-wing parties mobilizing citizens around asylum issues (4), frequent arson attacks on asylum centers (5), and the partial closing of Schengen borders.

As the crisis threatens national solidarity, the social contract, and continental unity, European policy-makers face increasing public pressure to find policy solutions. Although public preferences may not always directly translate into policies, a sizable political science literature has shown that, in democratic countries, particularly salient

and high-profile public policies often respond markedly to public opinion (6–8). In the context of this study, a case in point is the recent “Brexit” referendum in the United Kingdom in which the public voted for the United Kingdom to exit the European Union, a decision that has been attributed to rising anti-immigrant backlash in the United Kingdom (9). And whereas public opinion is a crucial factor, a key problem for both academic scholars and policy-makers alike is a lack of knowledge as to why some native-born citizens oppose and others support the welcoming of particular asylum seekers.

A large literature has examined public attitudes toward immigrants (10), ethnic minorities (11), and Muslims (12, 13) in general, but far fewer studies have looked at attitudes toward asylum seekers (14–21). The latter studies have provided important insights into the correlates of anti-asylum seeker sentiment, but either they are limited to particular countries or they rely on observational data from standard survey questions that ask about asylum seekers in general and do not use experiments to differentiate between different types of asylum seekers (22). Furthermore, they have mostly been conducted before the current asylum crisis. There still exists very little systematic and experimental evidence to inform the heated ongoing political debates over asylum policies with the voice of European voters. In particular, we lack a comprehensive assessment that captures which particular types of asylum seekers the European public is willing to accept given the current crisis.

To provide such an assessment, we designed a conjoint experiment and embedded it in a large-scale online public opinion survey that we fielded in 15 European countries (23). We used entropy balancing (24) to reweight our sample data to match the demographic margins from the populations of each country. Details about the sample, design, and statistical analysis can be found in the supplementary materials (SM) (25). All analyses, except otherwise noted, were prespecified in a preregistered analysis plan made available at the Political Science Registered Studies Dataverse (<http://dx.doi.org/10.7910/DVN/YUNKUL>).

Conjoint experiments ask subjects to evaluate hypothetical profiles with multiple, randomly varied attributes and are widely used in marketing and, increasingly, in other social science fields to measure preferences and the relative importance

¹Department of Political Science, Stanford University, Stanford, CA 94305-6044, USA. ²Immigration Policy Lab, Stanford University, Stanford, CA 94305-6044, USA and University of Zurich, 8050 Zurich, Switzerland. ³Graduate School of Business, Stanford University, Stanford, CA 94305-6044, USA. ⁴Department of Government, London School of Economics and Political Science, London WC2A 2AE, UK.

*The authors contributed equally to this work. †Corresponding author. Email: jhain@stanford.edu

of structural determinants of multi-dimensional decision-making (26, 27). Specifically, we used a conjoint experiment to ask 18,000 European eligible voters to evaluate 180,000 profiles of asylum seekers that randomly varied on nine attributes that asylum experts and the previous literature have identified as potentially important (table S1 and fig. S1) (28). This design allows us to test which specific attributes generate public support for or opposition to allowing asylum seekers to stay in the host country and how this willingness varies across different groups of eligible voters, countries, and types of asylum seekers.

The effects of the asylum-seeker attributes on the probability of acceptance pooling across all respondents (model 1 in table S9) are plotted in Fig. 2 (29). The results demonstrate that European voters do not treat all asylum seekers equally. Instead, the willingness to accept asylum seekers varies strongly with the specific characteristics of the claimant. In particular, preferences over asylum seekers appear to be structured by three main factors: economic considerations, humanitarian concerns, and anti-Muslim sentiment.

Asylum seekers who previously worked in higher-skill occupations—such as doctors, teachers, and accountants—are about 13 percentage points, 9 percentage points, and 8 percentage points, respectively, more likely to be accepted compared with asylum seekers who have been previously unemployed. We find a similar but smaller premium of about 5 to 6 percentage points, respectively, for asylum seekers who worked in lower-skill occupations, such as farmers or cleaners, compared with those who were unemployed. Respondents also attach high importance to language skills, such that asylum seekers are about 12 percentage points less likely to be accepted when they do not speak the host-country language than when they speak it fluently. Those who have limited host-country language proficiency face a penalty of 6 percentage points. Moreover, asylum seekers who are close to retirement age (62 years) are about 6 percentage points less likely to be accepted than young applicants (21 years). Overall, these results suggest that evaluations of the expected economic contribution or potential economic burden of asylum seekers play an important role in structuring asylum preferences.

Asylum seekers who apply because of fear of political, religious, or ethnic persecution are about 15 percentage points more likely to be accepted compared with those who migrate to seek better economic opportunities. Asylum seekers are also about 11 percentage points less likely to be accepted when they have major inconsistencies in their asylum testimony, compared with when they

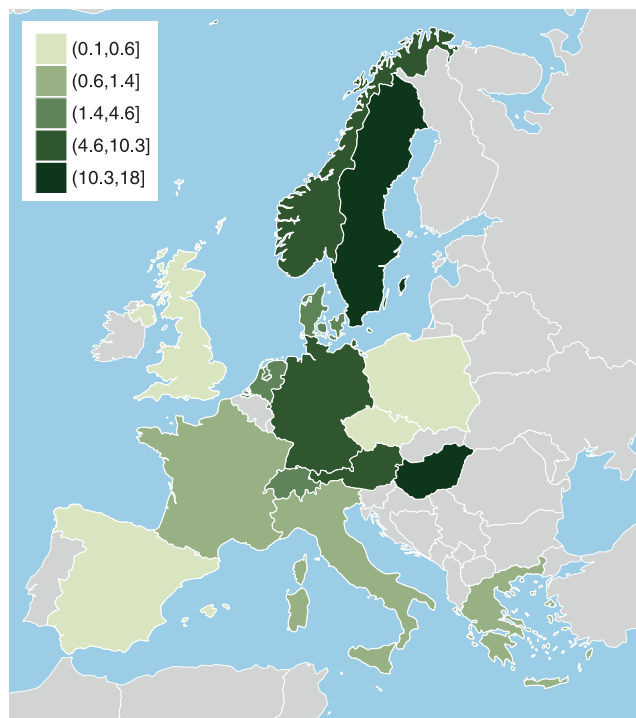


Fig. 1. Asylum applications per 1000 people from the local population, 2015. There is great heterogeneity in the number of asylum applications per capita in 2015 across the surveyed countries: Austria, Czech Republic, Denmark, France, Germany, Greece, Hungary, Italy, Netherlands, Norway, Poland, Spain, Sweden, Switzerland, and United Kingdom. [Data sources (42, 43)]

have no inconsistencies. Moreover, those who have been the victim of torture are about 11 percentage points more likely to be accepted than are those with no special vulnerabilities. Taken together, these results suggest that public preferences are also highly sensitive to humanitarian concerns about the deservingness and legitimacy of the asylum request, as well as the severity of the claimants' vulnerabilities. Moreover, the public is opposed to admitting asylum seekers whose principal motivation is to seek better economic opportunities and who therefore might be regarded as economic migrants who do not meet the legal definition of refugee status according to the 1951 Refugee Convention.

We also find that religion matters: Muslim asylum seekers are about 11 percentage points less likely to be accepted than otherwise similar Christian asylum seekers. This penalty is sizable and larger than the penalty applied to unemployed asylum seekers versus teachers. Moreover, the fact that Christian asylum seekers are only slightly preferred over agnostic asylum seekers suggests that the penalty mostly reflects a strong anti-Muslim bias, rather than a pro-Christian bias. As we show later, this penalty is not uniform across respondents but rather doubles in size for respondents who place themselves on the right of the political spectrum compared with those on the left. These results suggest that anti-Muslim sentiment is a third important factor that structures asylum preferences.

Last, once the other attributes are controlled for, the country of origin of an asylum seeker plays

only a minor role in generating support. Asylum seekers from Kosovo are least likely to be accepted, those from Syria and the Ukraine are most likely to be accepted, and those from Afghanistan, Iraq, Pakistan, and Eritrea fall in between. However, the differences are small in substantive terms; the maximum difference is only 4 percentage points between the most and least popular origin.

Do the effects of the attributes vary across different types of asylum seekers? For instance, based on psychological research on decision-making under conditions of uncertainty (30), we might expect that respondents rely more on their biases when evaluating profiles where the legitimacy of the claim is ambiguous. This suggests an interaction such that the anti-Muslim bias would be strongest when the applicant's asylum testimony has minor inconsistencies, rather than no inconsistencies or major inconsistencies. However, we find no substantively meaningful first-order interactions among any of the conjoint attributes; the lack of interaction suggests that the economic, humanitarian, and religious concerns are powerful determinants of attitudes toward asylum seekers across all types of profiles (figs. S22 to S48 and tables S32 to S61) (37).

How do asylum preferences vary across different types of voters? In order to test for interactions between respondent characteristics and the effects of the asylum-seeker attributes, we stratify the main analysis by voters' political ideology, age, education, and income (Fig. 3). Overall, we find that the effects of the attributes are broadly similar across the different subgroups; this suggests that there is a general consensus—among left- and right-wing, young and old, less and more highly educated, and richer and poorer voters—on which asylum seekers are preferred (table S10). Additional analyses using more fine-grained subgroups yield similarly homogenous results (figs. S5 to S10 and tables S15 to S20).

This effect homogeneity across subgroups also suggests that the concerns about employability are caused by sociotropic economic evaluations, meaning that respondents are concerned about the economic impact on the host country as a whole. This is in contrast to egocentric economic concerns, which pertain to the impact on the respondents' personal economic situation. If evaluations were shaped by egocentric concerns, we would have expected that preferences vary considerably given that different types of asylum seekers will differently affect a respondent's personal economic situation. For example, highly educated respondents should be more concerned about job competition from highly skilled asylum seekers, and less-educated respondents should be more concerned about competition from low-skilled asylum seekers. Similarly, given progressive tax systems, richer respondents should be

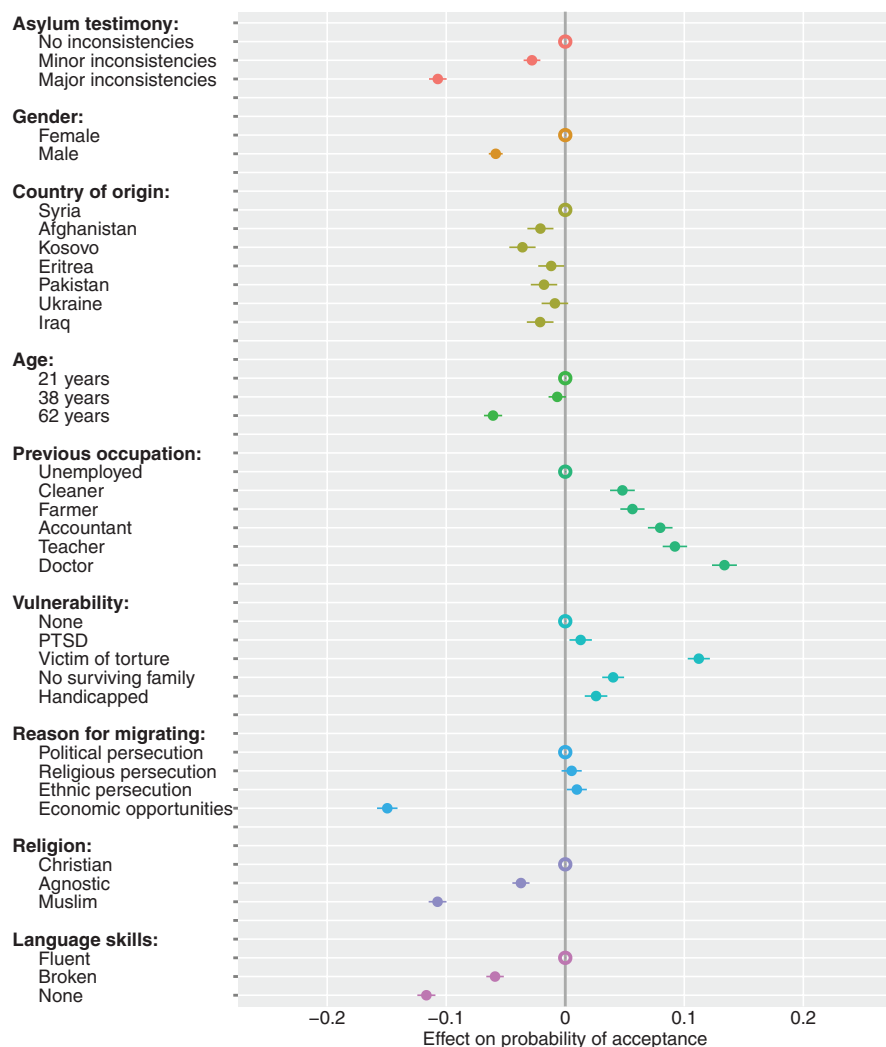


Fig. 2. Effects of asylum-seeker attributes on the probability that respondents accept the asylum seeker. Dots with horizontal lines indicate point estimates with cluster-robust 95% confidence intervals (CI) from linear (weighted) least squares regression. The unfilled dots on the zero line denote the reference category for each asylum-seeker attribute. Table S9 (model 1) displays the underlying regression results.

more concerned about the welfare burden imposed by unemployed asylum seekers than poorer respondents.

There is, however, a notable exception to this effect homogeneity: The top left two panels of Fig. 3 show that respondents on the left exhibit stronger humanitarian concerns and weaker anti-Muslim bias than voters on the right. First, the premium for asylum seekers with special vulnerabilities (e.g., victims of torture) and penalty for asylum seekers who migrated in search of economic opportunities are both larger among voters on the left than among those on the right. For instance, among voters on the right, economically motivated asylum seekers are about 13 percentage points less likely to be accepted than those who migrated for fear of political persecution. In contrast, this effect is 19 percentage points for voters on the left (the difference in effects between the left and the right is significant at $P < 0.0001$). This suggests that, although humanitarian concerns are shared among the left

and the right, those concerns play a somewhat stronger role in structuring attitudes toward asylum seekers for the left. Second, although the anti-Muslim bias exists among both left- and right-wing voters, the bias is about twice as large in the latter group (14 versus 7 percentage points, a difference that is significant at $P < 0.0001$). A more fine-grained analysis (figs. S3 and S4 and tables S13 and S14) shows that the anti-Muslim bias increases roughly monotonically moving from the left to the right of the ideological spectrum (32). Further analysis also shows that anti-Muslim sentiment is virtually constant across respondents with different levels of empathy (fig. S11 and table S21). This suggests that the responses are unlikely to be driven by social desirability bias, given the correlation between empathy and social desirability scales found in psychology research (33, 34).

The 15 surveyed countries exhibit major differences with regard to several potentially relevant factors for shaping domestic asylum preferences,

such as the number of immigrants, the number of asylum applications per capita (compare Fig. 1), the existence of a European Union external border, the generosity of their welfare states, their economic strength and levels of unemployment, and other general political and economic characteristics that have an impact on the number of asylum seekers they can integrate. Despite these differences, the asylum preferences follow a similar pattern across the 15 surveyed countries (fig. S2). The partial exceptions include that the magnitude of the anti-Muslim bias varies somewhat, and the penalty against asylum seekers who migrate for economic reasons is somewhat smaller in poorer countries (e.g., Czech Republic, Greece, Hungary, and Poland) compared with richer countries (e.g., Austria, Denmark, Germany, Netherlands, Norway, Sweden, and Switzerland).

This consensus on what types of asylum seekers are preferred also has cross-country implications for the average number of asylum seekers accepted, based on a dichotomized version of a rating variable that distinguishes between accepted and rejected profiles (table S2). The percentage of asylum seekers accepted by country is shown in Fig. 4. In most countries, the fraction of accepted asylum-seeker profiles is close to the average of 45% accepted in the pooled European sample (35). This suggests that, despite the major differences between the countries, there is a considerable consensus in terms of not only the types but also the overall number of asylum seekers that should be admitted. Furthermore, only a small percentage of respondents—9% overall and less than 14% in every country—categorically rejected all 10 of their asylum-seeker profiles (table S8 and fig. S49).

This study examined the impact of different asylum-seeker attributes on generating public support for granting asylum. We conducted a large-scale conjoint experiment and asked 18,000 voters in 15 European countries to evaluate profiles of asylum seekers that randomly varied on multiple attributes. We find that asylum seekers have a higher probability of being accepted when they are more employable and skilled, have special vulnerabilities, have more consistent asylum claims, and are Christian rather than Muslim. Furthermore, these effects are strikingly similar across sociodemographic subgroups and countries. Additional analysis reported in the SM also reveals that all the findings are similar regardless of whether we use a rating or choice outcome (table S2) to evaluate the asylum-seeker profiles (figs. S16 to S21 and tables S9 and S26 to S31). Finally, the results are similar across all five evaluation tasks asked of each respondent and when comparing respondents above and below the median time of survey completion (this test was not prespecified); this suggests that the results are not diluted by survey fatigue (figs. S14 and S15 and tables S24 and S25).

Although the experimental design of our study (i.e., the randomization of attributes) ensures its internal validity, as with all survey studies, there are potential external validity issues. However, four factors help to alleviate concerns about the

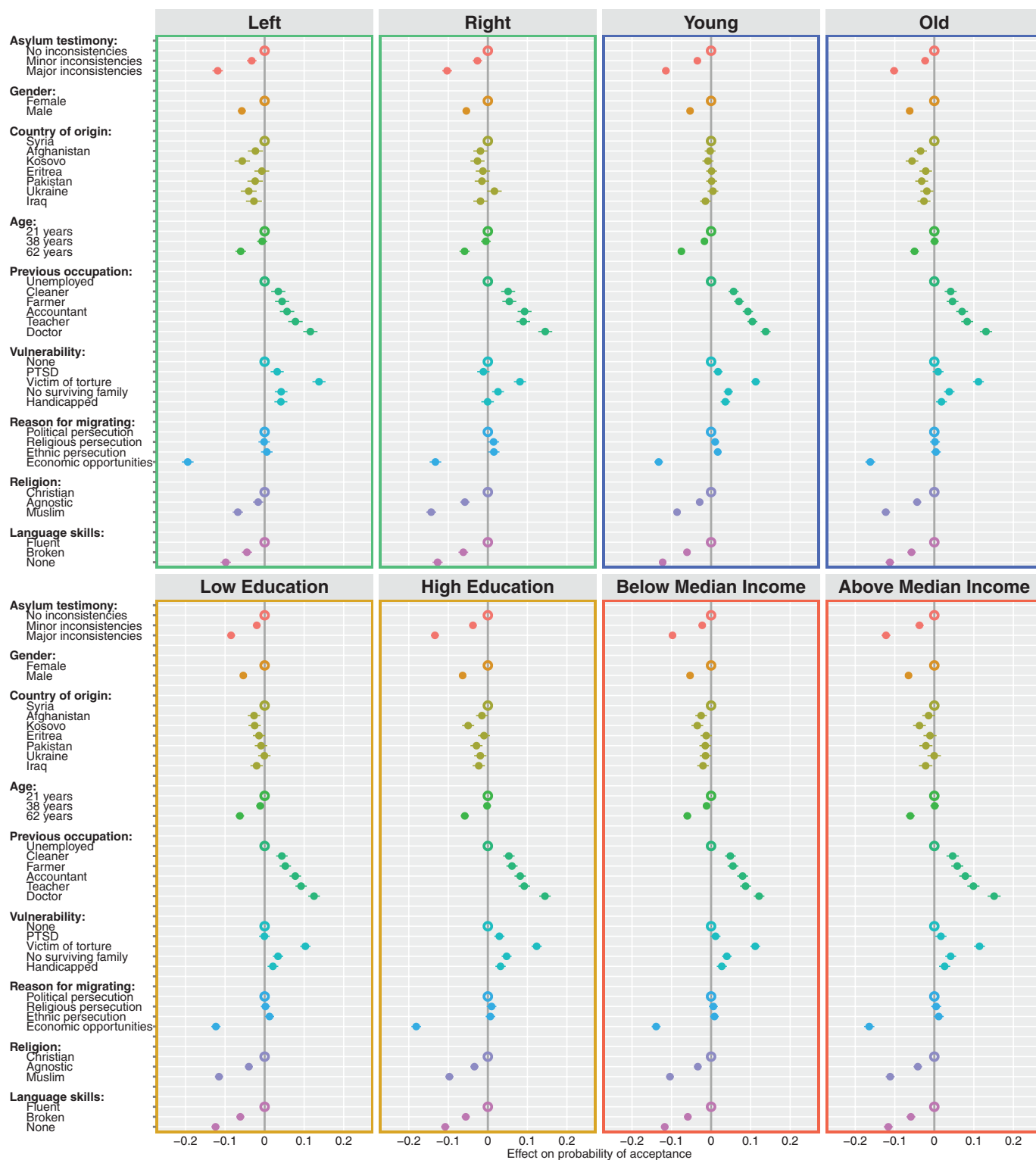


Fig. 3. Effects of asylum-seeker attributes on the probability of accepting the asylum seeker across subgroups of respondents. The effects of the various asylum-seeker attributes are similar across different sociodemographic subgroups, stratified by ideology (top left, green), age (top right, blue), education (bottom left, orange), and income (bottom right, red). Dots with horizontal lines indicate point estimates with cluster-robust 95% CI from linear (weighted) least squares regression. The unfilled dots on the zero line denote the reference category for each asylum-seeker attribute. The test for education and income was not specified in the preanalysis plan. The underlying regression results are displayed in table S10, and how the subset variables were coded is described in table S3.

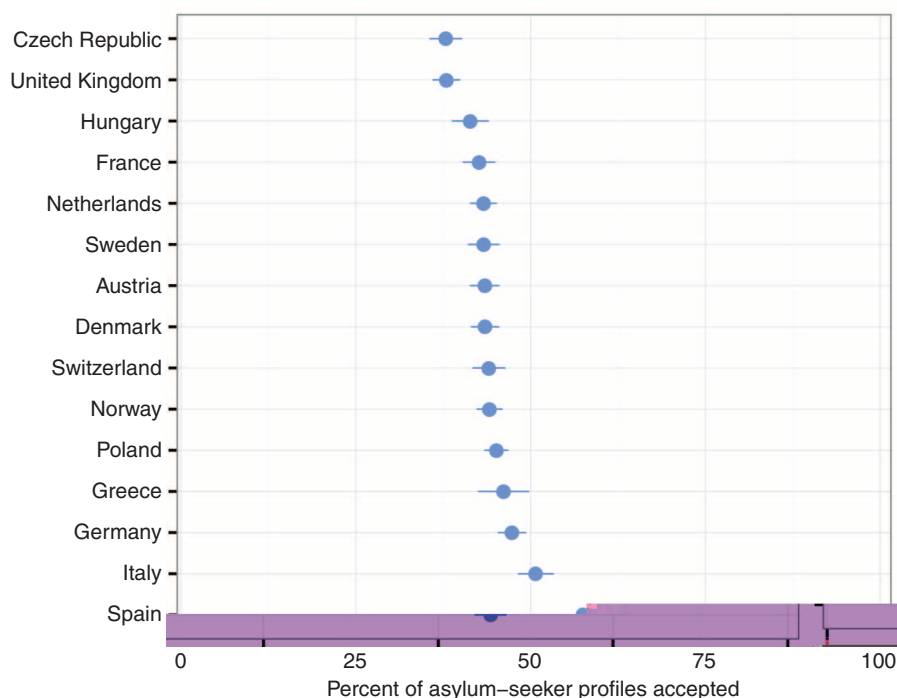


Fig. 4. Percentage of accepted asylum-seeker profiles by country. The percentage of accepted asylum-seeker profiles is similar across countries. Corresponding 95% CI are also shown.

external validity of our study. First, the one external validation test that we are aware of has shown that the paired conjoint design we used can achieve high external validity in reducing social desirability bias and replicating real-world voting behavior (36). Second, the number of profiles that each respondent accepted in their conjoint tasks, based on their ratings of the profiles, is highly correlated with respondents' general attitudes toward asylum seekers as measured by an additional question in our survey that asked respondents whether they want to decrease or increase the number of people granted asylum in their country (37). This suggests that respondents' judgments of individual cases are closely linked to their support for broader asylum policies. Third, given the homogeneity of the results across the countries and subgroups of respondents, it is unlikely that our results would have been substantially different had our sample contained different distributions on age, gender, education, or income—and in fact, the results are similar if we do not use reweighting for the analysis (table S9). Fourth, as already noted, the vast majority of respondents in all surveyed countries neither categorically rejected nor categorically accepted all of their asylum-seeker profiles. These results suggest that our findings on how voters condition their support on the basis of specific asylum-seeker attributes has broadly meaningful implications for European public attitudes toward asylum seekers rather than being applicable only on the margins.

These findings have important implications for our theoretical understanding of public opinion on asylum seekers and migrants more generally. Mirroring the findings from research on

the drivers of general anti-immigrant sentiment, we find strong evidence that sociotropic economic evaluations are shaping attitudes toward asylum seekers. In addition, we also find that humanitarian concerns with regard to asylum seekers' deservingness and vulnerability play a major role. Given that the sizable literature on immigration attitudes has largely ignored humanitarian concerns as a central explanatory factor (38), our results suggest that humanitarian concerns might be particularly important for structuring attitudes toward asylum seekers. Moreover, the finding of general agreement across different subsets of the population on which asylum seekers should be admitted echoes a similar consensus identified in previous research on American attitudes toward immigrants more broadly (39). However, to the extent that the respondents on the left exhibit a weaker anti-Muslim bias and place stronger emphasis on humanitarian considerations, our analysis also discovers new heterogeneity in attitudes toward migrants across the left-right ideological spectrum.

Our study also has important implications for policy. We find mixed evidence on the extent to which public preferences reflect the requirements of international law. It is important to note that all 15 countries included in the study are signatories to the 1951 Refugee Convention. This United Nations treaty commits its parties to granting asylum to persons with legitimate claims, which include asylum seekers who face political, religious, or ethnic persecution in their home countries. In light of these obligations, the results of our study can be interpreted in two ways. On the one hand, the results suggest that European policy-makers

are confronted with a disjuncture between public opinion and international legal norms (40, 41). The fact that our respondents exhibit anti-Muslim bias and a preference for higher employability, even when evaluating legally legitimate asylum seekers who face persecution, is at odds with the legal requirements that asylum not be given on the basis of religion or professional skills. On the other hand, the results reveal that humanitarian concerns have a pronounced effect, such that asylum seekers who face persecution, have consistent asylum testimonies, and have special vulnerabilities are substantially more likely to be accepted. Most important, these preferences are widely shared across countries and apply across all types of asylum seekers, regardless of their religion and employability. This suggests that the public has partially internalized the central pillars of international refugee law.

The results also inform the ongoing debate over how to resolve the current refugee crisis. In particular, they illuminate both challenges and opportunities for policy-makers who are struggling to meet their legal responsibilities to protect refugees while simultaneously respecting the public will on this salient and divisive issue. The public's strong anti-Muslim bias and preference for highly skilled asylum seekers who can speak the language of the host country points to a mounting challenge for solving the current crisis and successfully integrating asylum seekers, given that most asylum seekers currently originate from Muslim-majority countries and may lack the desired professional and language skills. Yet at the same time, the fact that the European public shares common humanitarian and sociotropic concerns suggests a clear narrative to increase support for accepting refugees. If the goal is to alleviate the social tensions of the current refugee crisis and generate more public acceptance of asylum seekers, European policy-makers have an opportunity to highlight refugees' deservingness and vulnerability, as well as their economic contributions to their host societies.

REFERENCES AND NOTES

1. United Nations High Commissioner for Refugees (UNHCR), "Global trends: Forced displacement in 2015" (UNHCR, 2016); www.unhcr.org/statistics/unhcrstats/576408cd7/unhcr-global-trends-2015.html.
2. UNHCR, "Refugees/migrants emergency response — Mediterranean" (UNHCR, 2016); <http://data.unhcr.org/refugees/migrants/emergency-response/mediterranean/regional.php>.
3. UNHCR, "UNHCR redefines role in Greece as EU-Turkey deal comes into effect" (UNHCR, 2016); www.unhcr.org/56f10d049.html.
4. A. Steinmayr, "Exposure to refugees and voting for the far-right: (Unexpected) results from Austria" (IZA discussion paper, Institute for the Study of Labor, 2016); <http://ftp.iza.org/dp9790.pdf>.
5. Bundeskriminalamt, "Anzahl der politisch motivierten Gewalttaten mit rechtsextremistischem Hintergrund in Deutschland von 2009 bis 2015 nach Art des Delikts" [Bundeskriminalamt (German Federal Criminal Police Office), 2016]; <http://de.statista.com/statistik/daten/studie/4690/umfrage/rechtsextremismus-entwicklung-der-gewalttaten-seit-2006>.
6. J. A. Stimson, M. B. MacKuen, R. S. Erikson, *Am. Polit. Sci. Rev.* **89**, 543–565 (1995).
7. P. Burstein, *Polit. Res. Q.* **56**, 29–40 (2003).
8. J. R. Lax, J. H. Phillips, *Am. Polit. Sci. Rev.* **103**, 367–386 (2009).

9. C. Calhoun, *New Perspect. Q.* **33**, 50 (2016).
10. J. Hainmueller, D. J. Hopkins, *Annu. Rev. Polit. Sci.* **17**, 225–249 (2014).
11. S. A. Weldon, *Am. J. Polit. Sci.* **50**, 331–349 (2006).
12. K. O. Kalkan, G. C. Layman, E. M. Uslaner, *J. Polit.* **71**, 847–862 (2009).
13. J. Sides, K. Gross, *J. Polit.* **75**, 583–598 (2013).
14. K. Betts, *People Place* **9**, 34 (2001).
15. M. Verkuyten, *Soc. Justice Res.* **17**, 293–314 (2004).
16. E. Ivarsson, *J. Elections Public Opin. Parties* **15**, 21–45 (2005).
17. A. E. Kessler, G. P. Freeman, *J. Common Mark. Stud.* **43**, 825–850 (2005).
18. A. Pedersen, J. Attwell, D. Heveli, *Aust. J. Psychol.* **57**, 148–160 (2005).
19. W. R. Louis, J. M. Duck, D. J. Terry, R. A. Schuller, R. N. Lalonde, *Eur. J. Soc. Psychol.* **37**, 53–73 (2007).
20. A. M. Nickerson, W. R. Louis, *J. Appl. Soc. Psychol.* **38**, 796–817 (2008).
21. F. H. McKay, S. L. Thomas, S. Kneebone, *J. Refug. Stud.* **25**, 113–133 (2012).
22. Pew Research Center, “Europeans fear wave of refugees will mean more terrorism, fewer jobs” (Pew, July 2016); www.pewglobal.org/2016/07/11/europeans-fear-wave-of-refugees-will-mean-more-terrorism-fewer-jobs.
23. The countries included in the study are Austria, the Czech Republic, Denmark, France, Germany, Greece, Hungary, Italy, the Netherlands, Norway, Poland, Spain, Sweden, Switzerland, and the United Kingdom. These countries were chosen to represent a diversity of national characteristics, including coastal and noncoastal border countries, large and small economies, countries with major and minor political influence, and countries with varying degrees of popularity as asylum-seeker destinations.
24. J. Hainmueller, *Polit. Anal.* **20**, 25–46 (2012).
25. Materials and Methods are available as SM on Science Online.
26. P. E. Green, V. R. Rao, *J. Mark. Res.* **8**, 355–363 (1971).
27. J. Hainmueller, D. J. Hopkins, T. Yamamoto, *Polit. Anal.* **22**, 1–30 (2014).
28. Supplementary figures and tables (e.g., table S1), are available as SM on Science Online.
29. In addition, the results for various subsamples can be found in the SM (tables S10 to S61).
30. J. F. Dovidio, S. L. Gaertner, *Psychol. Sci.* **11**, 315–319 (2000).
31. These tests were not prespecified.
32. The results are similar regardless of whether we use the respondents’ self-reported left-right ideological placement or the ideological placement of the political parties with which they identify. Tables S3 and S4 contain the details on these two ideology measures.
33. N. Eisenberg et al., *J. Pers. Soc. Psychol.* **66**, 776–797 (1994).
34. A. Preti et al., *Cogn. Neuropsychiatry* **16**, 50–70 (2011).
35. The asylum-seeker profiles were generated randomly, according to the experimental design; thus, the distribution of profiles is similar in each country in expectation. Therefore, the differences in the percentage of accepted profiles measures cross-country differences in the general level of support for accepting asylum seekers, and this measure is not confounded by the differences in the actual pools of asylum seekers in each country. This measure should not be interpreted as the level of support for the country-specific pool of asylum seekers.
36. J. Hainmueller, D. Hangartner, T. Yamamoto, *Proc. Natl. Acad. Sci. U.S.A.* **112**, 2395–2400 (2015).
37. See “General attitudes toward asylum seekers” in the Supplementary Text for more details.
38. B. J. Newman, T. K. Hartman, P. L. Lown, S. Feldman, *Br. J. Polit. Sci.* **45**, 583–607 (2015).
39. J. Hainmueller, D. J. Hopkins, *Am. J. Pol. Sci.* **59**, 529–548 (2015).
40. Some scholars of migration policy, e.g. (41), have used the term “liberal constraint” to refer to the inability of policy-makers in liberal democratic countries to cater to anti-immigration and anti-asylum public preferences, a constraint that is the result of the international norms and agreements to which those states are committed.
41. C. Boswell, *Int. Migr. Rev.* **41**, 75–100 (2007).
42. Eurostat, “Asylum and first time asylum applicants by citizenship, age, and sex” ([migr_asyappctzm](http://ec.europa.eu/eurostat/data/database)) (European

Commission, Brussels, 2016); http://ec.europa.eu/eurostat/statistics-explained/index.php/Asylum_statistics.
 43. Eurostat, Population (under demography and population) (European Commission, Brussels, 2016); <http://ec.europa.eu/eurostat/data/database>.

ACKNOWLEDGMENTS

We acknowledge funding from the Swiss National Science Foundation (grant 100017_159820) that enabled data collection and the Ford Foundation for operational support of the Immigration Policy Lab. For helpful advice, we thank E. Avina, M. Bechtel, S. Chauchard, T. Huddleston, S. Kurer, D. Laitin, D. Lawrence, L. Schmid, S. Schütz, L. Schwab, and J. Spiring. For replication code and data, see Harvard Dataverse (<http://dx.doi.org/10.7910/DVN/KLOFDF>). A preregistered analysis plan is available at the Political

Science Registered Studies Dataverse; <http://dx.doi.org/10.7910/DVN/YUNKUL>.

SUPPLEMENTARY MATERIALS

www.sciencemag.org/content/354/6309/217/suppl/DC1
 Materials and Methods
 Supplementary Text
 Figs. S1 to S49
 Tables S1 to S61
 References (44–48)

24 May 2016; accepted 6 September 2016
 Published online 22 September 2016
 10.1126/science.aag2147

MICROBIAL PHYSIOLOGY

Methane production from coal by a single methanogen

Daisuke Mayumi,^{1*} Hanako Mochimaru,^{1*} Hideyuki Tamaki,^{2*} Kyosuke Yamamoto,² Hideyoshi Yoshioka,¹ Yuichiro Suzuki,¹ Yoichi Kamagata,^{2†} Susumu Sakata^{1†}

Coal-bed methane is one of the largest unconventional natural gas resources. Although microbial activity may greatly contribute to coal-bed methane formation, it is unclear whether the complex aromatic organic compounds present in coal can be used for methanogenesis. We show that deep subsurface-derived *Methermicoccus* methanogens can produce methane from more than 30 types of methoxylated aromatic compounds (MACs) as well as from coals containing MACs. In contrast to known methanogenesis pathways involving one- and two-carbon compounds, this “methoxytrophic” mode of methanogenesis couples O-demethylation, CO₂ reduction, and possibly acetyl-coenzyme A metabolism. Because MACs derived from lignin may occur widely in subsurface sediments, methoxytrophic methanogenesis would play an important role in the formation of natural gas not limited to coal-bed methane and in the global carbon cycle.

Coal-bed methane (CBM), a form of natural gas distributed in coal seams or adjacent sandstones, is a relatively untapped energy source with a large potential: The global reserves in 2014 were estimated at 50 trillion m³, equivalent to 11% of conventional natural gas resources (1). Large-scale CBM production has been implemented in the United States, Canada, Australia, and other countries worldwide. The contribution of biogenic methane to CBM is quite large (2, 3); geochemical studies have estimated that 40% of CBM produced in the United States is of microbial origin (4). Live microbial communities are present in coal seams and are associated with methanogenesis from coal in subsurface environments (5–10). Geomicrobiological studies have shown that enhanced CBM production in coal seams might be achieved by the stimulation of methanogenic activity (11). Although extensive efforts have been made to de-

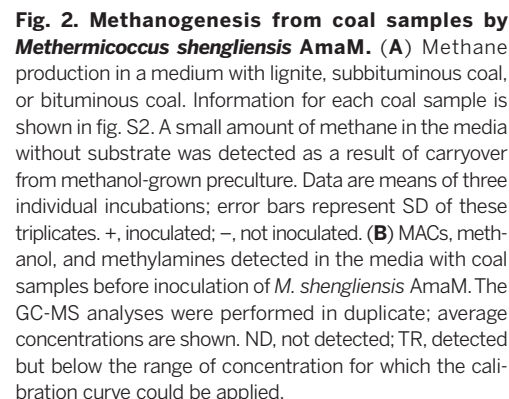
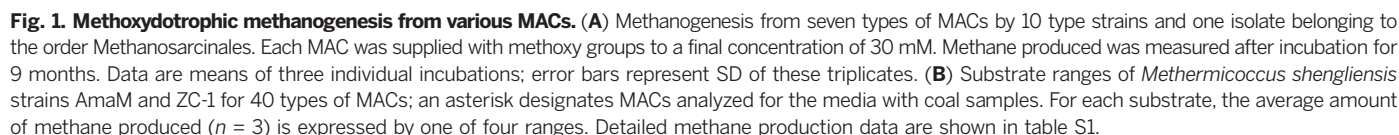
velop this technology, very little is known about what components of coal can be used for methanogenesis and which microorganisms possess the metabolic capabilities to do so.

Coal is an extremely complex and heterogeneous material whose structure consists of single and condensed aromatic rings (12, 13). Aromatic compounds in coal are derived from lignin monolignols and are often substituted with hydroxyl, methoxy, and carboxyl groups (14, 15). Methoxy groups are especially abundant and common in immature coal (14, 16). Because methanogenesis from coal tends to occur in immature coal rather than in mature coal (4, 17), coal-bed microorganisms may produce methane from methoxy groups. Methanogenic microorganisms in CBM fields are commonly dominated by methylotrophic methanogens belonging to the archaeal order Methanosarcinales (5, 18, 19). The methylotrophic methanogens are capable of using methyl compounds such as methanol, methylamines, and/or dimethylsulfide (20), but it is unclear whether they can directly use methoxylated aromatic compounds (MACs) as substrates.

To investigate the possibility of MACs as substrates for methylotrophic methanogens, we tested the methane production ability of one archaeal isolate (*Methermicoccus shengliensis* strain AmaM)

¹Institute for Geo-Resources and Environment, Geological Survey of Japan, National Institute of Advanced Industrial Science and Technology (AIST), 1-1-1 Higashi, Tsukuba 305-8567, Japan. ²Bioproduction Research Institute, AIST, 1-1-1 Higashi, Tsukuba 305-8566, Japan.

*These authors contributed equally to this work. †Corresponding author. Email: y.kamagata@aist.go.jp (Y.K.); su-sakata@aist.go.jp (S.S.)



obtained from a high-temperature deep subsurface oil reservoir in this study (fig. S1), and of 10 type strains belonging to the genera *Methanosarcina*, *Methanobolus*, *Methanohalophilus*, *Methanosaeta*, *Methanomicrococcus*, *Methanococcoides*, *Methanohalobium*, *Methanosalsum*, *Methanomethylovorans*, and *Methermicoccus* (i.e., *M. shengliensis* strain ZC-1) (21) in the order Methanosarcinales using seven types of MACs (2-methoxy-benzoate, 3-methoxy-benzoate, 4-methoxy-benzoate, 3,4,5-trimethoxy-benzoate, 3,4,5-trimethoxy-cinnamate, 1,2,3-trimethoxy-benzene, and 3,4,5-trimethoxy-benzylalcohol) as substrates. We only observed substantial methane production in the incubation of *Methermicoccus shengliensis* strains AmaM and ZC-1 with seven and six types of MACs, respectively (Fig. 1A). To investigate their substrate ranges, we incubated the strains AmaM and ZC-1 with 40 commercially available MACs. The results showed that the strains AmaM and ZC-1 used 35 and 34 types of MACs, respectively (Fig. 1B and table S1).

To confirm whether these “methoxydrotrophic methanogens” could produce methane from coal, we incubated *M. shengliensis* AmaM with coals of different maturity levels: lignite (most immature) and subbituminous and bituminous (most mature) coals (fig. S2). A small but substantial amount of methane (7.5 to 10.8 $\mu\text{mol/g-coal}$) was produced in all of the three lignites (L-A, L-B, and L-C) and even in the subbituminous coal S-A and the bituminous coal B-A (Fig. 2A). *M. shengliensis* AmaM used MACs, methanol, and methylamines as substrates for methanogenesis (Fig. 1 and fig. S1), which suggests that coal may have provided some of these substrates. We analyzed growth media with coal before incubation for the 26 types of MACs usable for *M. shengliensis* AmaM (marked with asterisks in Fig. 1B) by gas chromatography-mass spectrometry (GC-MS). We detected either two or three types of methoxylated benzoates in each medium from which methane production was observed (Fig. 2B). The total concentrations of methanol and methylamines as well as of MACs detected in the media were too low to account for the concentrations of methane produced in the coal cultures alone (Fig. 2); for example, in bituminous coal culture B-A, 0.09 $\mu\text{mol/g-coal}$ of MACs was detected but 9.39 $\mu\text{mol/g-coal}$ of methane was

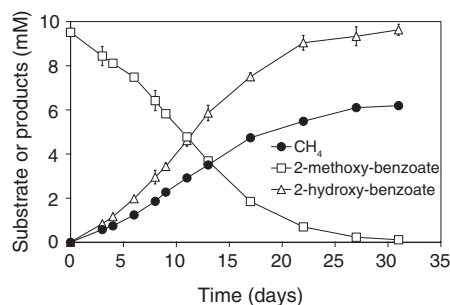


Fig. 3. Methanogenesis from 2-methoxy-benzoate by *Methermicoccus shengliensis* AmaM. All symbols represent means of three individual incubations; error bars represent SD of these triplicates.

produced. This result suggests that *M. shengliensis* AmaM produced methane from undetectable MACs dissolved in the media as well as those chemically or physically bound to the coal surface. This was supported by the ability of *M. shengliensis* AmaM to use a wide variety of MACs (>30 types of MACs) for methanogenesis (Fig. 1B).

If methoxydrotrophic methanogenesis proceeds in analogy to methylotrophic methanogenesis, it is expected from stoichiometry that $\frac{3}{4}$ mol of methane is produced from 1 mol of the methoxy group ($4\text{Ar-OCH}_3 + 2\text{H}_2\text{O} \rightarrow 4\text{Ar-OH} + 3\text{CH}_4 + \text{CO}_2$, where Ar denotes any aromatic group). During incubation with 2-methoxy-benzoate, *M. shengliensis* AmaM produced methane and 2-hydroxy-benzoate with a decrease in 2-methoxy-benzoate (Fig. 3). The 2-hydroxy-benzoate produced was nearly equivalent to the 2-methoxy-benzoate consumed, which suggests that *M. shengliensis* AmaM produced methane via O-demethylation of the methoxy group.

We conducted stable isotope tracer experiments to elucidate the mode of metabolism in the methoxydrotrophic methanogenesis. In the incubation of *M. shengliensis* AmaM with 2-[^{13}C]methoxy-benzoate, the ^{13}C contents of methane increased with increasing contents of ^{13}C at the methoxy group (Fig. 4A), indicating that the methoxy carbon was incorporated into methane. However, the incorporation efficiency from the methoxy group to methane, estimated as the slope of the regression line between the ^{13}C contents of methane and the methoxy group, was 63.6% (Fig. 4A). By contrast, in the incubation with [^{13}C]methanol, we estimated that nearly all (96.4%) of the methane carbon came from the substrate methanol. This implies that additional carbon (other than methoxy carbon) is incorporated into methane during MACs-driven methanogenesis.

To identify this additional carbon, we evaluated whether CO_2 was incorporated into methane via CO_2 reduction. We incubated *M. shengliensis* AmaM with 2-methoxy-benzoate or methanol in the medium amended with [^{13}C]bicarbonate.

Although the ^{13}C contents of methane increased only slightly in the presence of methanol, those of methane in the presence of 2-methoxy-benzoate increased far more substantially (Fig. 4B), indicating that CO_2 is also incorporated into methane via CO_2 reduction in methoxydrotrophic methanogenesis. The incorporation efficiency from CO_2 into methane, estimated as the slope of the regression line (Fig. 4B), was 29.6%. Considering that the incorporation efficiency from the methoxy group to methane is 63.6% (Fig. 4A), approximately one-third of methane carbon is derived from CO_2 and two-thirds of methane carbon from the methoxy group. In the incubation of *M. shengliensis* AmaM with a variety of coals in the presence of [^{13}C]bicarbonate, we observed the production of highly ^{13}C -enriched methane, which indicates that methane produced from coal was mostly derived from MACs (fig. S3).

Further tracer experiments incubating *M. shengliensis* AmaM with 2-methoxy-benzoate in the medium amended with 2-[^{13}C]acetate revealed a small but substantial incorporation of the acetate methyl carbon into methane (fig. S4). The acetate concentration in the medium did not change during growth, implying no intentional uptake of extracellular acetate through acetoclastic methanogenesis. We therefore infer that acetyl-coenzyme A (CoA) could be a catabolic intermediate in the methoxydrotrophic methanogenesis. *M. shengliensis* AmaM genes encode acetyl-CoA synthesis, acetyl-CoA oxidation, and CO_2 -reducing methanogenesis, but its genome lacks known acetogen-associated genes for O-demethylation of the methoxy group (e.g., Mtv system) (22, 23) and electron transport systems (e.g., Rnf, complete Fpo complex, etc.) (20) necessary for conventional methanogenesis (table S2). Although details of the metabolic pathway in the methoxydrotrophic methanogenesis remain elusive, all the results indicate that the mode of metabolism is clearly different from the conventional methylotrophic methanogenesis.

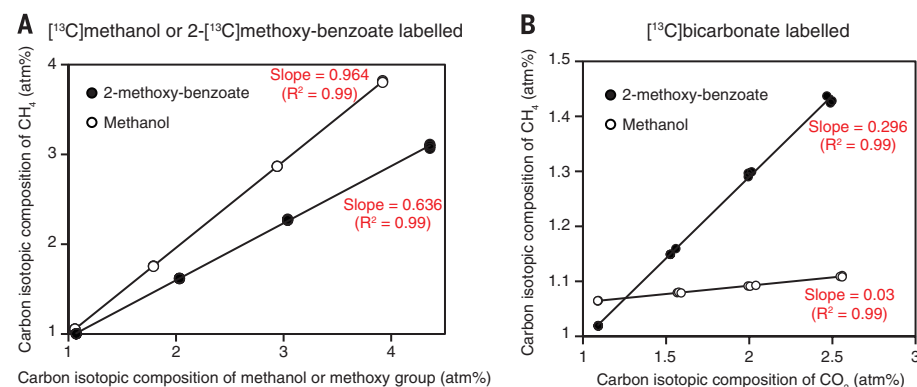


Fig. 4. Stable isotope tracer experiments to elucidate the mode of metabolism in methoxydrotrophic methanogenesis. (A) Carbon isotopic relationship between methane produced by *M. shengliensis* AmaM and either methanol or the methoxy group of 2-methoxy-benzoate added to the media. The slopes of the regression lines show the efficiency of carbon incorporation from each substrate into methane. (B) Carbon isotopic relationship between methane produced from either methanol or 2-methoxy-benzoate and carbon dioxide. The slopes of the regression lines show the efficiency of carbon incorporation from carbon dioxide into methane. Each symbol represents one of three individual incubations.

Our finding that MACs serve as a direct substrate for methanogens may not be limited to coal-bed environments. In the deep subsurface, MACs are contained in sedimentary organic matter derived from lignin in higher plants, namely kerogen, with quantitative variation depending on the maturity (24). In fact, alkyl-methoxyphenols with a short C₁-C₃ chain have been detected in the pyrolysates of immature kerogen extracted from a Cretaceous (Cenomanian) black shale (25). Kerogen is ubiquitous in sediments and accounts for most of the organic matter in subsurface environments (26). Microorganisms from the genus *Methermicoccus* and related clones have often been detected in deep subsurface environments worldwide (fig. S5). Methoxydotrophic methanogenesis may therefore play an important role in the biogeochemical carbon cycle in Earth as well as in the formation of biogenic gas, which accounts for more than 20% of natural gas resources, including CBM (27).

REFERENCES AND NOTES

1. World Energy Outlook 2015 (International Energy Agency, 2015).
2. D. Strapoć, M. Mastalerz, C. Eble, A. Schimmelmann, *Org. Geochem.* **38**, 267–287 (2007).
3. T. Thielemann, B. Cramer, A. Schippers, *Org. Geochem.* **35**, 1537–1549 (2004).
4. D. Strapoć et al., *Annu. Rev. Earth Planet. Sci.* **39**, 617–656 (2011).
5. S. Shimizu et al., *Geobiology* **5**, 423–433 (2007).
6. M. S. Green, K. C. Flanagan, P. C. Gilcrease, *Int. J. Coal Geol.* **76**, 34–45 (2008).
7. S. H. Harris, R. L. Smith, C. E. Barker, *Int. J. Coal Geol.* **76**, 46–51 (2008).
8. M. Krüger et al., *Geomicrobiol. J.* **25**, 315–321 (2008).
9. T. J. Penner, J. M. Foght, K. Budwill, *Int. J. Coal Geol.* **82**, 81–93 (2010).
10. F. Inagaki et al., *Science* **349**, 420–424 (2015).
11. D. Ritter et al., *Int. J. Coal Geol.* **146**, 28–41 (2015).
12. D. W. van Krevelen, *Coal: Typology, Chemistry, Physics, Constitution* (Elsevier, 1993).
13. M. Vandenbroucke, C. Largeau, *Org. Geochem.* **38**, 719–833 (2007).
14. S. A. Stout, J. J. Boon, W. Spackman, *Geochim. Cosmochim. Acta* **52**, 405–414 (1988).
15. H. A. Stafford, *Phytochemistry* **27**, 1–6 (1988).
16. P. G. Hatcher, D. J. Clifford, *Org. Geochem.* **27**, 251–274 (1997).
17. E. J. P. Jones et al., *Int. J. Coal Geol.* **76**, 138–150 (2008).
18. H. Guo et al., *Appl. Microbiol. Biotechnol.* **96**, 1587–1597 (2012).
19. D. Strapoć, M. Ashby, L. Wood, R. Levinson, B. Huizinga, in *Applied Microbiology and Molecular Biology in Oilfield Systems*, C. Whitby, T. Skovhus, Eds. (Springer, 2010), chap. 25.
20. R. K. Thauer, A.-K. Kaster, H. Seedorf, W. Buckel, R. Hedderich, *Nat. Rev. Microbiol.* **6**, 579–591 (2008).
21. L. Cheng et al., *Int. J. Syst. Evol. Microbiol.* **57**, 2964–2969 (2007).
22. E. Pierce et al., *Environ. Microbiol.* **10**, 2550–2573 (2008).
23. S. W. Ragsdale, E. Pierce, *Biochim. Biophys. Acta* **1784**, 1873–1898 (2008).
24. J. W. De Leeuw, C. Largeau, in *Organic Geochemistry*, M. H. Engel, S. A. Macko, Eds. (Plenum, 1993), chap. 2.
25. V. Salmon et al., *Org. Geochem.* **27**, 423–438 (1997).
26. B. Durand, *Kerogen, Insoluble Organic Matter from Sedimentary Rocks* (Editions Technip, 1980), chap. 1.
27. B. J. Katz, *Open Geol. J.* **5**, 75–83 (2011).

ACKNOWLEDGMENTS

We thank Japan Petroleum Exploration Co., Ltd. (JAPEx) for providing samples from an oil reservoir; F. Nozawa, K. Shuin, Y. Shinotsuka, T. Ujii, and X. Meng for technical support;

and M. Nobu for valuable comments. Supported by JSPS KAKENHI grants JP26709070, JP25289333, JP26710012, and JP26106004. *M. shengliensis* strain AmaM has been deposited as accession number NBRC 112467 in the Biological Resource Center, National Institute of Technology and Evaluation (NBRC). Genomic data of *M. shengliensis* strain AmaM are available in the Integrated Microbial Genomes system of the U.S. Department of Energy Joint Genome Institute with ID no. 2516653088 (Gold Project ID: Gp0021722).

jishaSG

GLOBAL CLIMATE CHANGE

Impact ejecta at the Paleocene-Eocene boundary

Morgan F. Schaller,^{1*} Megan K. Fung,¹ James D. Wright,² Miriam E. Katz,¹ Dennis V. Kent^{2,3}

Extraterrestrial impacts have left a substantial imprint on the climate and evolutionary history of Earth. A rapid carbon cycle perturbation and global warming event about 56 million years ago at the Paleocene-Eocene (P-E) boundary (the Paleocene-Eocene Thermal Maximum) was accompanied by rapid expansions of mammals and terrestrial plants and extinctions of deep-sea benthic organisms. Here, we report the discovery of silicate glass spherules in a discrete stratigraphic layer from three marine P-E boundary sections on the Atlantic margin. Distinct characteristics identify the spherules as microtektites and microkrystites, indicating that an extraterrestrial impact occurred during the carbon isotope excursion at the P-E boundary.

Ejecta from known impact strewn fields have common features that provide useful criteria for identifying previously undiscovered impact ejecta in the geologic record. An ejecta deposit typically results from an air-fall event and occurs in a discrete stratigraphic layer. If spherules are present, they generally are glasses (microtektites) and may contain crystallites (microkrystites), both of which have characteristic morphologies and may be either solidified melt ejecta or vapor condensates (1–3). Microkrystites show distinct internal crystallite textures that indicate rapid quenching from high temperature and, if they formed as a vapor condensate, they can be enriched in projectile material (3). Microtektites that form as melt droplets solidify at slightly lower temperatures and are more likely to be vesicular; they may contain inclusions of high-temperature components such as lechatelierite, a quartz glass that solidifies above 1750°C (4, 5). Shock-metamorphosed grains can be associated with microtektites but are not uniformly distributed throughout a strewn field. For example, the presence and abundance of shocked grains is spatially heterogeneous in the widespread Australasian strewn field [for which an impact crater has yet to be identified, despite being the largest and youngest Cenozoic tektite event at 0.8 million years ago (Ma)]. The Ivory Coast strewn field (next youngest

SUPPLEMENTARY MATERIALS

www.sciencemag.org/content/354/6309/222/suppl/DC1
Materials and Methods
Figs. S1 to S5
Tables S1 and S2
References (28–32)

12 May 2016; accepted 29 August 2016
10.1126/science.aaf8821

at 1.1 Ma) that emanated from Bosumtwi crater contains (micro)tektites but no shocked mineral grains [see (6) for review].

We examined three marine Paleocene-Eocene (P-E) boundary sections that encompass the onset of the carbon isotope excursion (CIE) that defines the P-E boundary (7) (Fig. 1): continental shelf sites Wilson Lake B (39.6598°N, 75.0472°W) and Millville [Ocean Drilling Program (ODP) Leg 174AX; 39.4046°N, 75.0889°W] (8), where the onset of the CIE coincides with the base of the thick Marlboro Clay unit of the Salisbury Embayment, and pelagic sediments at ODP Hole 1051B at Blake Nose (30.0531°N, 76.3578°W, water depth 1980.6 m) (9). To constrain the stratigraphic level of the CIE onset, we use detailed bulk sediment carbonate isotope records from Wilson Lake B and Millville (10) and Hole 1051B (11). We also report preliminary data from an exposure of the Marlboro Clay near Medford, New Jersey, to eliminate the possibility of spurious drilling-induced contamination as the source for the spherules [see (12)].

At the Wilson Lake B and Millville shelf localities, as well as Hole 1051B, peak spherule abundance occurs close to the P-E boundary as constrained by the $\delta^{13}\text{C}$ decrease in bulk sediment (Fig. 1). Spherules are found over a ~20-cm interval in each case, with the number of spherules increasing sharply up-section from zero below to a peak at or close to the P-E boundary. Maximum abundances in the >63- μm size fraction are between 2.5 and 3 spherules per g at Wilson Lake B and Millville and 4 spherules per g at Hole 1051B, followed by a gradual decline in abundance to zero over ~10 cm. At Wilson Lake B and Millville, the peak spherule abundance coincides with the

¹Earth and Environmental Sciences, Rensselaer Polytechnic Institute (RPI), Troy, NY 12180, USA. ²Earth and Planetary Sciences, Rutgers University, Piscataway, NJ 08854, USA.

³Lamont-Doherty Earth Observatory (LDEO), Columbia University, Palisades, NY 10964, USA.

*Corresponding author. Email: schall@rpi.edu

basal contact of the Marlboro Clay, which is gradational with some reworking of the underlying Vincentown Formation facies.

These abundances are similar to impact spherule abundances in distal ejecta layers linked to other extraterrestrial impact events, such as the Late Eocene clinopyroxene (cpx)-bearing spherule layer associated with the Popigai impact crater (13–15). Late Eocene cpx spherules that are found in ODP Site 738 in the southern Indian Ocean [~ 2 spherules per g ($>150\ \mu\text{m}$)], in ODP Site 689 in the Southern Ocean (~ 5 to 6 spherules per g ($>63\ \mu\text{m}$)) [see (13) for review], and at Massignano, Italy [~ 4 spherules per g ($>150\ \mu\text{m}$)] (16) show concentrations similar to ours.

The glassy spherules from Wilson Lake B and Millville range from 65 to 500 μm in diameter (average 302 μm), whereas those at Hole 1051B average 274 μm in diameter. They have generally spherical and rotational morphologies, as well as other characteristics of splash-form microtektites (1, 17) (Fig. 2), and are occasionally colorless, translucent green, or dark-brown/black. The spherules often have surface pits (Fig. 2, A and C) and in some cases microcraters (Fig. 2G and fig. S7), indicating relative velocities high enough to fracture the spherules on impact with one another or other objects after solidification. Such microcraters would be an unexpected feature of volcanic spherules. There are also occasional dumbbell forms and smaller spherules accreted to larger ones (Fig. 2F), often of different chemical composition (Fig. 3E), suggesting that they were sintered to one another in a molten form and quenched

rapidly. We conclude that the stratigraphic distribution and morphologies of the spherules are wholly consistent with the expected manifestation of an air-fall sedimentary event such as an impact ejecta bed, modified by minor and typical postdepositional bioturbation of marine sediments.

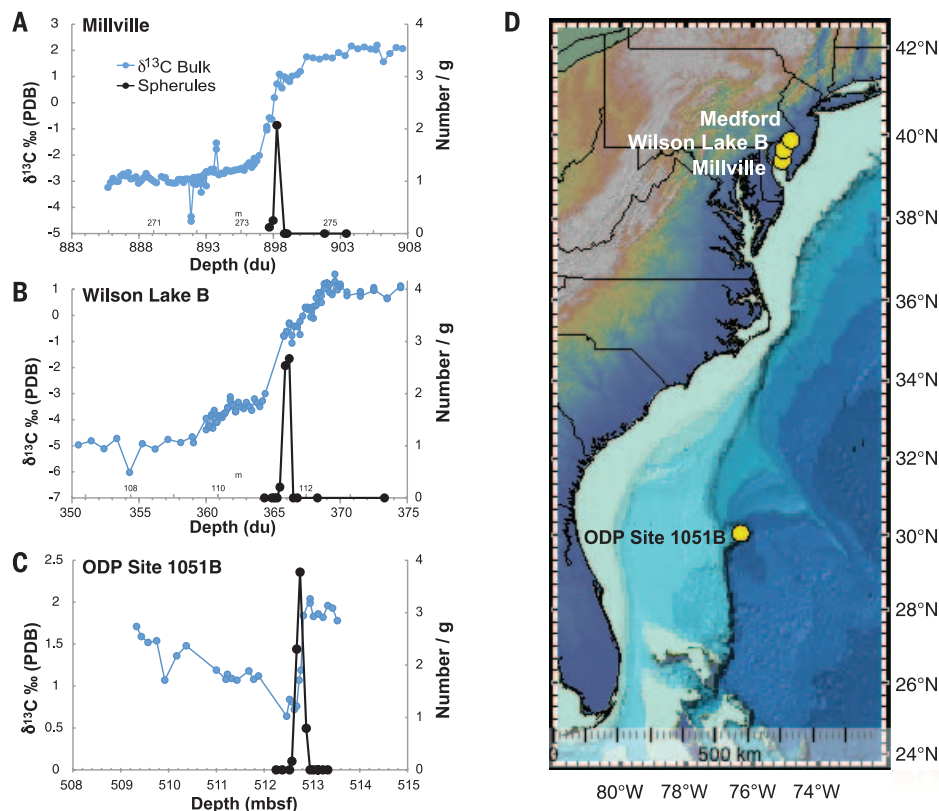
Major oxide chemistries of the P-E spherules show a wide range of compositions distributed equally among Wilson Lake B, Millville, and Hole 1051B (Fig. 4) (12). The spherules are ~ 33 to $\sim 50\%$ SiO_2 and have CaO contents between ~ 20 to $\sim 35\%$, which is consistent with a CaCO_3 -rich target rock, with Al_2O_3 and FeO as the second and third most abundant oxides, at around 15% and 10% on average, respectively. This variability is typical of tektite strewn fields and consistent with an impact origin of the spherules (18, 19). Impact melts have little time for homogenization, but a population of major oxide chemistries will generally follow broadly linear compositional trends with SiO_2 content because they were generated from the same source rock at the site of impact (18). In contrast, ashes or spherules from a volcanic eruption tend to exhibit inter- and intraspherule compositional homogeneity (19). Magma is generally well mixed during a single eruptive event, and hence volcanic spherules from the same eruptive sequence will be compositionally homogeneous and generally have much higher water content than impact spherules [up to a few weight % (wt %) (20)]. The water content of impact glasses is generally much lower than volcanic spherules (21, 22) because water is removed by vapor stripping during solidification (23). Field transmission infrared spectroscopy (FTIR)

on representative P-E spherules reveals water contents below 0.023 wt % (see table S5), much lower than expected for volcanic spherules but typical of impact-generated microtektites.

In cross section, the internal texture of most of the P-E spherules is glassy and relatively featureless (Fig. 3); exceptions are the less common microkrystites (discussed below). The glassy spherules also occasionally have microlites just inside the rims and are mildly vesicular. This vesicular nature, and the composition discussed above, are inconsistent with iron or stony micrometeorites and other cosmic spherules, which are generally either chondritic or differentiated and do not show evidence of volatile degassing (24).

A key observation is the presence of amorphous, occasionally vesicular, nearly pure SiO_2 glass (lechatelierite) inclusions within the microtektites (Fig. 3). Lechatelierite occurrence is confirmed by energy-dispersive x-ray spectroscopy (EDS) and micro-Raman spectroscopy in cross sections of spherules from Wilson Lake B, Millville, and Hole 1051B (see fig. S18). EDS was used to identify inclusions that are $>98\%$ SiO_2 , and Raman spectra from several of these are consistent with that of fulgurite (lightning-induced lechatelierite). Lechatelierite forms from melting of quartz and quenching to quartz glass, which generally occurs at temperatures $>1750^\circ\text{C}$ (4, 5). This indicates that the P-E spherules formed at temperatures at least this high, which excludes any known terrestrial volcanism as their origin. Melting of crustal silicates by impact sufficient to produce lechatelierite occurs at shock pressures of ~ 30 to 50 GPa

Fig. 1. Stratigraphic distribution of P-E spherules. (A to C) Stratigraphic distribution of P-E spherules from Millville (A), Wilson Lake B (B), and ODP Hole 1051B (C). Millville and Wilson Lake B core depths are in drilling units (du) of decimal feet; core depth in Hole 1051B is in meters below seafloor (mbsf). The carbon isotope composition of bulk carbonate from Millville and Wilson Lake B is from Wright and Schaller (10), and Hole 1051B is from Katz *et al.* (11). (D) Map showing location of the New Jersey (NJ) margin locations, including exposure in Medford, NJ, compared to that of Site 1051, Blake Nose. At both Wilson Lake B and Millville, the spherules are found in the basal Marlboro Clay Formation. Because the CIE has not been defined stratigraphically at the equivalent exposure of the Marlboro Clay at Medford, the stratigraphic placement of the spherules recovered there is only qualitative with respect to the P-E boundary (12).



(25, 26). This observation implies that the target rock, although not necessarily silica-rich, at least had silt-sized or larger quartz grains that were melted on impact.

We have identified a quartz inclusion in a microtektite from Millville that has Raman spectral characteristics indicative of shocked quartz (Fig. 3D and fig. S21). In particular, the relaxation of the spectral peak corresponding to SiO_2 bond-bending vibration from 464 to 460 cm^{-1} wave numbers observed in the Millville inclusion is consistent with observations from synthetic quartz experimentally shocked to peak pressures of 25.8 GPa (27) (fig. S21) and is considered diagnostic. Other characteristic spectral shifts unique to shocked quartz also match the Millville grain. An extensive search for individual shocked quartz among the abundant shelf quartz grains will be the subject of future investigation.

A subset of spherules shows quench-crystallization textures of clinopyroxene (Raman spectra most closely matching augite or diopside; see fig. S20), in an otherwise glassy matrix (Fig. 3), typical of microkrystites (3, 28). The feathered, dendritic, and chainlike textures of the P-E microkrystites are classic rapid-crystallization high-temperature quench features of impact glasses with lower silica content from other strewn fields (12). Examples are clinopyroxene (cpx) microkrystites of the upper Eocene spherule layer (17, 29, 30), attributed to the Popigai impact event (13, 15, 31), and the Cretaceous-Paleogene (K-Pg) spherules (also discussed below) (32). Among P-E microkrystites, vesicles are present but less common. Iron-rich inclusions are found in a few of the microkrystites and microtektites (fig. S16). These inclusions are generally noncrystalline and round or stringy. The presence of vesicles and lack of Ni-rich spinels in the P-E microkrystites are consistent with melt ejecta.

Within a given P-E spherule, the crystallite chemistry is close to the surrounding matrix glass. The distribution of major oxide chemistries is also similar to, but distinct from, the Late Eocene cpx spherules, which, like the P-E spherules, have high CaO contents (averaging only about 10 wt %, which is substantially lower than the P-E spherules). However, unlike the P-E spherules, the Late Eocene spherules have compositions much higher in SiO_2 and Na_2O , and lower in Al_2O_3 and FeO (18, 30, 33). The P-E microtektites and microkrystites are roughly equally represented at each of the three sites (Wilson Lake B, Millville, and Hole 1051B).

Impact ejecta, including spherules, are associated with the 66-Ma K-Pg boundary on the New Jersey coastal plain, such as in the Bass River core (34). For the following reasons, we find it implausible that the K-Pg spherules were reworked and redeposited at the P-E boundary. First, the chemistry of the P-E spherules differs significantly from those found at K-Pg boundary sections, with the latter being much higher in silica content (45 to 68%) (35). Newly discovered deposits of unaltered microtektites and microkrystites at a K-Pg ejecta layer in Gorgonilla Island, Colombia (32), have much higher SiO_2 and slightly lower Al_2O_3 than the P-E spherules, and Al_2O_3 generally

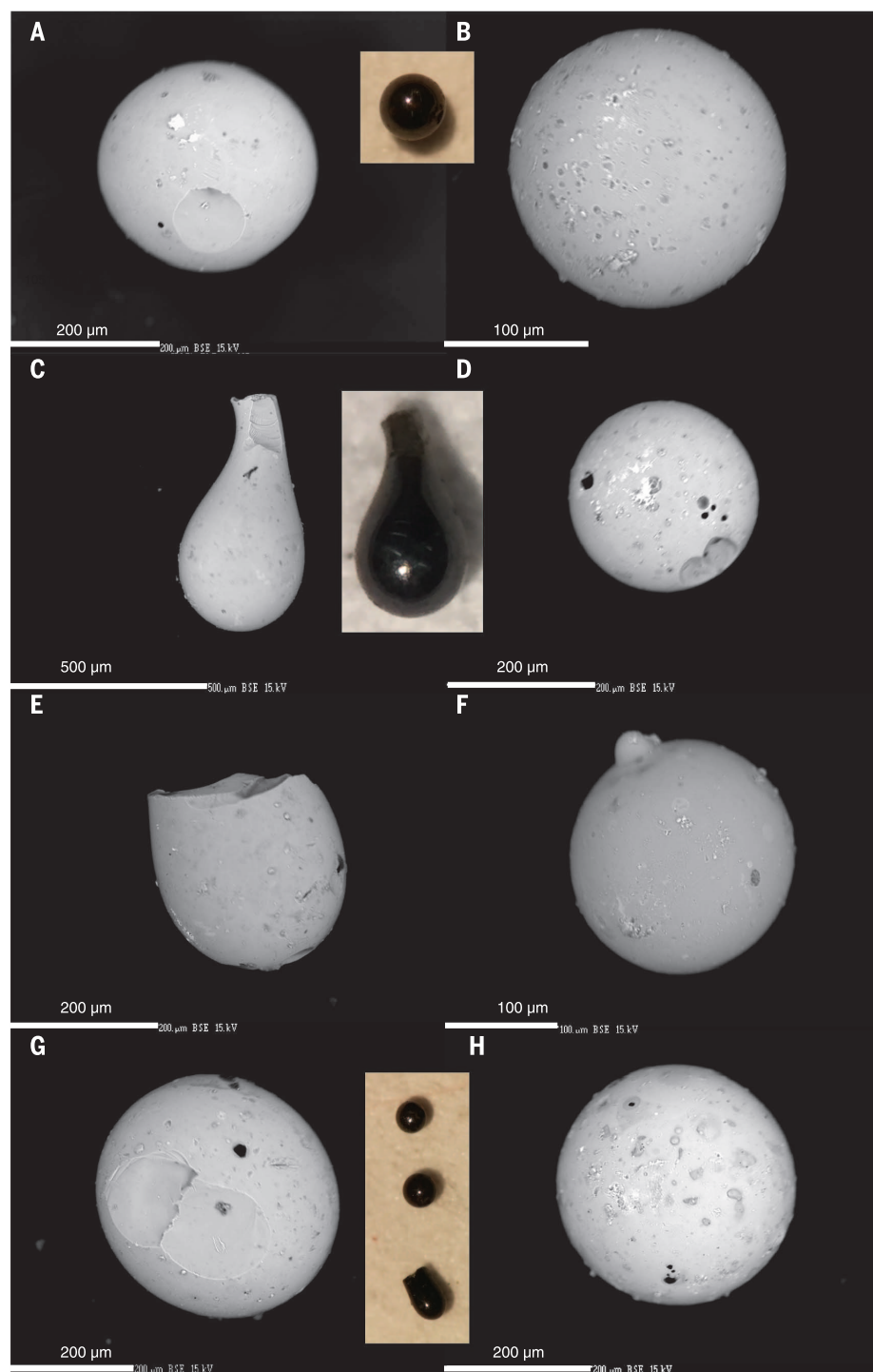


Fig. 2. Electron backscatter (15 kV) images of representative P-E spherules from Hole 1051B, Wilson Lake B, and Millville cores and the Medford exposure. Selected color micrographs are shown as insets. (A) Microtektite with a surface pit from ODP Hole 1051B (512.75 mbsf). (B) Microkrystite from ODP Hole 1051B (512.75 mbsf). Round features on surface of microkrystite are vesicles and small accretionary material. (C) Teardrop-shaped glass spherule from Millville 898.8 drilling units (du); inset is photomicrograph of same object. (D) Microkrystite with surface pit (spallation or microcrater?) from Millville (898.8 du). Dark round surface features are exposed vesicles. (E) Broken drop-form or dumbbell from Wilson Lake B (366.2 du). (F) Microtektite from Wilson Lake B (365.9 du), with a smaller spherule accreted to the side. This nature of deformation is typical of accretion occurring in partially molten state (compare to Fig. 3, E and F). (G) Microtektite with surface microcrater from the Medford, NJ Exposures. Inset shows several other forms found at Medford, which allows us to exclude drilling contamination as a source of the spherules. See table S4 for abundances. (H) Typical microkrystite from Wilson Lake B (366.2 du).

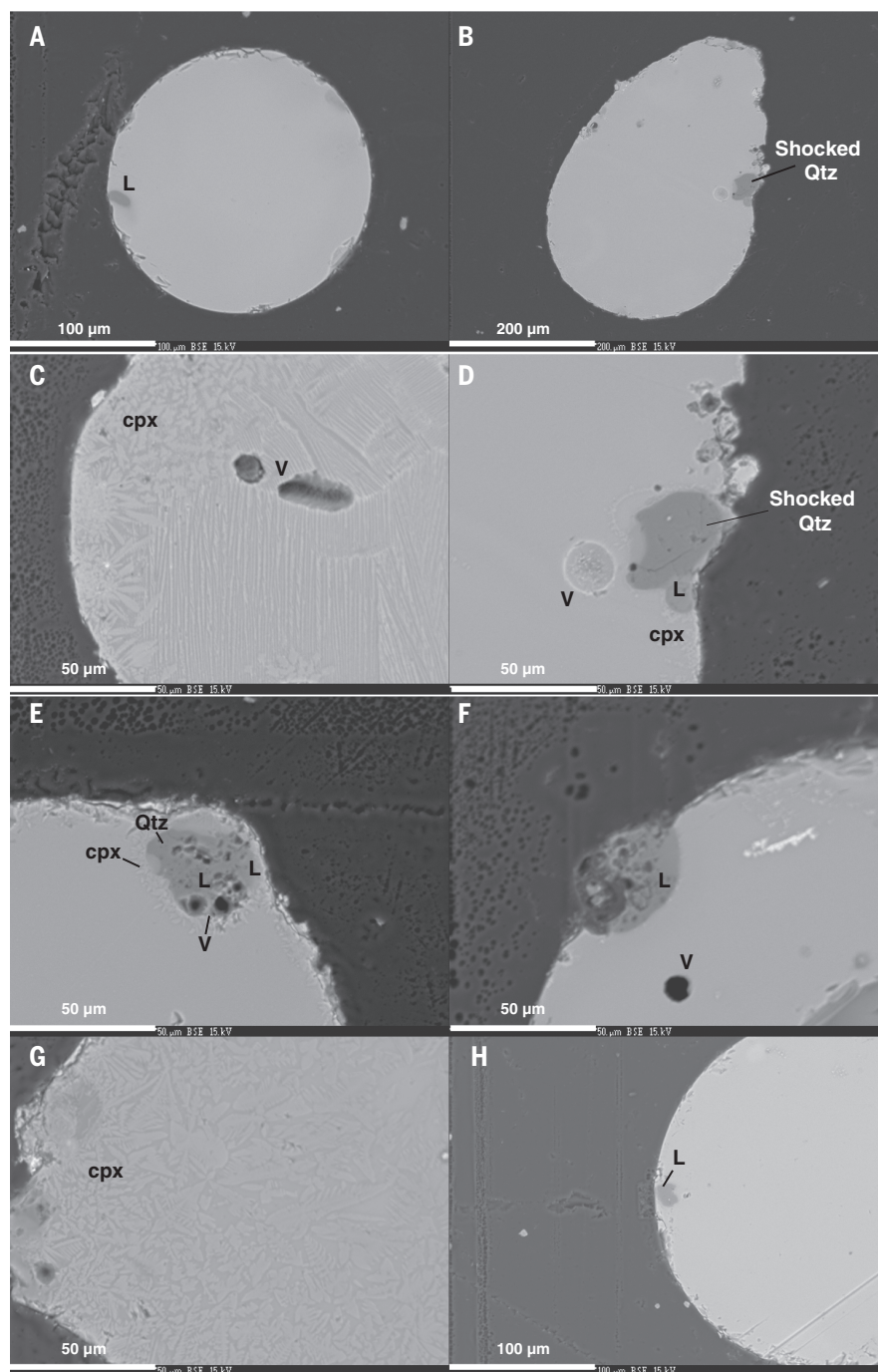


Fig. 3. Electron backscatter (15 kV) images of microtektites and microkrystites from polished cross sections. Scale in micrometers noted by white bars (L, lechatelierite inclusions; cpx, clinopyroxene microlites; V, vesicle). (A) Typical internal structure of a glassy microtektite from Wilson Lake B (365.5 du). (B) Teardrop microkrystite from Millville (898.5 du). Note quartz and lechatelierite inclusion at edge. (C) Quench-form crystallite morphologies in a microkrystite from Millville (898.5 du). Note “chain form” and dendritic structures of cpx crystals, typical of rapid quenching from high temperatures. (D) Enlargement of grain inclusion in (B) showing lechatelierite around a quartz grain. Raman spectra from this quartz grain show characteristic vibrational shifts associated with shocked quartz (see fig. S21). Also note fine-grained dendritic cpx microlites at edges of droplet. (E) Vesicular lechatelierite accretion/inclusion surrounded by clinopyroxene microlites from Millville (898.8 du). Light-colored inclusions are iron-rich crystallites (see fig. S16 for details). (F) Microtektite showing accretion of a grain or an exposed inclusion with lechatelierite around it, from Millville (898.8 du). (G) Close-up of microkrystite showing dendritic and feather-form crystallites of clinopyroxene from Hole 1051B (512.75 mbsf). (H) Typical microtektite with small lechatelierite inclusion from Hole 1051B (512.75 mbsf).

increases with increasing silica content. These K-Pg spherules are also several times more enriched in Na_2O (average ~3%) compared with the P-E spherules (0.2%) and have about half as much FeO (5.5% in the K-Pg versus 10% in the P-E). The presence of conchoidal fracture patterns in the P-E spherule glass is also inconsistent with surficial exposure and chemical weathering (e.g., Fig. 2 and fig. S2, E and F). The K-Pg ejecta are not preserved as glassy spherules on the coastal plain and are usually diagenetically altered; furthermore, they were buried by 20 to 30 m of sediment by the time of the P-E boundary (36) and would have been unlikely to survive unaltered on the terrestrial surface for 10 million years before a redeposition event at the P-E boundary. Indeed, the occurrence of the P-E microtektites in a discrete time-correlative stratigraphic layer at three separate locations separated by >1000 km, two from the New Jersey shelf and one in the open ocean (Blake Nose) (Fig. 1), makes a required focused reworking of relatively rare K/Pg spherules highly improbable. In addition, if the spherules were reworked, they would be accompanied by other material of the same age, such as K-Pg microfossils, which would have been much more abundant than spherules. Also, the discovery of spherules at the Medford outcrop section (Fig. 2) (12) that are identical in morphology and chemistry to those at Millville, Wilson Lake B, and Hole 1051B confirms that they are not an artifact of drilling disturbance.

We conclude that the spherule layer at Wilson Lake B, Millville, and ODP Site 1051 is best explained as air-fall ejecta (microtektites and microkrystites) generated by an impact close to the time of the P-E boundary. Ejecta fallout occurs over hours or days, implying that the spherule layer provides the most precise time-correlative feature for the P-E boundary among the three sites. The unprecedented high stratigraphic resolution of the Wilson Lake B and Millville sites, where the onset of the CIE is recorded over meters of section, compared with only a few centimeters in open ocean sections [e.g., ODP Sites 1051 and 690 (37)], provides the potential for temporal resolution that has not been heretofore possible and will surely be the target of important future work. Importantly, the virtually instantaneous time line provided by the microtektite horizon provides an opportunity to delineate the detailed sequencing of sedimentation and carbon cycling at a critical juncture in Earth's climate history. For example, the apparent variable offsets between the microtektite horizon and inflections in the bulk sediment $\delta^{13}\text{C}$ curves at Wilson Lake B and Millville, compared to the step function in foraminiferal $\delta^{13}\text{C}$ (fig. S22), must be viewed in this unfamiliar level of ultrahigh resolution and inspire greater scrutiny of the source(s) of the bulk carbon isotope excursion and its relation to the actual sequence of events at the P-E boundary.

It is worth noting that an Ir anomaly has been identified at a P-E boundary section at Zumaya, Spain (38), although it has been interpreted as volcanic in origin (39), and in flysch deposits from Slovenia (40); however, a large iridium anomaly is

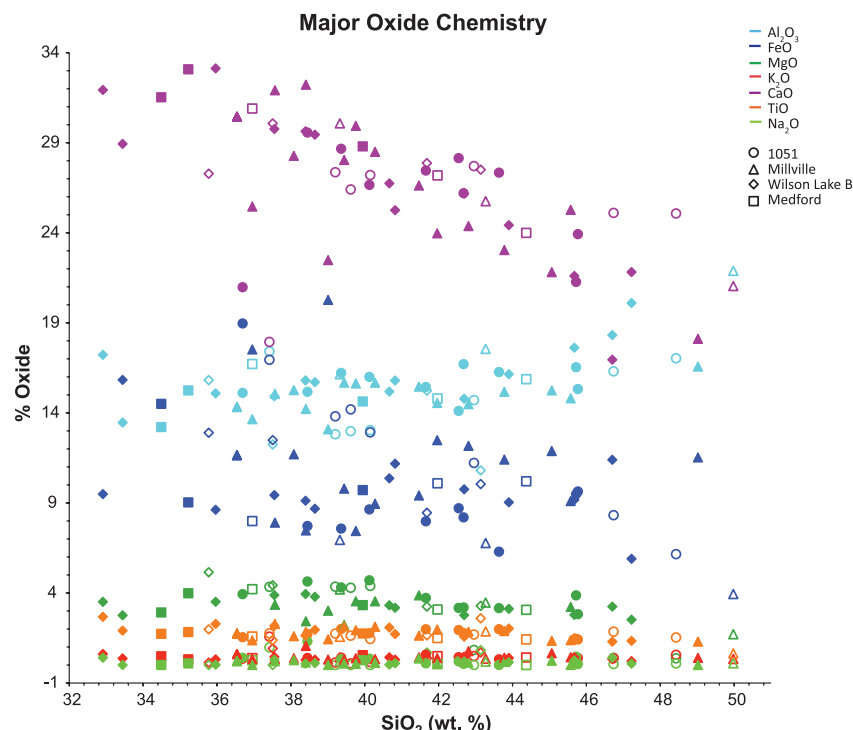


Fig. 4. Microtektite and microkrystite major oxide chemistry from Wilson Lake B, Millville, Medford, and Hole 1051B. Elemental abundances are corrected from EDS spectra and normalized to oxygen, assuming stoichiometry (see table S5). Closed symbols represent microtektites, and open symbols denote microkrystites.

not necessarily associated with all major impacts [e.g., the Chesapeake impact (47)]. These findings will motivate a search for impact ejecta at other sites to define the geographic footprint of the P-E strewn field, which will ultimately constrain the currently unknown location of an impact crater.

REFERENCES AND NOTES

1. B. P. Glass, *Geol. Soc. Am. Bull.* **85**, 1305–1314 (1974).
2. B. Glass, *Tectonophysics* **171**, 393–404 (1990).
3. B. Glass, C. A. Burns, in *Lunar and Planetary Science Conference Proceedings* (1988), vol. 18, pp. 455–458.
4. D. Stöffler, *J. Non-Cryst. Solids* **67**, 465–502 (1984).
5. D. Stöffler, F. Langenhorst, *Meteoritics* **29**, 155–181 (1994).
6. B. P. Glass, B. M. Simonson, *Distal Impact Ejecta Layers: A Record of Large Impacts in Sedimentary Deposits* (Springer Science & Business Media, 2012).
7. M.-P. Aubry, K. Ouda, C. Dupuis, W. A. Berggren, J. A. van Couvering, *Episodes* **30**, 271–286 (2007).
8. P. J. Sugarman et al., in *Proceedings of the Ocean Drilling Program, Initial Reports*, K. G. Miller, P. J. Sugarman, J. V. Browning, Eds. (Ocean Drilling Program, College Station, TX, 2005).
9. R. Norris, D. Kroon, A. Klaus, in *Proceedings of the Ocean Drilling Program, Initial Reports*, (1998), vol. 171, pp. 1–749.
10. J. D. Wright, M. F. Schaller, *Proc. Natl. Acad. Sci. U.S.A.* **110**, 15908–15913 (2013).
11. M. E. Katz, D. K. Pak, G. R. Dickens, K. G. Miller, *Science* **286**, 1531–1533 (1999).
12. All primary data are available as supplementary materials on Science Online.
13. S. Liu, B. Glass, F. T. Kytte, S. M. Bohaty, The late Eocene clinopyroxene-bearing spherule layer: New sites, nature of the strewn field, Ir data, and discovery of coesite and shocked quartz. *Geol. Soc. Am. Spec. Pap.* **452**, 37–70 (2009).
14. C. W. Poag, *Sediment. Geol.* **108**, 45–90 (1997).
15. F. Langenhorst, *Geology* **24**, 487–490 (1996).
16. B. P. Glass, S. Liu, A. Montanari, *Meteorit. Planet. Sci.* **39**, 589–597 (2004).
17. B. P. Glass, *Chemie Erde Geochem.* **62**, 173–196 (2002).
18. B. P. Glass, H. Huber, C. Koeberl, *Geochim. Cosmochim. Acta* **68**, 3971–4006 (2004).
19. C. Koeberl, *Tectonophysics* **171**, 405–422 (1990).
20. C. Koeberl, *Geol. Soc. Am. Spec. Pap.* **293**, 133–152 (1992).

21. C. Koeberl, A. Beran, in *Lunar and Planetary Science Conference Proceedings* (1988), vol. 18, pp. 403–408.
22. A. Beran, C. Koeberl, *Meteorit. Planet. Sci.* **32**, 211–216 (1997).
23. H. Melosh, N. Artemieva, *Lunar Planet. Sci.* **XXXV**, 1723 (2004).

PROTEIN EVOLUTION

Evolution of protein phosphorylation across 18 fungal species

Romain A. Studer,^{1,*} Ricard A. Rodriguez-Mias,^{2,*} Kelsey M. Haas,^{2,*} Joanne I. Hsu,² Cristina Viéitez,^{3,4} Carme Solé,³ Danielle L. Swaney,² Lindsay B. Stanford,² Ivan Liachko,² René Böttcher,³ Maitreya J. Dunham,² Eulàlia de Nadal,³ Francesc Posas,³ Pedro Beltrao,^{1,4,†} Judit Villén^{2,†}

Living organisms have evolved protein phosphorylation, a rapid and versatile mechanism that drives signaling and regulates protein function. We report the phosphoproteomes of 18 fungal species and a phylogenetic-based approach to study phosphosite evolution. We observe rapid divergence, with only a small fraction of phosphosites conserved over hundreds of millions of years. Relative to recently acquired phosphosites, ancient sites are enriched at protein interfaces and are more likely to be functionally important, as we show for sites on H2A1 and eIF4E. We also observe a change in phosphorylation motif frequencies and kinase activities that coincides with the whole-genome duplication event. Our results provide an evolutionary history for phosphosites and suggest that rapid evolution of phosphorylation can contribute strongly to phenotypic diversity.

Divergence in transcriptional regulation and gene expression is often considered the main driver of phenotypic variation across species (1). Comparative gene expression and chromatin immunoprecipitation se-

24. D. Parkin, R. Sullivan, J. Andrews, *Philos. Trans. R. Soc. London A: Math. Phys. Eng. Sci.* **297**, 495–518 (1980).
25. D. Stöffler et al., *Rev. Mineral. Geochem.* **60**, 519–596 (2006).
26. A. J. Gratz, D. K. Fiesler, B. F. Bohor, *Earth Planet. Sci. Lett.* **142**, 513–521 (1996).
27. P. F. McMillan, G. H. Wolf, P. Lambert, *Phys. Chem. Miner.* **19**, 71–79 (1992).
28. H. Vonhof, J. Smit, *Meteorit. Planet. Sci.* **34**, 747–755 (1999).
29. C. John, B. P. Glass, *Geology* **2**, 599–602 (1974).
30. B. Glass, C. A. Burns, J. R. Crosbie, D. L. DuBois, *J. Geophys. Res. Solid Earth* **90** (S01), 175–196 (1985).
31. S. Liu, D. Papanastassiou, H. Ngo, B. Glass, *Meteorit. Planet. Sci.* **41**, 705–714 (2006).
32. H. D. Bermúdez et al., *Terra Nova* **28**, 83–90 (2016).
33. S. L. D'Hondt, G. Keller, R. F. Stallard, *Meteoritics* **22**, 61–79 (1987).
34. R. K. Olsson, K. G. Miller, J. V. Browning, D. Habib, P. J. Sugarman, *Geology* **25**, 759–762 (1997).
35. W. Alvarez et al., *Geology* **20**, 697–700 (1992).
36. A. D. Harris et al., *Paleoceanography* **25**, PA3211 (2010).
37. S. Bains, R. M. Corfield, R. D. Norris, *Science* **285**, 724–727 (1999).
38. B. Schmitz et al., *Palaeogeogr. Palaeoclimatol. Palaeoecol.* **133**, 49–68 (1997).
39. B. Schmitz et al., *Earth Planet. Sci. Lett.* **225**, 1–17 (2004).
40. T. Dolenec, J. Pavšič, S. Lojen, *Terra Nova* **12**, 199–204 (2000).
41. A. Montanari, F. Asaro, H. V. Michel, J. P. Kennett, *Palaios* **8**, 420–437 (1993).

ACKNOWLEDGMENTS

We thank L. Lanci, B. Glass, and E. B. Watson for many helpful discussions. Samples were provided by IODP, which is sponsored by NSF and participating countries under management of the Joint Oceanographic Institutions, Inc. We also thank J. Singer for his help and expertise on the ion microprobe at RPI and C. Hoff for his valuable expertise in FTIR and Raman spectroscopy. We thank the four anonymous reviewers for their constructive input, which greatly strengthened this manuscript. This work was funded in part by the Comer Science and Education Foundation. LDEO contribution 8060.

SUPPLEMENTARY MATERIALS

www.sciencemag.org/content/354/6309/225/suppl/DC1
Supplementary Text
Figs. S1 to S22
Tables S1 to S6
References (42–49)
25 February 2016; accepted 16 September 2016
10.1126/science.aaf5466

identification of posttranslational modification (PTM) events. Studies of phosphosite evolution indicate that phosphorylation constrains protein evolution but that phosphosites can diverge quickly (3–7). However, we lack a phylogenetic understanding of phosphosite evolution. Thus, we examined the regulation of protein function by phosphorylation across 18 different fungal species that diverged from each other tens to hundreds of millions of years ago (Fig. 1A). Using MS, we identified a total of 73,340 high-confidence [$<1\%$ false discovery rate (FDR)] and well-localized phosphosites in these species (ranging from 3062 to 5286 phosphosites per species) (tables S1 and S2) (8). We found that most positions were phosphorylated only in a few species (fig. S1A), partly due to incomplete experimental coverage. As expected, the conservation of the phosphorylation state decreases with the evolutionary distance (fig. S1B).

We estimated the most likely origin for each phosphosite, taking into account the MS-derived phosphosites, sequence-based prediction of phos-

phorylation potential, and the phylogenetic tree (Fig. 1B) (8). We identified 44,877 origins of phosphorylation in 41,832 aligned positions (Fig. 1C and table S3). Only 890 sites (2.0%) are likely to have been present in the last common ancestor of all 18 species [≥ 731 million years (My), Y0], and 2194 sites (4.9%) are estimated to be ≥ 434 My old (Y0+Y1). These ancient sites tend to be conserved in higher eukaryotes, with 39.8% of the Y0 sites and 34.3% of the Y0+Y1 sites also phosphorylated in human or mouse. Phosphosites tend to be more conserved than expected by random sampling of phosphoacceptor residues (fig. S2).

For the 3884 phosphosites identified in *Saccharomyces cerevisiae* (Fig. 1D, left), 69% have an estimated age of ≤ 18 My, and 90% of sites are ≤ 182 My old. Age assignment could be biased due to site localization errors or neutral variation whereby the phosphorylation might occur in a neighboring, but not perfectly aligned, residue in an orthologous sequence. To take these into account, we obtained age estimates using a window of ± 3 positions around each phosphosite (8). As expected, this analysis shifted the estimates to older ages (Fig. 1D, right; fig. S3; and table S3). Using both approaches as bounds, we estimated that 39 to 69% of the *S. cerevisiae* sites are likely to be ≤ 18 My old, whereas 76 to 90% of sites are likely to be ≤ 182 My old. This suggests that the majority of observed phosphosites in extant species are evolutionarily novel and change at rates comparable to those observed

for transcription factor binding sites (9). Similar results were obtained when restricting the analysis to aligned regions of higher confidence, when mimicking a decrease in coverage, and when restricting the analysis to ancient proteins (figs. S3 and S4) (8). The latter suggests that phosphosites tend to be acquired via mutations in preexisting proteins. We also observed that coverage is not strongly biased by the environmental conditions (fig. S5).

By studying the phylogenetic history of ancient sites with known function in *S. cerevisiae*, we find cases such as T210 in the activation loop of Snf1p kinase, a phosphosite that is critical for viability and is strictly conserved (Fig. 1E). Alternatively, we find cases such as S22 of pyruvate kinase, which, in *S. cerevisiae*, regulates the catalytic activity of this enzyme (10) but which has been lost more than once during evolution (Fig. 1F). Plausibly, losses like these are compensated for by other mutations and may allow us to study neutral evolution at the level of phosphoregulatory networks. Alternatively, these phosphosites may be important only in specific conditions, resulting in these species occupying environmental niches where the losses are evolutionarily neutral. Out of 61 ancient sites with known function in *S. cerevisiae*, 17 (27.9%) are not phosphoacceptors in at least one species (fig. S6). Out of these cases, four were mutated to negatively charged residues that may mimic phosphorylation and result in constitutive regulation. Evolutionary transitions between phosphosites and acidic residues

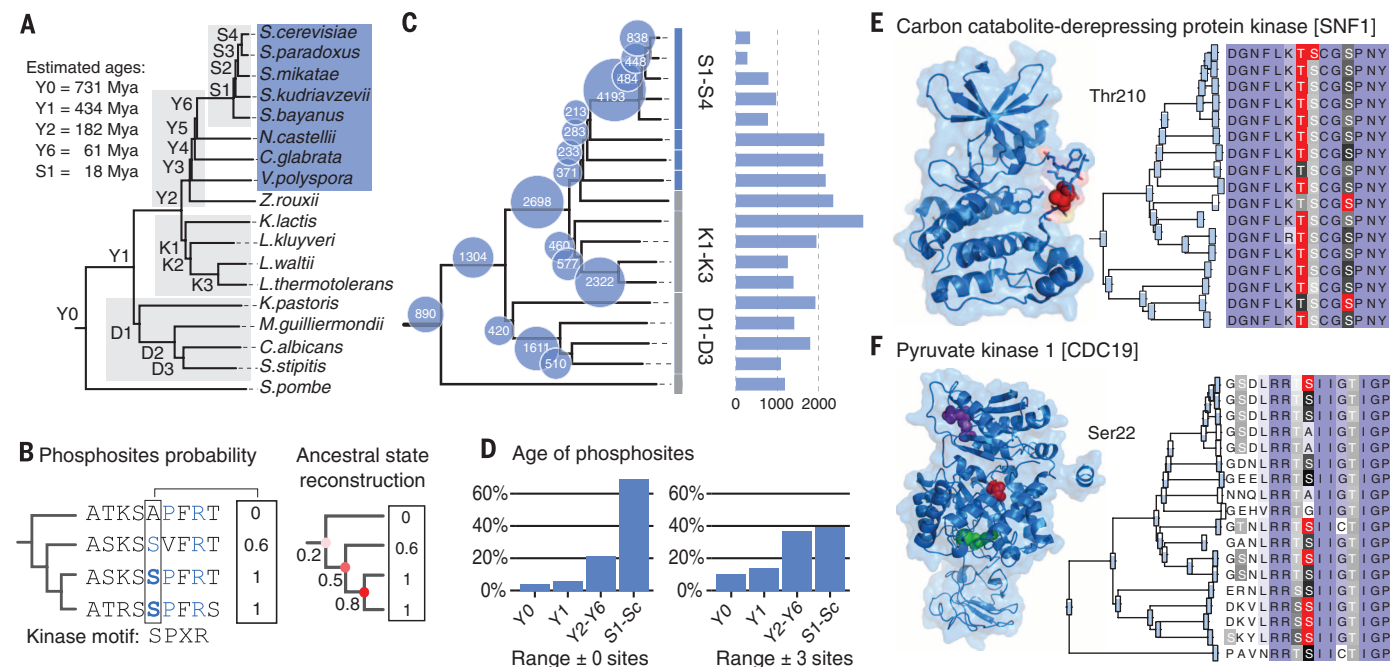


Fig. 1. Phylogenomics pipeline to estimate the age of phosphosites.

(A) Estimated consensus species tree. Post-whole-genome duplication event species are highlighted in the blue box. Age estimates are from timetree.org. (B) Example of ancestral state inference combining experimentally determined sites (bold) with sequence-based phosphosite predictions. (C) Number of predicted origins at each point in the phylogeny. The bar plot represents species-specific phosphosites. (D) Distribution of origins of phosphosites from *S. cerevisiae* (Sc).

(Left) Single-column age estimates. (Right) ± 3 window age estimates. (E and F) Predicted phylogenetic history for SNF1 T210 (E) and CDC19 S22 (F). Phosphosites are in red in the 3D structures. Phylogenetic tree: Red boxes denote experimental phosphosites; the white-to-black color scheme represents the probability of phosphorylation (0 to 1). Single-letter abbreviations for the amino acid residues are as follows: A, Ala; C, Cys; D, Asp; E, Glu; F, Phe; G, Gly; H, His; I, Ile; K, Lys; L, Leu; M, Met; N, Asn; P, Pro; Q, Gln; R, Arg; S, Ser; T, Thr; V, Val; W, Trp; and Y, Tyr.

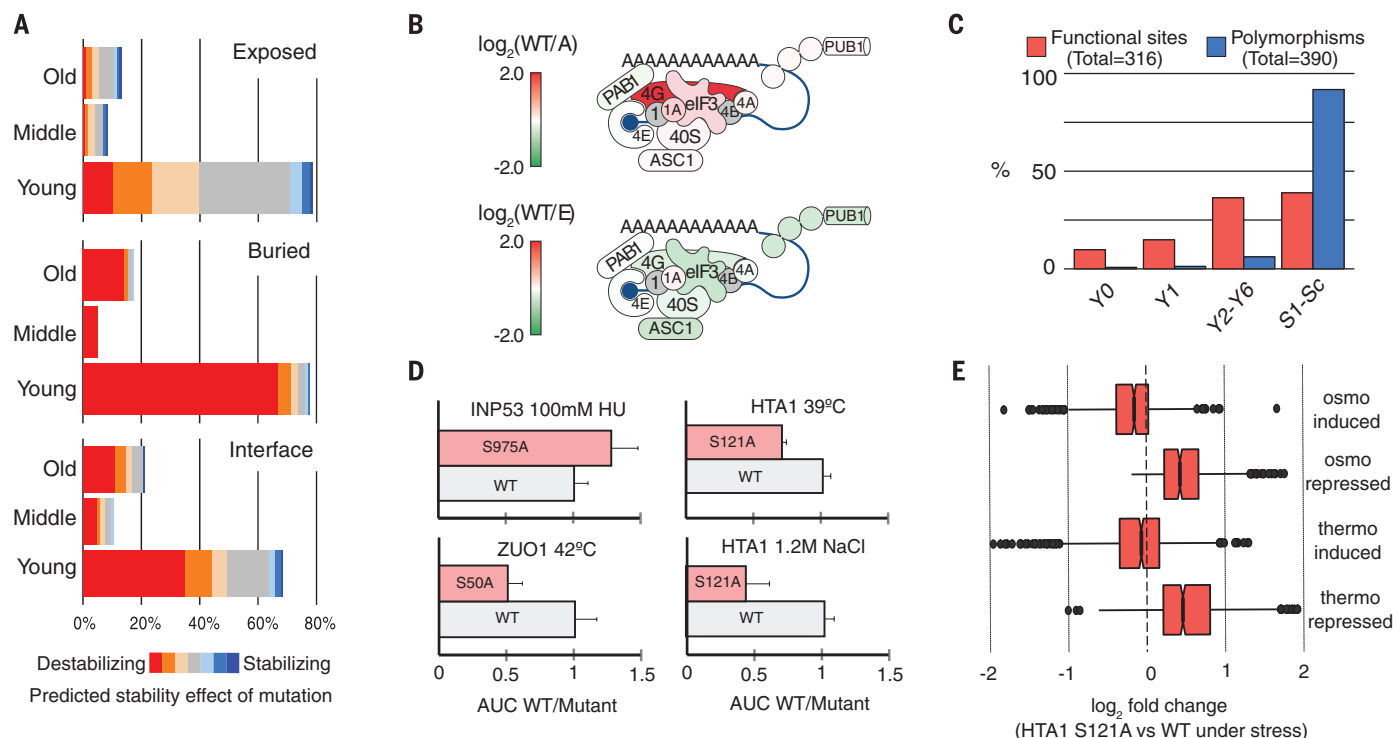


Fig. 2. Structural and functional characterization of sites. (A) Phosphosite distribution in interaction structures. The categories Old (>400 My), Middle (65 to 400 My), and Young (<65 My) correspond to Y0-Y1, Y2-Y6, and S1-Sc, respectively. (B) CDC33 (eIF4E) pulldown results color-coded on a model of a circular messenger ribonucleoprotein complex, with selected proteins involved in translation repression via P-body and/or stress-granule formation. (C) Age-group distributions for functional and polymorphic sites. (D) Fitness for WT and alanine-mutant strains, defined by the area under the curve (AUC). Error bars indicate SD. (E) Behavior of WT stress-responsive genes (defined by FDR < 0.05 and $|\log_2\text{FC}| > 1$) in an HTA1 S121A mutant upon stress.

have been reported (11) but were not commonly observed in our analysis (8).

Phosphosites with known functions show above-average conservation (6, 12). We therefore hypothesized that phosphosite age may correlate with functional importance. To test this hypothesis, we analyzed the age of *S. cerevisiae* sites at 2208 protein-protein interfaces, under the assumption that these could regulate protein interactions. We noted that there is a small but significant depletion of young phosphosites at interfaces relative to other exposed residues, supporting the view that sites with a putative function tend to be older (Fig. 2A; test of proportion, $P = 9.5 \times 10^{-4}$). This difference is not observed when normalizing for sequence conservation. Older interface phosphosites have, on average, a stronger predicted destabilizing effect compared with younger sites (Fig. 2A; Mann-Whitney, $P = 0.036$). This suggests that older interface sites are more likely to be at positions that contribute to the stability of the interface. We further characterized ancient site S28 in *S. cerevisiae* CDC33 (eIF4E), predicted to be at the interface with TIF4631 (eIF4G1) (fig. S7). We purified the CDC33 wild type (WT) and phosphodeficient [S28→A28 (S28A)] and phosphomimetic (S28E) mutants from yeast extracts and quantitatively compared interacting proteins (table S4A) (8). Several observations reveal the functional relevance of this phosphosite. First, both eIF4G paralogs TIF4631 and TIF4632 showed a strong increase (four- and twofold, respectively) in binding to CDC33 S28E and the WT versus

CDC33 S28A. Second, S28A and S28E mutations moderately compromise eIF4E binding to EAP1, a well-known eIF4E-interacting protein that competes with eIF4G. Third, several proteins involved in stress granule and P-body formation (ASC1, STIM1, and TIF34) showed substantially higher affinity for the S28E mutant than the S28A mutant (Fig. 2B). Fourth, the S28E mutant showed increased phosphorylation of neighboring sites at T15 and T22 on CDC33 (fig. S7 and table S4B). These data suggest that CDC33 S28 phosphorylation modulates eIF4E-eIF4G interaction and is a hotspot for translation initiation regulation.

We compared the age of *S. cerevisiae* phosphosites with functional annotations with those at polymorphic positions. We observed that functionally important phosphosites tended to be older relative to the polymorphic phosphosites (Fig. 2C). Age is predictive of functional phosphosites, even when accounting for sequence conservation (fig. S8), and can therefore be used to guide functional studies. As examples, we studied four ancient phosphosites: H2A1 S121 (S122 counting starting methionine), ZUO1 S50, INP53 S975 (Fig. 2D), and CDC10 T216. Compared with the WT controls, INP53 S975A showed an increased resistance to hydroxyurea (HU); ZUO1 S50A showed increased sensitivity to heat; and CDC10 T216 showed no phenotype under osmotic, heat, or HU stress (8). The alanine mutant of H2A1 (S121A), implicated in chromosome stability in *S. pombe* (13), rendered cells thermosensitive and osmosensitive compared with the WT on both solid and

liquid media (Fig. 2C and fig. S9). In nonstressed conditions, the WT and S121A have a very similar expression pattern, with only 32 genes significantly altered in the mutant (FDR < 0.05 and at least two-fold difference) (fig. S9B). Under stress conditions, a larger fraction showed altered gene expression (more than 600 and 800 genes in osmotic stress and heat stress, respectively). The expression of representative stress-responsive genes was validated by Northern blot (fig. S9C) and a single cell reporter system (fig. S9D). When stratifying stress-responsive genes by their WT response, genes that were stress-induced in the WT showed a decrease in up-regulation in the mutant, whereas genes that were repressed in the WT showed the opposite behavior (Fig. 2E). These results indicate that S121 on H2A1 is important for maintaining transcriptional control of stress-responsive genes.

The phylogenetic history of phosphosites was used to identify functions and complexes that are enriched in phosphosites of specific age groups (Fig. 3A). To guarantee that the enrichment is due to the age of sites and not the proteins, we normalized the enrichment for the age and average conservation level of the proteins in the corresponding group of genes (8). Several central processes, such as translation and protein folding, as well as some metabolic pathways and some central complexes are enriched in ancient sites (Y0, Fig. 3A). This indicates that the phosphoregulation of these processes and complexes is constrained. Conversely, some processes and complexes are enriched in recently arisen sites that could be

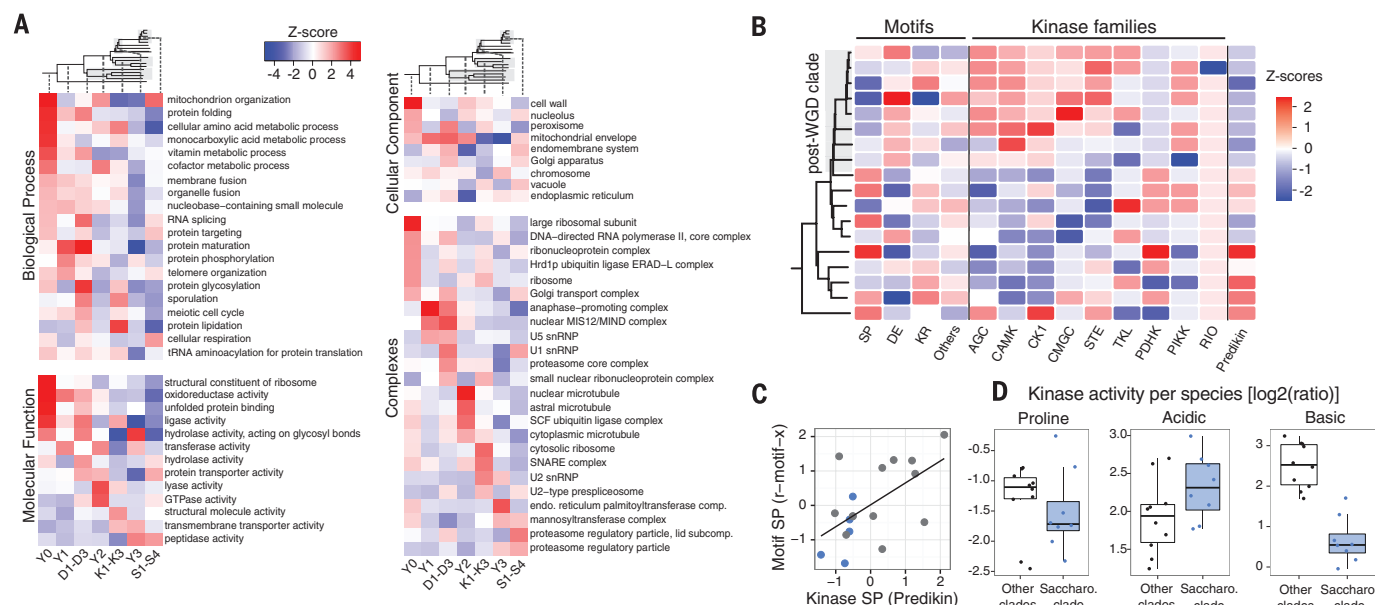


Fig. 3. Phylogenetic analysis of functional groups and kinase motif recognition. (A) Enrichment of gene ontology terms for phosphosites of different age groups. (B) Per-species enrichment in kinase types and phosphomotifs (SP, proline-directed; DE, acidic; KR, basic). Proline-directed kinase specificity was predicted with Predikin. (C) Correlation between the relative usage of predicted proline (SP) kinases and the relative usage of proline motifs. Blue dots represent the *Saccharomyces sensu stricto* group. (D) Enrichment ratio in KAYAK kinase activities for proline, acidic, or basic motifs.

associated with recent adaptations (Y3 and S1-S4 in Fig. 3A). Different spliceosome components show enrichment for sites of different ages. This potential change in the regulation is consistent with divergence in splicing across these species (14).

We next investigated whether the rapid divergence in phosphorylation is also accompanied by changes in the overall usage of phosphorylation motifs and the repertoire of protein kinases (Fig. 3B). We matched each phosphosite to common kinase motif preferences and calculated the relative motif usage across species (8). We observed a trend of lower relative usage of proline-directed motifs and higher relative usage of acidic motifs for species belonging to the post-WGD clade (15) and, in particular, for species in the *Saccharomyces sensu stricto* genus (Fig. 3B, columns one to four).

The differential usage of phosphorylation motifs is not due to a differential presence of the equivalent sequence motifs (figs. S10 and S11), so we speculated it could coincide with changes in the repertoire of protein kinases, their specificities, and/or their activities. We examined the fraction of kinases in each species assigned to different major groups of protein kinases (Fig. 3B, columns 5 to 13, and table S5). We observed a small increase in the fraction of CMGC and STE families in the *Saccharomyces* species and AGC and CAMK kinases in *Saccharomyces* species, *Candida glabrata*, and *Vanderwaltozyma polyspora*. However, kinase family membership is a poor predictor of kinase specificity. Thus, we focused on proline-directed (SP) kinases that can be accurately predicted from sequence (16). Such kinases tend to be depleted in the post-WGD clade (Fig. 3B, column 14), with the relative presence of SP phosphosites showing a significant correlation with the fraction of SP

kinases across species (Fig. 3C; Pearson's correlation coefficient $r^2 = 0.34$, $P = 0.011$).

To measure changes in basal kinase activities, we conducted KAYAK (kinase activity assay for kinome profiling) analysis (17). Cell lysates were reacted with peptide libraries matching proline-directed, acidic, and basic motifs. The extent of phosphorylation was used as a proxy for kinase activity toward these sequences (Fig. 3D). We selected nine species spanning our tree and performed two biological replicates ($r^2 = 0.98$; fig. S12A) (8). The measured kinase activities show a weak but significant correlation with the relative usage of phosphorylation motifs (Pearson's $r^2 = 0.09$, $P = 0.024$; fig. S12B). Relative to the others, *Saccharomyces* species show a significant difference in kinase activities across the three motif types (analysis of variance, $P = 8.0 \times 10^{-4}$). They tend to have lower activity toward proline and basic motifs and higher activity toward acidic motifs (Fig. 3D). Together, these results suggest that changes in the repertoire of kinases have altered the overall basal kinase activities, resulting in a differential usage of phosphorylation motifs across species.

On the whole, our results show that evolution of phosphoregulation is highly dynamic, and we suggest that changes in PTM regulation are on par with changes in transcriptional regulation in their capacity to quickly generate a diversity of solutions during evolution.

REFERENCES AND NOTES

- M. C. King, A. C. Wilson, *Science* **188**, 107–116 (1975).
- D. Villar, P. Flicek, D. T. Odom, *Nat. Rev. Genet.* **15**, 221–233 (2014).
- A. M. Moses, M. E. Liku, J. J. Li, R. Durbin, *Proc. Natl. Acad. Sci. U.S.A.* **104**, 17713–17718 (2007).
- L. J. Holt et al., *Science* **325**, 1682–1686 (2009).
- P. Beltrao et al., *PLOS Biol.* **7**, e1000134 (2009).
- C. R. Landry, E. D. Levy, S. W. Michnick, *Trends Genet.* **25**, 193–197 (2009).

- L. Freschi, M. Osseni, C. R. Landry, *PLOS Genet.* **10**, e1004062 (2014).
- See supplementary materials on Science Online.
- B. B. Tuch, D. J. Gajgoczy, A. D. Hernday, H. Li, A. D. Johnson, *PLOS Biol.* **6**, e38 (2008).
- P. Portela, S. Moreno, S. Rossi, *Biochem. J.* **396**, 117–126 (2006).
- S. M. Pearlman, Z. Serber, J. E. Ferrell Jr., *Cell* **147**, 934–946 (2011).
- P. Beltrao et al., *Cell* **150**, 413–425 (2012).
- S. A. Kawashima, Y. Yamagishi, T. Honda, K. Ishiguro, Y. Watanabe, *Science* **327**, 172–177 (2010).
- C. Neuvéglise, C. Marck, C. Gaillardin, C. R. Biol. **334**, 662–670 (2011).
- K. H. Wolfe, D. C. Shields, *Nature* **387**, 708–713 (1997).
- J. J. Ellis, B. Kobe, *PLOS ONE* **6**, e21169 (2011).
- Y. Yu et al., *Proc. Natl. Acad. Sci. U.S.A.* **106**, 11606–11611 (2009).

ACKNOWLEDGMENTS

MS data and identifications are accessible via MassIVE (<http://massive.ucsd.edu>, ID MSV000079428). RNA sequencing data are deposited in the Gene Expression Omnibus (www.ncbi.nlm.nih.gov/geo, accession number GSE80512). This work was supported by an Ellison Medical Foundation Award (AG-NS-0953-12 to J.V.), an Amgen scholarship (to K.M.H.), a Mary Gates scholarship (to J.I.H.), NSF grant 1243710 (to M.J.D.), Human Frontier Science Program award CDA00069/2013 (to P.B.), and European Research Council starting grant ERC-2014-STG 638884 – PhosFunc (to P.B.). M.J.D. is a Rita Allen Foundation Scholar and a Senior Fellow in the Genetic Networks program at the Canadian Institute for Advanced Research. F.P. and E.D.N. are recipients of ICREA (Institut Catalana de Recerca i Estudis Avançats) Acadèmia and are supported by Fundación Botín, Banco Santander, the Spanish government (BFU2015-64437-P, BFU2014-52333-P, FEDER), and the Catalan government (2014-SGR-599). We thank the laboratory of S. Fields for providing yeast strains and C. Landry and P. Flicek for critical reading of the manuscript.

SUPPLEMENTARY MATERIALS

www.sciencemag.org/content/354/6309/229/suppl/DC1
Materials and Methods
Supplementary Text
Figs. S1 to S12
Tables S1 to S5
References (18–58)

8 January 2016; accepted 16 August 2016
10.1126/science.aaf2144

SIGNAL TRANSDUCTION

Opposing effects of Elk-1 multisite phosphorylation shape its response to ERK activation

Anastasia Mylona,^{1*} Francois-Xavier Theillet,^{2†} Charles Foster,¹ Tammy M. Cheng,³ Francesc Miralles,^{1,4} Paul A. Bates,³ Philipp Selenko,² Richard Treisman^{1‡}

Multisite phosphorylation regulates many transcription factors, including the serum response factor partner Elk-1. Phosphorylation of the transcriptional activation domain (TAD) of Elk-1 by the protein kinase ERK at multiple sites potentiates recruitment of the Mediator transcriptional coactivator complex and transcriptional activation, but the roles of individual phosphorylation events had remained unclear. Using time-resolved nuclear magnetic resonance spectroscopy, we found that ERK2 phosphorylation proceeds at markedly different rates at eight TAD sites in vitro, which we classified as fast, intermediate, and slow. Mutagenesis experiments showed that phosphorylation of fast and intermediate sites promoted Mediator interaction and transcriptional activation, whereas modification of slow sites counteracted both functions, thereby limiting Elk-1 output. Progressive Elk-1 phosphorylation thus ensures a self-limiting response to ERK activation, which occurs independently of antagonizing phosphatase activity.

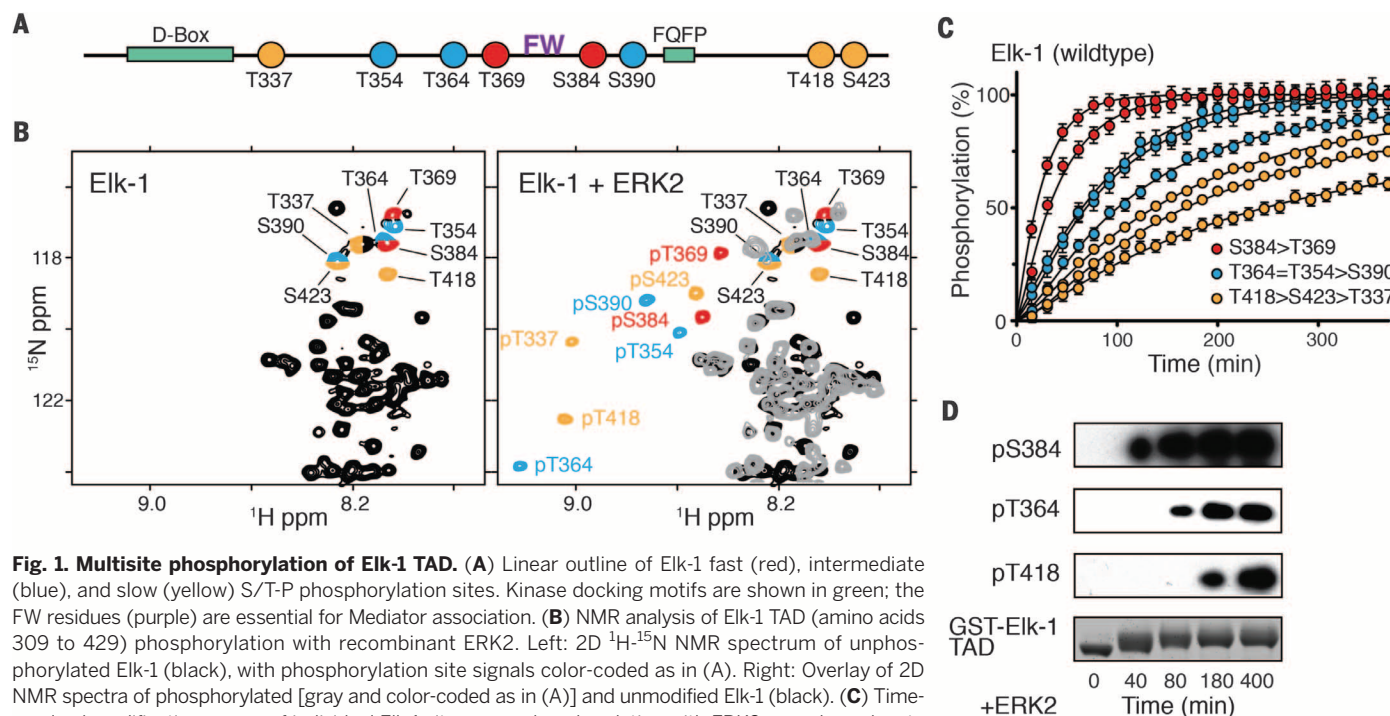
Multisite protein phosphorylation increases the complexity of functional signaling outputs that can be generated from single protein kinase inputs. It can set thresholds for activity or transform graded signals into switch-like responses (1–4). Many transcription factors and their interacting regulatory proteins are subject to multisite phosphorylation, which allows distinct aspects of protein function—including protein turnover, nuclear import and export, and specific protein interactions—to be

controlled independently (5). However, in general, the dynamics and functional roles of individual phosphorylation events are incompletely understood.

The ternary complex factor (TCF) subfamily of Ets-domain transcription factors, consisting of Elk-1, SAP-1, and Net, provides an example of multisite phosphorylation in transcriptional activation. TCFs, together with their partner protein SRF, function in many biological processes by coupling SRF target genes to mitogen-activated

protein kinase (MAP kinase) signaling (5). Mitogenic and stress stimuli induce phosphorylation of TCF C-terminal transcriptional activation domains (TADs) at multiple S/T-P (Ser or Thr-Pro) phosphorylation sequences, of which eight are conserved across the family (Fig. 1A and fig. S1) (6–11). Two MAP kinase docking sites, the D-box and the Phe-Gln-Phe-Pro (FQFP) motif, control phosphorylation of these sites (12–15). Multisite phosphorylation triggers transcriptional activation by TCFs, facilitating their interaction with the Mediator transcriptional coactivator complex (16–19), but the kinetics with which the different sites are phosphorylated, and whether they serve distinct functions, remain unclear.

To obtain atomic-resolution insights into phosphorylation of the Elk-1 TAD, we used nuclear magnetic resonance (NMR) spectroscopy (20) to monitor its modification by recombinant ERK2 in vitro (Fig. 1B and fig. S2A). Time-resolved NMR experiments revealed that each phosphorylation proceeded efficiently but at markedly different rates. Phosphorylation of Thr³⁶⁹ and Ser³⁸⁴, which flank the central Phe-Trp (FW) motif implicated in Mediator interaction (18), occurred faster than



modification of Thr³⁵⁴, Thr³⁶⁴, and Ser³⁹⁰, whereas residues Thr⁴¹⁸, Ser⁴²³, and Thr³³⁷ were modified more slowly (Fig. 1C), which we confirmed by immunoblotting (Fig. 1D). Chemical shift analysis (Ca, C β) showed no stable secondary structure elements in unmodified or phosphorylated Elk-1 TAD (fig. S2B).

As a first step toward understanding the basis for the phosphorylation sites' differential kinetic behavior, we devised a reaction model based on Michaelis-Menten enzyme kinetics. To simplify the mathematical treatment, we grouped Elk-1 sites into three classes: fast (Thr³⁶⁹ and Ser³⁸⁴), intermediate (Thr³⁵⁴, Thr³⁶⁴, and Ser³⁹⁰), and slow (Thr³³⁷, Thr⁴¹⁸, and Ser⁴²³). We assumed that ERK2 phosphorylation is distributive, that enzymatic rate constants (k_{cat}) are similar for all sites, and that the different sites have relative affinities for ERK2 modeled by increasing Michaelis-Menten constants ($K_M^{Fast} < K_M^{Int} < K_M^{Slow}$) (Fig. 2A and fig. S3A) (20). This model, which recapitulated the measured kinetics of in vitro Elk-1 phosphorylation well (Fig. 2B), predicted that removal of fast or intermediate sites should increase the phosphorylation rates of other sites. To test this idea, we analyzed the phosphorylation kinetics of Elk-1 TAD mutants in which we substituted all fast or intermediate phosphoacceptor residues with alanines (Elk-1F: Thr³⁶⁹ → Ala, Ser³⁸⁴ → Ala; Elk-1I: Thr³⁵⁴ → Ala, Thr³⁶⁴ → Ala, Ser³⁹⁰ → Ala) (Fig. 2A). In the fast-site mutant Elk-1F, phosphorylation rates of intermediate and slow sites increased, whereas those of the fast and slow sites increased in the intermediate-site mutant Elk-1I; in both cases, the altered kinetics fit well with those predicted by the model (Fig. 2B and fig. S3B). Thus, even the fast sites are not phosphorylated at the maximum possible rate in the wild-type protein. Moreover, phosphorylation of an Elk-1 TAD mutant in which Thr³⁶⁹ and Ser³⁸⁴ were replaced with aspartates was similar to Elk-1F, excluding the possibility that fast-site phosphorylation primes later modification events (fig. S3B).

To gain more insight into the factors affecting individual sites' phosphorylation kinetics, we assessed the role played by primary sequence. To do this, we exchanged the sequences surrounding the fast Thr³⁶⁹ and slow Ser⁴²³ sites. This also effectively exchanged their reactivities, which suggests that these sites' phosphorylation rates reflect their position relative to ERK docking sequences, rather than intrinsic differences in reactivity (Fig. 2C). We therefore examined the contributions of the D-box and FQFP ERK docking motifs to each site's phosphorylation kinetics. Deletion of the D-box decreased the rates of Thr³³⁷, Thr³⁵⁴, Thr³⁶⁴, and Thr³⁶⁹ phosphorylation but increased the rates of Ser³⁹⁰, Thr⁴¹⁸, and Ser⁴²³ modification (Fig. 2D). In contrast, deletion of the FQFP motif decreased the rate of Ser³⁸⁴ phosphorylation but enhanced modification of intermediate sites, including adjacent Ser³⁹⁰, with no effect on the C-terminal sites (Fig. 2D). Thus, the ERK docking motifs differentially affect each phosphorylation site's competitive behavior. Previous studies showed that Elk-1 TAD phosphorylation by JNK and p38

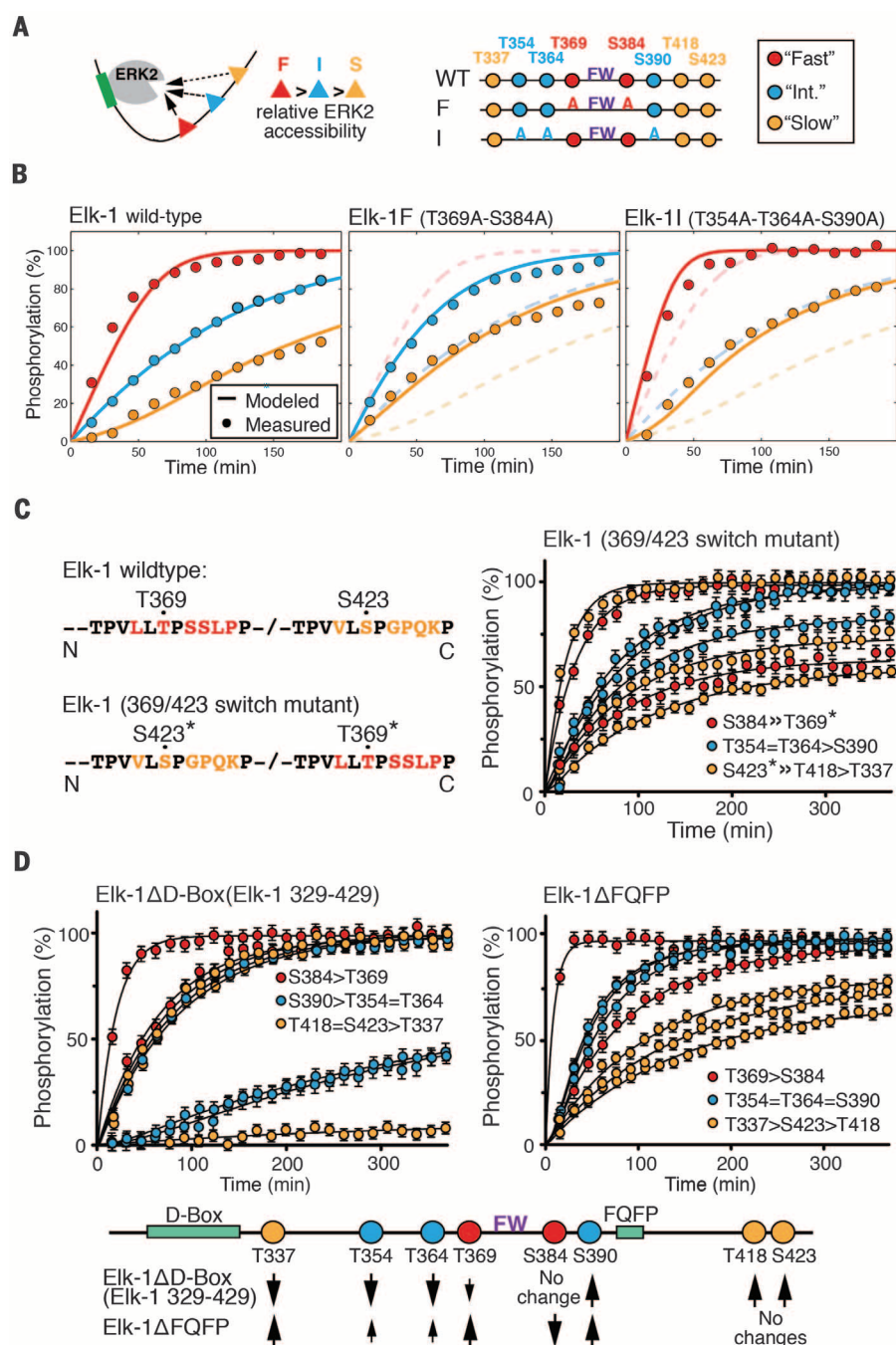


Fig. 2. Phosphorylation kinetics of Elk-1 TAD mutants. (A) Outline of analyzed Elk-1 TAD mutants. Substrate sites were classified as fast (red), intermediate (blue), or slow (yellow) for model calculations. (B) Left: Comparison of averaged measured data points of wild-type Elk-1 TAD fast-, intermediate-, and slow-site phosphorylation by ERK2 (circles) with calculated rates according to the competitive inhibition model (solid lines). Center: Fast-site alanine-substituted Elk-1 TAD (Elk-1F); dashed lines show wild-type Elk-1 TAD for comparison. Right: Intermediate-site alanine-substituted Elk-1 TAD (Elk-1I); dashed lines show wild-type Elk-1 TAD for comparison. (C) Time-resolved modification curves (right) of the Elk-1 369/423 switch mutant (left). Amino acid abbreviations: G, Gly; K, Lys; L, Leu; P, Pro; Q, Gln; S, Ser; T, Thr; V, Val. Error bars denote differences between replicate experiments on two independent samples. (D) Time-resolved modification curves of ERK docking-site mutants Elk-1ΔD-box (left) and Elk-1ΔFQFP (right), presented as in (C). Effects of D-box and FQFP site deletions on Elk-1 TAD phosphorylation rates are summarized below.

MAP kinases differs from phosphorylation by ERK (10, 21–24) and that this reflects differences in their docking interactions (12, 14, 15, 25). In-

deed, these kinases exhibited site preferences and phosphorylation rates that were distinct from that of ERK2 (fig. S3C). Taken together,

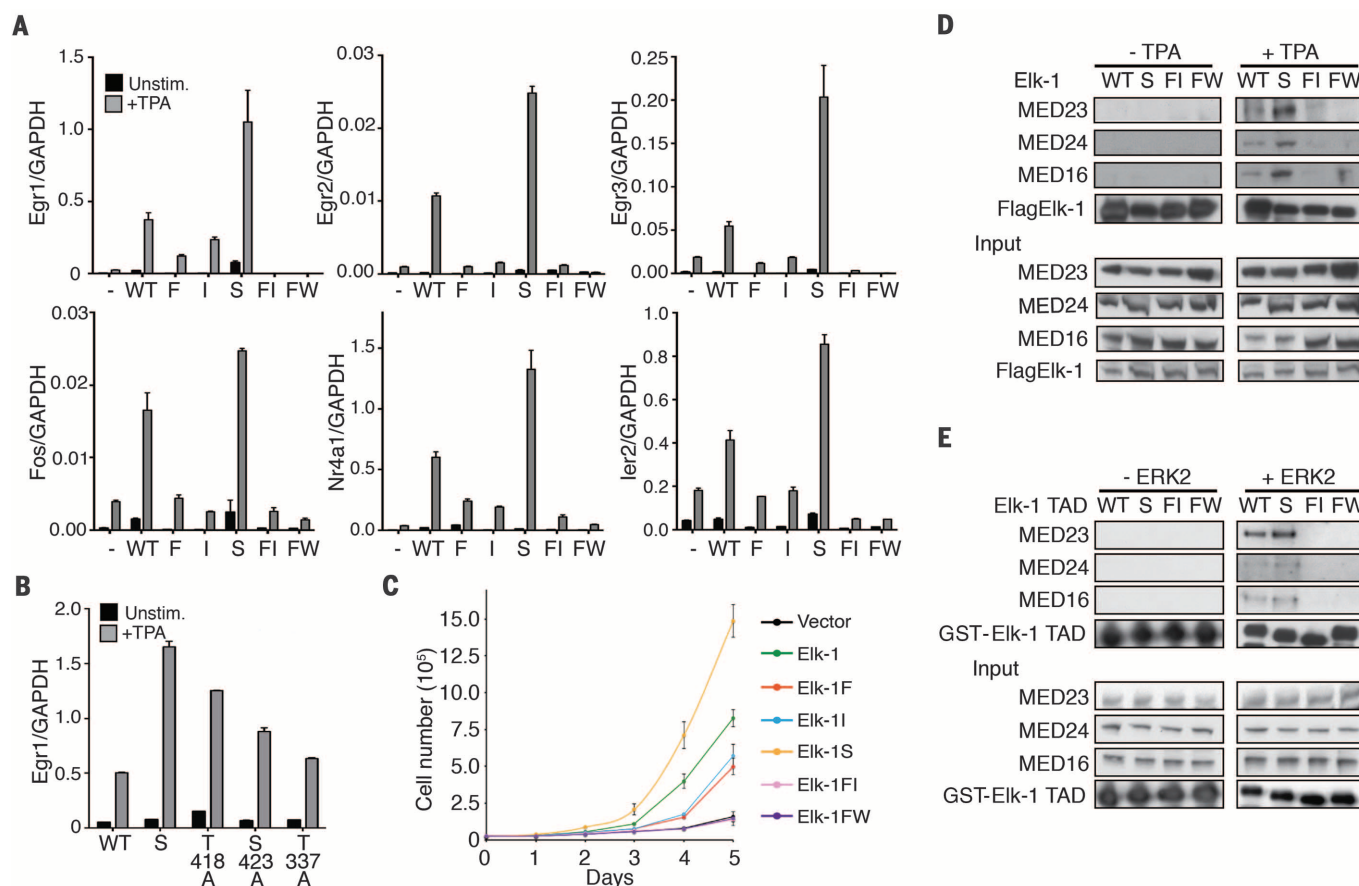


Fig. 3. Effects of Elk-1 TAD mutations on TCF target gene expression, cell proliferation, and Mediator binding. (A) Quantitative reverse transcription polymerase chain reaction (qRT-PCR) analysis of TCF target gene transcription in reconstituted TKO MEFs. Cells were reconstituted with wild-type mouse Elk-1 (WT) or fast-site (F), intermediate-site (I), slow-site (S), fast- and intermediate-site (FI), or alanine-substituted FW motif (FW) mutants. (B) Effects of individual slow-site alanine substitutions on *Egr1* expression. Data are expressed relative to expression of GAPDH. In (A) and (B), cells were stimulated with TPA (50 ng/ml)

where indicated. RNA levels are quantified relative to GAPDH; data are means \pm SEM, $n = 3$. (C) Proliferation of wild-type and mutant Elk-1 TKO MEFs. Data are means \pm SEM, $n = 3$. (D) Coimmunoprecipitation of Mediator with wild-type or mutant Flag-tagged Elk-1 from NIH3T3 cell extracts. Antibodies to Mediator subunits MED23, MED24, and MED16 were used for immunoblotting. (E) Mediator coprecipitation from unstimulated NIH3T3 cell extracts using wild-type and mutant GST-tagged Elk-1 TAD proteins with and without prior ERK2 phosphorylation.

our results show that the different rates of Elk-1 TAD phosphorylation by ERK2 follow a competition mechanism that is governed by the position of individual Elk-1 substrate sites relative to ERK2 docking interactions.

To test whether the different kinetic classes of Elk-1 TAD phosphorylation sites are functionally equivalent, we expressed Elk-1 mutants in fibroblasts derived from TCF-deficient (*Elk1*^{-/-}; *Elk3*^{8/8}; *Elk4*^{-/-}) triple-knockout mouse embryos (TKO MEFs; fig. S4, A to C). In these cells, immediate-early (IE) gene expression is defective, but expression of wild-type mouse Elk-1 restored the IE transcriptional activation seen in wild-type MEFs after activation of ERK by treatment with TPA (12-*O*-tetradecanoylphorbol-13-acetate) (fig. S4D). As expected, alanine substitutions of fast and/or intermediate sites, or of the FW motif, greatly diminished or abolished the ability of Elk-1 to activate TCF-SRF target gene transcription after TPA stimulation (Fig. 3A). Surprisingly, however, mutation of the slow sites substantially enhanced Elk-1-mediated activation of TCF-SRF target genes (Fig. 3A). Alanine substitutions at

individual slow sites also increased Elk-1 activity, with Thr⁴¹⁸ exhibiting the greatest effect (Fig. 3B and fig. S4, E to G). TCF-SRF signaling is important for cellular proliferation (26, 27), and TKO MEFs proliferated more slowly than wild-type MEFs. The reconstituted TKO MEFs exhibited enhanced proliferation rates, which correlated with the ability of each mutant to promote transcriptional activation (Fig. 3C).

Phosphorylation of Elk-1 promotes transcriptional activation by facilitating its MED23-dependent interaction with the Mediator complex (16–18). We therefore investigated whether the different transcriptional activities of the Elk-1 mutants reflected alterations in Mediator binding. We prepared extracts of TKO cells expressing wild-type or mutant Elk-1 proteins and assessed Elk-1 association with Mediator by coimmunoprecipitation of the MED23, MED24, and MED16 subunits. Consistent with the transcription experiments, Elk-1–Mediator interaction was induced by TPA stimulation and dependent on the FW motif; it was abolished by alanine substitutions of fast and intermediate sites, and increased in the slow-site Elk-1 mutant

(Fig. 3D). We obtained similar results when we used glutathione *S*-transferase (GST)–Elk-1 TAD proteins to recover Mediator proteins from unstimulated NIH3T3 cell extracts (Fig. 3E). In this assay, ERK2 phosphorylation time-course experiments showed that Mediator recovery by the wild-type Elk-1 TAD was most efficient prior to modifications of the slow sites (fig. S5, A and B). Taken together, these data show that according to the sites involved, ERK2 phosphorylation promotes or inhibits transcriptional activation by Elk-1, which reflects alterations in Elk-1–Mediator interactions.

Next, we investigated Elk-1 TAD phosphorylation kinetics in vivo. Previous studies were unable to distinguish the progressive phosphorylation of fast and slow Elk-1 sites (6). However, by incubating cells at 25°C to slow down reactions, we confirmed that phosphorylation rates can be ranked in the order Ser³⁸⁴ > Thr³⁶⁴ > Thr⁴¹⁸ and that different site classes exhibited a similar competitive behavior, as seen in vitro (fig. S6A). Reasoning that phosphorylation of the Elk-1 TAD might be sensitive to kinetic effects at limiting signal strengths, we titrated ERK activity using

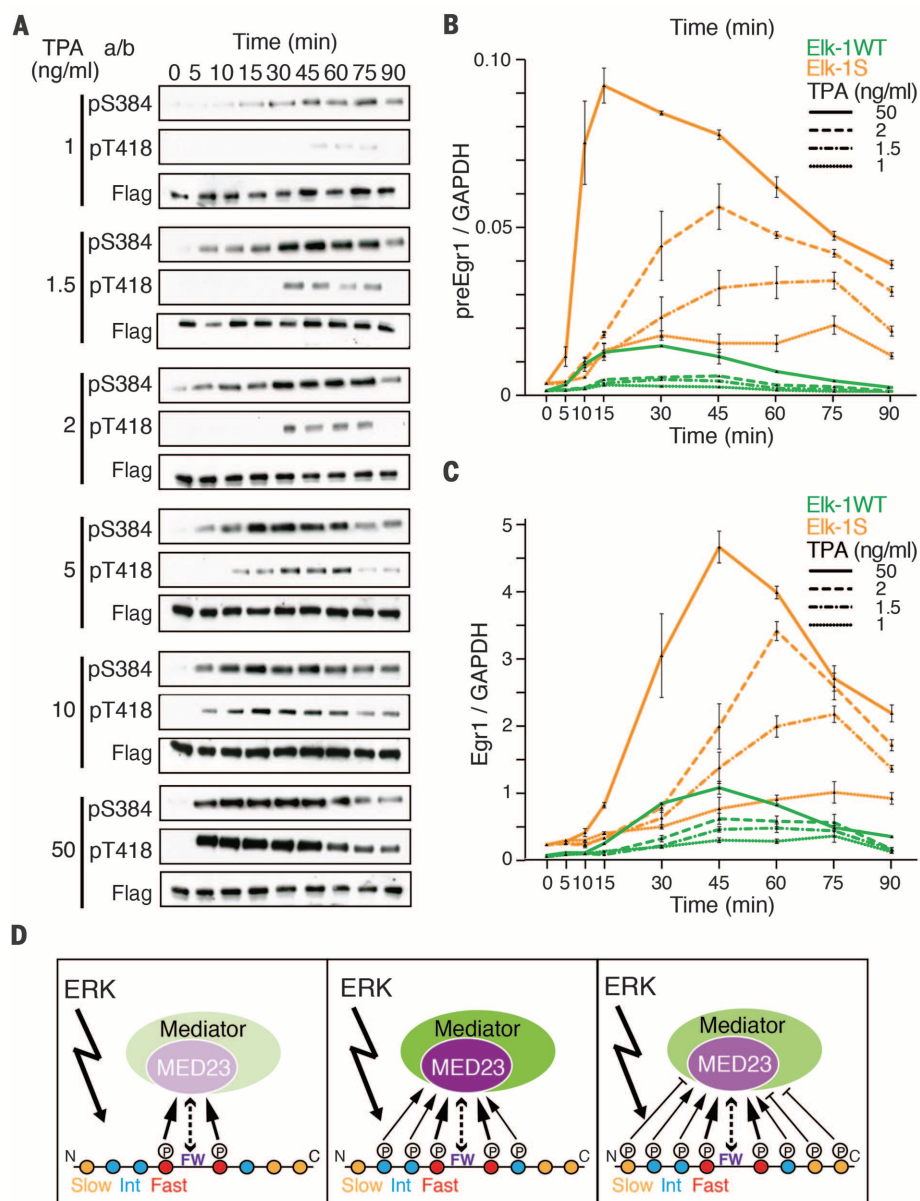


Fig. 4. Multisite phosphorylation of Elk-1 shapes the transcriptional response to ERK activation.

(A) Kinetics of Elk-1 fast- and slow-site phosphorylation in cells treated with increasing concentrations of TPA. (B) Transcription rate of the TCF-SRF target gene *Egr1* in TKO MEFs expressing wild-type Elk-1 or mutant Elk-1S. Precursor RNA was monitored by qRT-PCR after stimulation with different concentrations of TPA. Data are means \pm SEM; $n = 3$. (C) Kinetics of *Egr1* mRNA accumulation in cells as in (B) monitored by qRT-PCR. (D) Progressive Elk-1 phosphorylation by ERK has both activating (left and center) and inhibitory (right) effects on Mediator recruitment, as suggested by shading densities. A strong signal will rapidly reach the attenuated state shown at the right; a weak signal may reach this state only if sustained.

increasing amounts of TPA. This both increased the maximal extent of ERK activation and advanced the time at which it occurred (fig. S6B). At low TPA concentrations, Elk-1 fast-site (Ser³⁸⁴) and slow-site (Thr⁴¹⁸) modifications accumulated slowly over 1 hour, whereas at a saturating TPA dose they were maximal by 10 min. Both phosphorylations declined at late times, presumably owing to the action of Elk-1 phosphatases (Fig. 4A) (6, 28).

Having established that Elk-1 phosphorylation kinetics are tuned by signal strength, we

investigated their relationship to transcriptional activation. We compared the ability of wild-type Elk-1 and the slow-site mutant Elk-1S to activate transcription in response to signals of differing strengths. At saturating TPA concentrations, both proteins activated *Egr1* transcription with similar transient kinetics, although Elk-1S was much more active, reflecting the loss of the inhibitory sites (Fig. 4, B and C). At limiting TPA doses, however, their behaviors were markedly different. Whereas the activity of wild-type Elk-1 was almost

maximal by 15 min, that of Elk-1S increased substantially beyond this time (Fig. 4B), resulting in prolonged *Egr1* mRNA accumulation (Fig. 4C). Thus, progressive phosphorylation of the Elk-1 TAD by a single kinase, ERK, attenuates the transcriptional response of Elk-1, shaping it according to the strength and kinetics of ERK activation.

Our results show that phosphorylation of the Elk-1 TAD by ERK can either promote or inhibit Mediator interaction depending on the sites involved, thereby modulating transcriptional activation. Given that the TAD sequences are conserved in the other TCFs, our findings may also apply to them. The more rapidly phosphorylated sites are located in the substantially conserved central core of the TAD and are essential for transcriptional activation, lying close to the FW hydrophobic motif required for Elk-1-Mediator interaction (10, 18). Multisite phosphorylation of these residues might stabilize this interaction and perhaps also set a signaling threshold for it, similar to the way that multisite phosphorylation sets a threshold for the Sic1-Cdc4 interaction (29). In contrast, slowly phosphorylated sites located N- and C-terminal of the conserved TAD core act negatively. Their phosphorylation inhibits Mediator recruitment and limits transcriptional activation (Fig. 4D) and may also facilitate recruitment of negative regulators of Elk-1 activity. Together, these properties ensure that ERK phosphorylation of the Elk-1 TAD is self-limiting, whereby phosphorylation of slow sites attenuates TCF-SRF target gene expression under conditions of strong or sustained ERK signaling (Fig. 4D). Our results challenge the common assumption that multisite modification events act unidirectionally and can only be reversed or limited by antagonistic enzymes, such as phosphatases. Given the prevalence of such events in different biological processes, we expect that similar mechanisms may govern other regulatory interactions.

REFERENCES AND NOTES

1. J. Gunawardena, *Proc. Natl. Acad. Sci. U.S.A.* **102**, 14617–14622 (2005).
2. J. Gunawardena, *Biophys. J.* **93**, 3828–3834 (2007).
3. C. Salazar, T. Höfer, *FEBS J.* **276**, 3177–3198 (2009).
4. X. Liu, L. Bardwell, Q. Nie, *Biophys. J.* **98**, 1396–1407 (2010).
5. M. Karin, T. Hunter, *Curr. Biol.* **5**, 747–757 (1995).
6. F. H. Cruzalegui, E. Cano, R. Treisman, *Oncogene* **18**, 7948–7957 (1999).
7. R. Janknecht, W. H. Ernst, V. Pingoud, A. Nordheim, *EMBO J.* **12**, 5097–5104 (1993).
8. R. Marais, J. Wynne, R. Treisman, *Cell* **73**, 381–393 (1993).
9. R. Janknecht, W. H. Ernst, A. Nordheim, *Oncogene* **10**, 1209–1216 (1995).
10. M. A. Price, A. E. Rogers, R. Treisman, *EMBO J.* **14**, 2589–2601 (1995).
11. H. Gille et al., *EMBO J.* **14**, 951–962 (1995).
12. D. A. Fantz, D. Jacobs, D. Glossip, K. Kornfeld, *J. Biol. Chem.* **276**, 27256–27265 (2001).
13. S. H. Yang, P. R. Yates, A. J. Whitmarsh, R. J. Davis, A. D. Sharrocks, *Mol. Cell. Biol.* **18**, 710–720 (1998).
14. S. H. Yang, A. J. Whitmarsh, R. J. Davis, A. D. Sharrocks, *EMBO J.* **17**, 1740–1749 (1998).
15. D. Jacobs, D. Glossip, H. Xing, A. J. Muslin, K. Kornfeld, *Genes Dev.* **13**, 163–175 (1999).
16. J. L. Stevens et al., *Science* **296**, 755–758 (2002).
17. G. Wang et al., *Mol. Cell* **17**, 683–694 (2005).
18. M. A. Balamotis et al., *Sci. Signal.* **2**, ra20 (2009).

19. W. Wang *et al.*, *Dev. Cell* **16**, 764–771 (2009).
20. F. X. Theillet *et al.*, *Nat. Protoc.* **8**, 1416–1432 (2013).
21. M. Cavigelli, F. Dolfi, F. X. Claret, M. Karin, *EMBO J.* **14**, 5957–5964 (1995).
22. H. Gille, T. Strahl, P. E. Shaw, *Curr. Biol.* **5**, 1191–1200 (1995).
23. A. J. Whitmarsh, P. Shore, A. D. Sharrocks, R. J. Davis, *Science* **269**, 403–407 (1995).
24. M. A. Price, F. H. Cruzalegui, R. Treisman, *EMBO J.* **15**, 6552–6563 (1996).
25. D. L. Sheridan, Y. Kong, S. A. Parker, K. N. Dalby, B. E. Turk, *J. Biol. Chem.* **283**, 19511–19520 (2008).
26. E. R. Vickers *et al.*, *Mol. Cell. Biol.* **24**, 10340–10351 (2004).
27. M. A. Wozniak *et al.*, *Curr. Biol.* **22**, 2017–2026 (2012).
28. T. Sugimoto, S. Stewart, K. L. Guan, *J. Biol. Chem.* **272**, 29415–29418 (1997).
29. P. Nash *et al.*, *Nature* **414**, 514–521 (2001).

ACKNOWLEDGMENTS

Work in the Treisman group was supported by the Francis Crick Institute, which receives its core funding from Cancer Research UK (FC001-190), the UK Medical Research Council (FC001-190), and the Wellcome Trust (FC001-190), and by European Research Council (ERC) advanced grant 268690 ACTinNonSRF. Work in the Selenko group is funded by ERC consolidator grant 647474 NeuroInCellNMR. F.-X.T. is supported by Agence Nationale pour la Recherche grant ANR14-ACHN-0015-01. The authors have no conflicts of interest. Author contributions: A.M. conceived the project; A.M., C.F., and F.M. designed and performed molecular and cell biology experiments; F.-X.T., T.M.C., and P.A.B. developed the competitive inhibition model; F.-X.T. and P.S.

designed, executed, and interpreted the NMR experiments; and A.M., P.S., and R.T. designed and interpreted experiments and wrote the paper. We thank F. Gualdrini, C. Esnault, and P. Costello for characterizing gene regulation in reconstituted TKO MEFs, sharing their unpublished data, and generating reconstituted TKO MEF cells; the Crick Genomics and Flow Cytometry technology platforms for technical support; and A. Behrens, V. Calleja, A. Chakraborty, M. Diefenbacher, C. Duellberg, R. Nicolas, P. Riou, M. Skehel, and our group members for advice and discussions.

SUPPLEMENTARY MATERIALS

www.sciencemag.org/content/354/6309/233/suppl/DC1
Figs. S1 to S6
References (30–41)

5 August 2015; accepted 23 August 2016
10.1126/science.aad1872

VACCINES

Rapid development of a DNA vaccine for Zika virus

Kimberly A. Dowd,^{1*} Sung-Youl Ko,^{2*} Kaitlyn M. Morabito,² Eun Sung Yang,² Rebecca S. Pelc,¹ Christina R. DeMaso,¹ Leda R. Castillo,^{2,3} Peter Abbink,⁴ Michael Boyd,⁴ Ramya Nityanandam,⁴ David N. Gordon,¹ John Robert Gallagher,⁵ Xuejun Chen,² John-Paul Todd,² Yaroslav Tsybovsky,⁶ Audray Harris,⁵ Yan-Jang S. Huang,⁷ Stephen Higgs,⁷ Dana L. Vanlandingham,⁷ Hanne Andersen,⁸ Mark G. Lewis,⁸ Rafael De La Barrera,⁹ Kenneth H. Eckels,⁹ Richard G. Jarman,¹⁰ Martha C. Nason,¹¹ Dan H. Barouch,⁴ Mario Roederer,² Wing-Pui Kong,² John R. Mascola,² Theodore C. Pierson,^{1†} Barney S. Graham^{2†}

Zika virus (ZIKV) was identified as a cause of congenital disease during the explosive outbreak in the Americas and Caribbean that began in 2015. Because of the ongoing fetal risk from endemic disease and travel-related exposures, a vaccine to prevent viremia in women of childbearing age and their partners is imperative. We found that vaccination with DNA expressing the premembrane and envelope proteins of ZIKV was immunogenic in mice and nonhuman primates, and protection against viremia after ZIKV challenge correlated with serum neutralizing activity. These data not only indicate that DNA vaccination could be a successful approach to protect against ZIKV infection, but also suggest a protective threshold of vaccine-induced neutralizing activity that prevents viremia after acute infection.

The emergence of Zika virus (ZIKV) in the Americas and Caribbean follows a series of global threats to public health from mosquito-borne viral diseases over the past three decades. Because of the profound impact on individuals and society from a disabling congenital disease caused by ZIKV infection in pregnant women, the World Health Organization declared ZIKV a global health emergency in February 2016. Although it is likely that the incidence of ZIKV infection will decline considerably within 1 to 2 years (1), it is also likely that ZIKV will become endemic in tropical and subtropical regions, with sporadic outbreaks and potential for spread into new geographical areas, as observed with other emerging arboviruses such as West Nile (WNV) and chikungunya. Therefore, unless immunity is established before childbearing age, pregnant women will continue to be at risk for an infection that could harm their fetus. Further, because men can harbor ZIKV in semen for several months after a clinically unapparent

infection and can sexually transmit virus to a pregnant partner (2), even women in nonendemic regions will have some ongoing risk if exposed to men who have traveled to endemic regions. These characteristic features of transmission and disease suggest that there will be an ongoing need for a ZIKV vaccine to maintain a high level of immunity in the general population and in travelers to endemic regions to reduce the frequency of fetal infection.

To rapidly address the critical need for a preventive vaccine to curtail the ongoing ZIKV outbreak in the Americas, we chose a gene-based vaccine delivery approach that leverages our prior experience with a DNA-based WNV vaccine (3). Advantages of DNA vaccines include the ability to rapidly test multiple candidate antigen designs, the ability to rapidly produce material that conforms to good manufacturing practices, an established safety profile in humans, and a relatively straightforward regulatory pathway into clinical evaluation.

Antigen design was guided by prior knowledge about humoral immunity to flaviviruses. Vaccine-

elicited neutralizing antibodies (NAbs) are associated with protection from flavivirus-mediated disease (4). Because the most potent monoclonal flavivirus NAbs map to conformational epitopes in domain III (DIII) of the envelope (E) protein (5), or to more complex quaternary epitopes that bridge between antiparallel E dimers or between dimer rafts arrayed on the virus surface (6, 7), our goal was to identify constructs that produced particles that faithfully captured the antigenic complexity of infectious virions. Expression of the structural proteins premembrane (prM) and E are sufficient for the production and release of virus-like subviral particles (SVPs) with antigenic and functional properties similar to those of infectious virions (8, 9).

To identify promising vaccine candidates, prM-E constructs were synthesized and screened for expression and efficiency of particle release from transfected cells. prM-E sequences were inserted into a cytomegalovirus immediate early promoter-containing vector (VRC8400) that has been evaluated clinically in several previous studies (3, 10, 11). These constructs are distinct from one reported in recent studies by Larocca *et al.* (12) and Abbink *et al.* (13) that was based on a Brazilian isolate (strain

¹Viral Pathogenesis Section, National Institute of Allergy and Infectious Diseases, National Institutes of Health, Bethesda, MD 20892, USA. ²Vaccine Research Center, National Institute of Allergy and Infectious Diseases, National Institutes of Health, Bethesda, MD 20892, USA. ³Federal University of Rio de Janeiro, COPPE (Instituto Alberto Luiz Coimbra de Pós-Graduação e Pesquisa de Engenharia), Chemical Engineering Program, Rio de Janeiro, Rio de Janeiro, Brazil. ⁴Center for Virology and Vaccine Research, Beth Israel Deaconess Medical Center, Harvard Medical School, Boston, MA 02215, USA. ⁵Structural Informatics Unit, Laboratory of Infectious Diseases, National Institute of Allergy and Infectious Diseases, National Institutes of Health, Bethesda, MD 20892, USA. ⁶Electron Microscopy Laboratory, Cancer Research Technology Program, Leidos Biomedical Research, Frederick National Laboratory for Cancer Research, Frederick, MD 21702, USA. ⁷Department of Diagnostic Medicine/Pathobiology, College of Veterinary Medicine, Kansas State University, Manhattan, KS 66506, USA. ⁸Bioqual, Rockville, MD 20852, USA. ⁹Translational Medicine Branch, Walter Reed Army Institute of Research, Silver Spring, MD 20910, USA. ¹⁰Viral Diseases Branch, Walter Reed Army Institute of Research, Silver Spring, MD 20910, USA. ¹¹Biostatistics Research Branch, Division of Clinical Research, National Institute of Allergy and Infectious Diseases, National Institutes of Health, Bethesda, MD 20852, USA.

*These authors contributed equally to this work. †Corresponding author. Email: piersonc@niaid.nih.gov (T.C.P.); bgraham@mail.nih.gov (B.S.G.)

gairdner 2016 SYMPOSIA

LES PRIX CANADA GAIRDNER AWARDS

Rodolphe Barrangou

International

Philippe Horvath

International

Jennifer Doudna

International

Emmanuelle Charpentier

International

Feng Zhang

International

Frank Plummer

Wightman

Anthony Fauci

Global Health

Watch the
webcast LIVE at:

bit.ly/Gairdnerwebcast

Sylvain Moineau

Université Laval

Jonathan Weissman

University of California San Francisco

Daniel Durocher

Lunenfeld-Tanenbaum Research Institute,
University Of Toronto

Anthony James

University of California Irvine

Paula Cannon

Keck School Of Medicine,
University of Southern California

Françoise Baylis

Dalhousie University

2016 Canada Gairdner Awardees' Lectures

Thursday, October 27, 2016

9:00 am – 3:00 pm

University of Toronto

Macleod Auditorium

This year's Canada Gairdner Award winners join together after touring the country to explain and explore their discoveries in science. Our International Award winners will discuss the expanding potential of the CRISPR technique for gene editing, and our Wightman and Global Health awardees will share their experiences confronting HIV/AIDS and broader global health challenges.

Gene Editing: Bacterial Immunity To Global Impact

Friday, October 28, 2016

9:00 am – 2:30 pm

University of Toronto

Macleod Auditorium

Inspired by the gene-editing pioneers of the 2016 Canada Gairdner International Awards, this one-day symposium will step beyond the discovery of the CRISPR-Cas system to explore gene editing's potential across the biological spectrum, and how advances in human health, disease control & environmental engineering could change our perspective & place in the natural world. Featuring a Roundtable Discussion with the 2016 Canada Gairdner Award Laureates.

Gairdner Symposia are FREE events open to all interested members of the public

For further information visit us at www.gairdner.org or follow us on [Twitter](#) and [YouTube](#)

New: 4 liter capacity!



More Capacity

Centrifuge 5920 R

The new Centrifuge 5920 R delivers extraordinary high capacity in a very compact and ergonomic product design. Its state-of-the-art refrigeration system provides excellent cooling performance and keeps your temperature sensitive samples safe.

- > Max. capacity: 4 × 1000 mL or 52 × 50 mL conical
- > Outstanding rotor versatility
- > Space-saving design
- > Advanced temperature management
- > NEW: Eppendorf Conical Tubes, 15 mL and 50 mL



www.eppendorf.com/centrifugation

Eppendorf and the Eppendorf logo are registered trademarks of Eppendorf AG, Germany. U.S. Design Patents are listed on www.eppendorf.com/ip. All rights reserved, including graphics and images. Copyright © 2016 by Eppendorf AG.

Watch video!





DVS Analyzers

IGAsorp dynamic vapor sorption (DVS) analyzers from Hidden Isochema allow control of relative humidity (RH) at values up to 10 times lower than possible with traditional DVS analyzer methods. Climate-XT mode applies independent, intelligent control algorithms to the sample and humidifier thermostats to allow humidity setpoints below 0.2% RH. The analyzer's HIsorp software determines and applies the humidifier temperature(s) required to attain the full range of isotherm points as entered by the user. The process is fully automated, and the full kinetic data is recorded and analyzed along with the equilibrium data. Hidden's Climate-XT mode uniquely allows fully automated access to the complete range of humidity values up to 98% RH, with direct measurement of both humidity and temperature at the sample position. For a sample temperature of 50°C, humidity may be controlled as standard down to 0.1% RH, and further options are available for optimized temperature and humidity requirements.

Hidden Isochema

For info: +44-(0)-1925-244678
www.hiddenisochema.com

Real-Time Intracellular Oxygen Assay

MitoXpress Intra is a powerful new tool that facilitates real-time assessment of transient changes in cell respiration, oxygen gradients, and physiological responses across a range of cell models. Specifically, it simplifies the measurement of cellular oxygenation—a critical parameter across many fields of research including hypoxia and cancer metabolism. Traditionally, intracellular measurements have proven very difficult, requiring the use of invasive, laborious, low-throughput, technically challenging techniques. Using the MitoXpress Intra probe, researchers can monitor molecular oxygen in real time within the cell monolayer on a plate reader in a noninvasive, rapid manner. The assay is optimized for use on standard 96-/384-well plates and time-resolved fluorescence plate readers, enabling high-throughput analysis of multiple samples in parallel. Data produced is complementary to other intracellular parameters, such as reactive oxidative species and mitochondrial membrane potential.

AMS Biotechnology

For info: +44-(0)-1235-828200
www.amsbio.com



SPR System

Biacore 8K is the new eight-needle, high-sensitivity surface plasmon resonance system from GE Healthcare Life Sciences. It offers Biacore's high-quality kinetics and affinity data at a speed that shortens time to results by up to eightfold compared to single-needle systems. Its flexibility facilitates the analysis of small fragments as well as multidomain proteins, and it can also tackle new drug formats such as bispecific antibodies. Biacore 8K's sensitivity and stability generate high-quality binding data for small molecules binding to complex targets such as G-protein-coupled receptors, and provide an alternative to traditional immunoassays such as ELISAs. Its eight needles allow analysis of up to 2,300 small-molecule fragments per day, and the novel 2D kinetics methodology delivers full kinetic characterization data within 35 minutes, without the need for extensive assay development. Affinity and kinetic ranking enables rapid selection of biotherapeutic or small-molecule hits, while detailed kinetic and affinity data help characterize and optimize selected binders.

GE Healthcare Life Sciences

For info: 800-526-3593
www.gelifesciences.com

guaranteeing specific staining. The assay offers a rapid, quantitative approach to monitoring autophagy in live cells without the need for cell transfection.

Enzo Life Sciences

For info: 1-800-942-0430
www.enzolifesciences.com

Organoid Resource Lab

Trevigen is pleased to announce the opening of the Organoid Resource Laboratory (ORL) at its Gaithersburg, Maryland, location. The purpose of the ORL is to provide the research community with the matrices, reagents, growth factors, organoid progenitor cells, protocols, and technical support needed to promote the establishment of organoid cultures. Researchers have devised means to propagate 3D cultures, which most closely mimic the physiological response patterns of the tissue of origin. The ultimate form of 3D culture is the organoid, which is cultured from progenitor stem cells taken from a fresh target organ. The cells never come in direct contact with glass or plastic labware and under stringent, prescribed conditions, can be cultured to become mini-organs that closely resemble the original source organ and exhibit the proper physiological response patterns. Trevigen now offers highly qualified organoid culture products, along with protocols for use and technical services support, to assist the adoption of organoid cultures by both new and experienced labs alike.

Trevigen

For info: 301-216-2800
www.trevigen.com

Autophagy Detection Kit

CYTO-ID Autophagy Detection Kit 2.0 measures and labels autophagic vacuoles and monitors autophagic flux in lysosomally inhibited live cells using a novel dye. The dye has been optimized through the identification of titratable functional moieties that allow for minimal staining of lysosomes while exhibiting bright fluorescence upon incorporation into pre-autophagosomes, autophagosomes, and autolysosomes (autophagolysosomes). As such, the dye ensures a low background while

Electronically submit your new product description or product literature information! Go to www.sciencemag.org/about/new-products-section for more information.

Newly offered instrumentation, apparatus, and laboratory materials of interest to researchers in all disciplines in academic, industrial, and governmental organizations are featured in this space. Emphasis is given to purpose, chief characteristics, and availability of products and materials. Endorsement by *Science* or AAAS of any products or materials mentioned is not implied. Additional information may be obtained from the manufacturer or supplier.



There's only one **Science**

Science Careers Advertising

For full advertising details, go to ScienceCareers.org and click For Employers, or call one of our representatives.

Tracy Holmes

Worldwide Associate Director
Science Careers
Phone: +44 (0) 1223 326525

THE AMERICAS

E-mail: advertise@sciencecareers.org
Fax: +1 (202) 289 6742

Tina Burks

Phone: +1 (202) 326 6577

Nancy Toema

Phone: +1 (202) 326 6578

Online Job Posting Questions

Phone: +1 (202) 312 6375

EUROPE/INDIA/AUSTRALIA/ NEW ZEALAND/REST OF WORLD

E-mail: ads@science-int.co.uk
Fax: +44 (0) 1223 326532

Sarah Lelarge

Phone: +44 (0) 1223 326527

Kelly Grace

Phone: +44 (0) 1223 326528

Online Job Posting Questions

Phone: +44 (0) 1223 326528

JAPAN

Katsuyoshi Fukamizu (Tokyo)

E-mail: kfukamizu@aaas.org
Phone: +81 3 3219 5777

Hiroyuki Mashiki (Kyoto)

E-mail: hmashiki@aaas.org
Phone: +81 75 823 1109

CHINA/KOREA/SINGAPORE/ TAIWAN/THAILAND

Danny Zhao

E-mail: dzhao@aaas.org
Phone: +86 131 4114 0012

All ads submitted for publication must comply with applicable U.S. and non-U.S. laws. Science reserves the right to refuse any advertisement at its sole discretion for any reason, including without limitation for offensive language or inappropriate content, and all advertising is subject to publisher approval. Science encourages our readers to alert us to any ads that they feel may be discriminatory or offensive.

Science Careers

FROM THE JOURNAL SCIENCE AAAS

ScienceCareers.org

POSITIONS OPEN



POSTDOCTORAL FELLOWSHIPS

The Geophysical Laboratory, Carnegie Institution of Washington, invites applications for **POSTDOCTORAL FELLOWSHIPS**. The Geophysical Laboratory emphasizes interdisciplinary experimental and theoretical research in fields spanning geoscience, microbiology, chemistry, and physics. The Laboratory supports world-class facilities in high-pressure research; organic, stable isotope and biogeochemistry; mineral physics and petrology; and astrophysics.

Please visit website: <https://jobs.carnegiescience.edu/jobs/carnegie-fellowships-for-the-geophysical-laboratory-4/> to view a list of required materials and application instructions. Also, see website <http://www.glcw.edu/> for a listing of personnel, current research interests, and major facilities.

Completed applications for Carnegie fellowships should be submitted by **November 30, 2016**.

The Geophysical Laboratory is located in Washington, DC, and is an Equal Opportunity Employer.

U.S. POSTAL SERVICE

Statement required by the Act of 12 August 1970, Section 3685, Title 39, United States Code, showing the ownership, management, and circulation of: 1-9. Science, Publication No. 0036-8075, is published weekly on Friday, except the last week in December, at 1200 New York Avenue, N.W., Washington, DC 20005. Date of filing: 26 September 2016. This is also the address of the publisher, the editor, and the managing editor, who are, respectively, Bill Moran, Jeremy Berg, and Monica M. Bradford.

10. The owner is the American Association for the Advancement of Science, 1200 New York Avenue, N.W., Washington, DC 20005. Stockholders: None.

11. Known bondholders, mortgages, and other security holders owning or holding 1 percent or more of total amount of bonds, mortgages, or other securities: None.

12. The purpose, function, and nonprofit status of this organization and the exempt status for federal income tax purposes have not changed during the preceding 12 months.

13-15. The average number of copies of each issue during the preceding 12 months is (A) Total number of copies printed: 86,041; (B) Paid circulation: 70,141; (1) Paid/Requested outside-county mail subscriptions stated on form 3541: 60,218; (2) Paid/Requested in-county subscriptions stated on form 3541: 0; (3) Sales through dealers and carriers, street vendors, counter sales: 9,912; (4) Other classes mailed through USPS: 11; (C) Total paid circulation: 70,141; (D) Free distribution: samples, complimentary, and other free copies: 13,891; (1) Outside-county as stated on form 3541: 2,504; (2) In-county as stated on form 3541: 0; (3) Other classes mailed through the USPS: 2; (4) Free distribution outside of mail carrier or other means: 11,385; (E) Total free distribution: 13,891; (F) Total distribution: 84,032; (G) Copies not distributed: 2,023; (H) Total: 86,055; (I) Percent paid and/or Requested Circulation: 83.5%.

Actual number of copies of single issue (9/9/2016) published nearest to filing date are (A) Total number of copies printed: 68,050; (B) Paid circulation: 62,763; (1) Paid/Requested outside-county mail subscriptions stated on form 3541: 53,781; (2) Paid/Requested in-county subscriptions stated on form 3541: 0; (3) Sales through dealers and carriers, street vendors, counter sales: 8,971; (4) Other classes mailed through USPS: 11; (C) Total paid circulation: 62,763; (D) Free distribution: Samples, complimentary, and other free copies: 3,266; (1) Outside-county as stated on form 3541: 2,442; (2) In-county as stated on form 3541: 0; (3) Other classes mailed through the USPS: 2; (4) Free distribution outside of mail: Carrier or other means: 822; (E) Total free distribution: 3,266; (F) Total distribution: 66,029; (G) Copies not distributed: 2,021; (H) Total: 68,050; (I) Percent paid and/or Requested Circulation: 95.1%.

I certify that the statements made above are correct and complete. (signed) Bill Moran, Publisher.

POSITIONS OPEN

ASSOCIATE PROFESSOR of TERRESTRIAL REMOTE SENSING

Geospatial Sciences Center of Excellence
South Dakota State University

The Geospatial Sciences Center of Excellence seeks a person with research experience and teaching interests focused on remote sensing science and applications with expertise in one or more of these focal areas: land cover and land use, agriculture, hydrology, and biogeochemistry. This 12-month position is funded by state funds and carries a workload of 80% research, 10% teaching, and 10% service. Responsibilities include securing externally funded research grants, recruiting and mentoring doctoral students and post-doctoral researchers, and delivering one graduate course per year. Minimum qualifications include an earned Ph.D. degree in an appropriate field with a background in remote sensing; minimum of five years' experience conducting externally funded research; scholarly activity, including collaborative research and peer-reviewed publications as first author; and a demonstrated ability to communicate effectively. A record of sponsored research, experience with geospatial technologies and quantitative methods, and experience mentoring students and staff are desired qualifications. For questions on the position, contact the search committee chair, **Dr. David Roy** via email at (605) 688-5352 or david.roy@sdstate.edu. Application deadline is November 3, 2016. To view a full position description and to apply, visit website: <https://yourfuture.sdbor.edu/applicants/Central?quickFind=60522>, and click on "apply for this posting." For questions on the electronic employment process, contact SDSU Human Resources at (605) 688-4128. SDSU is an AA/EEO Employer. Women, minorities, veterans, and persons with disabilities are encouraged to apply.

FACULTY POSITION(S) IN HEALTH DISPARITIES IN CANCER RESEARCH PROGRAM

The Mitchell Cancer Institute at the University of South Alabama (USAMCI) is recruiting faculty at the junior and mid-career stage for its newly developed research program in "Cancer Health Disparities". This program will broaden the institute's overall expertise-base and complement existing research programs at USAMCI. Interested applicants, who are already conducting cancer health disparities research or plan to use their basic and translational research skills to expand their portfolio into this exciting and much needed area of research, are encouraged to apply. Candidates with a track record of independent funding and publications in high impact journals will be given the highest consideration. Successful candidates will be expected to run a vibrant collaborative program supported by external funding. A competitive salary and research start-up package will be provided. Position(s) will be within the Department of Oncologic Sciences, Mitchell Cancer Institute at the University of South Alabama and are tenure-track.

To apply, please send your curriculum vitae, a brief summary of your research plans, and three letters of recommendation to: **Ajay P. Singh, PhD; Professor of Oncologic Sciences & Head, Health Disparities in Cancer Research Program, Mitchell Cancer Institute, 1660 Springhill Avenue, Mobile, AL 36604** or by email to dkeasler@health.southalabama.edu. Applications will be reviewed and evaluated on an ongoing basis. The University of South Alabama is an Equal Opportunity Employer-Minorities/Females/Veterans/Disabled.

Post Your Jobs

• 1,449,418 unique job seekers

• 235,960 job applications in 2015

Science Careers





Wales wants more scientists

Wales may be small but it has big plans for science. New initiatives to fund over 100 new fellowships and hire up to 30 top scientists, combined with infrastructure investments in the physical sciences, are turning Wales into a land of opportunity. **By Gunjan Sinha**

Mumbles Lighthouse, Wales

Advanced materials aren't usually associated with Wales, but it's high time they were, says **James Durrant**, professor of photochemistry at Imperial College London. In 2013, Durrant accepted a joint appointment as the *Sêr Cymru* (Stars Wales) Solar Energy Research Chair at Swansea University in Wales. Now he also coordinates research to build the country's reputation as a pioneer in new materials that expand the reach of solar energy. At Swansea's Sustainable Product Engineering Centre for Innovative Functional Industrial Coatings (SPECIFIC), Durrant helps develop technologies that enable buildings to produce, store, and release their own energy. Durrant already leads a successful research lab at Imperial, but his joint appointment now allows him to connect fundamental science expertise at Imperial with engineering and manufacturing expertise at Swansea. "Imperial is a world-class place for research, but London is not an environment that focuses on manufacturing," he says. Swansea was historically a manufacturing hub and remains so—and today that legacy continues at the university's campuses, where you are just as likely to see industry experts roaming the labs at SPECIFIC as you are to spot academics, Durrant says.

Durrant was one of the first beneficiaries of the Welsh Government's *Sêr Cymru* initiative, which was announced in 2012 as part of the government's science strategy to identify areas of research where Wales "has a fighting chance to be the best in the world," says **David Allen**, chair of the Higher Education Funding Council for Wales. The first phase of *Sêr Cymru* committed up to £50 million (US\$66.2 million) to bring prestigious research chairs to Welsh universities and also to support national research networks in three "grand challenge" areas: life sciences and health; low carbon, energy, and environment; and advanced engineering and materials. These networks are intended to "get the Welsh universities to think horizontally rather than vertically," says Allen, and to strengthen their reputation as centers for scientific enquiry. A second £60 million (US\$79.5 million) phase of *Sêr Cymru*, launched in December 2015, is further boosting research capacity by offering fellowships to

mid- or early-career scientists and those currently on a career break. Through both initiatives, Wales hopes to draw in 20 to 30 "rising star" researchers and support 120 fellows "to produce critical mass around our strengths," says **Julie Williams**, chief science adviser to the Welsh Government. "Our ambition is to grow research."

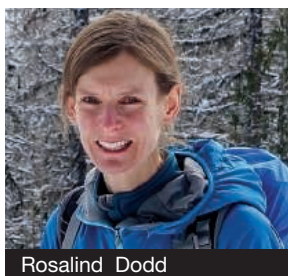
To boost capacity even further, the Welsh universities of Cardiff, Swansea, Bangor, and Aberystwyth have also been investing heavily in infrastructure such as new buildings and equipment.

Like other countries that see knowledge-growth as a pillar of their economies, Wales has created a science agenda that aims not only to expand academic science, but to translate science and technology into applications that lead to economic growth. Consequently, it is inviting industry to work with academics in research areas deemed to have the greatest promise of commercial success, adds Williams.

World-class brain imaging at Cardiff

At Cardiff University, the goal of close industry collaboration has morphed into a new physical space: the £300 million (US\$393.6 million) Innovation Campus. The campus, which is being constructed in phases, aims to bring business development staff on hand to assist with access to university research, facilities, and services. It will feature social networking and creativity spaces to encourage problem solving, open innovation, and collaboration. The campus will house other research facilities in the future, and is already home to the Cardiff University Brain Research Imaging Centre (CUBRIC)—a £44 million (US\$58.3 million) facility financed by a combination of public funds and charitable trusts.

Among its five new scanners, CUBRIC boasts Europe's most powerful microstructural brain scanner, the Siemens 3 Tesla Connectome magnetic resonance imaging (MRI) system, a specially adapted MRI scanner of which there is only one other in the world, located at Harvard University in the United States. Because its powerful technology can measure microstructural features in the brain, such as **cont.**>



Rosalind Dodd

Upcoming Features

Top Employers Survey—October 28 ■ **Regional Focus: China—November 4** ■ **Regional Focus: China—December 16**

the diameter of nerve cell axons, it enables researchers to answer entirely new questions, says CUBRIC director **Derek Jones**. “Rather than merely brain mapping, we can start to address more biologically specific questions like, ‘How do individual differences in axon diameter correlate with differences in impulsivity?’” he says.

Jones arrived at Cardiff in 2006 as codirector of CUBRIC. His job was to establish a neuroimaging research program where none existed. A medical physicist by training, Jones had the good fortune to work alongside two other physicists with complementary backgrounds. Together they came up with the idea and a business plan for establishing a new, comprehensive neuroimaging research center at Cardiff. The proposal dovetailed nicely with Wales’ greater science agenda to establish itself as world class in a few key areas. “I think they were excited at the vision of the university having something genuinely unique,” Jones recalls. Their plan was approved. The new CUBRIC boasts a combination of imaging equipment that is unique in all of Europe.

Anyone can approach the center with a research proposal, says Jones, and it will work with both academics and industry partners on brain stimulation technologies, including pharmaceutical companies investigating the effects of experimental medicines. Jones’s own research employs the center’s equipment to achieve the best estimates of myelination, axon characteristics such as density and diameter, and brain connectivity. He then uses that information to understand individual differences in brain electrophysiology and cognition. A recent experiment, for example, showed that six weeks of cognitive training could produce detectable differences in brain microstructure.

Translating research at Swansea

At Swansea, much of the research for Sêr Solar (funded under Sêr Cymru) is focused on commercialization. Durrant and his colleagues at Imperial’s Centre for Plastic Electronics are working on developing and understanding new ink-based coatings that can be printed onto surfaces as semiconductor materials in order to capture solar energy. Researchers at Swansea, in collaboration with industry, are taking these printable materials and focusing on the challenges of scalability and stability to develop new classes of solar cells. “The vision is to print the ink directly onto roofing products,” he says.

Durrant is an academic at heart. “I’d love my research to be useful,” he says, “but I’m not very good at applying it.” At Swansea he can concentrate on basic research, while others working alongside him can develop applications. He points out that the CEO of SPECIFIC previously worked in the steel industry. “That type of industrial perspective permeates the culture of SPECIFIC, and so you have a huge drive to turn science into practical applications. I’m happy to be involved,” adds Durrant.

A pilot plant for the coated roofing has already been built at the Innovation and Knowledge Centre—located about 16 km (10 miles) away from Swansea University’s Singleton Park campus. The £20 million (US\$26.5 million), five-year SPECIFIC project will develop coated steel and glass products to incorporate into new and existing buildings, enabling walls and roofs to generate, store, and release energy. Such coatings on buildings



could reduce the United Kingdom’s CO₂ output by millions of tons a year. The project is a partnership that in addition to Swansea, involves several universities including Imperial College, Bangor, and Cardiff, as well as multinational companies such as Tata Steel and BASF International.

Swansea University recently expanded and in 2015 opened its Bay

Campus, a £450 million (US\$580.6 million) science and innovation space situated on a 65-acre beachfront site not far from the Singleton Park Campus. The campus currently hosts the College of Engineering and the School of Management and boasts a hall that seats 800, an extensive library, and student housing, among other amenities. The multipartner, public-private project was largely funded by the university and the Welsh Government through the European Regional Development Fund.

Wales builds strength in environmental science

In striving for excellence in select areas, Wales is following a tried and tested recipe. **Chris Thomas** came to Aberystwyth University in 2007 to help build up the Institute of Biological, Environmental and Rural Sciences (IBERS). Thomas is a wildlife biologist by training, but he now uses technology such as satellite remote sensing and software applications such as geographic information systems to model vector disease transmission. “I was attracted to Wales by the big investment in environmental and agricultural studies,” Thomas says. “We are very proud of what’s gone on there.”



David Thomas

In 2013, Thomas was appointed Pro Vice-Chancellor of Research at Aberystwyth. His primary goal is to ensure the success of the current science strategy. With translational research high on the agenda, Thomas is also overseeing the conception and construction of the new £40.5 million (US\$53.6 million) Innovation and Enterprise Campus at Aberystwyth, which will focus on agricultural innovation. The university is already world

renowned for research in pasture-based agriculture, which encompasses many areas including grass breeding, nutritional characterization of different grass breeds, and the use of different plant species in applications ranging from flood control to altering the nutritional value of meat and milk via the grasses animals eat.

Through the £7 million (US\$9.2 million) Sêr Cymru National Research Network for Low Carbon, Energy and Environment—one of the three grand challenge areas—Welsh universities hope to capitalize even more on their expertise in pasture-based agriculture. The network encourages interdisciplinary research across departments and universities, so that environmental scientists collaborate with energy scientists, for example, and architects with plant scientists, says **David Thomas**, director of the Bangor University-based network. “The network has been the catalyst to bring them into the same room,” he adds. “It encourages collaborations to be more innovative.”

FEATURED PARTICIPANTS

Aberystwyth University
www.aber.ac.uk

Bangor University
www.bangor.ac.uk

Cardiff University
www.cardiff.ac.uk

CUBRIC
sites.cardiff.ac.uk/cubric

**Higher Education Funding Council
for Wales**
www.hefcw.ac.uk/home/home.aspx

**Institute of Biological,
Environmental and Rural Sciences**
www.aber.ac.uk/en/ibers

Learned Society of Wales
www.learnedsociety.wales

**National Research Network
for Low Carbon, Energy and
Environment**
www.nrn-lcee.ac.uk

SPECIFIC
www.specific.eu.com

Swansea University
www.swansea.ac.uk



Institute of Biological, Environmental and Rural
Sciences at Aberystwyth University

The collaborative environment is what **Rosalind Dodd** enjoys most about working in the network. “We’ve got some great researchers who are very engaged and great to work with,” she says. Dodd came to Bangor University in January after completing a postdoc at the University of Arkansas in the United States. She found the work in Arkansas interesting, but wanted “something more ambitious in terms of size and scope.” Dodd is part of a cluster within the network focused on smart grass: Her group studies the impact of extreme weather on different varieties of grass and the ecosystem. The research will become important across agricultural regions, she says, as climate change is expected to increase the frequency of extreme weather events around the world.

A sustainable future built on strong science

Agriculture has and continues to make up a major share of Wales’ economy—support for research in this area continues to be strong. Wales’ science agenda is not only driven by its existing strengths in the life sciences, but also by a vision of where it wants to go. “Wales is trying to brand itself as a sustainable nation,” says Allen. “It defines the sort of Wales we want to be.”

Population growth, climate change, environmental destruction, and aging populations are global challenges. There is a widespread belief that only science and technology can provide solutions to these potentially catastrophic societal and environmental issues. Wales isn’t the only country investing in the science of sustainability—but it has found niches in which it either already excels or has the potential to shine.

The country’s recent capacity-building initiatives are not arbitrary. The Welsh Government’s *Sêr Cymru* program was largely based on studies showing that Welsh universities were not winning the percentage of competitive Research Councils UK grants commensurate with the size of the Welsh population (5% of the UK total). Evidence gathered by **Peter Halligan**, chief executive of the Learned Society of Wales, showed that the problem lay not in the quality of science but rather in the number of researchers. Wales has had a deficit of researchers—over 600 fewer relative to its population than Scotland, for example. Among the largest deficits have been researchers in science, technology, engineering, mathematics, and medicine—areas largely funded by high-spending agencies such as the Medical Research Council and the Engineering and Physical Sciences Research Council.

Despite this work force deficit, Welsh science overall now outperforms many other similarly small countries such as

Norway, Ireland, and New Zealand, according to commonly used measures of efficiency and science quality. Using field-weighted citation impact (a recognized measure of mean citations per article, normalized for subject field), Wales’ citation impact increased from 39% above the world average in 2004 to 68% in 2014. Citations per Welsh researcher also moved from an average of 7.6 in 2007–2011 to 9.6 in 2014—“that’s two percentage points above the UK average,” says the Learned Society of Wales’ Halligan. As Wales’ first national academy, the Learned Society of Wales—established in 2010—brings together the nation’s most successful and talented fellows to advance and promote research excellence in all scholarly disciplines.

Halligan’s research provided valuable support for extending *Sêr Cymru* into its second phase. *Sêr Cymru II* is a suite of schemes partly funded by the European Commission through the Horizon 2020 Marie Skłodowska-Curie Actions COFUND scheme, or by the Welsh European Funding Office through the European Regional Development Fund. In addition to funding fellowships and promising scientists, *Sêr Cymru* offers 12 additional fellowships to scientists returning to their fields after a long absence.

The level of government commitment has made a powerful impression on researchers. “I have been stunned at how accessible the leadership in Cardiff has been to me,” Durrant says. “Wales has the level of political engagement and the determination to focus their resources that is creating really world-class centers.”

Welsh universities also provide other perks that go beyond the quality of their science offerings. “People are very open and relaxed when talking about ideas,” says Dodd. “They don’t seem to worry about how they are going to be perceived.” This sentiment was echoed by Jones: “This university is the most collegial place I’ve ever worked.”

And contrary to the stereotypical view of a small institution being a professional handicap, “I haven’t needed to be in a large institution to be a successful scientist,” says Bangor University’s Thomas, who has been in Wales for over 20 years. Also worth mentioning is the proximity to ocean, mountains, and other natural beauty that together, says Thomas, make Wales “a blindingly good place to live.”

Gunjan Sinha is a freelance writer living in Berlin, Germany.

DOI: 10.1126/science.opms.r1600169

Do you have a passion for cutting-edge biodiversity science and making a real-world impact?

The California Academy of Sciences seeks three outstanding Ph.D. scientists focused on changing the world through biodiversity/ecological science, broader science communication, increasing diversity in science, and connecting their work to real-world sustainability outcomes. This year, we seek candidates working in biological or physical anthropology, herpetology, and the botany of western North America.

The Academy offers a powerful setting for scientific research and engagement: a LEED platinum natural history museum, aquarium, planetarium, and ~46 million specimens. Our new hires will join ~100 scientists, students, and post docs.

We seek candidates with skills in different areas, including evolutionary biology, taxonomy and systematics, genomics, innovative methods for field- and collections-based research, ecology, global environmental changes, GIS, visualization approaches, and connecting their work to larger sustainability challenges. Applicants must have a Ph.D. at time of application.

For further details, see <http://calacademy.snaphire.com/home?source=CAS>. Review of complete applications will begin November 14, 2016. Interviews will be held spring 2017.

The California Academy of Sciences is an Equal Opportunity Employer and committed to ensuring that all employees and applicants receive equal consideration and treatment.



CALIFORNIA
ACADEMY OF
SCIENCES

55 Music Concourse Drive
San Francisco, CA 94118
www.calacademy.org

The Leipzig School of
Human Origins

The Leipzig School of Human Origins

- An International Max Planck Research School -

by the
University of Leipzig
and the

Max Planck Institute for Evolutionary Anthropology

The **Leipzig School of Human Origins** offers a unique interdisciplinary graduate program to study the evolutionary history and origins of humans and other primates. Graduate students are accepted into one of the following areas, but are encouraged to take part in courses and seminars from all four disciplines:

Comparative and Molecular Primatology

Paleogenomics

Paleoanthropology

Human Behavioral Ecology and Developmental Psychology

The language of the school is English. Visit www.leipzig.de for information on living in Leipzig, Germany, in the center of Europe.

For project and application details go to
www.leipzig-school.eva.mpg.de

or contact us at:
e-mail: leipzig-school@eva.mpg.de
phone: ++49 (0) 341 3550-0
fax: ++49 (0) 341 3550-119

Application deadline: December 01, 2016



DANA-FARBER
CANCER INSTITUTE



HARVARD MEDICAL SCHOOL
TEACHING HOSPITAL

DIRECTOR OF CANCER CELL THERAPY PROGRAM

Dana-Farber Cancer Institute is seeking an academic leader to serve as the Director of the Cancer Cell Therapy Program at the Dana-Farber Cancer Institute with an appointment as Associate Professor or Professor of Medicine at Harvard Medical School.

This individual will be responsible for the full scope of research, preclinical and educational activities of the Program as well as collaborative activities with other departments at Harvard Medical School and its affiliated institutions.

Candidates should have an MD and or PhD degree, at least 10 years of experience in the field of cellular therapies, an established record as a mentor and as a teacher, national recognition for research accomplishments, and possess effective leadership, managerial, and collaborative skills. Ideally, she/he would be a proven leader with an international reputation in cancer cell therapy, who can develop a leading translational program in cellular therapy at the Dana-Farber Cancer Institute.

Interested candidates are requested to submit a cover letter and current Curriculum Vitae to the email address below for consideration to:

Committee Chair

Jerome Ritz, MD, Dana-Farber Cancer Institute
jerome_ritz@dfci.harvard.edu

We are an Equal Opportunity Employer and all qualified applicants will receive consideration for employment without regard to race, color, religion, sex, sexual orientation, gender identity, national origin, disability status, protected veteran status, or any other characteristic protected by law.

Advance your
career with expert
advice from
Science Careers.



Download Free Career Advice Booklets!
ScienceCareers.org/booklets

Featured Topics:

- Networking
- Industry or Academia
- Job Searching
- Non-Bench Careers
- And More



Science Careers
FROM THE JOURNAL SCIENCE

THE FIRST INTERNATIONAL YOUNG SCHOLARS SHENZHEN FORUM OF SUN YAT-SEN UNIVERSITY

Organizer: Sun Yat-sen University
Date: December 24-26, 2016

The First International Young Scholars Shenzhen Forum of Sun Yat-sen University is now officially open for online registration.

[Introduction]

Sun Yat-sen University was established in 1924 by Dr. Sun Yat-sen. A top-tier comprehensive research university recognized both at home and abroad for its remarkable strengths in a wide range of disciplines. Sun Yat-sen University has fostered an exceptional learning environment and a favorable academic atmosphere.

[Start of Forum] The University started to organize the International Young Scholars Forum in 2015. Shenzhen Forum 2016 is the third session.

[Forum purpose] The Forum aims to bring together young scholars from China and abroad for exploring the frontiers of academic topics, tracking hot academic issues, and promoting academic exchanges and cooperation while serving as a venue for introducing the University to top-level international talent.

[Forum organize] Presentations, workshops, discussions and will provide opportunities for talent recruitment.

[Subject areas] Shenzhen Forum will include in broad disciplines, especially in these academic fields: Clinical Medicine, Basic Medicine, Public Health and Preventive Medicine, Pharmaceutical Science, Biomedical Engineering, Materials Science and Engineering, Information and Communication Engineering, Aeronautics and Astronautics Science and Technology, Intelligent Manufacturing, and etc.

中山大学国际青年学者深圳论坛
International Young Scholars Shenzhen Forum of Sun Yat-sen University
Sun Yat-sen University
December 24-26, 2016



中山大學
SUN YAT-SEN UNIVERSITY

[Application Conditions]

Applicants must be: under the age of 40; holders of a PhD degree from a well-known university abroad, or holders of a PhD degree from a domestic university but with more than 2 years of research experience abroad; must have demonstrated academic achievements or academic potential in their respective research fields, and intending to apply for Professor or Associate Professor of Sun Yat-sen University's "100 Top Talents Program", Research Fellow or Postdoctoral Researcher.

[Application Process]

Applicants can access the online application system found at (<http://survey.sysu.edu.cn/en>), provide the information as required on the web page, and submit it. To check whether or not you have been invited, you will receive an email with results by December 9. The applicants who have received an invitation and intend to attend the forum should fill in the confirmation note within a week upon receiving the invitation.

[Travel and Accommodation Arrangements]

Meals and accommodation will be arranged by the organizer, and travel subsidies will be provided as well.

[Contact]

Human Resources Department
Sun Yat-sen University
Guangzhou, Guangdong, China 510275
Tel: +86-20-84114884
Fax: +86-20-84115959
Contact: Ms. Fan Sun, Ms. Manrong Chi
E-mail: rsrccgc@mail.sysu.edu.cn
SYSU Recruitments Official webpage:
<http://rsc.sysu.edu.cn/Article/invitation/Professor/201609/7612.html>



香港中文大學(深圳)
The Chinese University of Hong Kong, Shenzhen

PROFESSOR/ASSOCIATE PROFESSOR/ASSISTANT PROFESSOR IN THE SCHOOL OF SCIENCE AND ENGINEERING

Located in the Longgang District of Shenzhen, The Chinese University of Hong Kong, Shenzhen [CUHK(SZ)] is a research-intensive university, established in 2014 through a Mainland-Hong Kong collaboration with generous support from the Shenzhen Municipal Government. It inherits the fine academic traditions of The Chinese University of Hong Kong and will develop its academic programmes in phases and offer courses in Schools of Science and Engineering, Management and Economics, and Humanities and Social Science. The language of instruction will be in both English and Chinese, and the students will receive degrees of The Chinese University of Hong Kong.

● POST SPECIFICATION

The School of Science and Engineering (www.cuhk.edu.cn/en/Xueyuan/ligong.html) invites applications for faculty positions in all areas of Bioinformatics, Biomedical Science and Engineering, Chemistry, Material Science and Physics, Computer Science and Engineering, Electrical and Information Engineering, New Energy Science and Engineering, Statistical Science, Data Science, Mathematics, Financial Engineering and Quantitative Finance. Applications in other areas will also be considered.

Junior applicants should have (i) a PhD degree (by the time of reporting for duty) in related fields; and (ii) high potential in teaching and research. Candidates for Associate and Full Professor posts are expected to have demonstrated academic leadership and strong commitment to the highest standards of excellence. Appointments will normally be made on contract basis for up to three years initially, leading to longer-term appointment or tenure later subject to review. Exceptional appointments with tenure will be considered for candidates of proven ability.

● SALARY AND FRINGE BENEFITS

Salary will be comparable to international standards, commensurate with experience and accomplishments. Appointments will be made under the establishment of CUHK(SZ), and employee benefits will be provided according to the relevant labor laws of Mainland China as well as CUHK(SZ) regulations. Subsidies from various government sponsored talent programs will also be made available for eligible candidates <http://www.cuhk.edu.cn/UploadFiles/talentsProgramoutline.pdf>

Applications (with CV and contact information of three referees) should be emailed to: talents4sse@cuhk.edu.cn

RECRUITMENT FOR GLOBAL HIGH-LEVEL TALENTS (ONLINE + ON SPOT)

Job Vacancies in China's Universities
and Research Institutes

Holding Date:

ONLINE: 9:00-16:00 (GMT+8), October 26th, 2016
ON SPOT: October 28th, 2016—November 4th, 2016
(Britain+Germany)

Recruitment requirements:

Overseas Scholars, Doctors and Post-doctors

Participating Universities:

Shanghai University Of Engineering Science
Shanghai Normal University
Southwest University

Northeast Forestry University

Harbin Engineering University

Southwest Jiaotong University

Third Military Medical University

OTHER MORE UNIVERSITIES

AND MORE INFORMATION

PLEASE VISIT www.edu.cn/cv

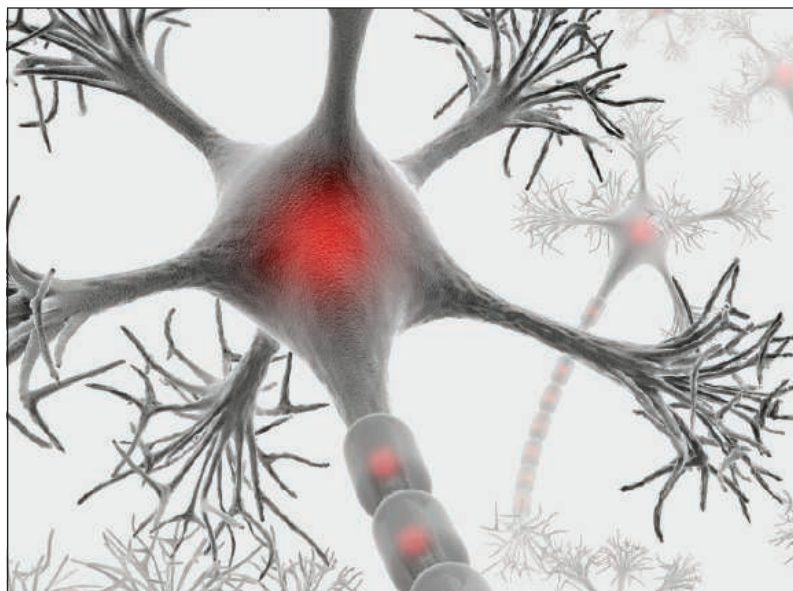
Participation Approaches:

Please send your CV to

consultant@acabridge.edu.cn

Want to recommend talents or consult more
information?

Please contact consultant@acabridge.edu.cn



Special Job Focus:

Neuroscience

Issue date: November 4

Book ad by October 18 to
guarantee space

Ads accepted until October 28
if space allows

For recruitment in science, there's only one *Science*.

What makes *Science* the best choice?

- Read and respected by 400,000 readers around the globe
- 75% of readers read *Science* more often than any other journal
- Your ad dollars support AAAS and its programs, which strengthens the global scientific community.

Why choose this job focus for your advertisement?

- Relevant ads lead off the career section with special neuroscience banner
- Bonus distribution to Society for Neuroscience, November 12–16, San Diego, CA.

Expand your exposure.

Post your print ad online to benefit from:

- Link on the job board homepage directly to neuroscience jobs
- Dedicated landing page for jobs in neuroscience
- Additional marketing driving relevant job seekers to the job board.

Deliver your message to a
global audience of targeted,
qualified scientists.

129,574

subscribers in print
every week

49,518

unique active job seekers
searching for **neuroscience**
positions in 2015

34,780

applications submitted for
neuroscience positions
in 2015



Produced by the *Science*/AAAS Custom Publishing Office.

SCIENCECAREERS.ORG

ScienceCareers

FROM THE JOURNAL *SCIENCE* AAAS

To book your ad: advertise@sciencecareers.org

The Americas
+202 326 6582
Japan
+81 3 3219 5777

Europe/RoW
+44 (0) 1223 326500
China/Korea/Singapore/Taiwan
+86 186 0082 9345



ASSISTANT PROFESSOR EXPERIMENTAL LOW ENERGY NUCLEAR PHYSICS

The Department of Physics and Astronomy at the University of Tennessee Knoxville invites applications for a tenure-track faculty position at the rank of **Assistant Professor** in the field of Experimental Low Energy Nuclear Physics (LENP). The successful applicant will have a PhD in Physics or related field, several years of post-PhD experience, and a strong research record in Experimental LENP as evidenced by a publication record. The candidate is expected to define a vital program in nuclear structure, reactions, and/or nuclear astrophysics that will attract independent external research funding and provide state-of-the-art training for graduate students and postdoctoral researchers. The successful candidate will contribute to the teaching mission of the department at both the undergraduate and graduate levels.

The experimental LENP group at the University of Tennessee, Knoxville (UT) leads experiments at user facilities in the US, and worldwide, using decay and low-energy nuclear reaction techniques to study the structure of the atomic nucleus and its interactions, particularly those relevant to element production through the astrophysical r- and rp-processes. This research is strongly aligned with the program of the Facility for Rare Ion Beams (FRIB). Our group has led the development and construction of the Versatile Array for Neutron Detection at Low Energies (VANDLE) and the Hybrid Array for Gamma Ray Detection (HAGRID) and is at the cutting-edge of developments with digital data acquisition used for decay and reaction studies. UT is a key member of the Center of Excellence for Radioactive Ion Beam Studies for Stewardship Science, funded by the National Nuclear Security Agency, and maintains significant funding from the DOE Office of Science. UT has an established partnership with Oak Ridge National Laboratory (ORNL) through the Joint Institute for Nuclear Physics and Applications. The successful candidate is expected to strengthen the UT LENP group program and will be encouraged to explore research opportunities at the future FRIB facility. This appointment is expected to begin August 1, 2017.

The University welcomes and honors people of all races, creeds, cultures, and sexual orientations, and values intellectual curiosity, pursuit of knowledge, and academic freedom and integrity. The Knoxville campus of the University of Tennessee is seeking candidates who have the ability to contribute in meaningful ways to the diversity and intercultural goals of the University. Applicants should send a cover letter, CV, list of publications, a description of teaching and research experience, and their proposed research program, and also arrange for at least three letters of reference to be submitted separately. All application materials should be submitted on-line at <https://apply.interfolio.com/36687>. Only electronic applications will be considered, and acceptable file formats are .pdf or .doc. Review of applications will begin on November 15, 2016 and continue until the position is filled.

ASSISTANT PROFESSOR SYNTHETIC ORGANIC OR POLYMER CHEMISTRY

The Department of Chemistry at The University of Tennessee at Knoxville <https://www.chem.utk.edu> invites applications for a tenure track faculty position in the area of Synthetic Organic or Polymer Chemistry, broadly defined, with an anticipated start date of October 15, 2017. Ideally, the applicant's proposed research program will augment existing expertise in the department. The position will be at the rank of Assistant Professor and requires a Ph.D. degree in chemistry, or a closely related field, and at least one year of post-doctoral research experience. Successful candidates are expected to develop an internationally recognized, externally funded research program and contribute to the Department's teaching and service missions. Interested applicants should submit a cover letter, CV, description of proposed research, and teaching philosophy as a single pdf document to organicpolymersearch@ion.chem.utk.edu. Furthermore, applicants should arrange for three letters of recommendation to be sent to the same email address. Review of applications will begin on November 1, 2016 and continue until the position is filled.

The Department is in a vigorous growth phase and currently consists of 28 faculty members, ~130 graduate students, and ~220 chemistry majors. The Department offers excellent support facilities including five NMR spectrometers (solution and solid state), four mass spectrometers ranging from walk on to proteomics instruments, a Raman spectrometer, powder and single crystal X-ray diffractometers, and a state-of-the-art polymer characterization laboratory. A competitive start-up package will be provided to supply the successful candidates with the time and funds required to initiate a strong research program. The University, and in particular the Chemistry Department, enjoys strong collaborative research ties to the nearby Oak Ridge National Laboratory (ORNL). All of our faculty members have unique collaborative research opportunities with ORNL, UT-ORNL Joint Institutes for Biological Sciences, Computation, Neutron Sciences, and Advanced Materials and the School for Genome Science & Technology.

The University of Tennessee, Knoxville, is Tennessee's flagship state research institution, a campus of choice for outstanding undergraduates, and a premier graduate institution. Knoxville is the gateway to multiple beautiful and historically significant National Park Service destinations, including the Great Smoky Mountains NP and the Big South Fork NRR. East Tennessee offers a blend of convenient urban and rural living settings with easy access to miles of inland waterways, ~1000 acres of trails in Knoxville's Urban Wilderness, and diverse cultural opportunities. Downtown Knoxville is a thriving neighborhood adjacent to campus, filled with restaurants, shops, indoor and outdoor entertainment venues, and is a musical mecca with Tennessee Shines, the Big Ears Music Festival, Knoxville Symphony & Opera, Jazz on the Square, Alive at Five, and other events.

The University of Tennessee is an EEO/AA/Title VI/Title IX/Section 504/ADA/ADEA institution in the provision of its education and employment programs and services. All qualified applicants will receive equal consideration for employment without regard to race, color, national origin, religion, sex, pregnancy, marital status, sexual orientation, gender identity, age, physical or mental disability, or covered veteran status.

ASSISTANT/ASSOCIATE PROFESSOR STRUCTURAL BIOLOGY/BIOPHYSICS POSITION

The Biochemistry & Cellular and Molecular Biology Department (BCMB) at the University of Tennessee at Knoxville (UT) is soliciting applications for a full-time, tenure-track position at the rank of **ASSISTANT PROFESSOR** or **ASSOCIATE PROFESSOR** to begin August 1, 2017. The BCMB Department (<https://bcmb.utk.edu>) has 40 active faculty with core strengths in structural/computational biochemistry & biophysics, plant/microbial biology, and developmental genetics. We seek applicants who use modern structural or biophysical approaches to study complex cellular, sub-cellular, or molecular systems. These approaches may include but are not limited to Cryo-EM single particle analysis or tomography, single-molecule biophysics/optical spectroscopy, neutron/X-ray crystallography/scattering, and NMR. These approaches should be applied to explore the fundamental molecular, cellular, or physiological nature of complex systems that may include macromolecular complexes, biomembranes, organelles, and nanomachines. The candidate will be required to develop an innovative and extramurally funded research program that complements existing areas of computational and experimental biophysics within the BCMB. UT is located near Oak Ridge National Laboratory (ORNL) and candidates interested in building collaborative or joint research programs in biophysics and structural biology with ORNL are particularly encouraged to apply <http://web.ornl.gov/sci/ees/bsd/index.shtml>.

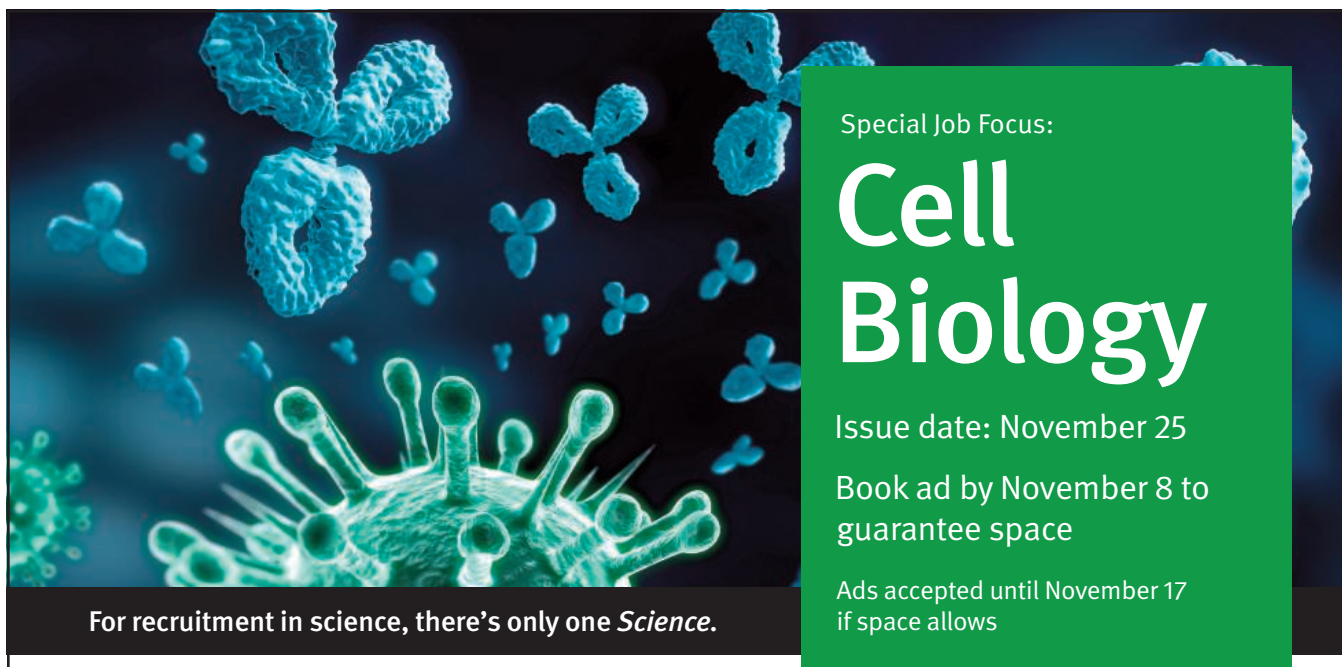
Applicants must have a Ph.D. and postdoctoral experience in an appropriate discipline with evidence of high quality research and the interest/ability to teach biochemistry and/or physical biochemistry plus graduate courses in their area. Applicants should send a single PDF containing a cover letter, *curriculum vitae*, current and future research interests with funding prospects, and statement of teaching philosophy to experimentalbio@utk.edu. Following initial review, the top applicants will be contacted and requested to arrange three letters of recommendation to be sent electronically to utkreferences@utk.edu. Direct further inquiries to Dr. Barry D. Bruce, (865-974-4082; bbruce@utk.edu). Review of applications will begin on November 4, 2016 and continue until the position is filled.

ASSISTANT PROFESSOR THEORETICAL BIOPHYSICS

The Department of Physics and Astronomy at the University of Tennessee (UT) invites applications for a tenure-track faculty position at the rank of **Assistant Professor** in the field of Theoretical Biophysics. Candidates should have a PhD in Physics or another field closely related to Physics. The candidate is expected to have a strong research record in Theoretical Biophysics and is expected to develop a first-class, externally funded research program, to provide training for graduate students and postdoctoral researchers, and to contribute to the teaching mission of the department at both the undergraduate and graduate levels. The preferred expertise of the candidate should be in the broad area of Soft Matter Physics applied to living systems, including but not limited to non-equilibrium statistical mechanics, cellular biomechanics, multi-scale molecular dynamics and Monte Carlo simulations, and polymer physics. A strong interest in interacting with ongoing programs at UT, such as computational physics and theoretical condensed matter physics research, is highly desirable. The appointment is expected to begin August 1, 2017.

The successful candidate will benefit greatly from available computational resources, the location on campus of the National Institute for Mathematical and Biological Synthesis (NIMBioS), and by the proximity to unique research facilities at Oak Ridge National Laboratory, including the Joint Institutes for Computational Sciences, Biological Sciences, Advanced Materials, and Neutron Sciences.

The University welcomes and honors people of all races, creeds, cultures, and sexual orientations, and values intellectual curiosity, pursuit of knowledge, and academic freedom and integrity. The Knoxville campus of the University of Tennessee is seeking candidates who have the ability to contribute in meaningful ways to the diversity and intercultural goals of the University. Applicants should send a CV, list of publications, a description of research and teaching experience, a proposed research program, and also arrange for at least three letters of reference to be submitted separately. All application materials should be submitted on-line at <https://apply.interfolio.com/36843>. Only electronic applications will be considered and acceptable file formats are .pdf or .docx. To guarantee consideration please submit all materials by December 1, 2016.



Special Job Focus:

Cell Biology

Issue date: November 25

Book ad by November 8 to guarantee space

Ads accepted until November 17 if space allows

For recruitment in science, there's only one *Science*.

What makes *Science* the best choice?

- Read and respected by 400,00 readers around the globe
- 75% of readers read *Science* more often than any other journal
- Your ad dollars support AAAS and its programs, which strengthens the global scientific community.

Why choose this job focus for your advertisement?

- Relevant ads lead off the career section with special cell biology banner
- Bonus distribution to American Society for Cell Biology, December 3–7, San Francisco, CA.

Expand your exposure. Post your print ad online to benefit from:

- Link on the job board homepage directly to cell biology jobs
- Dedicated landing page for jobs in cell biology
- Additional marketing driving relevant job seekers to the job board.

Deliver your message to a global audience of targeted, qualified scientists.

129,574

subscribers in print every week

42,242

unique active job seekers searching for **cell biology** positions in 2015

50,136

applications submitted for **cell biology** positions in 2015



Produced by the *Science*/AAAS Custom Publishing Office.

SCIENCECAREERS.ORG

ScienceCareers

FROM THE JOURNAL SCIENCE  AAAS

To book your ad: advertise@sciencecareers.org

The Americas
+202 326 6582
Japan
+81 3 3219 5777

Europe/RoW
+44 (0) 1223 326500
China/Korea/Singapore/Taiwan
+86 131 4114 0012



Call for Application JAXA International Top Young Fellowship (ITYF) 2016

ITYF application

The Japan Aerospace Exploration Agency (JAXA) International Top Young Fellowship (ITYF) invites world's top-level young researchers to work at the Institute of Space and Astronautical Science (ISAS)/JAXA for 3 years. In addition to producing outstanding academic achievements in their areas of specialization, ITYF fellows are expected to contribute to creating new academic trends in collaboration with researchers inside and/or outside ISAS. An excellent remuneration package is offered, including research budget (including travel expense) so that the fellow can extend their international profile, as well as developing collaborations within Japan.

**The application deadline: 23:59 (JST),
November 27, 2016**

Please see the below link for further details.
<http://www.isas.jaxa.jp/e/researchers/young-fellowship/appli.shtml>

Contact Information
E-mail: ITYF_ADMIN@jaxa.jp



ASSISTANT PROFESSOR Tenure-Track, Biology

Adelphi University invites applications for a tenure-track position for an organismal physiologist to begin fall 2017. A Ph.D. is required and postdoctoral experience is highly preferred. Teaching responsibilities will include undergraduate and graduate physiology, human anatomy & physiology and could include courses such as animal behavior, pathophysiology for nursing students, introductory biology, and/or additional specialty courses. The successful applicant will have a commitment to teaching students from diverse cultural backgrounds and excellent potential as a teacher, plus a record of significant research accomplishment and the potential to develop a fundable independent research program involving undergraduate and master's students.

For more information about the department, visit <http://academics.adelphi.edu/artsci/bio/>. We are strongly committed to achieving excellence through cultural diversity. Adelphi is a private university with the spirit of a liberal arts college, committed to combining teaching and scholarship, and located in suburban Long Island within easy reach of New York City. More detailed descriptions of the position and application are available through www.adelphi.edu/positions/faculty. **Deadline for applications: November 15, 2016.**

Adelphi University is an equal opportunity/affirmative action employer committed to building a diverse workforce and strongly encourages applications from women, under-represented groups, members of the LGBT community, people with disabilities and veterans.

Four Tenure-Track Professors Division of Nutritional Sciences

The Division of Nutritional Sciences at Cornell University is hiring four tenure-track Professors. These positions are fully-funded, nine-month appointments with excellent benefits.

The Division of Nutritional Sciences is a broadly based interdisciplinary unit that integrates theories and methods from across many academic disciplines to understand the complex relationships among biology, nutrition, food systems and lifestyle patterns, social and institutional environments and governmental policies in human health.

Candidates are expected to demonstrate promise for/or to already have vibrant, independent and extramurally-funded research programs, to bring their unique expertise and perspectives to the Cornell curriculum for graduate and/or undergraduate education, and to mentor graduate students in the Field of Nutrition and other fields at Cornell University.

Review of applications and interviews will occur on a rolling basis until these positions have been filled.

Assistant Professor of Public Health and Community Nutrition <https://academicjobsonline.org/ajo/jobs/8070>

Candidates should have experience in interdisciplinary research at the interface of food, human nutrition and public health, and demonstrated expertise in social and behavioral sciences, community-based interventions, policy and/or dissemination or implementation research. Demonstrated research excellence in areas of interest include, but are not limited to, maternal and child nutrition, obesity and chronic disease prevention, and nutrition disparities. Research excellence should be demonstrated through publications in journals and authored books. Scholarship related to nutrition and public health should be central to the candidate's research program.

Assistant Professor of Molecular Nutrition and Metabolomics <https://academicjobsonline.org/ajo/jobs/7327>

Candidates should have experience in the development and use of metabolomics and related biomarkers of human metabolism, nutritional status and/or dietary exposure, and demonstrated expertise in metabolomics studying human metabolism and/or related model systems, and an interest in understanding the relationships among metabolism, nutritional status and human health. Areas of expertise include, but are not limited to analytical chemistry/biochemistry, mass spectrometry, systems biology, and/or genomics/metabolomics. Research areas of interests include, but are not limited to, the study of biomarkers of human metabolism, human disease, nutritional status or dietary exposure and/or the role of essential and/or non-essential bioactive food/plant components in human health.

Assistant, Associate or Full Professor in Global Health and Nutrition <https://academicjobsonline.org/ajo/jobs/7319>

Candidates should have experience in interdisciplinary research in global health and nutrition and an interest in studying the biological and/or social dimensions of nutrition in human populations. Areas of expertise include epidemiology and intervention targeting and evaluation. Scholarship related to nutrition and human health, in the broadest sense, should be central to the candidate's research interests. Demonstrated research excellence in areas of interest include, but are not limited to, maternal and child nutrition, obesity and chronic disease prevention, and food systems for health and nutrition disparities. This position is aligned with University initiatives in big data, information sciences, and global and public health. The qualifications of the candidate will determine the rank of appointment.

Assistant, Associate or Full Professor of Functional Mouse Genomics <https://academicjobsonline.org/ajo/jobs/7028>

Candidates should have experience in metabolism, cell biology, genetics, biochemistry, developmental biology and/or experimental genomics with an interest in exploring the interactions among nutrients, metabolism and the genome in health and disease. Research areas of interest include energy metabolism, systems biology, stem cells, mammalian developmental and metabolic programming, epigenetics and/or complex metabolic diseases. Preference will be given to candidates with expertise in mouse models. Research excellence should be demonstrated by the existence or potential for building an active, externally-funded research program as well as by a strong record of publication in recognized journals. Scholarship related to nutrition and human health, in the broadest sense, should be central to the candidate's research program. The qualifications of the candidate will determine the rank of appointment.

Please visit <http://www.human.cornell.edu/dns/jobopenings.cfm> for more information on the Division of Nutritional Sciences and to access full descriptions.

Candidates are required to apply through Academic Jobs Online and upload a cover letter, CV, research statement and a teaching statement. Applicants must also arrange to have three confidential letters of recommendation submitted through Academic Jobs Online.



Diversity and Inclusion are a part of Cornell University's heritage. We're an employer and educator recognized for valuing AA/EEO, Protected Veterans, and Individuals with Disabilities.

AMERICAN ASSOCIATION FOR THE ADVANCEMENT OF SCIENCE

Career Development Center



Career Development Center

Meet career challenges head-on with online courses
designed for scientists

- Public engagement
- R&D funding analysis
- Effective communication
- Proposal writing
- Career development
- Science policy and advocacy

REGISTER TODAY
CareerDevelopment.aaas.org



Assistant Professors (Tenure Track) of Computer Science

→ The Department of Computer Science (www.inf.ethz.ch) at ETH Zurich invites applications for assistant professorships (tenure track) with focus on the following broad areas within computer science. For each area, several possible examples (not exhaustive) of expertise are provided.

- **Programming Languages and Software Engineering** (language design and implementation, testing and debugging, compilers and language runtimes, programming models, dynamic languages)
- **Robotics and Cyber-physical Systems** (artificial intelligence, human-robot interaction, planning and control, virtual/augmented reality, internet of things, embedded systems, data acquisition systems)
- **Data Science** (machine learning, language/media processing, data privacy, medical applications, data centers architecture and management, programming and runtime platforms for data centers and cloud computing)
- All other areas in **Computer Science** (while there is focus on the three areas above, ETH Zurich is broadly looking in all areas)

→ Please only apply for one of the above four areas as all applications will be jointly reviewed.

→ Applicants should be strongly rooted in computer science, have internationally recognized expertise in their field and pursue research at the forefront of computer science. Successful candidates should establish and lead a strong research program. They will be expected to supervise doctoral students and teach both undergraduate and graduate level courses (in German or in English). Collaboration in research and teaching is expected both within the department and with other groups of ETH Zurich and related institutions.

→ Assistant professorships have been established to promote the careers of younger scientists. ETH Zurich implements a tenure track system equivalent to other top international universities. For candidates with exceptional research accomplishments, applications for a tenured associate or full professorship will also be considered.

→ Please apply online (application period starts on 31 October 2016) at: www.facultyaffairs.ethz.ch

→ Applications include a curriculum vitae, a list of publications with the three most important ones marked, a statement of future research and teaching interests, the names of three references, and a description of the three most important achievements. The letter of application should be addressed to the **President of ETH Zurich, Prof. Dr. Lino Guzzella**. The closing date for applications is **15 December 2016**. ETH Zurich is an equal opportunity and family friendly employer and is further responsive to the needs of dual career couples. We specifically encourage women to apply.



UNIVERSITY OF MINNESOTA

Medical School

DEPARTMENT OF NEUROSCIENCE

THE UNIVERSITY OF MINNESOTA seeks candidates at the tenure-track (Assistant Professor) or tenured (Associate or Full Professor) level for appointment in the Department of Neuroscience within the Medical School (see www.neurosci.umn.edu). Candidates with research programs in the broadly-defined field of neuroscience will be considered; though the primary goal of this appointment is to augment and complement existing departmental strengths (e.g., neurodegenerative disease, neuronal-glia interactions, neurobiology of pain, complex cognitive processes). Faculty will be expected to participate in our vigorous Graduate Program in Neuroscience, as well as in other interdisciplinary graduate programs at the University of Minnesota (www.neuroscience.umn.edu). Faculty will have access to exceptional core facilities in magnetic resonance and optical imaging, genomics and proteomics, and behavioral phenotyping. Also, there are numerous opportunities to participate in outstanding centers including the Institute for Translational Neuroscience, Center for Neuroengineering and Center for Immunology.

The University of Minnesota is a land-grant institution, enjoying generous state support for research initiatives. The University is committed to the success and retention of its faculty and offers excellent benefits. Quality of life in the Twin Cities is also exceptional. The Twin Cities ranked first in 2015 as a place to live (Patch of Earth), is also one of the greenest cities in the US (Wallet Hub), best cities for foodies (Travel and Leisure), and best cities for biking (Forbes), walkability and public transportation (bestcolleges.com).

The University of Minnesota is committed to the development of a diverse workforce. The Department of Neuroscience therefore actively encourages applications from an inclusive group of candidates that furthers the goal of increasing the representation of women and members of groups underrepresented in science within our faculty.

At the tenure-track level of appointment, candidates are expected to have doctoral and postdoctoral training in the neurosciences, and to develop a nationally recognized and extramurally-funded independent research program. Appointment at the tenured level requires demonstrated independence and research productivity, including a strong track record of major external funding and quality publications in peer-reviewed journals. Salary, start-up funds and research space are competitive and commensurate with education and experience.

Candidates must have a PhD and/or MD degree and must be US citizens or must be able to secure permanent resident status. The Minneapolis campus of the University of Minnesota – Twin Cities is an urban campus overlooking the Mississippi River and houses many colleges in addition to the Academic Health Center, which includes the Medical School. The starting date is negotiable with appointment available as early as July 1, 2017.

Review of applications will commence **December 1, 2016** and continue until the position is filled. Those seeking a position at the Assistant Professor level should send a current curriculum vitae, statement of research interests and intentions, and three letters of reference to the Neuroscience Faculty Search Committee. Those looking at the Associate or Full Professor levels should send a current curriculum vitae, statement of research interests and intentions, and the names of three individuals to provide letters of reference to: **Neuroscience Faculty Search Committee, Attention: Ms. Kathleen Beterams, Department of Neuroscience, University of Minnesota, 6-145 Jackson Hall, 321 Church St SE, Minneapolis, MN 55455 USA** or electronically by e-mail to kbeteram@umn.edu. Applicants also need to complete the online application at <http://www1.umn.edu/ohr/employment/index.html>. Those seeking a position at the **Assistant Professor** level can find the application by searching for requisition **#313006** under key words. Those looking at the **Associate or Full Professor** levels can search for requisition **#313075**.

As an Equal Opportunity Educator and Employer, the University of Minnesota is committed to attracting and retaining employees with varying identities and backgrounds. To learn more about diversity at the University of Minnesota visit <https://diversity.umn.edu/>.

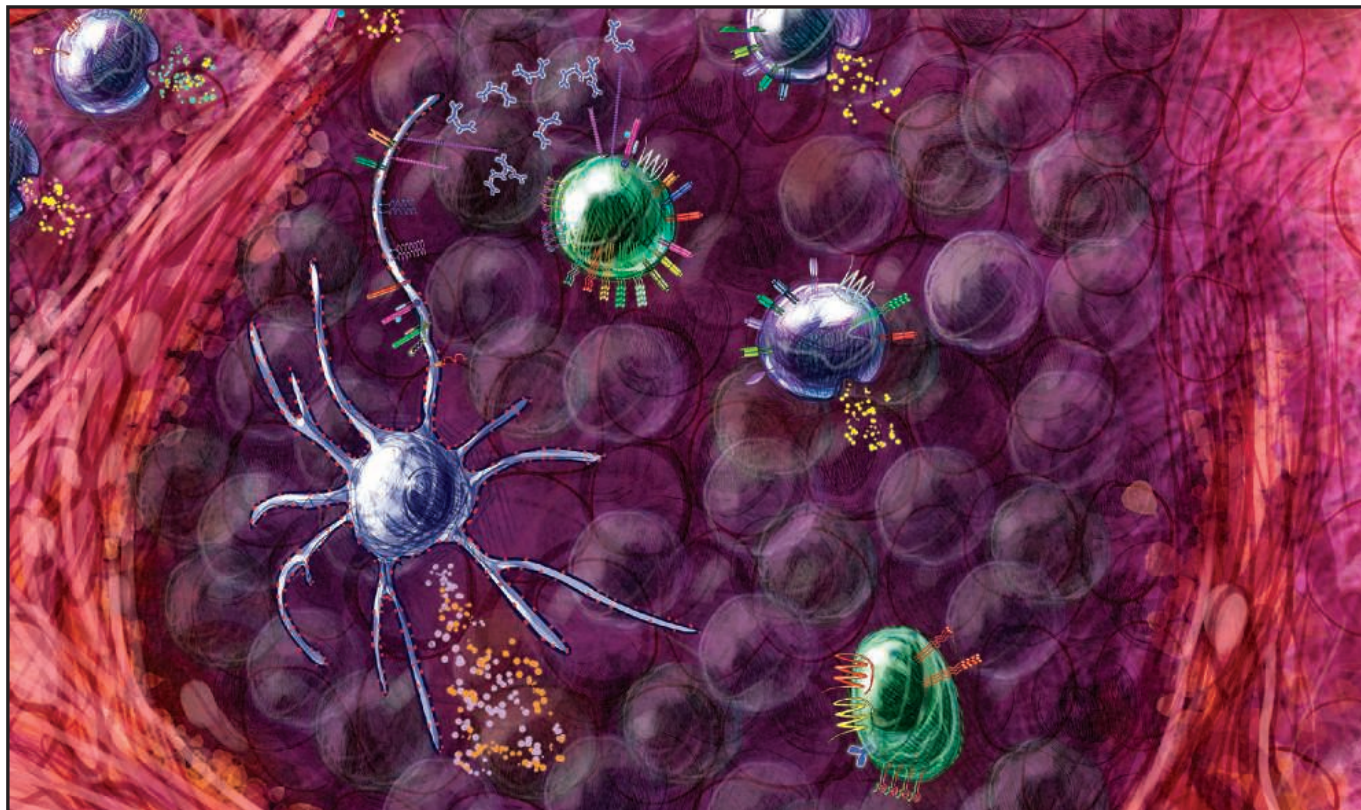
Webinar

Immune response monitoring

What can we learn about immunotherapy, pathogen response, and autoimmunity?

WEDNESDAY, OCTOBER 26, 2016

12 noon Eastern, 9 a.m. Pacific, 5 p.m. UK (BST), 6 p.m. CEST



The role of the immune system in health and well-being is perhaps more far-reaching than previously imagined. An insufficient or overactive immune response impacts cancers, autoimmune diseases, and infectious diseases. Monitoring immune responses by measuring cytokine levels has become an integral part of disease-related research, providing clues to the state of the immune system and how it could be targeted therapeutically. Also, knowing which cytokines to measure is essential for gaining a better understanding of the complexity of immune responses.

This webinar will address the role that insufficient or overactive immune responses play in disease, which cytokines are most commonly used to monitor inflammation and immunosuppression, and whether the use of common biomarkers is good enough, or if a broader set of measurements is required.

The panel will be available to answer questions live from the online audience.

SPEAKERS



Abul K. Abbas, MBBS
University of California,
San Francisco
San Francisco, CA



Adrian Bot, M.D., Ph.D.
Kite Pharma Inc.
Santa Monica, CA



Sacha Gnjatic, Ph.D.
Icahn School of Medicine
at Mount Sinai
New York, NY

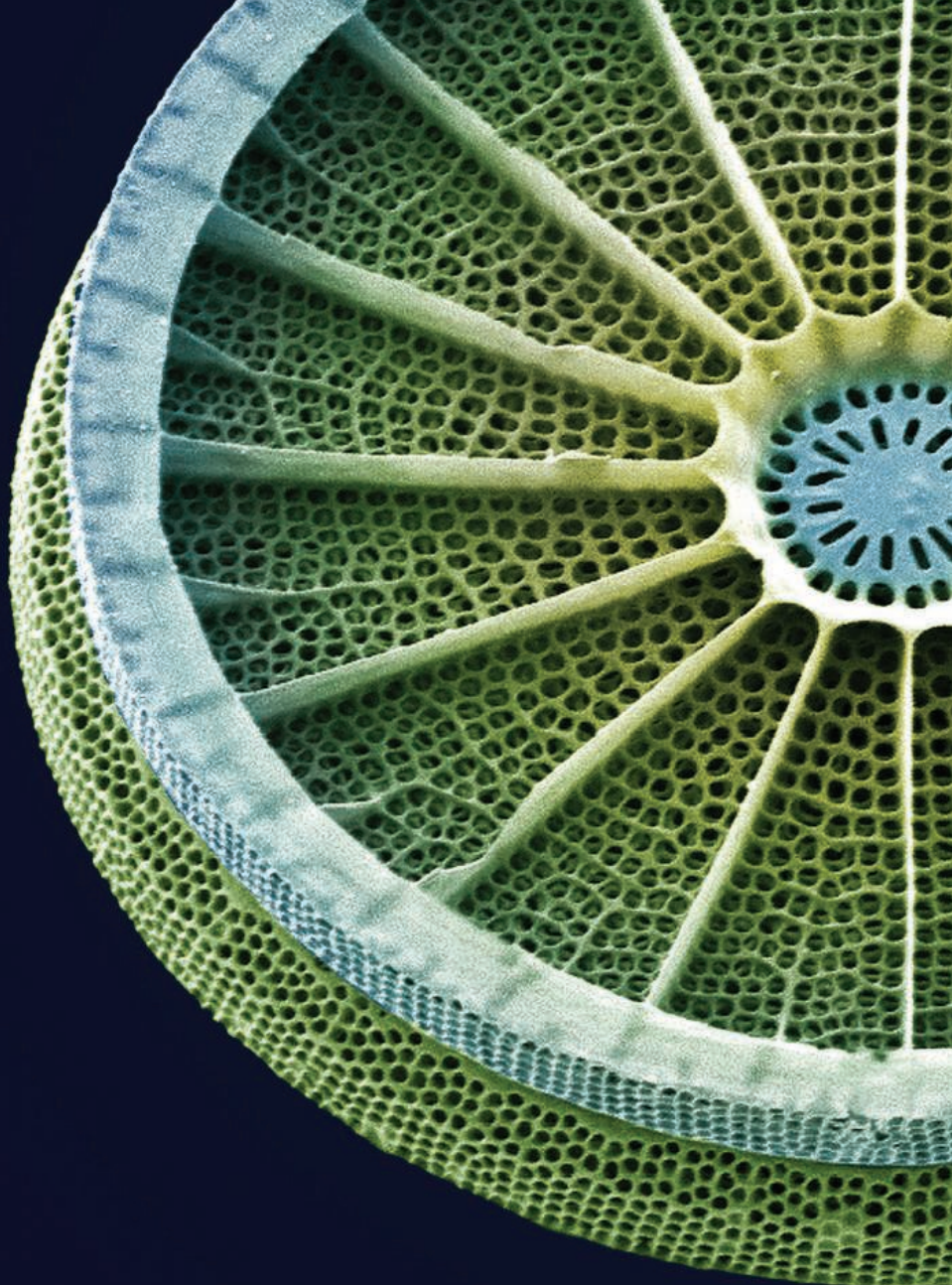
REGISTER AT
www.bit.ly/2dVBpMI

Sponsored by

biotechne®

Brought to you by the Science/
AAAS Custom Publishing Office

Science AAAS



Target with precision.

Introducing the NEBNext Direct[™] Cancer HotSpot Panel

Using a unique approach, the NEBNext Direct Cancer HotSpot Panel enriches for 190 common cancer targets from 50 genes prior to next generation sequencing. Combining a novel method for hybridization-based target enrichment with library preparation, the NEBNext Direct technology reduces processing time and minimizes sample loss. Ideal for automation, NEBNext Direct enables highly-specific deep sequencing of genomic regions of interest for the discovery and identification of low frequency variants from challenging sample types.

Visit **NEBNextDirect.com** to learn more
and to inquire about sampling this product.

TARGETS INCLUDE REGIONS FROM THE FOLLOWING CANCER-RELATED GENES, INCLUDING >18,000 COSMIC FEATURES:

ABL1	EGFR	GNAQ	KRAS	PTPN11
AKT1	ERBB2	GNAS	MET	RB1
ALK	ERBB4	HNF1A	MLH1	RET
APC	EZH2	HRAS	MPL	SMAD4
ATM	FBXW7	IDH1	NOTCH1	SMARCB1
BRAF	FGFR1	IDH2	NPM1	SMO
CDH1	FGFR2	JAK2	NRAS	SRC
CDKN2A	FGFR3	JAK3	PDGFRA	STK11
CSF1R	FLT3	KDR	PIK3CA	TP53
CTNNB1	GNA11	KIT	PTEN	VHL

For research use only; not intended for diagnostic use.

NEW ENGLAND BIOLABS[®] and NEB[®] are registered trademarks of New England Biolabs, Inc.
NEBNext DIRECT[™] is a trademark of New England Biolabs, Inc.

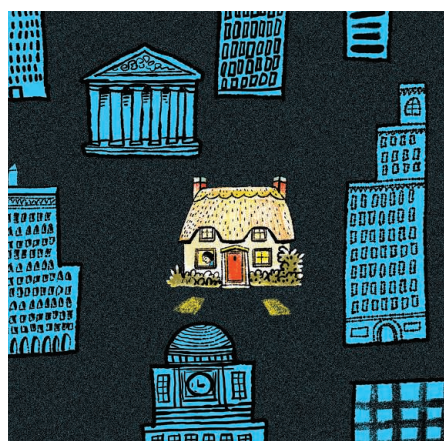
Making my own home

In the spring of 2015, after interviewing for yet another tenure-track faculty position—about my 185th application in 5 years—I was excited to hear that I was the top candidate. But despite that encouraging sign, once again I didn't get the offer. For years, I had been committed to pursuing the traditional academic path because I wanted to run an independent research program and teach. I thought a tenure-track faculty position was the one job that offered both. My efforts, however, had resulted in a handful of interviews but no offers. By the time I got that last rejection, my outlook had changed. A faculty post would have been nice, but I had a startup to run.

I fully committed to the startup life when I began thinking more deeply about what I wanted from my career. As my faculty job search stalled, I asked for advice from friends and mentors. Some talked through my interview approach with me, trying to help me figure out where I was going wrong. Others said that they would have quit the search, and they admired that I had not. One said that I should start considering jobs in industry. My mother told me not to give up. The only consistent point was that I had to re-evaluate my journey.

I asked myself whether I actually needed a faculty position to bring my ideas to life. The answer, I realized, was no. I had a Ph.D., which gave me a diverse skill set: analytical thinking, independence, the ability to write grants, and more. I also had teaching opportunities, as an adjunct lecturer and courtesy faculty member. What I needed was a home for my research. So, instead of trying to find a spot at an existing institution, I decided to create my own. It was a eureka moment!

I had unintentionally laid some of the groundwork a few years earlier, after completing a traditional postdoc and a time-limited position at the U.S. Department of Agriculture, where I established my own research program investigating nematode pheromone signaling, among other projects. I still wanted to do research, but I no longer had a permanent position. So, in 2012, while I continued applying for faculty jobs, I also established a company. I teamed up with academic and governmental researchers to submit collaborative grant applications to support my work. (As a bonus, I thought that winning a grant would make me a more competitive faculty candidate.) I bought lab equipment whenever I saw good deals at surplus auctions and on eBay, and I stockpiled it in my



“I [didn't need] a faculty position. ... What I needed was a home for my research.”

garage. I was ready to get my research started if and when I got funded.

That happened in late 2014, for a project to explore nematodes' relationship with their symbiotic bacteria. As a result, when I decided to stop applying for faculty jobs the next year, I was in a position to pursue both the funded project and the one I planned to commercialize: improving beneficial nematodes' efficacy for pest control.

Upon opting to fully dedicate myself to my startup, I realized that federal grants would not be enough to bring a product to market. I needed to be in the right ecosystem with the right mentors. I applied to a program at a University of Florida-affiliated business incubator, which provided office space; business mentors; and training on

topics including value proposition, market analysis, pain points, and investor pitches. The hardest part was learning how to explain my work to the nonscientists I was collaborating with. I also learned the importance of working with business professionals to bring a product to the market.

Now, I have a rented laboratory at the incubator and a grant to train my small but growing team. I am still raising funds from diverse sources, and I still have a lot to learn. But I'm glad I've found a way to pursue independent research outside the confines of academia while also maintaining some connection with my teaching. In the end, it's very rewarding that all those years of scientific training and endless hours of research are finally turning into a product that can contribute to improving the world. ■

Fatma Kaplan is the co-founder, co-owner, and CEO of Kaplan Schiller Research, LLC in Gainesville, Florida. Send your story to SciCareerEditor@aaas.org.